ABSTRACT

Title of dissertation: SYMBOLIC AND NUMERIC SOLUTIONS OF MODIFIED BANG-BANG CONTROL STRATEGIES FOR PERFORMANCE-BASED ASSESSMENT OF BASE-ISOLATED STRUCTURES

Robert R. Sebastianelli, Jr.,
Doctor of Philosophy, 2005

Dissertation directed by: Associate Professor Mark A. Austin
Department of Civil and Environmental
Engineering and Institute for
Systems Research

This work explores symbolic and numeric solutions to the Lyapunov matrix equation as it applies to performance-based assessment of base-isolated structures supplemented by modified bang-bang control. Traditional studies of this type rely on numeric simulations alone. This study is the first to use symbolic analysis as a means of identifying key "cause and effect" relationships existing between parameters of the active control problem and the underlying differential equations of motion. We show that symbolic representations are very lengthy, even for structures having a small number of degrees of freedom. However, under certain simplifying assumptions, symbolic solutions to the Lyapunov matrix equation assume a greatly simplified form (thereby avoiding the need for computational solutions).

Regarding the behavior of the bang-bang control strategy, further analysis shows: (1) for a 1-DOF system, the actuator force acts very nearly in phase, but in opposite direction to the velocity (90° out of phase and in opposite direction to the displacement), and (2) for a wide range of 2-DOF nonlinear base-isolated models, bang-bang control is insensitive to nonlinear deformations in the isolator devices. Through nonlinear time-history analysis, we see that one- and two-DOF models are good indicators of behavior in higher DOF models.

An analytical framework for system assessment through energy- and power-balance analysis is formulated. Computational experiments on base-isolated systems are conducted to identify and quantitatively evaluate situations when constant stiffness bang-bang control can significantly enhance overall performance, compared to base isolation alone, and assess the ability of present-day actuator technologies to deliver actuator power requirements estimated through simulation.

SYMBOLIC AND NUMERIC SOLUTIONS OF MODIFIED BANG-BANG CONTROL STRATEGIES FOR PERFORMANCE-BASED ASSESSMENT OF BASE-ISOLATED STRUCTURES

by

Robert R. Sebastianelli, Jr.

Dissertation submitted to the Faculty of the Graduate School of the
University of Maryland, College Park in partial fulfillment
of the requirements for the degree of
Doctor of Philosophy
2005

Advisory Committee:

Associate Professor Mark A. Austin, Chair/Advisor
Associate Professor Raymond Adomaitis
Professor Emeritus Pedro Albrecht
Professor Bilal M. Ayyub
Assistant Professor Ricardo A. Medina

This dissertation is dedicated to my wife, Mary. For her love, taste, judgment, and style.

ACKNOWLEDGMENTS

One of the things that has sustained me in this endeavor has been the thought that I would at some stage have the opportunity to formally thank the many people that have supported me. My first thanks goes to my advisor, Mark Austin. He has always made himself available to give advice, help, and encouragement. There has never been a time when I have knocked on his door and he has not given me his time. Special thanks are due to my committee members, Professors Raymond Adomaitis, Pedro Albrecht, Bilal Ayyub, and Ricardo Medina for agreeing to serve on my dissertation committee, reviewing my dissertation, and their constructive comments.

I gratefully remember Conrad Hemond for his early influence and encouragement.

I thank John O'Fallen and Hamid Ghasemi from the Federal Highway Administration for their guidance and support. Fellowship grants from the Federal Highway Administration provided some financial support for this dissertation. This support is gratefully acknowledged.

I thank the management at my employer, Houston Associates, Inc., for their financial and professional support and flexibility. I gratefully acknowledge the understanding and support given to me by David Butt, Anthony DeStefano, and

Robert Seitz. A special thanks goes to Trevor Vaughan who selflessly gave me advice for automating the simulations. Numerous other friends at Houston Associates, have provided me with continuous support and encouragement. For this, I am grateful.

My appreciation goes to my family, so happily extended by marriage, and particularly my sister, Jennifer, for endless amounts of support and encouragement. I would especially like to thank my parents for molding me through faith, love, and example.

I owe my deepest appreciation to my wife, Mary, who spent countless, late nights proofreading the manuscript and supporting me. Without her love, this dissertation would be a distant dream. She has sustained me in this endeavor. She is the best thing to ever happen to me.

Lastly, I know that all good things come from the Lord who has undoubtedly shined his light upon me, his unworthy servant. For this, I am blessed and grateful.

TABLE OF CONTENTS

LIST OF TABLES

LIST OF FIGURES

Chapter 1

Introduction

1.1 Background

The roots of structural control in civil engineering can be traced back to aerospace-related problems of tracking and pointing of spacecraft and rockets. Starting with the conceptual study by Yao [98] in 1972, the technology moved into the field of civil engineering. The field continued to mature quickly, and in 1990,

> "... in recognition of the growing worldwide awareness by civil engineers of the potential of active protective systems for earthquake hazard mitigation ..." [33]

the U.S. Panel on Structural Control was formed. The panel sponsored the U.S. National Workshop on Structural Control held at the University of Southern California in 1990. Subsequent meetings including the Japan National Workshop, the U.S.-Italy Workshop in 1992, and an international workshop held in Hawaii in 1993. One of the most significant events took place at the Tenth World Conference on Earthquake Engineering in Madrid, Spain in 1992 where several technical sessions were dedicated to structural control. The International Association for Structural Control (IASC) was formed the next year. The efforts of this governing body led to the First World Conference on Structural Control in 1994 where 337 participants from 15 countries met to present and discuss the results of their research. Additional activity in the area of structural control include the 10th and 11th World Conferences on Earthquake Engineering, held in Madrid and Acapulco, respectively, the First European Conference on Structural Control in Barcelona, Spain, the Second

International Workshop on Structural Control, which was held in Hong Kong in 1996, the Second World Conference on Structural Control held in Tokyo in 1998, the Third World Conference on Structural Control held in Como, Italy in 2002. According to Spencer and Nagarajaiah [68], as of July 2003, there have been over 40 buildings that have employed feedback control strategies (see table 2.2). The vast majority of these have been hybrid control systems.

1.2 Motivation

To assist engineers in the design of base-isolated structures, recent AASHTO and UBC design codes [1, 86] contain code provisions prescribing a series of standard performance levels for design, together with acceptable levels of structural and non-structural damage, and suggested methods of analysis for performance evaluation. Under minor and moderate earthquake loadings, for example, base-isolated structures should suffer no structural damage. For design earthquakes corresponding to the maximum credible ground motion for the site, the main structural members are expected to remain essentially elastic, with nonlinear deformations (i.e., damage) restricted to the isolation devices. Simplified methods of design for base-isolated structures have been proposed by Turkington et al. [83, 82], Antriono and Carr [3, 2], Mayes et al. [48], and Ghobarah and Ali [30], among others. While the overall benefits of base isolation systems are well known [2, 3, 30, 48, 83, 82, 84], there is a mounting body of evidence that base isolation may not always provide adequate protection [99]. One concern is the possibility of localized buckling of the isolator devices and/or collapse of the structure caused by truly excessive lateral displacements of isolator elements (details on the appropriate analysis procedures can be found in Naeim and Kelly [49]). A second area of concern, raised by Johnson et al. [36] and Spencer et al. [68], points to the inability of base isolation to

protect structures against near-source, high-velocity, long-period pulse earthquakes. In similar studies, Hall et al. [31] and Heaton et al. [32] express concerns about excessively large base drifts caused by strong, near-fault ground motions.

Base isolation is one of the most successful methods for protecting structures against seismic ground motion; however, due to the simplicity and passive nature of base isolation mechanisms, coupled with the unpredictable nature of future ground motions, base isolation is not a guaranteed means of effective protection during a wide range of seismic events [99]. One complicating factor is the sensitivity of "optimal designs" to localized site effects – an isolation system designed for a El Centro-type earthquake typically will not be optimal for a Northridge-type earthquake. Due to the uncertainty in ground motion prediction, there is a need for an isolation system that is adaptable. Johnson et al. [36] and Spencer et al. [68] point out that recently there has been significant concern regarding the effectiveness of base isolation to protect structures against near-source, high-velocity, long-period pulse earthquakes. Such earthquake motions are difficult to accommodate. For example, a base-isolated structure in one region of Los Angeles that may have readily survived the 1994 Northridge earthquake, may have well been destroyed if it were located elsewhere in the region [47]. Also, Housner et al. [33] and Reinhorn et al. [58] observe that since base isolation generally reduces the interstory drift and absolute acceleration of the structure at the expensive of large base displacement, the combination of active control with base isolation is able to achieve both low interstory drift, and at the same time, limit the maximum base displacement with a single set of control forces. Also, base-isolated systems are limited in their ability to adapt to changing demands for structural response reduction. By supplementing base isolation with a active control mechanisms, the hope is that higher levels of performance will be possible without a substantial increase in cost.

In a first step toward addressing these issues (and potentially achieving a higher level of performance), researchers have proposed systems where the main isolation devices are supplemented by active control mechanisms [58, 33]. Bang-bang control is a natural choice for the implementation of such a system. While numerical algorithms exist for solving the Lyapunov matrix equation, systematic procedures for modeling base-isolated structures, supplemented by bang-bang control are still lacking [33]. Unresolved research questions include: What kinds of "performance improvement" are possible with active components? Are there earthquakes whose ground motion characteristics make isolation an unsuitable option for design? What are the limitations of present-day active component technologies? Answers to these questions are important because of their practical ramifications to design – base isolation alone is capable of reducing both the interstory drift and absolute accelerations structures at the expense of slight increases in base displacement. Looking ahead, we foresee base isolation supplemented by active control being able to achieve simultaneously low interstory displacements, low absolute accelerations, and controlled maximum base displacements [33, 68].

1.3 Equation of Motion

The well known general equation of motion for a multi-degree of freedom system subject to an earthquake load and external active controlling forces is as follows:

$$\mathbf{M}\ddot{x}(t) + \mathbf{C}\dot{x}(t) + \mathbf{K}x(t) = \mathbf{H}u(t) - \mathbf{M}r\ddot{x}_g(t). \tag{1.1}$$

In equation 1.1, $x(t)$ is a n-dimensional vector representing the relative displacements of the n degrees of freedom. $\mathbf{M}$, $\mathbf{C}$, and $\mathbf{K}$ are the mass, damping, and stiffness n x n matrices, respectively. $\ddot{x}_g(t)$ represents the earthquake ground ac-

celeration, $\mathbf{H}$ is an n x p matrix that designates the location of the controller(s), while $u(t)$ is a p-dimensional vector that represents the control force of p-number of controllers.

The first-order differential equation, or state-space, form of equation 1.1 is given by the following:

$$\dot{z}(t) = \mathbf{A}z(t) + \mathbf{B}u(t) - \mathbf{W}\ddot{x}_g(t). \tag{1.2}$$

In equation 1.2,

$$z(t) = \begin{bmatrix} x(t) \\ \dot{x}(t) \end{bmatrix}; \tag{1.3}$$

$$\mathbf{A} = \begin{bmatrix} \mathbf{0} & \mathbf{1} \\ -\mathbf{M^{-1}K} & -\mathbf{M^{-1}C} \end{bmatrix}; \tag{1.4}$$

$$\mathbf{B} = \begin{bmatrix} \mathbf{0} \\ \mathbf{M^{-1}H} \end{bmatrix}; \tag{1.5}$$

$$\mathbf{W} = \begin{bmatrix} 0 \\ r \end{bmatrix}. \tag{1.6}$$

While most modern control makes use of the first-order differential equation 1.2, this proposal will try wherever possible to use the more familiar second-order differential equation of motion shown by equation 1.1. Using the second-order form of the equation of motion has the following advantages:

1. Numerical iterative time-step methods for solving equation 1.1 are well established. Numerical methods such as Newmark's time step method have been shown to be either conditionally stable or absolutely stable dependent on the assumption of the behavior of acceleration between time steps.

2. Several numerical algorithms exist for solving for the unknowns of the system in the form of equation 1.1 that has a property (i.e., stiffness) nonlinearity. The force-displacement behavior of base-isolated structures subjected to moderate to severe ground motion loadings is expected to be nonlinear. We will use existing numerical algorithms for solving for the time-history of base-isolated structures subjected to earthquake loads.

3. The second-order form has a representation that is closely aligned to the physical intuition of experienced structural designers. The second-order form facilitates valuable insight as to how adding/modifying the active control force effects the behavior of the structure.

1.4 Bang-Bang Control Law

One of the well-known control laws in optimal control theory is the bang-bang control law [11, 92, 93]. The key characteristic of optimal bang-bang control is a control force, $u(t)$, that switches from one extreme to another (i.e., the control force is always exerting its maximum force in either the positive or negative direction). Since the control force always takes on maximum values, the full capabilities of the actuators can be exploited. Numerical simulation studies have shown that bang-bang control can provide better control efficiency than the well-known Linear Quadratic Regulator (LQR) Control Law [93].

Control Objective. The control objective for bang-bang control is to minimize:

$$J = \frac{1}{2} \int_0^{t_f} \left(z^T(t) \mathbf{Q} z(t) \right) dt. \tag{1.7}$$

where $z(t)$ is a $2n$ x 1 state vector of system displacements and velocities (for structural control, the state variables represent the displacements and velocities at

the n-degrees of freedom), and $\mathbf{Q}$ is a positive semi-definite matrix whose content is left for the designer to choose. The well known optimal control solution [11, 92, 93] for a system in the form of equation 1.2 and which minimizes equation 1.7 is:

$$u(t) = -u_{max}\text{sgn}\left[\mathbf{B^T}\lambda(t)\right]; \tag{1.8}$$

where $\lambda(t)$ is known as the costate vector that is obtained by solving the following differential equation:

$$\dot{\lambda}(t) = -\mathbf{A^T}\lambda(t) - \mathbf{Q}z(t); \tag{1.9}$$

and u_{max} is a scalar that represents the maximum actuator control force. The other matrices in equations 1.8 and 1.9 are as previously defined. As part of the time history calculation of base-isolated structures influenced by bang-bang active control, equation 1.9 must be solved at each time step. Numerically stable integration algorithms such as the discrete implicit Runge-Kutta (DIRK2) method can be used to accomplish this task. Theoretical considerations can guide the selection of initial conditions for SDOF systems. However, for all other problems of practical importance, solutions to equation 1.9 are complicated by a lack of theoretical guidance for choosing the differential equation's initial conditions. An incorrect assumption (on the initial conditions) will lead to a numerical solution with time-varying characteristics that are correct, but is out of phase with the "correct optimal control solution." This may lead to an active controlled response that is worse than an uncontrolled response! We also note that the computational effort needed to solve 1.9 may be unwarranted, especially when the considerable uncertainties associated with the modeling of seismically-resistant structures (e.g., ability to predict details of future ground motions, limitations of damping models) are taken into account.

1.5 Modified Bang-Bang Control Law

To avoid solving equation 1.9 at each time step for the entire time history response, a modified bang-bang control law is proposed by Wu and Soong [93].

Control Objective. Instead of minimizing equation 1.7, the objective of modified bang-bang control is to minimize the derivative of the following generalized energy function:

$$V[z(t)] = z^T(t)\mathbf{S}z(t). \tag{1.10}$$

Equation 1.10 is also referred to as the Lyapunov function, where the $\mathbf{S}$ matrix is the solution to the following Lyapunov matrix equation:

$$\mathbf{A^T S} + \mathbf{SA} = -\mathbf{Q}. \tag{1.11}$$

Taking the time derivative of equation 1.10 and substituting in the closed-loop state equation leads to the following equation results [37, 93]:

$$\dot{V}[z(t)] = -z^T(t)\mathbf{Q}z(t) + 2u^T(t)\mathbf{B^T S}z(t). \tag{1.12}$$

Close inspection of equation 1.12 indicates that in order for this equation to be a minimum for all possible state variables, $z(t)$, the second term on the right-hand side of equation 1.12 should result in a negative scalar for all possible $z(t)$, and moreover, $u(t)$ must be set to a maximum, say u_{max}. An appropriate choice for $u(t)$ that fulfills these two criteria is:

$$u(t) = -u_{max}\text{sgn}\left[\mathbf{B^T S}z(t)\right]. \tag{1.13}$$

This selection of $u(t)$ minimizes the derivative of the Lyapunov function at each

time step, and hence, also minimizes the Lyapunov function itself (equation 1.12 at each time step of the response).

Equation of Motion. The effect of modified bang-bang control on the second-order differential equation of motion for a seismically-resistant structure is obtained by substituting equation 1.3 into equation 1.13, and then substituting the resultant equation into equation 1.1. The equation of motion is as follows:

$$\mathbf{M}\ddot{x}(t) + \mathbf{C}\dot{x}(t) + \mathbf{K}x(t) = -\mathbf{H}u_{max}\text{sgn}\left[\mathbf{B^T S}\begin{pmatrix} x(t) \\ \dot{x}(t) \end{pmatrix}\right] - \mathbf{M}r\ddot{x}_g(t); \qquad (1.14)$$

where the matrix, $\mathbf{S}$, is the $2n$ x $2n$ matrix solution to the Lyapunov matrix equation given in equation 1.11 and $\mathbf{B}$ is a $2n$ x p matrix as defined by equation 1.5.

Reference to "Bang-Bang Control" in This Dissertation. For the remainder of this dissertation, solutions to the Lyapunov equation for bang-bang control will be simply referred to as bang-bang control.

Linear Properties of the Lyapunov Matrix Equation. The multi-objective design of bang-bang control strategies is simplified by noting that for a given linear system, matrix $\mathbf{A}$ is fixed and matrix $\mathbf{S}$ is linearly dependent on $\mathbf{Q}$. In other words, given two Lyapunov matrix equations:

$$\mathbf{A^T S_1} + \mathbf{S_1 A} = \mathbf{Q_1}; \qquad (1.15)$$

and

$$\mathbf{A^T S_2} + \mathbf{S_2 A} = \mathbf{Q_2}; \qquad (1.16)$$

linearity of the Lyapunov matrix equations with respect to $\mathbf{S}$ implies:

$$\mathbf{A}^{\mathbf{T}}\left(a\mathbf{S_1}+b\mathbf{S_2}\right)+\left(a\mathbf{S_1}+b\mathbf{S_2}\right)\mathbf{A}=a\mathbf{Q_1}+b\mathbf{Q_2}. \tag{1.17}$$

where a and b are arbitrary coefficients. A proof of the linear matrix properties of the Lyapunov matrix equation is given by Belanger [10].

Trade-offs between our two control objectives may be investigated by solving equation 1.17 with $a = 1$ and $b = 0$ and with $a = 0$ and $b = 1$. The solution matrices $\mathbf{S_1}$ and $\mathbf{S_2}$ may be scaled to obtained any desired combination of a and b.

Observation Regarding the $\mathbf{B^TS}$ Matrix Product. Consider the matrix product $\mathbf{B^TS}$ for an n degree of freedom system. Since $\mathbf{B}$ has dimensions $2n$ x p and $\mathbf{S}$ has dimensions $2n$ x $2n$, the matrix product $\mathbf{B^TS}$ has dimensions p x $2n$. Since, by definition, the upper half of the $\mathbf{B}$ matrix is a n x p matrix of zeros, at most, only terms in rows $n + 1$ through $2n$ of $\mathbf{S}$ make any contribution to the matrix product $\mathbf{B^TS}$. We will employ this observation in our symbolic analysis of the inner workings for the bang-bang active control strategy.

1.6 Energy-Based Bang-Bang Control

From equations 1.11 and 1.13, it is evident that $\mathbf{Q}$ plays a central role in the bang-bang control strategy. It is therefore somewhat surprising that state-of-the-art procedures for structural control design tend to be ad hoc, letting iterative "trail and error" procedures and mathematical convenience drive the selection of terms in $\mathbf{Q}$ over first principles of engineering. While linear quadratic regulator (LQR) control is used extensively in control systems designed for structural control applications, the literature is scare in guidelines and justification for selection of design parameters $\mathbf{Q}$ (or $\mathbf{R}$). Kailath [37] (see page 219) states that the choice of the quantities is more of an art than science and is being further investigated. Both

Belanger [10] (see pg. 305) and Connor [21] (see pg. 603) refer to perturbing terms in the weighing matrices until a desired result is obtained. Cai et al. [13] (see pg. 1653) uses the LQR method for comparison to their proposed sliding-mode bang-bang control method. In the LQR formulation, Cai et al. [13] sets the diagonal, elements of $\mathbf{Q}$ as relative, arbitrary values, and the off-diagonal terms simply to zero.

A key tenet of our work is that the terms in $\mathbf{Q}$ should be selected so that the bang-bang control strategy has a well defined physical meaning. Wu, Soong, Gattulli, and Lin [94] suggest that under the LQR performance criteria, vibratory energy within the structure may be minimized by choosing $\mathbf{Q}$ to be one of the following options:

$$\mathbf{Q} = \begin{bmatrix} \mathbf{0} & \mathbf{0} \\ \mathbf{0} & \mathbf{M} \end{bmatrix}; \mathbf{Q} = \begin{bmatrix} \mathbf{K} & \mathbf{0} \\ \mathbf{0} & \mathbf{0} \end{bmatrix}; \mathbf{Q} = \begin{bmatrix} \mathbf{K} & \mathbf{0} \\ \mathbf{0} & \mathbf{M} \end{bmatrix}. \tag{1.18}$$

For the design of base-isolated structures supplemented by active control, distributions of structural stiffness, together with system displacements, determine quantities of internal energy present within portions of the structure. A complicating factor is the heterogeneous role played by elements within the structure. While elements in the system superstructure are expected to remain essentially elastic (and, therefore, undamaged), the base isolation elements are expected to protect the superstructure by deforming well into the inelastic range without losing strength. To capture this duality, Austin [5, 8, 9] and Takewaki [80] suggest that overall input energy be partitioned into two parts: (1) input energy directed to the main structural system, and (2) input energy directed to the isolation devices. This energy-based approach to bang-bang control is valid because for the design of base-isolated structures supplemented by active control, distributions of structural stiffness, together with system displacements, determine quantities of internal energy present within

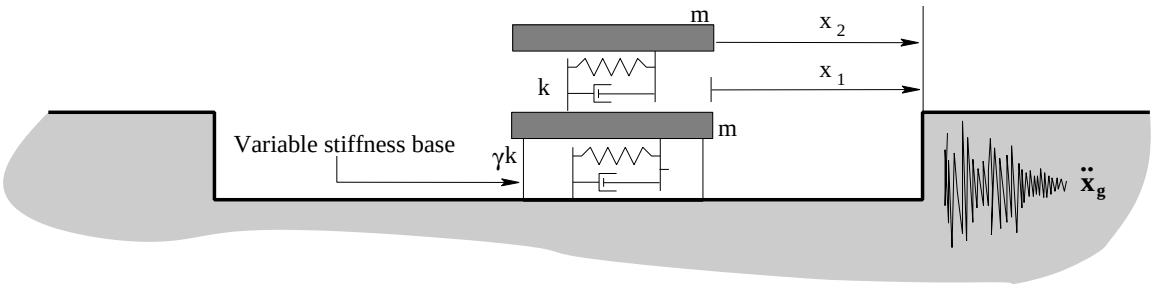

Figure 1.1: 2-DOF System

portions of the structure. Internal energy increases in proportion to the square of the displacements – hence, indirectly, internal energy is a measure of displacements, which in turn, is related to peak displacements and the likelihood of non-structural and structural damage. Models of structural performance need to capture force-displacement nonlinearities in the isolation devices.

1.6.1 Minimization of Superstructure Internal Energy

Since the relative displacement of the endpoints of a structural element are proportional to the square root of internal energy within the element, a reasonable control objective is minimization of the internal energy in the superstructure (i.e., everything except the base isolation devices).

Example 1. Internal Energy for the Superstructure of a Two Story Shear Structure. In mathematical terms, the internal energy in a single element of stiffness k is given by the following equation:

$$\text{Element I.E.(t)} = \frac{1}{2}k\left(x_2(t) - x_1(t)\right)^2 = \frac{1}{2}\begin{pmatrix} x_1(t), & x_2(t) \end{pmatrix}\begin{bmatrix} k & -k \\ -k & k \end{bmatrix}\begin{pmatrix} x_1(t) \\ x_2(t) \end{pmatrix}; \tag{1.19}$$

where $x_1(t)$ and $x_2(t)$ represent the end displacements of nodes 1 and 2, respectively. Now lets consider the 2-DOF system shown in Figure 1.1. The superstructure and

base isolation systems have lateral stiffness k, and γk, respectively. Typically γ will lie in the interval 0.0-0.15. The internal energy of the superstructure (element 2) can be minimal by choosing $\mathbf{Q}$ as:

$$\mathbf{Q} = \begin{bmatrix} k & -k & 0 & 0 \\ -k & k & 0 & 0 \\ 0 & 0 & 0 & 0 \\ 0 & 0 & 0 & 0 \end{bmatrix}. \tag{1.20}$$

Substituting equation 1.20 into equation 1.7 and rearranging terms gives the following expression for J:

$$J = \frac{1}{2} k \int_0^{t_f} (x_1(t) - x_2(t))^2 \, dt; \tag{1.21}$$

which is simply the integral of the internal energy in element 2 over the time history of the structure.

For bang-bang control, substituting equation 1.20 into equation 1.12 leads to the following equation:

$$\dot{V}[z(t)] = k(x_1(t) - x_2(t))^2 + 2u^T(t)\mathbf{B^T S}z(t). \tag{1.22}$$

The first term on the right-hand side of equation 1.22 is an energy term corresponding to double the amount of internal energy in element 2 at any time, t. Physical considerations dictate that the second term on the right-hand side of equation 1.22 must also be in terms of energy. Since the actuator force, $u(t)$, is present in equation 1.22, this term may be thought of as the work done by the actuator force(s) on the structure at any time, t.

1.6.2 Base Isolator Internal Energy

Because base isolator elements are designed to exhibit nonlinear hysteretic behavior without a loss of strength occurring [1, 59, 66], large base displacements are expected during severe earthquake loadings. From a performance viewpoint, however, truly excessive lateral displacement of the isolator elements should be avoided because they can lead to localized buckling of the isolator devices and/or collapse of the structure (details on the appropriate analysis procedures can be found in Naeim and Kelly [49]). Control of peak displacements must be balanced against a need for the base isolators to yield during an earthquake event and, therefore, do plastic work and dissipate energy. When the ground motions cease, ideally, permanent, plastic deformation of the isolator devices will be close to zero – indeed, we hope that the active control strategy and actuators will work towards this objective.

Example 2. Internal Base Isolator Energy for a Two Story Shear Structure. These performance criteria can be addressed indirectly through control of internal energy in the base isolators. Assuming that base isolators will be firmly attached to the ground (with full fixity), the internal energy is given by the following equation:

$$\text{Base Isolator Element Internal Energy(t)} = \frac{1}{2}\gamma k x_1(t)^2; \tag{1.23}$$

where γk is the lateral stiffness of the base isolator element and $x_1(t)$ represents the base isolator element degree of freedom that undergoes a displacement relative to the displacement of the ground. To minimize the internal energy in the base isolator (element 1) of the system shown in Figure 1.1, an appropriate choice for $\mathbf{Q}$ is:

$$\mathbf{Q} = \begin{bmatrix} \gamma k & 0 & 0 & 0 \\ 0 & 0 & 0 & 0 \\ 0 & 0 & 0 & 0 \\ 0 & 0 & 0 & 0 \end{bmatrix}. \tag{1.24}$$

Substituting equation 1.24 into equation 1.7 gives an expression for J that is the integral of the internal energy in the base isolator (element 1) over the time history of the structure.

For the bang-bang control case, substituting equation 1.24 into equation 1.12 gives an expression for $\dot{V}[z(t)]$ that represents the amount of internal energy in the base isolator (element 1) and a second energy term that represents the amount of work done on the structure by the actuator(s).

1.7 Research Objectives and Scope

Looking ahead, we envision performance-based design methods that will provide engineers with guidance in selecting appropriate control objectives and analysis procedures for base isolated buildings and bridges supplemented by active control. This vision is more likely to be realized if designers are provided with guidance on the performance capabilities and cause-and-effect relationships governing the active control. A key tenet of our work is that terms in the control design matrix ($\mathbf{Q}$) should have well defined physical meaning, thereby opening a pathway for identifying and understanding basic cause-and-effect mechanisms that might exist in the implementation of passive/active base isolation systems. Wu, Soong, Gattulli, and Lin [94] suggest, for example, designing $\mathbf{Q}$ so that energy is minimized in the structure.

In a departure from previous research efforts [5, 59, 66, 83, 82, 93], and in an attempt to bridge this gap, this dissertation explores three avenues of inves-

tigation in the hope of better understanding the potential benefits of bang-bang control mechanisms as a supplement to performance-based design of base-isolated structures. We are particularly interested in the role that symbolic and numeric analysis procedures associated with the Lyapunov equation can play. The research avenues are as follows:

1. **Symbolic Analysis For Single-Degree-of-Freedom Systems.** We explore the extent to which symbolic analysis can provide insight into the connection between an appropriate selection of $\mathbf{Q}$ and the active control strategy that follows through $\mathbf{B^T S}z(t)$. First, we use Mathematica© to compute symbolic solutions to coefficients in $\mathbf{B^T S}$ for systems having one and two degrees of freedom. We will soon see that for structures having more than two-degrees of-freedom, the symbolic expressions are computationally intractable, even for Mathematica©.

2. **Symbolic Analysis For Multi-Degree-of-Freedom Systems.** Starting with relatively simple expressions for solutions to $\mathbf{B^T S}$, in a one degree of freedom structure, we determine the restrictions on the structural model that allow the solution to be scaled up to a n-DOF system.

3. **Sensitivity Analysis.** In the final part of this dissertation, we explore the effect of bang-bang control strategies on the nonlinear base isolator deformations.

These research avenues lead to the formulation of simplified solutions to the Lyapunov equation that result from active control strategies driven by potential, kinetic, and total energy concerns. Key results and modeling assumptions that lead to simplified solutions to the Lyapunov equation are given in section 3.2.3. Numerical experiments were conducted to verify the predictions made during the analytical phase of the dissertation.

In the second half of the dissertation, we formulate energy- and power-balance equations for a base-isolated structure supplemented with constant stiffness bang-bang (CKBB) control. CKBB control is discussed in detail in section 4.4. While quantitative measurements such as absolute roof acceleration are a good indicator of damage to light internal equipment, occupant discomfort, and other non-structural damage [40], energy- and power-balanced based metrics of system performance provide a means for accurately estimating the capacity of a structure to resist forces elastically and dissipate energy associated with damping and key structural elements undergoing cyclic nonlinear deformations. In addition, since the control objective of CKBB control is energy-based, analyzing the system response from an energy point of view will help us to validate the CKBB control theoretical formulation.

A second set of numerical experiments is conducted in which we employ modeling techniques and a base-isolated building structure assembled from a variety of previous research efforts. The parameters of the model are the same as used by Ramallo et al. [57]. Nonlinear time-history analyses with energy- and power-balance assessment are computed for a 6-DOF base-isolated building system. With this computational framework in place, the specific research objectives of this second numerical experiment is as follows:

1. From an energy-balance and base drift viewpoints, compare the performance of a base-isolated building subjected to a variety of design criteria and earthquakes.

2. Compare demands on actuator power to the capabilities of actuator technology.

Experimental permutations in the design and ground motion excitations include: (1) Base isolation alone (with no control); (2) Base isolation supplemented with bang-bang control; (3) Moderate earthquakes; (4) Near-source, high-velocity, severe

earthquakes. We demonstrate that when the model parameters/behavior do not satisfy the assumptions needed to derive simplified representations for active control, it seems that good performance can still result. We say "it seems" because our modeling assumptions represent control under a "best case" scenario. As we move toward modeling of full-scale structures, several modeling assumptions would need to be reexamined: (1) A singular control-force requirement possible, (2) Availability of state variables (i.e., displacements and velocities at all DOFs), (3) No time delay between the measured displacements and velocities and the application of the control forces, and (4) The presence of only one actuator that is located at the top of the base isolator.

1.8 Dissertation Outline

The remainder of this dissertation is organized in the following manner:

Chapter 2 presents a literature survey of topics related to this research.

Chapter 3 presents a symbolic analysis of the bang-bang structural control problem. Three research avenues use tractable 1- and 2-DOF models to understand the relationship between the bang-bang control algroithm and model parameters (stiffness, damping, etc.) and model response (displacements and velocities).

Chapter 4 describes a numerical experiment that calculates the time history response of a 5-DOF nonlinear mass-spring-damper system with and without bang-bang control. The results of this numerical experiment are compared to the relationships obtained in Chapter 3.

Chapter 5 presents a theortical energy- and power-balance framework for estimating demand on structural subsystems.

Chapter 6 describes a numerical experiment that calculates the time history response of a scaled 6-DOF nonlinear mass-spring-damper system with and without bang-bang control. Using the framework presented in Chapter 5, the energy demand on structural subsystems are calculated. Senarios are used to determine when bang-bang control is most likely to be beneficial to base isolation. Senario parametrics include base isolator/bang-bang control design and severity of earthquake.

Chapter 7 describes the intellectual contributions and conclusions of this dissertation. It also identifies anticipated benefits of this research and gives suggestions for future extension of the work described in this dissertation.

Chapter 2

Related Research

2.1 Benchmark Studies in Structural Control

2.1.1 Benchmark Studies for Buildings

First Generation Benchmark Study for Buildings. In order to provide a clear basis for the evaluation and efficiency of various structural control systems in 1995, the American Society of Civil Engineers (ASCE) Committee on Structural Control initiated a benchmark study in structural control. Two benchmark structures, both scale models of a three-story building, were employed. The difference between these models is that one used an AMD controller while the other used an active tendon controller. The control model consisted of a 20-state linear system control model. The main variable for the designer was the type of control theory which to implement. A comparison between the analytical (control designs which were submitted to this benchmark study) and corresponding experimental results are yet to be published. These benchmark problems are known as the "First Generation Building Benchmark Problems" [71].

Building on the foundation laid by the ASCE Committee on Structural Control in 1995, plans for the next generation of benchmark structural control studies were initiated by the Working Group on building Control during the Second International Workshop on Structural Control. The Working Group's goal in this effort is to develop benchmark models to provide systematic and standardized means by which competing control strategies, including devices, algorithms, sensors, etc. may be evaluated. While the First Generation Benchmark Problem provided a basis

for evaluation of the various structural control systems, the problem lacked the complexity associated with full-scale applications. The goal of the next generation benchmark problem is to take the structural control community another step toward the realization and implementation of innovative control strategies for hazard mitigation [71].

Second Generation Benchmark Study for Buildings. The second generation building benchmark problems in structural control were more complex. Two models were proposed — one for wind excitation and a second for earthquake excitation. A high-fidelity, linear time-invariant state space control model was developed for each model.

Wind Model. The wind-excited model is based on a 76-story concrete tower proposed for Melbourne, Australia. This reinforced concrete building consists of a concrete core and concrete frame. The core is designed to resist the wind load whereas the frame is designed to carry the gravitational loads and part of the wind loads. Though all the structural members were designed, the building has not been constructed [97].

The 76-story building is modeled as a vertical cantilever beam. The finite element model has 76 rotational DOFs and 76 translational DOFs. Then, all the 76 rotational DOFs are removed by static condensation. By retaining the first 46 complex modes of the original system, the model is further reduced to 23 DOFs. Also, simplifications concerning the wind loading are made to further reduce the computational effort. It is the task of the designer/researcher to choose whether to use an active, semi-active, or passive control system. In the case of active control systems, either an active tuned mass damper (ATMD) or an AMD can be installed on the top floor. In the case of passive or semi-active systems, such as viscous

dampers, visco-elastic dampers, etc., control devices can be installed in any selected story units. It is also up to the designer/researcher to choose the type of control algorithm in which to use [97].

Earthquake Model. The earthquake-excited model is based on a 20-story building typical of mid- to high-rise buildings designed for the Los Angeles region. Although not actually constructed, the structure meets seismic code requirements for this region. The building's lateral load-resisting system is comprised of steel perimeter moment-resisting frames (MRFs). The interior bays contain simple framing with composite floors (i.e., concrete and steel) which provides diaphragm action (assumed rigid in the horizontal plane). The benchmark study focuses on an in-plane (2-D) analysis for one-half of the entire structure; the frame being considered is one of the N-S MRFs (in the short direction of the building) [70].

Based on the physical description of the 20-story structure, an in-plane finite element model of the N-S MRF is developed. The linear response of the structure is shown to be a reasonable approximation that is used in this benchmark study. The structure is modeled as plane-frame elements, and the mass and stiffness matrices for the structure are determined. Guyan reduction is used to reduce the number of DOFs to a more manageable size while still maintaining the important dynamic characteristics of the full-model. This results in a 62 state control model. Control implementation constraints and evaluation criteria are outlined. It is up to the designer/researcher to choose a control algorithm, control device (either passive, active, semi-active, or a combination thereof, may be considered), and the placement of sensors and actuators [70].

Third Generation Benchmark Study for Buildings. At the First World Conference on Structural Control in 1994, the necessity of taking into ac-

count structural nonlinearity was identified. During the Second World Conference on Structural Control in 1998 and as a result of the success of the second generation benchmark study for buildings, it was decided that the nonlinear analysis for the seismically excited buildings would be pursued. Also, at the Second World Conference on Structural Control, a third generation wind-excited benchmark model was developed.

Earthquake Model. Three earthquake excited nonlinear building models were developed. Nonlinear evaluation models of 3-story, 9-story, and 20-story buildings were developed that portrays the salient features of the structural system. The task of each participant in this benchmark study was to define (including sensors and control algorithms), evaluate and report on their proposed control strategies. These 3-story, 9-story and 20-story nonlinear buildings were designed for the SAC project for the Los Angeles, California region. The SAC project is a joint venture between the Structural Engineers Association of California (SEAOC), the Applied Technology Council (ATC), and Consortium of Universities for Research in Earthquake Engineering (CUREE). The members of each of these organizations realized that they were uniquely qualified to investigate the damage to welded steel moment frame buildings in the 1994 Northridge earthquake and developing repair techniques and new design approaches to minimize damage to steel moment frame buildings in future earthquakes.

Wind Model. Following the development of the wind model used in the second generation benchmark study in December 1997, wind tunnel testing was been conducted on a 1:400 scale model of the 76-story building to measure wind load time history on different floors of the building. The response control performance cri-

terion was been reformulated using experimentally measured wind loads from this wind tunnel testing.

2.1.2 First Generation Benchmark Study for Bridges

At the Second International Workshop on Structural Control (December 18-20, 1996), the Working Group on Bridge Control developed plans for the First Generation Bridge Benchmark Study. The bridge proposed for the benchmark study was the Jindo Bridge in South Korea. In order for the finite element model of the bridge to be created, it was necessary to increase the understanding of how the complexities associated with modeling cable-stayed bridges, such as nonlinear behavior and the participation of highly coupled, high order, vibration modes affect the active control schemes. Additionally, computational considerations associated with control analyses require the size of the model be significantly reduced without the loss of important vibration characteristics of the bridge. The First Generation Bridge Benchmark Study focuses on seismic response control [63].

Schemmann and Smith [61] studied the issues involved with modeling a flexible bridge structure. Due to the cable elements and the geometric nonlinearity associated with the Jindo Bridge, the following nonlinear issues were addressed in creating the control model: (i) the axial force deformation relationship of the inclined cables caused by the dead weight induced sag; (ii) the axial force-bending moment interaction of the towers and longitudinal girders (*i.e.,* beam-column interaction); (iii) the geometry change due to large deformations; (iv) multiple support excitation, caused by the exposure of the bridge towers to the spatially random seismic excitation; and (v) the participation of coupled, high order, three-dimensional vibration modes in the overall dynamic response. Material nonlinearities, which are typically avoided in such large structures were not taken into account in the model.

Also, three separate reduced-order modeling techniques for creating effective control models are studied: the IRS method, the internal balancing method, and a modal reduction method. These methods are compared on their ability to capture the complex dynamic response of cable-stayed bridges subjected to multiple-support excitation and their ability to create viable state space models for control analyses.

The resulting three-dimensional finite element model (FEM) has 316 DOFs (before model reduction). The deck is represented by a single central spine of space frame elements with lumped masses attached. Rigid links are used to represent the offset between the cables and the spine. Additionally, to induce coupling of the torsional and transverse modes of the deck, rotary inertia of the masses is included at the appropriate DOFs. The first twenty undamped natural frequencies of the FEM are used in the study. For illustration, figure 2.1 displays the first order torsional mode (7), fifth order vertical mode (8), fourth order lateral deck mode (20), and the first longitudinal tower mode (18). Observe that the model has mode shapes which span all three dimensions and that many modes are coupled—a three dimensional model is clearly required and ground motion should have components in all three orthogonal directions. The next step is a time-history analyses to obtain the modes that participate most directly in the structure's force response. The Northridge accelerogram was used for the time-history analyses.

The study by Schemmann and Smith [61] shows the importance of multiple-support excitation. Compared to uniform-support excitation, bending moments are increased significantly at numerous locations and entirely different sets of modes are excited. The drawback of time-history analysis is that different earthquakes with different frequency content may excite other modes. Thus, time-history analyses should be performed using a larger set of ground motions to obtain more general results. Also, usually modes which cause the largest displacements also generate

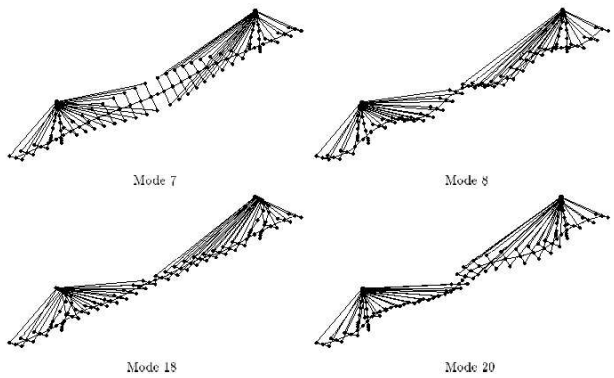

Figure 2.1: Finite Element Mode Shapes 7, 8, 18, 20 [61]

the largest forces; however, as it is shown here, higher order modes which do not significantly participate in the displacement response, participate significantly in the force response, the control algorithm will have to insure that the internal forces and not just the displacements are reduced. The modal reduction technique proves to be most promising in this area because of its ability to select only those modes which cause the largest force and displacement response.

A companion study, also by Schemmann and Smith [62], considers the application of active control to the model created in the above study. In this study, LQR control theory is implemented. One of the central components to this control theory is the performance index J. The second part of this paper by Schemmann and Smith considers the problem of control through output feedback and use of a Kalman filter. In both parts of this paper, different actuator configurations are compared. Not only are the force responses considered, but the peak control force put forth by the actuator should also be considered since this determines actuator size.

Results from the companion study indicate that the high order modes do not contribute significantly to the displacement response but do contribute significantly to the force response for the case of uniform-support excitation. For the case

multiple-support excitation, considerable attenuation of the force response can be achieved by only controlling the first order modes. Controlling higher order modes can reduce the force response, but not very significantly. In regard to full state feedback versus output feedback using a Kalman filter, a comparison between the displacement and force response of the model is presented implementing full state feedback and output feedback control. The same control effort is exerted for output feedback control as for state feedback control. As expected, full state feedback control outperforms output feedback control in all cases, but output feedback control does perform reasonably well. Output feedback control with sensor noise usually achieves approximately 90-97% of the force response attenuations obtained when full state feedback control without sensor noise is considered.

2.2 Structural Control Algorithms

There are 6 main categories of control algorithms that are applicable to structural systems. Each will be briefly described herein. However, as pointed out by Housner et al. [33], research and development in the field of control algorithms that are applicable to structural systems is still in its infancy. There is still no answer to the simple question:

> "... How does one design a controller to limit the peak stress (or displacements) in the presence of an arbitrary earthquake motion of strength X?..." [33]

Optimal Control. Optimal control implies the "best" design. However, this is somewhat misleading because every stabilizing controller is optimal by some criterion. Optimal is good only if the function being minimized is truly meaningful for the system. Housner et al. [33] that this is usually not the case. Indeed, in most cases, quadratic functions of the shown in equation 1.7 usually do not have

any physical significance but are used to weight two items that each have physical significance. Bang-bang control falls into the area of optimal control. Other types of optimal control are: Input Constraint Control (ICC) and Output Constraint Control (OCC) which are discussed by Zhu et al. [101], Linear Quadratic Regulator (LQR) control which is discussed by Belanger [10], and Linear Quadratic Gaussian (LQG) control which is discussed by Spencer et al. [76].

Stochastic Control. The application of stochastic control principles to civil engineering structures is rather a natural given the acceptance of uncertainty of modeling and reliability methods in design. According to Housner et al. [33], stochastic control addresses the following characteristics that are inherent to structures. Modeling – there is uncertainty in both the inherent nature of the structure as well as in the forces that it see. Second, there is measurement – the structures are not completely observable from sensors located at a single point; the sensors are also contaminated with noise. In the most general sense, stochastic control assumes that the disturbances and measurement noise, and even perhaps the parameter variations are random processes, the system response will therefore also be a random process. According to Stengel [78], the application of stochastic control to general nonlinear systems is difficult and limited. The application of stochastic control is mainly limited to LQG control and its frequency domain analog, H_2 control. When used with LQG control and H_2 control, stochastic methods are mainly beneficial in the areas of state estimation, covariance control, and robustness assessment. State estimation using noisy acceleration measurements has been examined by Dyke et al. [23]. Probabilistic stability robustness has been examined by Field et al. [29], and Spencer et al. [74].

Adaptive Control. An adaptive controller is one with adjustable parameters, incorporating a mechanism for adjusting these parameters. Adaptive control methods

generally are divided into: (1) direct; and (2) indirect methods. According to Housner et al. [33], in the direct methods, the controller parameters are adjusted directly based on the error between the measured and desired outputs. In the indirect methods, the parameters of a model for the unknown plant are estimated online, and the controller parameters are calculated as the solution of an underlying controller design problem based on the estimated plant parameters. The direct model reference adaptive control (MRAC) method presented by Kaufman et al. [38] has several properties that are attractive to our problem area and has been successfully applied to structural control problems.

Sliding Mode Control. For sliding mode control, a hypersurface, called the sliding surface, is defined in state space. Housner et al. [33] state that the error between actual and desired response is zero when the state falls on the sliding surface. Initially, controls are applied such that a arbitrary initial state will be brought to the sliding surface. Different controls are applied while the state is in different regions of the state space. Once on the the sliding surface, the system is said to be in the sliding mode, and controls are applied to keep the system in the sliding mode toward the equilibrium point. Yang et al. [96] presented experimental results of controlling a three-story building on a shaker table using sliding mode control.

Robust Control. Robust control focuses on the issues of performance and stability in the presence of uncertainty, both in parameters of the system and inputs to which it is subjected. According to Housner et al. [33], the development of robust control theory was motivated by the inability of the LQG or H_2 theories to directly accommodate plant uncertainties. The need to address uncertainty in a systematic way led to the development of the H_∞ problem. The interested reader is referred to Zhou et al. [100] for a description of the H_∞ problem. H_∞ control has been applied to a number of civil engineering structures. For example, Spencer et al. [75]

summarized a detailed comparison between H_2 and H_∞ control done by Suhardjo [79].

Intelligent Control. Intelligent control uses techniques from the fields of artificial intelligence, operations research, and automatic control to sense, reason, plan, and act in an "intelligent" manner. Housner et al. [33] state that conventional control techniques do not have the capabilities of intelligent control in dealing with qualitative, uncertain, and incomplete information. Two main technologies related to intelligent control have been developed: (1) artificial neural networks, and (2) fuzzy logic. Artificial neural networks were developed as a methodology for emulating the biology of the human brain, resulting in systems that learn by experience. Fuzzy logic is a means of processing imprecise and vague information. Fuzzy logic uses imprecise data to reason and derive control actions. Casciati and Yao [15] give an overview of fuzzy and neural techniques for the control of structures.

2.3 State of the Art of Actuator Technology

2.3.1 Background

Civil engineering structures generally require large control forces, on the order of a meganewton, and for seismic excitations, response times on the order of milliseconds. Moreover, the requirement for force coupled with the constraint on energy demand is very difficult to achieve [21]. There are hydraulic, electromechanical, and electromagnetic devices capable of delivering such a large force, but they also have a high energy demand. Considerable research is underway to develop new, large, controllable force capacity actuators that have a low energy demand. Semiactive control devices have a lot of promise in addressing this actuator technology challenge. Semiactive control devices offer the versatility and adaptability of active

control devices without requiring the large power sources. In fact, many semiactive control devices operate on battery power, which is critical during ground excitations when the power source to the structure may fail. Spencer and Sain [69] note that when implemented appropriately semiactive damping systems perform significantly better than passive devices and have the potential to achieve, or even surpass, the performance of fully active systems. Thus, semiactive control devices offer the possibility of effective response reduction during a wide array of ground excitations. In this section, we review both active, and semiactive, including material-based actuators, that are applicable to controlling civil engineering structures. A summary of the characteristics of the actuators that we review is shown in Table 2.1.

2.3.2 Active Control System Actuators

An active control system is one in which an external source powers control actuator(s) that apply forces to the structure in a prescribed manner. These forces can be used to both add and dissipate energy in the structure. Since an active control system can add mechanical energy to the structure, this type of system has the possibility of destabilizing the structure. The energy stability theorem of bounded energy input results in bounded energy output is violated. Examples of active control system actuators fall into the categories of hydraulic, electromechanical, and electromagnetic devices.

Hydraulic Actuators. Hydraulic mechanisms force fluid in or out of a cylinder through an orifice to maintain a certain pressure on the face of a piston head. Precise control movement and force can be achieved with a suitable control system. Dorey and Moore [22] points out that hydraulic mechanisms can produce forces on the order of meganewtons. However, the disadvantages of hydraulic mechanisms are the requirements for fluid storage system, complex valves and pumps are required to

regulate the fluid flow and pressure, and that seals require continuous maintenance.

Electromechanical Actuators. Electromechanical actuators generate force by moving a piston with a gear mechanism that is driven by an electric motor. The force is controlled by adjusting the power input to the motor. Response time is high, on the order of tenths of seconds. Electric actuators rated for 600 kN of force are commercial available. There are several manufacturers of linear electromechanical actuators. One such manufacturer is Raco (www.raco.de). Connor [21] notes that because electromechanical actuators are composed of many parts that are in contact with each other, there is a high risk of breakdown.

2.3.3 Semiactive Control System Actuators

Semiactive control mechanisms have a low ratio of energy demand to force output, and according to presently accepted definitions, a semiactive control device is one that cannot inject mechanical energy into the controlled structural system, i.e., semiactive devices act as energy dissipating mechanisms according to Spencer and Sain [69]. Thus, unlike active control mechanisms, semiactive control mechanisms do not have the potential to destabilize the structural system in a bounded input/bounded output sense. Examples of semiactive control system actuators fall into the categories of adaptive configuration-based actuators and controllable fluid-based actuators. Adaptive configuration-based actuators have the characteristic of being able to generate a large force by changing their physical makeup while controllable fluid-based actuators contain a fluid that is characterized by it's ability to change to a semisolid in milliseconds. Examples of adaptive configuration-based actuators include variable orifice dampers, variable stiffness devices, piezoelectric actuators, and smart tuned mass dampers (STMDs). Examples of controllable fluid-based actuators include electroheological (ER) and magnetorheological (MR) based

actuators.

Electromagnetic Actuators. Electromagnetic force mechanisms are based on the interaction between the magnetic field generated by the stationary field magnet and the current in the driving coil. A driving coil is attached to the piston, which translates with respect to the housing. Since electromagnetic actuators are driven by magnetic forces, they do not require mechanical contact and are therefore theoretically more reliable than hydraulic or electromechanical actuators. According to Connor [21], electromagnetic actuators with a force capacity up to several kilonewtons are commercially available and the force response time is on the order of milliseconds. Research and development of larger capacity actuators is currently underway. Connor [21] also points out that Chaniotakis et al. at the Massachusetts Institute of Technology is currently developing a large-scale electromagnetic actuator that may have full-scale applications. Disadvantages of electromagnetic actuator technology is a commercially available product in the meganewton range is still in the research and development phase and probably the voltage and current requirements for such a actuator can not be satisfied with conventional electrical power supply technology.

Variable Orifice Dampers. Variable orifice dampers use a control valve to alter the resistance to flow of a conventional hydraulic fluid damper. The valve opening adjusts according to force demand that is determined by a feedback control algorithm. Since the valve motion is perpendicular to the flow, the force required to adjust the valve position is small and energy demand is low (usually on the order of 30-50 watts) according to Connor [21] and Spencer and Nagarajaiah [68]. Variable orifice dampers were implemented by Kurata et al. [43] in a large-scale, three-story frame structure and Sack and Patten [60] and Patten et al. [54] developed a variable orifice damper and Patten et al. [55] installed a hydraulic actuator with a

controllable orifice on a bridge in Oklahoma.

Variable Stiffness Devices. Kobori et al. [42] conceived of using a full-scale variable orifice damper in on-off mode – a high stiffness device due to the lack of compressibility of hydraulic fluid when the valve is closed or a device with no stiffness when the valve is open – as a semiactive variable stiffness system. However, this system was not able to vary stiffness continuously from one state to another. However, according to Spencer and Nagarajaiah [68], Nagarajaiah has developed a semiactive variable-stiffness device (SAIVS) (U.S. Patient No. 6,098,969). Nagarajaiah and Mate [50] has shown in a scaled structural model that SAIVS can effectively smoothly vary the stiffness of a structure and produce a nonresonant system.

Piezoelectric Actuators. Piezoelectric actuators are fabricated with piezoceramic block-type elements or piezopolymer films. When a voltage is applied, these piezoceramic/piezopolymer materials extend or contract. When these materials are attached to a surface which restrains their motion and a voltage is applied, contact forces between the object and the restraining medium are produced. Two configurations are available. According to Connor [21], one configuration produced by Kinetic Ceramics, Inc. (www.kineticceramics.com) used piezoceramic wafers stacked vertically and produces a maximum force of 20 kN with a response time of several milliseconds. A second configuration produced by Active Control Experts (www.acx.com) uses piezoceramic wafers distributed over an area in a regular pattern produces a maximum force of 500 N at 200 volts with millisecond response.

Smart Tuned Mass Dampers (STMDs) Conventional tuned mass dampers (TMDs) are not adaptable due to their fixed design. An alternative is the STMD that continuously retunes its frequency due to real time control thus making it robust to changes in building stiffness and damping. Nagarajaiah and Varadarajan

[51] have shown the effectiveness of the SAIVS device to act as an integral part of the STMD system by controlling a small-scale three story structural model. Varadarajan and Nagarajaiah [88] studied the response control of an analytical model of a 76-story concrete office tower. The SAIVS device was part of a 500 ton STMD system that was demonstrated to substantially reduce the building when compared to a TMD system and reduce a similar response to a active mass damper system (AMD) system based on a LQG controller, but with a magnitude less power consumption. comparable to active tuned mass dampers, but with a order of magnitude less power consumption. STMD systems have also been proposed based on controllable tuned sloshing dampers (CTSDs). Tuned sloshing dampers (TSDs) use the liquid sloshing in a tank to add damping to the structure. Lou et al. [45] has proposed a semiactive CTSD device in which the length of the sloshing tank is altered to change the properties of the device.

Electrorheological (ER) and Magnetorheological (MR) Based Actuators. The common characteristic of both ER and MR fluids is their ability to change from free-flowing (in this state the fluid may be modeled as Newtonian) to a semisolid with a controllable yield strength in milliseconds. However, only MR fluids have been shown to be tractable for civil engineering applications according to Spencer and Sain [69]. MR fluids typically consist of micronsized, magnetically polarizable particles dispersed in a carrier medium such as mineral or silicone oil, and Spencer and Nagarajaiah [68] that MR fluid actuators have been shown to be readily controlled with low power (e.g. less than 50 W), low voltage (e.g. $\sim$12-24 V), and a power supply only outputting $\sim$ 1-2 A. Simulations and laboratory model experiments have shown that MR significantly outperform comparable passive damping configurations and requires only a fraction of the input power needed by active controllers (Spencer and Sain [69], Spencer et al. [72], Spencer [67], Dyke et al. [25, 26], Xu et al. [95], Ramallo et al. [57], Madden et al. [46], and Yoshioka et al. [99]).

Carlson and Spencer [14] and Spencer et al. [77] have studied a 200-kN capacity MR damper which may be used for full-scale applications. Figure 2.2 [68] shows the measured force-displacement loops for this damper.

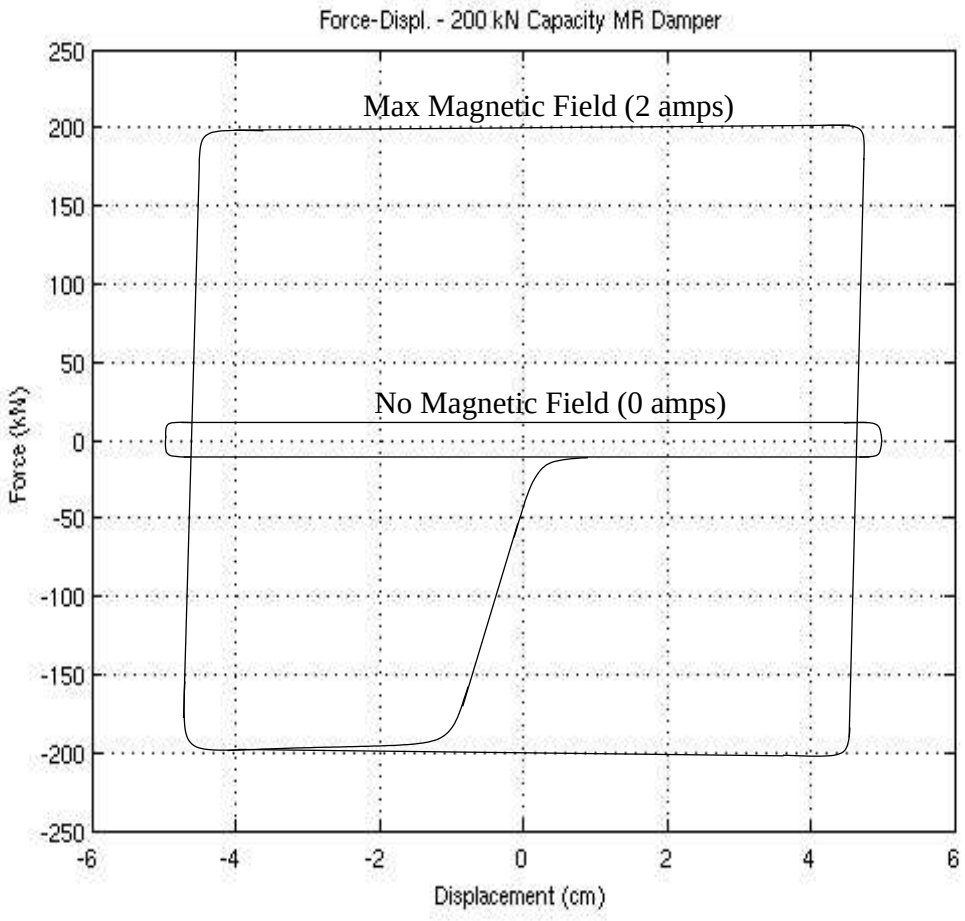

Figure 2.2: Hysteresis for 200-kN MR Damper [68]

Actuator Type	**Peak Force**	**Response Time**	**Watts/Volts/Amps Required**
Hydraulic	meganewtons	∼10-100 ms	high
Electromechanical	∼600 kNs	tenths of secs	high
Electromagnetic	several kNs	milliseconds	low
Variable Orifice Dampers	∼10-30 kNs	milliseconds	∼50W
Variable Stiffness Damper	∼8-10 kNs +	milliseconds	low
Piezoelectric Actuators	∼20 kNs	milliseconds	∼1000 V
Smart TMDs	∼25 kNs +	milliseconds	low
MR Actuators	∼200 kNs +	milliseconds	∼50W ∼12-24 V ∼1-2 A

Table 2.1: Summary of Characteristics of Active/Semiactive Control System Actuators

2.4 Full Scale Applications of Structural Control

The first full-scale application of active control was completed in 1989 at the Kyobahi Seiwa building in Tokyo, Japan. The control system consisted of two active mass dampers (AMDs); a pictorial representation of an AMD control system is in Figure 2.3. Since then, over 40 buildings and 10 bridges (during erection) have employed feedback control strategies in full-scale implementations. Full-scale building implementations are shown in table 2.2. For a list of full-scale bridge implementations with structural control, the interested reader is referred to Spencer and Nagarajaiah [68]. With the exception of one experimental system installed on a bridge in Oklahoma, none of these full-scale active control installations are located in the United States. According to Spencer and Nagarajaiah [68], there are many possible reasons for this disparity. For instance, the civil engineering profession and construction industry in the United States are conservative, and the absence of verified and consensus-approved analysis, design, and testing procedures represents addition impediments to the application of structural control technology.

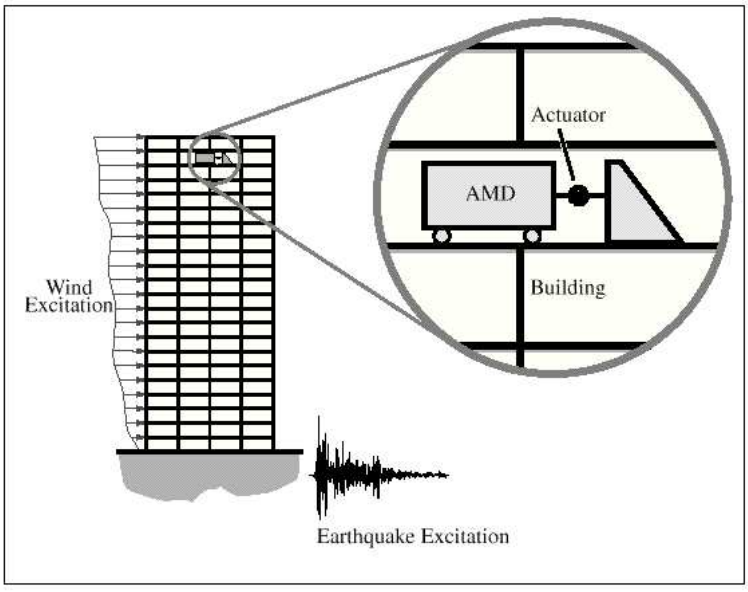

Figure 2.3: Concept of the AMD Control System [73]

Full-scale application of hybrid control systems, in particular hybrid mass dampers (HMD), are the most common control device implemented. The popularity of hybrid control stems from their ability address many of the challenges particular to structural control. These challenges include: (i) reduction of capital cost and maintenance, (ii) eliminating reliance on external power, (iii) increasing system reliability and robustness, and (iv) gaining acceptance of nontraditional technology [68]. Because multiple control devices are operating, hybrid control systems can alleviate some of the limitations and restrictions that exist when each system is acting alone. The resulting hybrid control system can be more reliable than a fully active system because should a failure occur with the active system, protection from the passive system is still in place. For these reasons, the majority of structural control research has been concentrated in the area of hybrid control.

Table 2.2: Summary of Controlled Buildings/Towers [68]

Full-Scale Structure (Year Completed)	**Location**	**Scale of Building**	**Control System Employed**	**AMD/HMD**		**Actuation Mechanism**
				No.	**Mass (tons)**	
Kyobashi Seiwa (1989)	Tokyo, Japan	33m, 400 ton, 11 stories	AMD	2	5	hydraulic
Kajima Research Institute KaTRI No. 21 Bldg. (1990)	Tokyo, Japan	12m, 400 ton, 3 stories	Active Variable Stiffness System (6 devices)	-	-	hydraulic
Sendagays INTES (1992)	Tokyo, Japan	58m, 3,280 ton 11 stories	AMD	2	72	hydraulic
Applause Tower (1992)	Osaka, Japan	161m, 13,943 tons 34 stories	HMD	1	480	hydraulic
Kansai Int. Airport Control Tower (1992)	Osaka, Japan	161m, 2,570 tons 7 stories	HMD	2	10	servo motor
Osaka Resort City 2000 (1992)	Osaka, Japan	200m, 56,980 tons 50 stories	HMD	2	200	servo motor
Yokohama Land Mark Tower (1993)	Yokohama, Japan	296m, 260,610 tons 70 stories	HMD	2	340	servo motor
Long Term Credit Bank (1993)	Toyko, Japan	129m, 40,000 tons 21 stories	HMD	1	195	hydraulic
Ando Nishikicho (1993)	Tokyo, Japan	54m, 2,600 tons 14 stories	HMD (DUOX)	1	22	servo motor
Hotel Nikko Kanazawa (1994)	Kanazawa, Japan	131m, 27,000 tons 29 stories	HMD	2	100	hydraulic
Hiroshima Riehga Royal Hotel (1994)	Hiroshima, Japan	150m, 83,000 tons 35 stories	HMD	1	80	servo motor
Shinjuku Park Tower (1994)	Toyko, Japan	227m, 130,000 tons 52 stories	HMD	3	330	servo motor

continued on next page

Table2.2 – continued

Full-Scale Structure (Year Completed)	Location	Scale of Building	Control System Employed	AMD/HMD No.	AMD/HMD Mass tons	Actuation Mechanism
MHI Yokohama Building (1994)	Yokohama, Japan	152m, 61,800 tons 34 stories	HMD	1	60	servo motor
Hamamatsu ACT Tower (1994)	Hamamatsu, Japan	212m, 107,500 tons 46 stories	HMD	2	180	servo motor
Riverside Sumida (1994)	Tokyo, Japan	134m, 52,000 tons 33 stories	AMD	2	30	servo motor
Hikarigaoka J-City (1994)	Tokyo, Japan	110m, 29,300 tons 26 stories	HMD	2	44	servo motor
Miyazaki Phoenix Hotel Ocean 45 (1994)	Tokyo, Japan	154m, 83,650 tons 43 stories	HMD	2	240	servo motor
Osaka WTC Bldg. (1994)	Osaka, Japan	252m, 80,000 tons 52 stories	HMD	2	100	servo motor
Dowa Kasai Phoenix Tower (1995)	Osaka, Japan	145m, 26,000 tons 28 stories	HMD (DUOX)	2	84	servo motor
Rinku Gate Tower North Building (1995)	Osaka, Japan	255m, 75,000 tons 56 stories	HMD	2	160	servo motor
Hirobe Miyake Building (1995)	Tokyo, Japan	31m, 273 tons 9 stories	HMD	1	2.1	servo motor
Plaza Ichihara (1995)	Chiba, Japan	61m, 5,760 tons 12 stories	HMD	2	14	servo motor
Kaikyo Dream Tower (1996)	Yamaguchi, Japan	190m, 5,400 tons	HMD	1	10	servo motor
Herbis Osaka (1997)	Osaka, Japan	153m, 62,450 tons 40 stories	HMD	2	320	hydraulic
TC Tower (1997)	Kao Hsung, Taiwan	85 stories	HMD	2	350	servo motor

continued on next page

Table2.2 – continued

Full-Scale Structure (Year Completed)	Location	Scale of Building	Control System Employed	AMD/HMD No.	AMD/HMD Mass tons	Actuation Mechanism
Itoyama Tower (1997)	Tokyo, Japan	89m, 9,025 tons 18 stories	HMD	1	48	servo motor
Bunka Gakuen (1998)	Tokyo, Japan	93m, 43,488 tons 20 stories	HMD	2	48	servo motor
Daiichi Hotel (1998)	Ohita, Japan	101m, 20,942 tons 21 stories	HMD	2	50	hydraulic
Odakyu Southern Tower (1998)	Tokyo, Japan	150m, 50,000 tons 36 stories	HMD	2	60	linear motor
Otis Shibayama Tower (1998)	Chiba, Japan	154m, 6,877 tons 39 stories	HMD	1	61	hydraulic
Yokohama Sheraton (1998)	Yokohama, Japan	115m, 33,000 tons 27 stories	HMD	2	122	servo motor
Kajima Shizuoka (1998)	Shizuoka, Japan	20m, 1,100 tons 5 stories	semiactive	-	-	variable-orifice
Century Park Tower (1999)	Tokyo, Japan	170m, 124,540 tons 54 stories	HMD	4	440	servo motor
Laxa Osaka (1999)	Nagoya, Japan	115m, 33,000 tons 27 stories	semiactive TMD	2	330 hydraulic damper	variable-orifice
Nanjing Tower (1999)	Nanjing, China	310m	AMD	1	60	hydraulic
Shin-Jei Bldg. (1999)	Taipei, Taiwan	99m, 22 stories	AMD	3	120	servo motor
Shinagawa Intercity (1999)	Tokyo, Japan	144m, 50,000 tons, 22 stories	HMD	2	150	servo motor
Incheon Airport Control Tower (2000)	Incheon, Korea	100m	HMD	2	12	servo motor hydraulic

continued on next page

Table2.2 – continued

Full-Scale Structure (Year Completed)	**Location**	**Scale of Building**	**Control System Employed**	**AMD/HMD**		**Actuation Mechanism**
				No.	**Mass tons**	
Keio Univ. Engr. Bldg. (2000)	Tokyo, Japan	29m, 25,460 tons, 9 stories	smart base isolation	-	-	variable-orifice damper
Osaka Airport Control Tower (2001)	Osaka, Japan	69m, 3,600 tons, 5 stories	HMD	2	10	servo motor
Dentsu Office Bldg. (2002)	Tokyo, Japan	210m, 130,000 tons, 48 stories	HMD	2	440	servo motor
Hotel Nikko Osaka (2002)	Osaka, Japan	138m, 37,000 tons, 33 stories	HMD	2	124	servo motor

Chapter 3

Symbolic Analysis

In this chapter, we establish a theoretical foundation for the symbolic representation and sensitivity analysis of bang-bang control strategies tailored toward the nonlinear behavior and design of base-isolated structures. We note that a key shortcoming in using numerical analysis packages to solve the Lyapunov equation for matrix $\mathbf{S}$, followed by the computation of $\mathbf{B^T S}z(t)$, is that any potential insight into the appropriate cause-and-effect relationships is buried inside the numerical procedure. To mitigate this shortcoming, in this chapter we explore the extent to which symbolic analysis procedures can provide insight into the connection between an appropriate selection of $\mathbf{Q}$ and the active control strategy that follows through $\mathbf{B^T S}z(t)$.

3.1 Research Avenue 1. Symbolic Analysis of Single-Degree-of-Freedom Systems

In this section, we use Mathematica© to compute a symbolic solution to coefficients in $\mathbf{B^T S}$ for a one degree of freedom system. We then investigate the circumstances under which the bang-bang control force will change sign, and prove that under a damped steady state system response, the bang-bang control is neither perfectly in phase with the displacements nor velocities.

3.1.1 Symbolic Representation for 1-DOF Bang-Bang Control Strategy

Consider a 1-DOF system with stiffness, k, mass, m, and damping, c= $\alpha \cdot m + \beta \cdot k$. Assume that the 1-DOF system has an actuator acting on the DOF. For the following general choice of $\mathbf{Q}$,

$$\mathbf{Q} = \begin{bmatrix} k^\star & 0 \\ 0 & 0 \end{bmatrix}, \tag{3.1}$$

where $k^\star$ is a real, positive number, the symbolic representation for the $\mathbf{B^T S}$ matrix product, as determined by Mathematica© is as follows:

$$\mathbf{B^T S} = \begin{bmatrix} 0 & \frac{1}{m} \end{bmatrix} \begin{bmatrix} \frac{mk^\star}{2(\alpha \cdot m + \beta \cdot k)} + \frac{(\alpha \cdot m + \beta \cdot k)k^\star}{2k} & \frac{mk^\star}{2k} \\ \frac{mk^\star}{2k} & \frac{m^2 k^\star}{2k(\alpha \cdot m + \beta \cdot k)} \end{bmatrix} = \begin{bmatrix} \frac{k^\star}{2k} & \frac{mk^\star}{2k(\alpha \cdot m + \beta \cdot k)} \end{bmatrix}. \tag{3.2}$$

When the terms in $\mathbf{Q}$ are selected to minimize potential energy in the 1-DOF system (i.e., $k^\star = k$), equation 3.2 simplifies to:

$$\mathbf{B^T S} = \begin{bmatrix} 0 & \frac{1}{m} \end{bmatrix} \begin{bmatrix} \frac{mk}{2(\alpha \cdot m + \beta \cdot k)} + \frac{\alpha \cdot m + \beta \cdot k}{2} & \frac{m}{2} \\ \frac{m}{2} & \frac{m^2}{2(\alpha \cdot m + \beta \cdot k)} \end{bmatrix} = \begin{bmatrix} \frac{1}{2} & \frac{m}{2(\alpha \cdot m + \beta \cdot k)} \end{bmatrix}. \tag{3.3}$$

Similarly, when

$$\mathbf{Q} = \begin{bmatrix} 0 & 0 \\ 0 & m^\star \end{bmatrix}, \tag{3.4}$$

where $m^\star$ is a real, positive number, the $\mathbf{B^T S}$ matrix product was calculated symbolically using Mathematica© as:

$$\mathbf{B^T S} = \begin{bmatrix} 0 & \frac{1}{m} \end{bmatrix} \begin{bmatrix} \frac{m^\star k}{2(\alpha \cdot m + \beta \cdot k)} & 0 \\ 0 & \frac{m m^\star}{2(\alpha \cdot m + \beta \cdot k)} \end{bmatrix} = \begin{bmatrix} 0 & \frac{m^\star}{2(\alpha \cdot m + \beta \cdot k)} \end{bmatrix}. \tag{3.5}$$

If the kinetic energy, $T(\dot{x}(t))$, in this 1-DOF system is minimized, i.e., $m^{\star} = m$, equation 3.5 becomes:

$$\mathbf{B^T S} = \begin{bmatrix} 0 & \frac{1}{m} \end{bmatrix} \begin{bmatrix} \frac{mk}{2(\alpha \cdot m + \beta \cdot k)} & 0 \\ 0 & \frac{m^2}{2(\alpha \cdot m + \beta \cdot k)} \end{bmatrix} = \begin{bmatrix} 0 & \frac{m}{2(\alpha \cdot m + \beta \cdot k)} \end{bmatrix}. \tag{3.6}$$

Due to the linear properties of the Lyapunov matrix equation, the $\mathbf{B^T S}$ matrix product that minimizes the total (potential + kinetic) energy of this 1-DOF system is the sum of equations 3.3 and 3.6.

3.1.2 Effectiveness of Bang-Bang Control in a 1-DOF System

In this section we investigate the effectiveness of bang-bang control in the situation of a linearly elastic 1-DOF system subject to a simplified ground motion. Initially, we assume: (1) the ground motion can be modeled as a periodic forcing function, and (2) steady state system response. Then in part two, we look at the effectiveness of bang-bang control when the 1-DOF system is in transient free vibration. We prove that the actuator works neither perfectly in phase with displacements nor perfectly in phase with velocities.

Note that when the variable β is used in the context of damping, it represents the stiffness coefficient in the linear viscous damping model otherwise, β represents the ratio of the applied loading frequency to the natural free vibration frequency.

Steady State Response

Let us assume that the forcing function due to ground accelerations is:

$$p(g,t) = A\sin(gt) \tag{3.7}$$

where "g" matches the "most dominant" natural circular frequency for ground shaking. If $\beta = (g/w)$ then the steady-state displacement and velocity are [17]:

$$x(t) = \left[\frac{A}{k}\right] \cdot \left[\frac{(1-\beta^2)\sin(gt) - 2\xi\beta\cos(gt)}{(1-\beta^2)^2 + (2\xi\beta)^2}\right] \tag{3.8}$$

and

$$\dot{x}(t) = \left[\frac{Ag}{k}\right] \cdot \left[\frac{(1-\beta^2)\cos(gt) + 2\xi\beta\sin(gt)}{(1-\beta^2)^2 + (2\xi\beta)^2}\right] \tag{3.9}$$

Amplitude of Response. From the trigonometric identity,

$$\sin(gt+\phi) = \sin(gt)\cdot\cos(\phi) + \cos(gt)\cdot\sin(\phi) \tag{3.10}$$

it follows that equation 3.8 can be written,

$$x(t) = \left[\frac{A}{k}\right] \cdot \left[\frac{1}{(1-\beta^2)^2 + (2\xi\beta)^2}\right] \cdot \sin(gt+\phi) \tag{3.11}$$

where

$$\tan(\phi) = \left[\frac{-2\xi\beta}{(1-\beta^2)}\right]. \tag{3.12}$$

The amplitude of the displacement vector is:

$$\|x(t)\| = \left[\frac{A}{k}\right] \cdot \left[\frac{1}{(1-\beta^2)^2 + (2\xi\beta)^2}\right]. \tag{3.13}$$

Similarly, the amplitude of the velocity vector is:

$$\|\dot{x}(t)\| = \left[\frac{Ag}{k}\right] \cdot \left[\frac{1}{(1-\beta^2)^2 + (2\xi\beta)^2}\right]. \tag{3.14}$$

Bang-Bang Control Strategy. When the terms in **Q** are selected to minimize potential energy in the 1-DOF system (i.e., $k^\star = k$), the matrix product $B^T S$ simplifies to:

$$\mathbf{B^T S} = \begin{bmatrix} 0 & \frac{1}{m} \end{bmatrix} \begin{bmatrix} \frac{mk}{2(\alpha \cdot m + \beta \cdot k)} + \frac{\alpha \cdot m + \beta \cdot k}{2} & \frac{m}{2} \\ \frac{m}{2} & \frac{m^2}{2(\alpha \cdot m + \beta \cdot k)} \end{bmatrix} = \begin{bmatrix} \frac{1}{2} & \frac{m}{2(\alpha \cdot m + \beta \cdot k)} \end{bmatrix}. \quad (3.15)$$

Substituting equations 3.8 and 3.9 into $\mathbf{Z}(t) = [x(t), \dot{x}(t)]^T$ and pre-multiplying by equation 3.15 gives:

$$\mathbf{B^T S Z} = \left[\frac{A}{2k}\right] \cdot \left[\frac{(1-\beta^2)\sin(gt) - 2\xi\beta\cos(gt) + \frac{mg}{c}(1-\beta^2)\cos(gt) + \frac{2mg}{c}\xi\beta\sin(gt)}{(1-\beta^2)^2 + (2\xi\beta)^2}\right] \quad (3.16)$$

Amplitude of Displacement and Velocity Contributions. The amplitude of displacement and velocity terms in equation 3.16 is:

$$\| \quad \text{displacement component}(t) \quad \| = \left[\frac{A}{2k}\right] \cdot \left[\frac{1}{(1-\beta^2)^2 + (2\xi\beta)^2}\right] \quad (3.17)$$

and

$$\| \quad \text{velocity component}(t) \quad \| = \left[\frac{Amg}{2ck}\right] \cdot \left[\frac{1}{(1-\beta^2)^2 + (2\xi\beta)^2}\right]. \quad (3.18)$$

Notice that as $c \to 0$, the velocity component amplitude increases in size relative to the amplitude of the displacement term.

Strategy for Switching Direction of the Actuator Force. From the viewpoint of bang-bang control, we want to know in which direction the actuator will push as a function of the displacement/velocity state variables, and how the strategy varies

as a function of the problem parameters. The actuator will switch directions in the force application when:

$$(1-\beta^2)\sin(gt) - 2\xi\beta\cos(gt) + \frac{mg}{c}(1-\beta^2)\cos(gt) + \frac{2mg}{c}\xi\beta\sin(gt) = 0. \quad (3.19)$$

Collecting and rearranging common terms:

$$\left[(1-\beta^2) + \frac{2mg}{c}\xi\beta\right]\sin(gt) = \left[2\xi\beta - \frac{mg}{c}(1-\beta^2)\right]\cos(gt) \quad (3.20)$$

gives:

$$\tan(gt) = \left[\frac{\left[2\xi\beta - \frac{mg}{c}(1-\beta^2)\right]}{\left[(1-\beta^2) + \frac{2mg}{c}\xi\beta\right]}\right] \quad (3.21)$$

Now recall that $\xi = c/2mw$ and $\beta = g/w$. The expression,

$$\frac{2mg}{c}\xi\beta \qquad \text{simplifies to...} \qquad \beta^2, \quad (3.22)$$

and

$$\frac{mg}{c}(1-\beta^2) \qquad \text{can be re-written as...} \qquad \frac{\beta}{2\xi}\cdot(1-\beta^2). \quad (3.23)$$

Hence, equation 3.21 simplifies to:

$$\tan(gt) = \left[2\xi\beta - \frac{\beta}{2\xi}\cdot(1-\beta^2)\right] \quad (3.24)$$

Case 1. The actuator works perfectly in phase with displacements when a change in actuator force and displacements occurs at the same time. From equation 3.8, x(t) = 0 when:

$$(1-\beta^2)\sin(gt) - 2\xi\beta\cos(gt) = 0. \tag{3.25}$$

i.e.,

$$\tan(gt) = \left[\frac{2\xi\beta}{(1-\beta^2)}\right] \tag{3.26}$$

Case 2. The actuator works perfectly in phase with velocities – i.e., to oppose the direction of motion – when $\dot{x}(\mathrm{t}) = 0$. i.e.,

$$(1-\beta^2)\cos(gt) + 2\xi\beta\sin(gt) = 0. \tag{3.27}$$

i.e.,

$$\tan(gt) = \left[\frac{(\beta^2-1)}{2\xi\beta}\right] \tag{3.28}$$

Theorem 1. For values of $\beta \neq 0$, the actuator works neither perfectly in phase with displacements nor perfectly in phase with velocities.

Proof. From equations 3.24 and 3.26 it is evident that in order for the actuator to work perfectly in phase with displacements we require:

$$\frac{2\xi\beta}{(1-\beta^2)} = \left[2\xi\beta - \frac{\beta}{2\xi}\cdot(1-\beta^2)\right] \tag{3.29}$$

The trivial ... and not very useful ... solution is $\beta = 0$. Rearranging the remaining terms gives,

$$\xi^2 = \left[\frac{-(1-\beta^2)^2}{4\beta^2}\right]. \tag{3.30}$$

Physical considerations dictate that ξ must be greater than zero (i.e., we want the

bang-bang control strategy and damping in the physical system to be well defined). From equation 3.30 it is evident, however, that no value of β exists for which this will occur. The left- and right-hand sides of equation 3.30 will be closest in value when $\beta = 1$ and $\gamma \approx 0$ (i.e., a very lightly damped system is forced near its resonance frequency).

Similarly, in order for the actuator to work perfectly in phase with velocities we require:

$$\frac{(\beta^2 - 1)}{2\xi\beta} = \left[2\xi\beta - \frac{\beta}{2\xi} \cdot (1 - \beta^2)\right] \tag{3.31}$$

Rearranging terms gives,

$$\xi^2 = \left[\frac{(\beta^2 - 1)(1 - \beta^2)}{4\beta^2}\right] = \left[\frac{-(1 - \beta^2)^2}{4\beta^2}\right]. \tag{3.32}$$

There are no values of β, including $\beta = 0$, which will make make the right-hand side of equation 3.32 positive.

Plots of Phase Shift vs Beta

Figures 3.1 through 3.3 show the phase shift in displacements, velocities and actuator force change as a function of β for contours of damping, $\xi = 0.01$, $\xi = 0.05$ and $\xi = 0.09$, respectively. Notice that the contours of displacement and velocity phase shift are separated by $\pi/2$ radians. Moreover, as predicted by the theorem, phase shift for the bang-bang control is synchronized with displacement phase shift at only two points – $\beta = 0$ and 1. What the mathematics doesn't show is that bang-bang control is "almost in phase" with velocities for β values covering the interval 0.8 through 1.2.

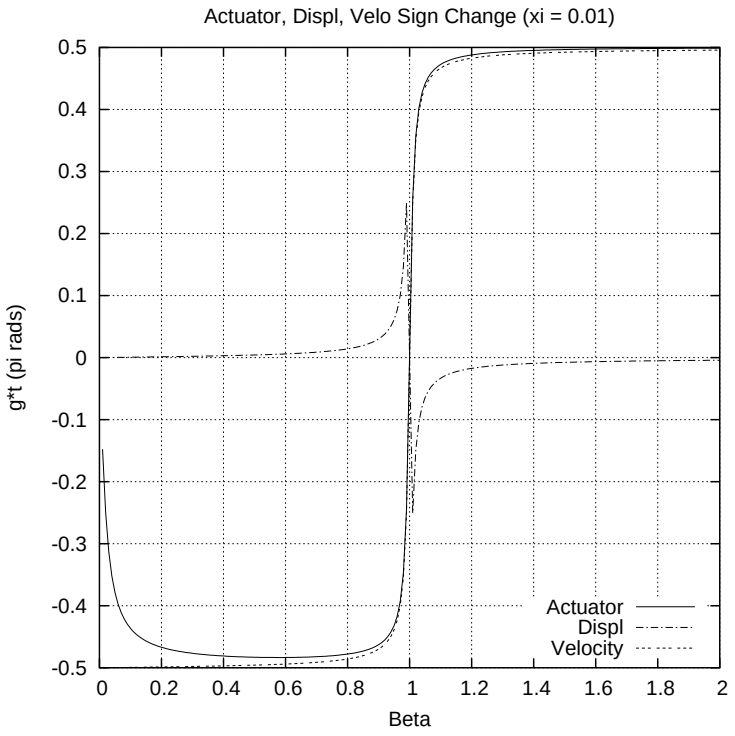

Figure 3.1: Actuator, Displacement, and Velocity Sign Change ($\xi = 0.01$)

Free Vibration Response

Now let us assume that the ground acceleration ceases and the structure enters a free vibration response,

$$x(t) = e^{-\xi w_o t} \left[A \cos(w_d t) + B \sin(w_d t) \right] \tag{3.33}$$

with initial displacement and velocity $x(0)$ and $\dot{x}(0)$, respectively. The time history of displacement and velocity are,

$$x(t) = e^{-\xi w_o t} \left[x(0) \cos(w_d t) + \frac{\dot{x}(0) + x(0)\xi w_o}{w_d} \sin(w_d t) \right] \tag{3.34}$$

and

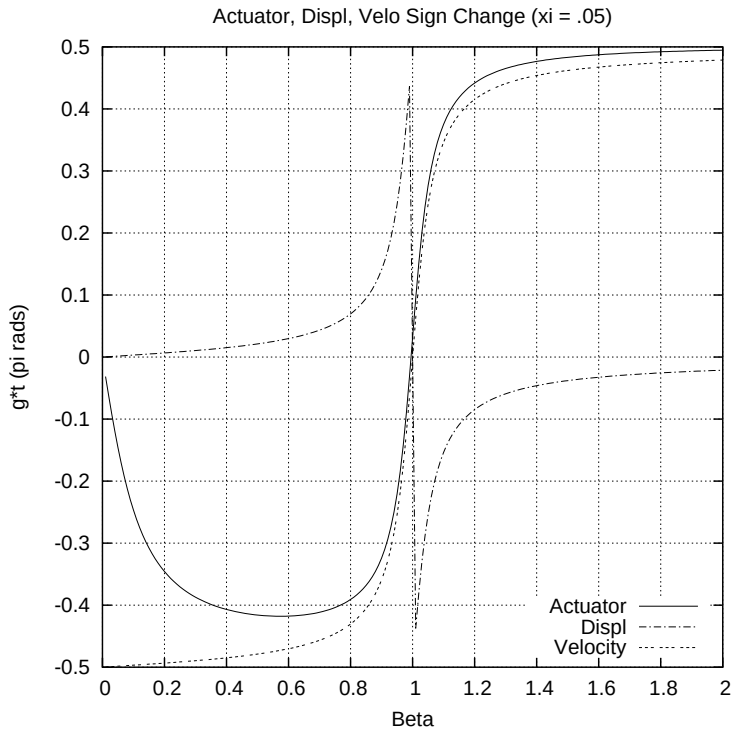

Figure 3.2: Actuator, Displacement, and Velocity Sign Change ($\xi = 0.05$)

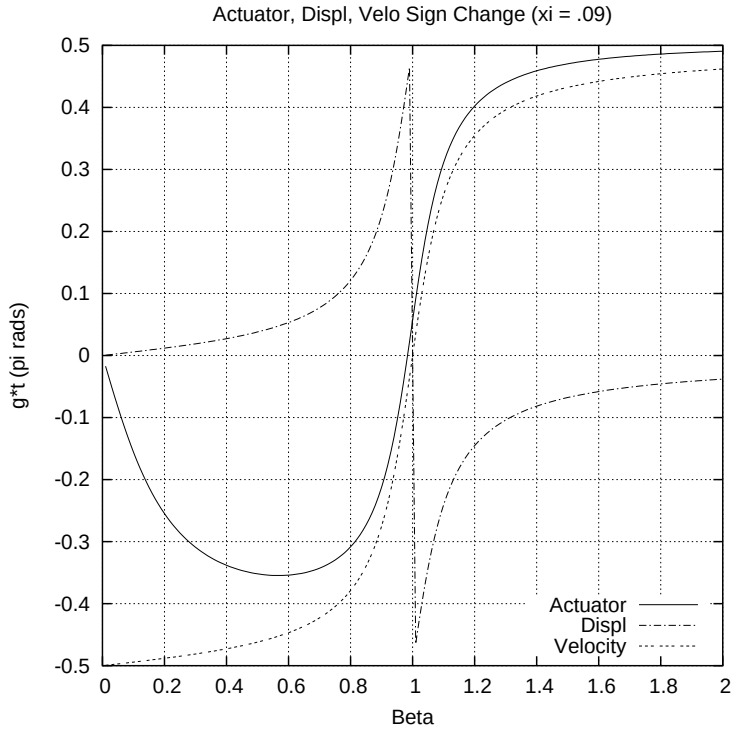

Figure 3.3: Actuator,Displacement, and Velocity Sign Change ($\xi = 0.09$)

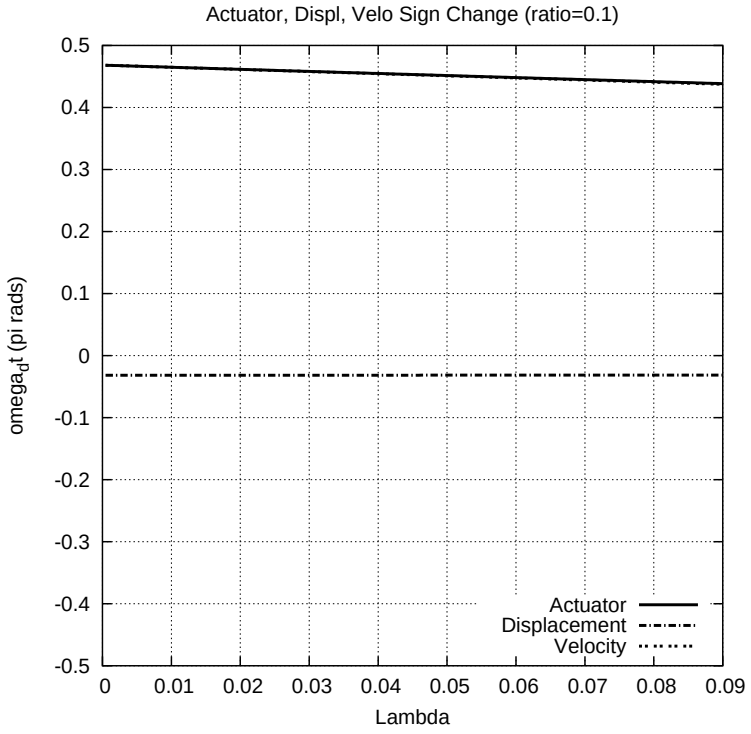

Figure 3.4: Actuator, Displacement, and Velocity Sign Change During Free Vibration ($\rho = 0.1$)

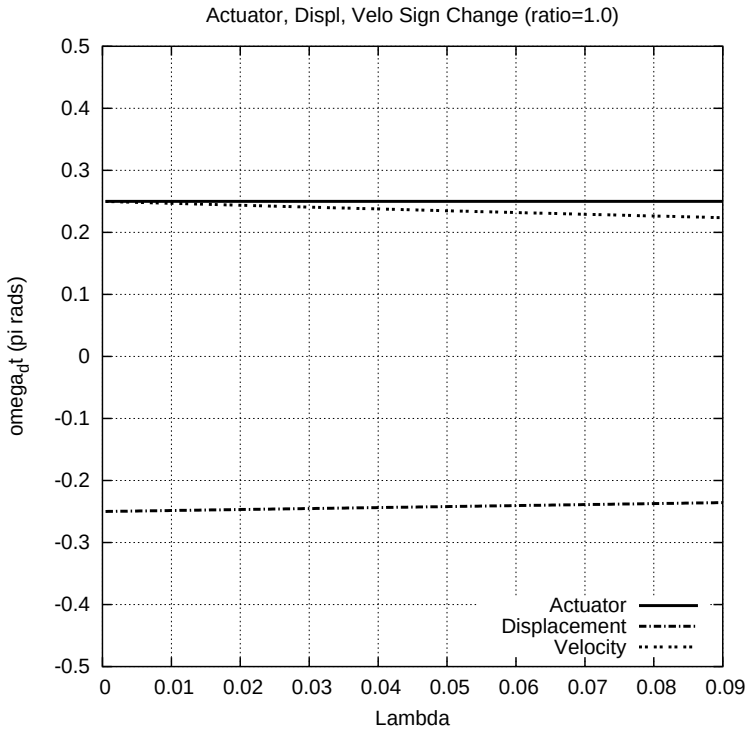

Figure 3.5: Actuator, Displacement, and Velocity Sign Change During Free Vibration ($\rho = 1$)

$$\dot{x}(t) = e^{-\xi w_o t}\left[\dot{x}(0)\cos(w_d t) - \frac{1}{\sqrt{1-\xi^2}}\left(\xi\dot{x}(0) + (\xi + \sqrt{1-\xi^2})w_o x(0)\right)\sin(w_d t)\right]. \tag{3.35}$$

Bang-Bang Control Strategy. Substituting equations 3.34 and 3.35 into $\mathbf{Z}(t) = [x(t), \dot{x}(t)]^T$ and pre-multiplying by equation 3.15 gives:

$$\mathbf{B^T S Z} = \left[\frac{1}{2}\right] x(t) + \left[\frac{m}{2c}\right]\dot{x}(t) = \left[\frac{1}{2}\right]\left[x(t) + \frac{1}{2\xi w}\dot{x}(t)\right]. \tag{3.36}$$

Strategy for Switching Direction of the Actuator Force. The actuator will switch directions in the force application when:

$$C\cos(w_d t) + D\sin(w_d t) = 0, \tag{3.37}$$

where

$$C = \frac{x(0)}{2} + \frac{\dot{x}(0)}{4\xi w_o} \tag{3.38}$$

and

$$D = \frac{\dot{x}(0)}{2} + \frac{x(0)\xi w_o}{2w_o\sqrt{1-\xi^2}} - \frac{1}{4\xi w_o\sqrt{1-\xi^2}}\left(\xi\dot{x}(0) + (\xi + \sqrt{1-\xi^2})w_o x(0)\right). \tag{3.39}$$

Substituting equations 3.38 and 3.39 into equation 3.37 and collecting terms, we have:

$$\tan(\omega_d t) = \left[\frac{(2\xi w_o x(0) + \dot{x}(0))\sqrt{1-\xi^2}}{\xi\dot{x}(0) + (\xi + \sqrt{1-\xi^2})w_o x(0)}\right] \tag{3.40}$$

Zero Displacements. The system displacements will change sign when,

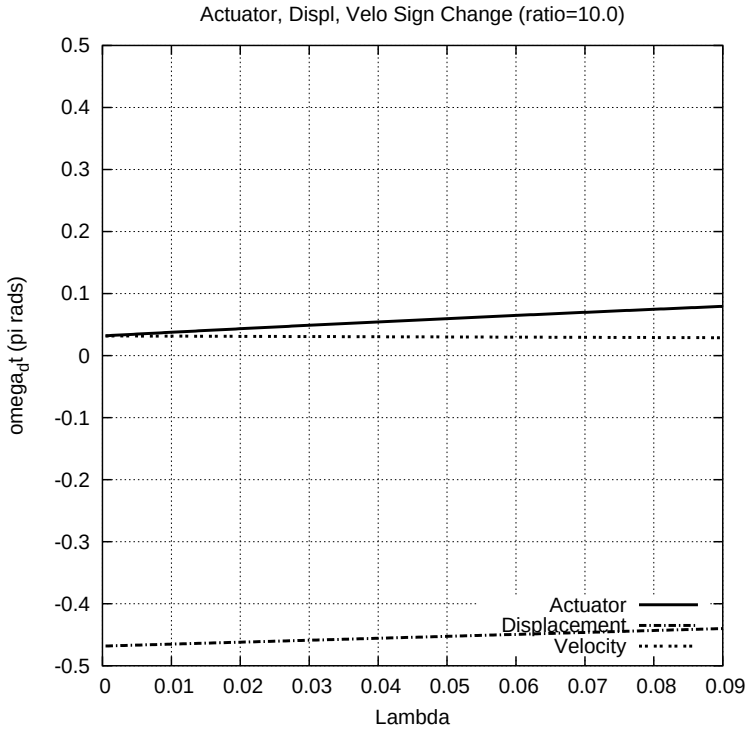

Figure 3.6: Actuator, Displacement, and Velocity Sign Change During Free Vibration ($\rho = 10$)

$$\tan(w_d t) = \frac{-\sqrt{1-\xi^2}x(0)w_o}{\dot{x}(0) + x(0)w_o\xi}. \tag{3.41}$$

Zero Velocities. The system velocities will be zero when,

$$\tan(w_d t) = \frac{\dot{x}(0)\sqrt{1-\xi^2}}{\xi\dot{x}(0) + (\xi + \sqrt{1-\xi^2})w_o x(0)}. \tag{3.42}$$

Plots of "Phase of Bang-Bang Control" vs ξ.

Because the number of degrees of freedom in the model of free vibration response is one fewer than the corresponding steady state model (i.e., β is a constant value), one plot can display a complete picture of how the direction of control force application changes as a function of the remaining problem parameters. We simplify the problem by defining the dimensionless ratio,

$$\rho = \frac{x(0)w_o}{\dot{x}(0)}. \tag{3.43}$$

Figures 3.4 through 3.6 are generated by solving equation 3.43 for $x(0)w_o$ and substituting into equations 3.40, 3.41, and 3.42 gives when the actuator, displacement and velocity of the system are zero in terms of ρ and ξ.

During the free vibration response, switching of the actuator force direction occurs almost in phase with the sign of velocity. This indicates that like the damping model, active control works to oppose changes in system displacement. Moreover, again notice that the displacement and velocity phase shifts are separated by $\pi/2$ radians. The "steady state" and "'free vibration" phase shift models are consistent if latter is viewed as a "steady state response" resulting from a very high forcing frequency (i.e., $\beta = \mathrm{g/w} \to \infty$).

3.2 Research Avenue 2. Symbolic Analysis of Multi-Degree-of-Freedom Systems

3.2.1 Symbolic Representation for 2-DOF Bang-Bang Control Strategy

In this section, we develop symbolic representation for the 2-DOF bang-bang control strategy under three objectives: (1) Minimization of potential energy, (2) Minimization of kinetic energy, and (3) Minimization of total (potential+kinetic) energy. We will soon see that "general symbolic expressions" are huge (even for a two degree of freedom structure) and computationally intractable (even for Mathematica©) for large problems.

Minimizing Potential Energy

Recent research [9] suggests that overall "blanket minimization" of structure-level energy (i.e., potential and kinetic energy) is an overly simplified view of desirable behavior. Instead, analysis procedures should allow for potential energy terms in the system superstructure to be considered separately from potential energy in the base isolation devices. For the 2-DOF mass-spring-damper system shown in Figure 1.1, a suitable form for $\mathbf{Q}$ is:

$$\mathbf{Q} = \begin{bmatrix} a\gamma k + bk & -bk & 0 & 0 \\ -bk & bk & 0 & 0 \\ 0 & 0 & 0 & 0 \\ 0 & 0 & 0 & 0 \end{bmatrix}. \tag{3.44}$$

The parameter setting $(a = 1, b = 0)$ corresponds to minimization of potential energy in the isolation device alone. Conversely, the parameter setting $(a = 0, b = 1)$ corresponds to minimization of potential energy in the superstructure alone. The analysis assumes linear viscous damping of the form $\mathbf{C} = \alpha \cdot \mathbf{M} + \beta \cdot \mathbf{K}$ and that actuators may be located at either or both DOFs (weight on minimizing the potential energy in the first and second stories may be different).

Symbolic Solution. The symbolic solution to $\mathbf{A^T S} + \mathbf{SA} = -\mathbf{Q}$ takes the form:

$$\mathbf{B^T S}(\mathbf{H}, m, k, \alpha, \beta, \gamma, a, b) = \mathbf{H^T} \begin{bmatrix} \frac{f_{11}}{\text{Den 1}} & \frac{f_{12}}{\text{Den 1}} & \frac{f_{13}}{\text{Den 2}} & \frac{f_{14}}{\text{Den 2}} \\ \frac{f_{21}}{\text{Den 1}} & \frac{f_{22}}{\text{Den 1}} & \frac{f_{23}}{\text{Den 2}} & \frac{f_{24}}{\text{Den 2}} \end{bmatrix}. \tag{3.45}$$

Terms in the denominator are:

$$\begin{aligned} \text{Den 1} &= 2(2\beta^2\gamma(2+\gamma)k^2 + \alpha\beta(4+8\gamma+\gamma^2)km + m((4+\gamma^2)k + 2\alpha^2(2+\gamma)m)), \\ \text{Den 2} &= 2(\beta^2\gamma k^2 + \alpha\beta(2+\gamma)km + \alpha^2m^2)(2\beta^2\gamma(2+\gamma)k^2 + \alpha\beta(4+8\gamma+\gamma^2)km \end{aligned}$$

$$+ m((4+\gamma^2)k + 2\alpha^2(2+\gamma)m)).$$

And terms in the numerator are:

$$\begin{aligned}
f_{11} &= bm((1+\alpha\beta)(2+\gamma)k + 2\alpha^2 m) + a(2\beta^2\gamma(2+\gamma)k^2 \\
&\quad + \alpha\beta(2+7\gamma+\gamma^2)km + m((2-\gamma+\gamma^2)k + 2\alpha^2(1+\gamma)m)), \\
f_{12} &= (a-b)m((1+\alpha\beta)(2+\gamma)k + 2\alpha^2 m) \\
&= -bm((1+\alpha\beta)(2+\gamma)k + 2\alpha^2 m) + am((1+\alpha\beta)(2+\gamma)k + 2\alpha^2 m), \\
f_{13} &= m(bm(\alpha m((2+\gamma)k + 2\alpha^2 m) + \beta k(2\gamma k + 2\alpha^2 m + \alpha^2\gamma m)) \\
&\quad + a(2\beta^3\gamma(2+\gamma)k^3 + \alpha\beta^2(4+12\gamma+3\gamma^2)k^2 m + \alpha m^2((2-\gamma+\gamma^2)k \\
&\quad + 2\alpha^2(1+\gamma)m) + \beta km((4-2\gamma+\gamma^2)k + \alpha^2(6+9\gamma+\gamma^2)m)))), \\
f_{14} &= m(-bm(-\beta\gamma^2 k^2 + \alpha^2\beta(2+3\gamma)km + 2\alpha^3 m^2 \\
&\quad + \alpha k(\beta^2\gamma(2+\gamma)k - (-2+\gamma)m)) + a(2\beta^3\gamma(2+\gamma)k^3 \\
&\quad + 2\alpha\beta^2(2+5\gamma+\gamma^2)k^2 m + \alpha m^2(-(-2+\gamma)k + 2\alpha^2 m) \\
&\quad + \beta km(4k + \alpha^2(6+5\gamma)m)))), \\
f_{21} &= (a-b)(2\beta^2\gamma(2+\gamma)k^2 + \alpha\beta(2+5\gamma)km + m((2-3\gamma)k + 2\alpha^2 m)) \\
&= -b(2\beta^2\gamma(2+\gamma)k^2 + \alpha\beta(2+5\gamma)km + m((2-3\gamma)k + 2\alpha^2 m)) \\
&\quad + a(2\beta^2\gamma(2+\gamma)k^2 + \alpha\beta(2+5\gamma)km + m((2-3\gamma)k + 2\alpha^2 m)), \\
f_{22} &= am((1+\alpha\beta)(2+\gamma)k + 2\alpha^2 m) + b(2\beta^2\gamma(2+\gamma)k^2 + \alpha\beta(2+7\gamma+\gamma^2)km \\
&\quad + m((2-\gamma+\gamma^2)k + 2\alpha^2(1+\gamma)m)), \\
f_{23} &= f_{14}, \\
f_{24} &= m(b(2\beta^3\gamma^2(2+\gamma)k^3 + \alpha\beta^2\gamma(8+10\gamma+\gamma^2)k^2 m + \beta km(2\gamma k + \gamma^3 k + 2\alpha^2 m \\
&\quad + 11\alpha^2\gamma m + 3\alpha^2\gamma^2 m) + \alpha m^2((2-\gamma+\gamma^2)k + 2\alpha^2(1+\gamma)m)) + a(2\beta^3\gamma(2+\gamma)k^3 \\
&\quad + \alpha\beta^2(4+8\gamma+\gamma^2)k^2 m + \alpha m^2((2+\gamma)k + 2\alpha^2 m) + \beta km((4+2\gamma+\gamma^2)k + 3\alpha^2(2+\gamma)m)
\end{aligned}$$

Points to note are as follows:

1. This analysis demonstrates that symbolic representations for the $\mathbf{B^T S}$ matrix product are huge, even for a simple 2-DOF system.

2. There are only two symbolic expressions for the denominators of $\mathbf{B^T S}$, one for the displacement coefficients, and a second for the velocity terms.

Special Cases

We have found that under a number of circumstances, the lengthy symbolic expressions simplify significantly.

Minimize Potential Energy ($k* = k$). When $\mathbf{Q}$ contains the structural stiffness matrix in the upper-left quadrant (i.e., $a = b = 1$), $\mathbf{B^T S}$ simplifies to:

$$\mathbf{B^T S} = \begin{bmatrix} \frac{\mathbf{H^T}}{2} & \frac{\mathbf{H^T M}(\alpha \cdot \mathbf{M} + \beta \cdot \mathbf{K})^{-\mathbf{1}}}{2} \end{bmatrix}. \tag{3.46}$$

This result is consistent with the n-DOF model derived in the next section.

Perfect Isolation ($\gamma = 0$). For structures that are perfectly isolated (i.e., $\gamma = 0$), the symbolic expressions simply to:

$$\mathbf{B^T S}(\mathbf{H}, m, k, \alpha, \beta, \gamma, a, b) = \mathbf{H^T} \begin{bmatrix} \frac{a+b}{4} & \frac{a-b}{4} & \frac{a(2\beta k+\alpha m)+b\alpha m}{4\alpha(2\beta k+\alpha m)} & \frac{a(2\beta k+\alpha m)-b\alpha m}{4\alpha(2\beta k+\alpha m)} \\ \frac{a-b}{4} & \frac{a+b}{4} & \frac{a(2\beta k+\alpha m)-b\alpha m}{4\alpha(2\beta k+\alpha m)} & \frac{a(2\beta k+\alpha m)+b\alpha m}{4\alpha(2\beta k+\alpha m)} \end{bmatrix}. \tag{3.47}$$

Two special cases exist. When $a = b = 1$, equation 3.47 simplifies further:

$$\mathbf{B^T S}(\mathbf{H}, m, k, \alpha, \beta, \gamma, 1, 1) = \mathbf{H^T} \begin{bmatrix} \frac{1}{2} & 0 & \frac{\beta k+\alpha m}{2\alpha(2\beta k+\alpha m)} & \frac{\beta k}{2\alpha(2\beta k+\alpha m)} \\ 0 & \frac{1}{2} & \frac{\beta k}{2\alpha(2\beta k+\alpha m)} & \frac{\beta k+\alpha m}{2\alpha(2\beta k+\alpha m)} \end{bmatrix}. \tag{3.48}$$

Notice that symbolic expressions for the coefficient denominators will be non-zero as long as $\alpha \neq 0$ (here we assume that m and k will never be zero) and hence, generally, the bang-bang control strategy is well defined even for structures that are perfectly isolated. The second special case occurs for $a = 0$ and $b = 1$ (i.e., we want to minimize energy within the superstructure alone). Now equation 3.47 simplifies to:

$$\mathbf{B^T S}(\mathbf{H}, m, k, \alpha, \beta, \gamma, 0, 1) = \mathbf{H^T} \begin{bmatrix} \frac{1}{4} & -\frac{1}{4} & \frac{\alpha m}{2\alpha(2\beta k+\alpha m)} & -\frac{\alpha m}{2\alpha(2\beta k+\alpha m)} \\ -\frac{1}{4} & \frac{1}{4} & -\frac{\alpha m}{2\alpha(2\beta k+\alpha m)} & \frac{\alpha m}{2\alpha(2\beta k+\alpha m)} \end{bmatrix}. \quad (3.49)$$

In a typical base-isolated structure, the time history response will be dominated by the first mode of vibration (i.e., $x_1(\mathrm{t}) \approx x_2(\mathrm{t})$ and $\dot{x}_1(\mathrm{t}) \approx \dot{x}_2(\mathrm{t})$). We observe that displacement and velocity pairs of this type will have little influence on the control strategy. Rather, it will be dominated by second-mode displacements.

Minimizing Kinetic Energy

This exercise can be repeated for minimization of kinetic energy in the base isolator and superstructure. For the 2-DOF mass-spring-damper system shown in Figure 1.1, a suitable form for $\mathbf{Q}$ is:

$$\mathbf{Q} = \begin{bmatrix} 0 & 0 & 0 & 0 \\ 0 & 0 & 0 & 0 \\ 0 & 0 & cm & 0 \\ 0 & 0 & 0 & dm \end{bmatrix}, \quad (3.50)$$

The symbols c and d in equation 3.50 represent relative amount of weight a designer places on minimizing kinetic energy in the first and second stories of the structure, respectively.

When $c = d = 1$, the symbolic representation of $\mathbf{B^T S}$ simplifies to:

$$\mathbf{B^T S} = \left[\begin{array}{cc} \mathbf{0} & \frac{\mathbf{H^T M}(\alpha \cdot \mathbf{M} + \beta \cdot \mathbf{K})^{-1}}{2} \end{array} \right]. \tag{3.51}$$

Minimizing Total (Potential+Kinetic) Energy

Notice that because solutions to the Lyapunov matrix equation are linear with respect to $\mathbf{S}$, $\mathbf{B^T S}$ that minimizes the total (potential + kinetic) is simply the sum of equations 3.46 and 3.51.

3.2.2 Limitations of Symbolic Analysis with Mathematica©.

We attempted to compute symbolic expressions for systems having more than two degrees of freedom, but Mathematica's© demands for storage space are greater than what is available on standard workstations. Instead of returning symbolic expressions, the Mathematica© calculation either "times out" or aborts.

3.2.3 Symbolic Analysis of a N-DOF System

When we first obtained symbolic expressions for the matrix elements in $\mathbf{B^T S}$, it was not immediately evident that when $a = b = 1$ and $c = d$, the lengthy formulas would simplify to the formats shown in equations 3.46 and 3.51. This surprising result made us think about other possibilities. Specifically, "starting with relatively simple expressions for solutions to $\mathbf{B^T S}$ in a one degree of freedom structure, we wondered if it would it be possible – perhaps under certain restrictions – to scale this solution up to a N-DOF system?" This pathway of investigation has two key benefits. Unlike numerical procedures for solution to the Lyapunov equation, symbolic expressions provide physical insight into the inner workings of the bang-bang control strategy. And second, when the matrix restrictions apply, symbolic expres-

sions remove the need for nontrivial numerical solutions to the Lyapunov matrix equation. We now present a summary of the key results and observations.

Minimizing Potential Energy

To minimize the potential energy in a n-DOF system, an appropriate choice for the $\mathbf{Q}$ matrix would be:

$$\mathbf{Q} = \begin{bmatrix} \mathbf{K} & \mathbf{0} \\ \mathbf{0} & \mathbf{0} \end{bmatrix}; \tag{3.52}$$

where $\mathbf{K}$ is the n x n structural stiffness matrix and $\mathbf{0}$ is a n x n matrix of zeros. Substituting equation 3.52 into the Lyapunov matrix equation shown in equation 1.11 and solving results in the following $\mathbf{B^T S}$ matrix product:

$$\mathbf{B^T S} = \begin{bmatrix} \frac{\mathbf{H^T}}{2} & \frac{\mathbf{H^T M}(\alpha \cdot \mathbf{M} + \beta \cdot \mathbf{K})^{-\mathbf{1}}}{2} \end{bmatrix}; \tag{3.53}$$

where $\mathbf{H}$ is a n by p matrix that designates the location of the controller(s). Appendix A shows the derivation of equation 3.53.

Requirements for Scalability. Equation 3.53 holds when: (1) the mass matrix $\mathbf{M}$ is diagonal and uniform (i.e., $m_1 = m_2 = ... = m_n$), and (2) linear viscous damping is present in the form $\alpha \cdot \mathbf{M} + \beta \cdot \mathbf{K}$. If the damping matrix sum $\alpha \cdot \mathbf{M} + \beta \cdot \mathbf{K}$ becomes rank deficient, then a unique solution to $\mathbf{B^T S}$ does not exist.

Remark. By substituting equation 3.53 into equation 1.12, the system parameters that are being minimized by the bang-bang control objective results:

$$\dot{V}[x(t), \dot{x}(t)] = -x^T(t)\mathbf{K}x(t) + u^T(t)\mathbf{H^T}[\mathbf{I}x(t) + \mathbf{M}(\alpha \cdot \mathbf{M} + \beta \cdot \mathbf{K})^{-1}\dot{x}(t)]. \tag{3.54}$$

The first term on the right-hand side of equation 3.54 is an energy term that corresponds to double the amount of potential energy in the system at any time, t. Physical considerations dictate that the second term on the right-hand side of equation 3.54 must also be in terms of energy. Since the actuator force, $u(t)$, is present in equation 3.54, this term may be thought of as being made up of displacement and velocity terms that account for work that is done by the actuator force(s) at any time, t.

Minimizing Kinetic Energy

The kinetic energy of a mass-spring system, $T(t)$, may be represented by the following equation:

$$T(\dot{x}(t)) = \frac{m_1\dot{x}_1(t)^2}{2} + \frac{m_2\dot{x}_2(t)^2}{2} + ... + \frac{m_n\dot{x}_n(t)^2}{2}. \tag{3.55}$$

Minimizing the squares of the velocities of a system response may not seem like an important parameter, but internal non-structural damage (e.g., to internal walls, plumbing, etc.) is correlated to peak velocities within a structure [52]. Accordingly, an appropriate choice for $\mathbf{Q}$ is as follows:

$$\mathbf{Q} = \begin{bmatrix} \mathbf{0} & \mathbf{0} \\ \mathbf{0} & \mathbf{M} \end{bmatrix}; \tag{3.56}$$

where $\mathbf{M}$ is the n by n structural mass matrix and $\mathbf{0}$ is a n by n matrix of zeros. Substituting equation 3.56 into the Lyapunov matrix equation results in the $\mathbf{B^T S}$ matrix product:

$$\mathbf{B^T S} = \begin{bmatrix} \mathbf{0} & \frac{\mathbf{H^T M}(\alpha\cdot\mathbf{M}+\beta\cdot\mathbf{K})^{-1}}{2} \end{bmatrix}. \tag{3.57}$$

In equation 3.57, $\mathbf{0}$ is a p by n matrix of zeros and $\mathbf{H}$ is a n by p matrix that designates the location of the controller(s). Appendix 2 shows the derivation of equation 3.57.

Requirements for Scalability. Equation 3.57 has the same scalability requirements as equation 3.53.

Remark. By substituting equation 3.57 into equation 1.12 the system parameters that are being minimized by the bang-bang control objective results:

$$\dot{V}[\dot{x}(t)] = -\dot{x}^T(t)\mathbf{M}\dot{x}(t) + u^T(t)\mathbf{H^T}[\mathbf{M}(\alpha \cdot \mathbf{M} + \beta \cdot \mathbf{K})^{-1}\dot{x}(t)]. \tag{3.58}$$

In a manner analogous to the case for minimizing the potential energy in a n-DOF system, the first term on the right-hand side of equation 3.58 is an energy term corresponding to double the amount of kinetic energy in the system at any time, t. Since the actuator force, $u(t)$, is present in the second term on the right-hand side of equation 3.58, this term may be thought of as being made up of only velocity terms that account for work that is done by the actuator force(s) at any time, t. It is noteworthy that by choosing the $\mathbf{Q}$ matrix as shown in equation 3.56, the bang-bang control objective works toward minimizing system velocities, and not system displacements.

Minimizing Total (Potential+Kinetic) Energy

The total energy in an n-DOF system can be minimized by setting $\mathbf{Q}$ to:

$$\mathbf{Q} = \begin{bmatrix} \mathbf{K} & \mathbf{0} \\ \mathbf{0} & \mathbf{M} \end{bmatrix}. \tag{3.59}$$

Solutions to the Lyapunov equation corresponding to equation 3.59 are given by the sum of equations 3.52 and 3.56. In other words,

$$\mathbf{B^T S} = \begin{bmatrix} \frac{\mathbf{H^T}}{2} & \frac{\mathbf{H^T M(\alpha \cdot M + \beta \cdot K)^{-1}}}{2} \end{bmatrix} + \begin{bmatrix} \mathbf{0} & \frac{\mathbf{H^T M(\alpha \cdot M + \beta \cdot K)^{-1}}}{2} \end{bmatrix} = \begin{bmatrix} \frac{\mathbf{H^T}}{2} & \mathbf{H^T M(\alpha \cdot M + \beta \cdot K)^{-1}} \end{bmatrix}. \tag{3.60}$$

Remark. Substituting equation 3.60 into 1.12 gives the following equation:

$$\dot{V}[x(t), \dot{x}(t)] = -[x^T(t)\mathbf{K}x(t) + \dot{x}^T(t)\mathbf{M}\dot{x}(t)] + u^T(t)\mathbf{H^T}[\mathbf{I}x(t) + 2\mathbf{M}(\alpha \cdot \mathbf{M} + \beta \cdot \mathbf{K})^{-1}\dot{x}(t)]. \tag{3.61}$$

It is clear that equation 3.61 is equal to the sum of equations 3.54 and 3.58. The first and second terms on the right-hand side of equation 3.61 are energy terms corresponding to double the sum of potential and kinetic energy in the system at any time, t. The third term on the right-hand side of equation 3.61 may be thought of as being made up of displacement and velocity terms that account for work that is done by the actuator force(s) at any time, t.

3.3 Research Avenue 3. Symbolic Analysis of the Effect of Nonlinear Deformations to Bang-Bang Control

In this section, we explore the sensitivity of parameters in bang-bang control to localized nonlinear deformations in the base isolation devices. A key observation is that in a typical base-isolated structure, the initial stiffness of the base isolators will be 10-20% of the stiffness of elements in the superstructure. After the isolators have yielded, the tangent stiffness may drop to 2-10% of elements in the superstructure. From a research perspective, the question of interest is "do these nonlinearities have a significant impact on the control strategy that should be employed?" We

address this concern by conducting a symbolic analysis of the control strategy for minimization of potential energy; see equation 3.53.

3.3.1 Case Study Problem (2-DOF Mass-Spring System)

The case study problem is the 2-DOF system shown in Figure 1.1. When controllers act on both degrees of freedom, $\mathbf{H}$ is as follows:

$$\mathbf{H} = \begin{bmatrix} 1 & 0 \\ 0 & 1 \end{bmatrix}. \tag{3.62}$$

Substituting equation 3.62 into equation 3.53 gives:

$$\mathbf{B^T S} = \begin{bmatrix} \frac{1}{2} & 0 & B^T S(1,3) & B^T S(1,4) \\ 0 & \frac{1}{2} & B^T S(2,3) & B^T S(2,4) \end{bmatrix} = \begin{bmatrix} \frac{\mathbf{H^T}}{2} & \frac{\mathbf{H^T M}(\alpha \cdot \mathbf{M} + \beta \cdot \mathbf{K})^{-1}}{2} \end{bmatrix}. \tag{3.63}$$

In the bang-bang control strategy, coefficients on the left- and right-hand sides of $\mathbf{B^T S}$ are multiplied by the system displacements and velocities, respectively. The terms $B^T S(1,3)$ through $B^T S(2,4)$ are elements of the matrix product $\frac{\mathbf{H^T M}(\alpha \cdot \mathbf{M} + \beta \cdot \mathbf{K})^{-1}}{2}$. Due to symmetry of the mass and stiffness matrices, $B^T S(2,3) = B^T S(1,4)$.

Our research goal is to identify conditions in the problem formulation where coefficients for the system velocities will be either very large or, conversely, very small, compared to the displacement coefficients. The former condition will lead to control strategies heavily influenced by system velocities. The latter will lead to control strategies dominated by system displacements.

3.3.2 Symbolic Expressions for Velocity Components of Bang-Bang Control

Let us assume that linear viscous damping is present in the form $\alpha \cdot \mathbf{M} + \beta \cdot \mathbf{K}$ such that there is percentage, ξ, of critical damping of the first two modes of

vibration. Since detailed information on the variation of damping with frequency is seldom available, it is common practice for analysis procedures to assume equal damping ratios to both frequencies [20] (i.e., $\xi = \xi_1 \approx \xi_2$ where ξ_1 and ξ_2 represent the damping ratios for the first two modes of vibration, respectively). The damping matrix coefficients α and β are as follows:

$$\alpha = \frac{2\xi\omega_2\omega_1}{\omega_2 + \omega_1}, \tag{3.64}$$

and

$$\beta = \frac{2\xi}{\omega_2 + \omega_1}, \tag{3.65}$$

where ω_1 and ω_2 are the first and second natural frequencies of the system, respectively. From eigenvalue analysis, the natural frequencies of vibration are:

$$\omega_1(\gamma, m, k) = \sqrt{\frac{k(\gamma + 2 - \sqrt{\gamma^2 + 4})}{2m}}, \tag{3.66}$$

and

$$\omega_2(\gamma, m, k) = \sqrt{\frac{k(\gamma + 2 + \sqrt{\gamma^2 + 4})}{2m}}. \tag{3.67}$$

Symbolic expressions for $B^T S(1,3)$, $B^T S(1,4)$ and $B^T S(2,4)$ in terms of ξ, γ, and the simplifying notation $\tau = m/k$ (units of seconds^2) are obtained in three steps. First, equations 3.66 and 3.67 are substituted into 3.64 and 3.65. Equations 3.64 and 3.65 are then substituted into equation 3.63. Finally, we note that $\omega_1\omega_2\tau = \sqrt{\gamma}$. The latter observation provides a pathway for simplifying the symbolic expressions to the point where key trends in the "velocity coefficients" can be identified. The symbolic expressions are as follows:

$$B^T S(1,3) = \left[\frac{\sqrt{\tau/8}\left[\sqrt{(\gamma+2)-\sqrt{\gamma^2+4}}+\sqrt{(\gamma+2)+\sqrt{\gamma^2+4}}\right](1+\sqrt{\gamma})}{\sqrt{\gamma}\cdot\left[4+2\gamma+4\sqrt{\gamma}\right]\cdot\xi} \right] \tag{3.68}$$

$$B^T S(1,4) = \left[\frac{\sqrt{\tau/8}\left[\sqrt{(\gamma+2)-\sqrt{\gamma^2+4}}+\sqrt{(\gamma+2)+\sqrt{\gamma^2+4}}\right]}{\sqrt{\gamma}\cdot\left[4+2\gamma+4\sqrt{\gamma}\right]\cdot\xi} \right] \tag{3.69}$$

$$B^T S(2,4) = \left[\frac{\sqrt{\tau/8}\left[\sqrt{(\gamma+2)-\sqrt{\gamma^2+4}}+\sqrt{(\gamma+2)+\sqrt{\gamma^2+4}}\right](1+\gamma+\sqrt{\gamma})}{\sqrt{\gamma}\cdot\left[4+2\gamma+4\sqrt{\gamma}\right]\cdot\xi} \right] \tag{3.70}$$

Remark. We need to make sure that the parameter values τ and γ are selected in such way that the natural periods of vibration are representative of systems that occur in practice. The derivation is straightforward. From equations 3.66 and 3.67 we obtain:

$$T_1 = \frac{2\pi}{w_1} = 2\pi\sqrt{\frac{2\tau}{\left(\gamma+2-\sqrt{\gamma^2+4}\right)}}, \tag{3.71}$$

and

$$T_2 = \frac{2\pi}{w_2} = 2\pi\sqrt{\frac{2\tau}{\left(\gamma+2+\sqrt{\gamma^2+4}\right)}}. \tag{3.72}$$

Table 3.1 summarizes the first and second natural periods of vibration (i.e., T_1 and T_2) for γ natural periods of vibration for γ covering the interval [0.0001, 0.15] at various levels of τ.

Generally speaking, low values of τ (i.e., $\tau \leq 0.0001$ secs^2) correspond

$\tau = 0.0001$ (sec^2)	$\gamma = 0.001$	$\gamma = 0.005$	$\gamma = 0.01$	$\gamma = 0.05$	$\gamma = 0.10$	$\gamma = 0.15$
T_1 (sec)	2.8103	1.2574	0.8897	0.3999	0.2846	0.2338
T_2 (sec)	0.0444	0.0444	0.0444	0.0442	0.0439	0.0436
$\tau = 0.0010$ (sec^2)	$\gamma = 0.001$	$\gamma = 0.005$	$\gamma = 0.01$	$\gamma = 0.05$	$\gamma = 0.10$	$\gamma = 0.15$
T_1 (sec)	8.8869	3.9763	2.8134	1.2646	0.8999	0.7395
T_2 (sec)	0.1405	0.1404	0.1403	0.1396	0.1387	0.1378
$\tau = 0.010$ (sec^2)	$\gamma = 0.001$	$\gamma = 0.005$	$\gamma = 0.01$	$\gamma = 0.05$	$\gamma = 0.10$	$\gamma = 0.15$
T_1 (sec)	28.1028	12.5742	8.8969	3.9989	2.8457	2.3385
T_2 (sec)	0.4442	0.4440	0.4437	0.4415	0.4387	0.4359

Table 3.1: First and Second Natural Periods of Vibration (i.e. T_1 and T_2) versus τ and γ

to systems having a stiff superstructure. High values of τ (i.e., $\tau \geq 0.01$ secs^2) correspond to systems having a flexible superstructure. During a nonlinear time-history response, instantaneous values of γ vary according to elastic/plastic states of the systems. In contrast, values of τ remain constant. Hence, from an analysis and design perspective, we need to explore sensitivity of parameters in the bang-bang control strategy to systematic variations in γ while holding τ constant.

3.3.3 Sensitivity Analysis

In an effort to understand the relative importance of displacement and velocity terms in the bang-bang control strategy, we employ a combination of mathematics and graphics to identify and validate trends in the "system velocity coefficients" versus ξ, γ and τ. First, notice that although each formula has many terms, the relationship among these coefficients is simple:

$$\frac{B^T S(1,3)}{B^T S(1,4)} = 1 + \sqrt{\gamma} \quad \text{and} \quad \frac{B^T S(2,4)}{B^T S(1,4)} = 1 + \gamma + \sqrt{\gamma}. \tag{3.73}$$

For large values of γ (e.g., $\gamma = 0.15$), the ratios $B^T S(1,3)/B^T S(1,4)$ and $B^T S(2,4)/B^T S(1,4)$ are 1.38 and 1.53, respectively. For small values of γ (i.e., $\gamma \sim 0.00$), the ratios $B^T S(1,3)/B^T S(1,4)$ and $B^T S(2,4)/B^T S(1,4)$ approach 1. Hence, while the left-hand side of $\mathbf{B^T S}$ has coefficient values 1/2 along the diagonal elements and zeros elsewhere, for small values of γ, values of the four system velocity components are approximately the same. Moreover, we note that:

$$\text{limit}_{\gamma \to 0} \left[\frac{\sqrt{(\gamma+2) - \sqrt{\gamma^2+4}} + \sqrt{(\gamma+2) + \sqrt{\gamma^2+4}}}{\left[4 + 2\gamma + 4\sqrt{\gamma}\right]} \right] = \frac{1}{2}. \tag{3.74}$$

Hence, for small values of γ, the velocity coefficients $B^T S(1,3)$, $B^T S(1,4)$ and $B^T S(2,4)$ increase in proportion to $1/\sqrt{\gamma}$. Also, for a fixed value of γ, the velocity coefficients increase in proportion to $\sqrt{\tau}$ and $1/\xi$ (the damping ratio of the structure).

Figures 3.7 through 3.9 validate these observations and show two important trends. In these figures, the damping ratio, $\xi = 0.05$. First, we observe that τ increases monotonically as one moves vertically along contours of constant γ. We conclude from this trend that the influence of system velocities on bang-bang control will increase as the superstructure becomes progressively more flexible. (Conversely, bang-bang control will be most influenced by system displacements when the superstructure is stiff.) Second, within the interval $\gamma \in$ [0.05,0.15], the coefficient values are relatively constant. We surmise from this observation that "bang-bang control strategies" will be insensitive to localized nonlinearities in the base isolation devices, especially when γ(t) remains within the interval [0.05,0.15]. As such, simplified design procedures might be justified. For design applications where post-yield

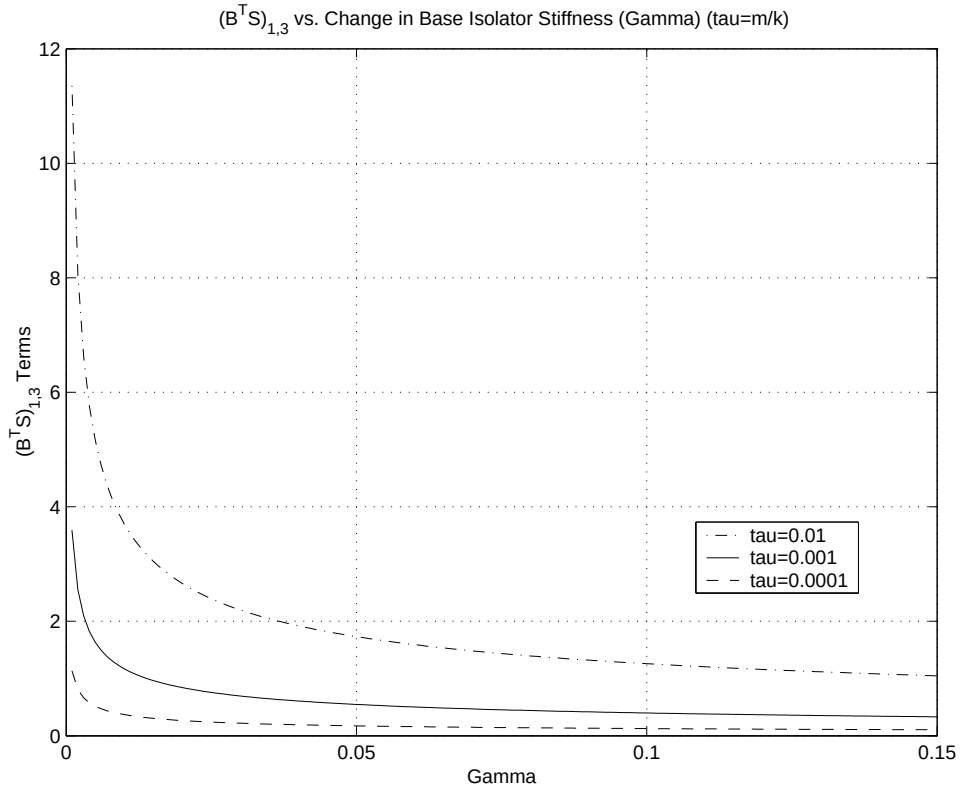

Figure 3.7: Velocity coefficient $B^T S(1,3)$ versus γ for contours of constant τ ($\xi = 0.05$)

stiffnesses are very low (i.e., $\min(\gamma(t)) \approx 0$), the bang-bang control strategy is likely to switch between two modes: (1) a displacement driven strategy for pre-yield states, and (2) a velocity driven strategy for post-yield states. At this point these observations are preliminary predictions. Numerical simulations are needed to validate the accuracy of these observations.

3.3.4 Consistency Check

At a glance this result would seem to be at odds with the symbolic expressions derived in Research Avenue 2. However, this isn't the case. Unlike the analysis in Section 3.2.1, the formulation here assumes that the damping matrix coefficients α and β, i.e.,

$$\alpha = \frac{2\xi\omega_2\omega_1}{\omega_2 + \omega_1} \qquad \text{and} \qquad \beta = \frac{2\xi}{\omega_2 + \omega_1}, \tag{3.75}$$

will vary according to ω_1 and ω_2, the first and second natural circular frequencies of the system, respectively. As γ approaches zero, the natural periods of vibration move toward infinity. Hence, it is evident from equation 3.75 that as ω_1 and ω_2 approach 0, β increases toward infinity. The case for α is less clear. We note that $w_1 < w_2$ (generally) and rewrite the symbolic expression for α as

$$\alpha = \frac{2\xi\omega_1}{\left[1 + \frac{\omega_1}{\omega_2}\right]}. \tag{3.76}$$

The denominator will evaluate to a small finite number as γ approaches zero. Hence, α also approaches 0. Moreover, from equation 3.48 we see that as α approaches 0, coefficients $B^T S(1,3)$ and $B^T S(1,4)$ increase in value toward infinity. Coefficients $B^T S(1,3)$ and $B^T S(1,4)$ also approach each other in value. Therefore, these observations are completely consistent with the symbolic analysis in section 3.1.

Remark. Although Rayleigh damping models are not associated with single degree-of-freedom systems, it can be easily shown that if $w_1 = w_2$ in equations 3.75, the damping coefficient

$$c = \left[\frac{1}{6\lambda\omega}\right]. \tag{3.77}$$

Hence, even in the single degree-of-freedom case, the coupling of Rayleigh damping models to the bang-bang control strategy forces the damping coefficient to increase toward infinity as ω approaches zero.

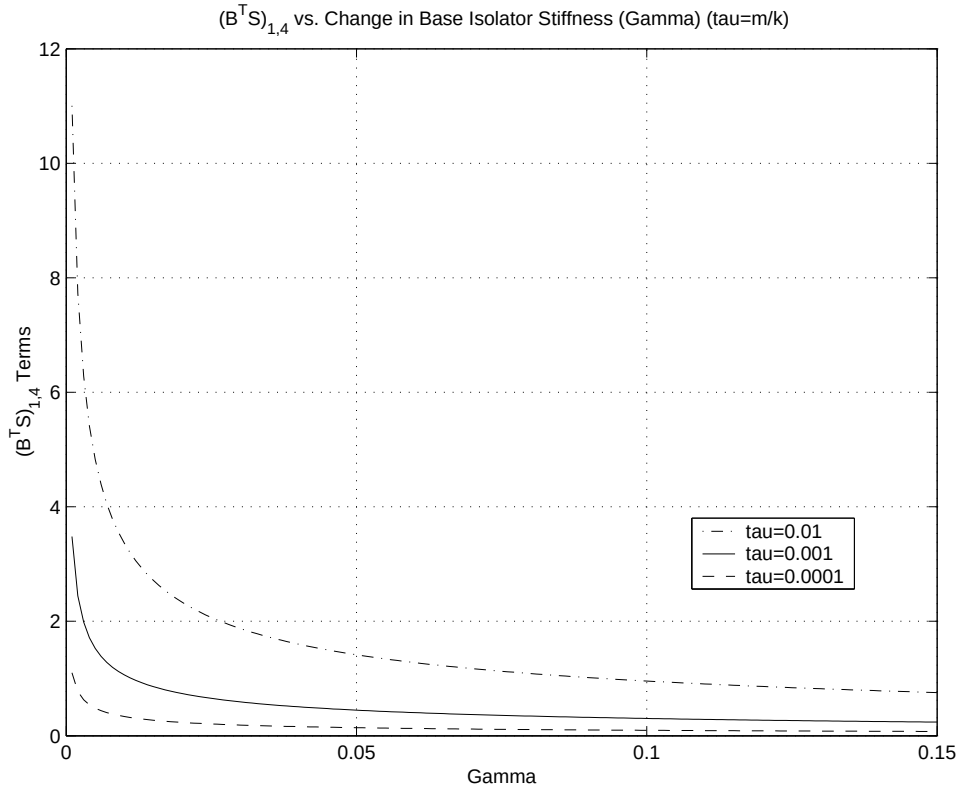

Figure 3.8: Velocity coefficient $B^T S(1,4)$ versus γ for contours of constant τ ($\xi = 0.05$)

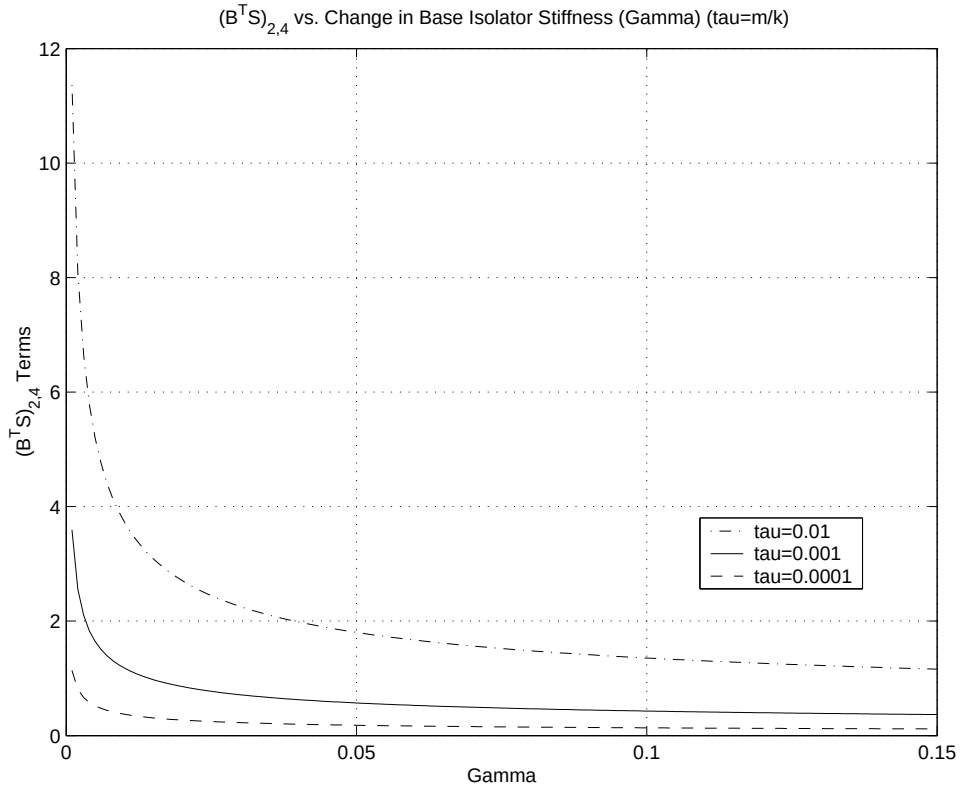

Figure 3.9: Velocity coefficient $B^T S(2,4)$ versus γ for contours of constant τ ($\xi = 0.05$)

Chapter 4

Numerical Analysis: Effect of Bang-Bang Control Strategy

For a wide range of moderate-to-large ground motion events, base-isolated structures are expected to exhibit nonlinear displacement behavior at the isolator level, leaving the main structural system undamaged. In Section 3.3, we formulated symbolic expressions for parameters in the bang-bang control strategy as a function of localized nonlinear deformations in the isolator devices. Figures 3.7 through 3.9 indicate that over the interval $\gamma \in [0.05, 0.15]$, the magnitude of velocity coefficients in $\mathbf{B^T S}$ will be insensitive to variations in γ. From a design perspective, however, we need to know whether small variations in the magnitude of velocity coefficients will lead to large perturbations in peak values of system response? To resolve this issue, in this chapter we use the Aladdin scripting language [6, 7] to compute the time-history response of a five-DOF actively controlled nonlinear mass-spring-damper system subject to an ensemble of severe earthquake ground motions. The purposes of this experiment are to: (1) Validate by experiment the theoretical formulation for bang-bang control, (2) Demonstrate that localized nonlinear displacements in the base isolation devices are insensitive to the bang-bang strategy used (the bang-bang strategies considered are described in section 4.4), and (3) Show the characteristic high frequency switching of the control force from one extreme to another after the ground excitation ends. The latter points to the limitations of constant amplitude bang-bang control, and the strong need for a time-varying adaptive strategy.

	Floor	Stiffness (kN/m)		Period (secs)		Part. Factor (Γ)	
DOF/Mode	Mass (kg)	Pre-yield	Post-yield	Pre-yield	Post-yield	Pre-yield	Post-yield
1	160,000	27,000	4,500	1.20	2.70	1.11	1.02
2	160,000	150,000	150,000	0.31	0.33	0.15	0.03
3	160,000	150,000	150,000	0.17	0.17	0.04	0.01
4	160,000	150,000	150,000	0.13	0.13	0.02	0.00
5	160,000	150,000	150,000	0.11	0.11	0.01	0.00

Table 4.1: Properties of Five DOF Mass-Spring-Damper System

4.1 Actively Controlled Mass-Spring-Damper System

Figures 4.1 and 4.2 show elevation views of an idealized mass-spring-damper base-isolated system. Within the superstructure (elements 2-5), five lumped masses are connected via four linearly elastic springs. Element 1 is modeled with a bi-linear, force-displacement relationship that follows the kinematic hardening rule. Element 1 is used by Lin [44] and is a model of a laminated rubber base-isolator with a lead core. The purpose of element 1 is to isolate the superstructure from the inertia forces generated by the ground displacements. The left-hand side of Table 4.1 contains a summary of mass and stiffness properties for the structural model.

As shown on the right-hand side of Table 4.1, the first and second natural periods of vibration are 1.2 and 0.31 seconds, respectively. When the base isolator yields the first and second natural periods of vibration increase to 2.70 and 0.33 seconds. Also notice that in both the pre- and post-yield states, the modal participation factors indicate that the overall system response should be dominated by first mode displacements – this is particularly the case for post-yield displacements.

The yield force and displacement for element 1 are 350 kN and 13.0 mm, respectively. Damping effects are accounted for through linear viscous damping. In the equation $\mathbf{C} = \alpha\mathbf{M} + \beta\mathbf{K}$, the coefficients α and β are chosen so that there is 5% critical damping in the first two modes. Boundary conditions for our model are

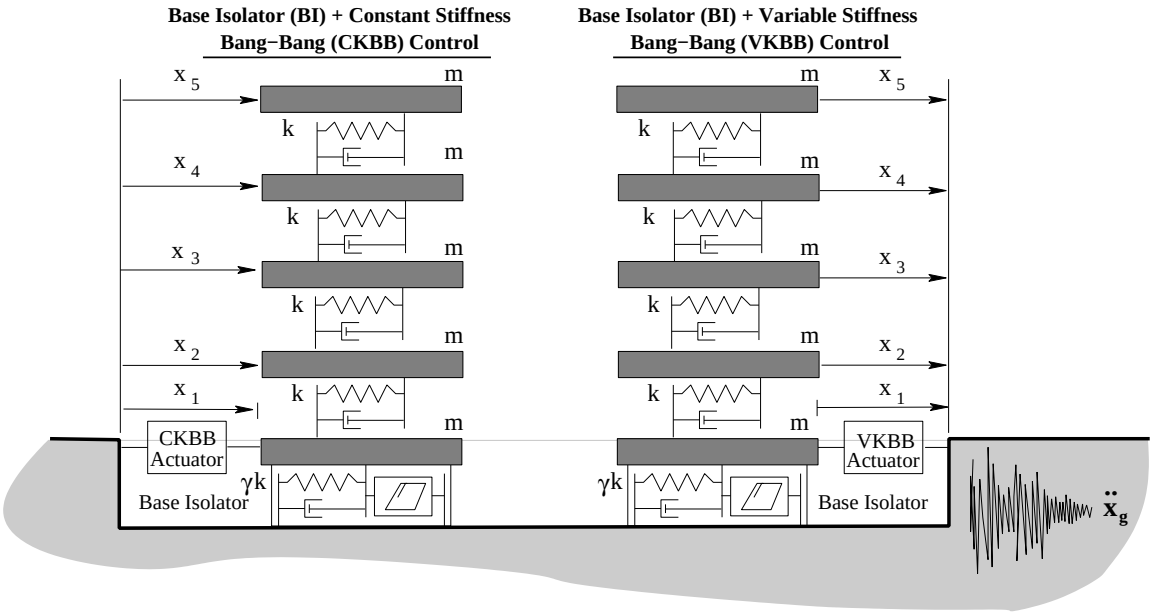

Figure 4.1: Elevation View of 5 DOF Linear/Nonlinear Mass-Spring-Damper System

full-fixity at the base, and full-fixity against vertical displacements and rotations at nodes 2 through 5.

With respect to parameters in the symbolic analysis, the pre- and post-yield values of γ are 0.18 and 0.03 and the value for τ is 0.00106 secs^2. To see where these parameters lie with respect to the two-DOF system in Table 3.1, we partition the overall mass into two "roughly equivalent" masses. The ratio $\tau = 2.5m/k = 0.00265$ secs^2. These parameter settings: (1) put the pre-yield five-DOF between the bottom right-hand corner and middle right-hand side of Table 3.1, and (2) indicate that the study problem is consistent with the class of problems covered by the symbolic analysis.

4.2 Actuator Placement and Characteristics

For the purposes of illustrating the potential benefits of active control, an actuator is located at the top of the lead-rubber base isolator (degree of freedom

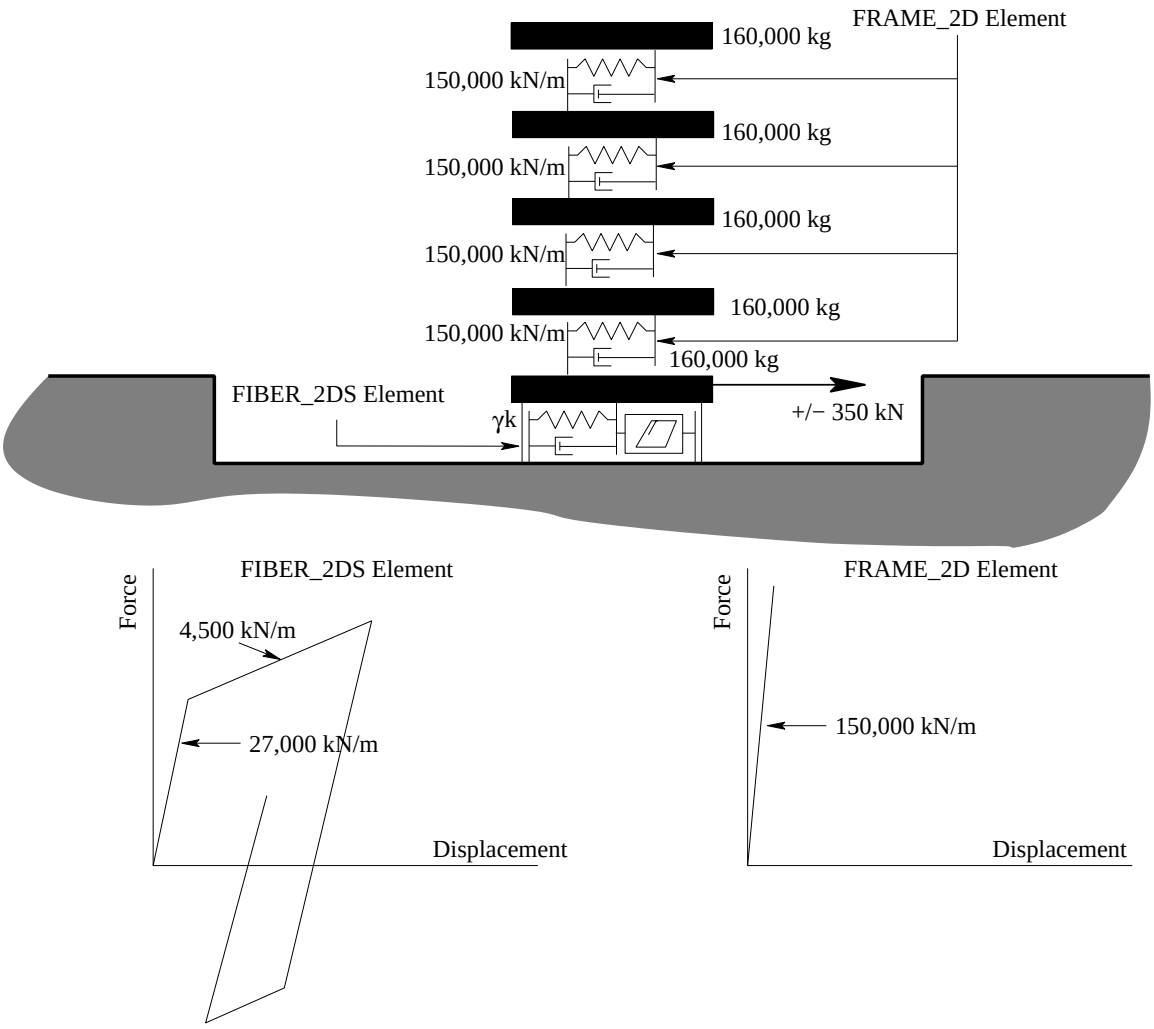

Figure 4.2: Model of Mass-Spring-Damper System

1). Unfortunately, at this time there is a complete lack of guidance in the literature on the selection of appropriate max/min forces in the actuator. Hence, in this dissertation, we proceed under the assumption that the hybrid system will not add value to the overall system performance unless the passive and active components of control can work in concert. For the passive control system, stiffness and yield force design parameters are selected so that the structure will have appropriate natural periods of vibration and yield before excessive forces occur within the main structural system. We observe that since the actuators will not affect the natural periods of vibration, as a first cut, peak actuator forces should be balanced against

the yield capacity of the isolators. Therefore, for this dissertation, the maximum force that may be generated by the actuator matches the yield force of the base isolator (i.e., $u_{max} = 1F_y = 350$ kN).

4.3 Ground Excitation

The numerical experiments are based on 15 second segments of ground motion recorded at San Fernando and Northridge, CA., Kobe, Japan, and Duzce, Turkey (Source, Earthquake Engineering Research (PEER) Center Strong Motion Database [27]). The details of each accelerogram are as follows:

1. 1971 San Fernando – 164° south-south-west component of the February 9, 1971, San Fernando, CA. USA. earthquake (unscaled magnitude 6.6). Recorded at the 279 Pacoima Dam substation (CDMG station #279). The closest distance of the substation to the fault rupture is 2.8 kilometers.

2. 1994 Northridge – east-west component of the January 17, 1994, Northridge, CA. USA. earthquake (unscaled magnitude 6.7). Recorded at the 24436 Tarzana, Cedar Hill substation (CDMG station 24436). The closest distance of the substation to the fault rupture is 17.5 kilometers.

3. 1995 Kobe – north-south component of the January 16, 1995, Kobe, Japan earthquake (unscaled magnitude 6.9). Recorded at the Kobe Japanese Meteorological Agency (KJMA). The closest distance of the substation to the fault rupture is 0.6 kilometers.

4. 1999 Duzce – north-south component of the November 12, 1999, Duzce, Turkey earthquake (unscaled magnitude 7.1). Recorded at the 375 Lamont Doherty Earth Observatory substation. The closest distance of the substation to the fault rupture is 8.2 kilometers.

Time histories of ground acceleration vs time are shown in Figures 4.3 through 4.6. The ground motions are digitized at intervals of 0.02 seconds. Each record was translated along the y-axis to remove residual velocity effects. Park and Otsuka [53] have classified these earthquakes as being severe – therefore, expected structural behavior is large plastic deformations in the isolators and essentially elastic behavior in the system superstructure.

Frequency Content of Ground Motions. The Fourier transform is a frequency domain analysis technique that is used to determine dominant frequency. Figures 4.7 through 4.10 show the frequency content of ground motion for the Kobe, San Fernando, Northridge and Duzce accelerograms, respectively. Each plot is annotated with the dominant frequency (Hz) and corresponding period (sec) of ground shaking (i.e., 0.68, 0.21, 0.35 and 0.34 seconds). It is important to note that in all cases, the base isolation design effectively separates the dominant period of vibration in the ground shaking from the natural periods of the structure ($T_1 = 1.2$ seconds). The corresponding values of $\beta = g/w$ are 1.76, 5.76, 3.44, and 3.52.

Ground Motion Scaling. Using peak ground acceleration (PGA) and Arias Intensity as metrics of ground shaking severity, the accelerograms were scaled so that they have approximately the same potential for imparting damage to a structure. Arias Intensity is a measure of energy in an accelerogram [4]. Kayen and Mitchell [39] note that as a scaling parameter, Arias Intensity has two key advantages over PGA, namely:

1. Arias Intensity is computed over the duration of the acceleration record. It therefore incorporates all amplitude cycles that occur. PGA, in contrast, utilizes a single amplitude that is independent of shaking duration, and

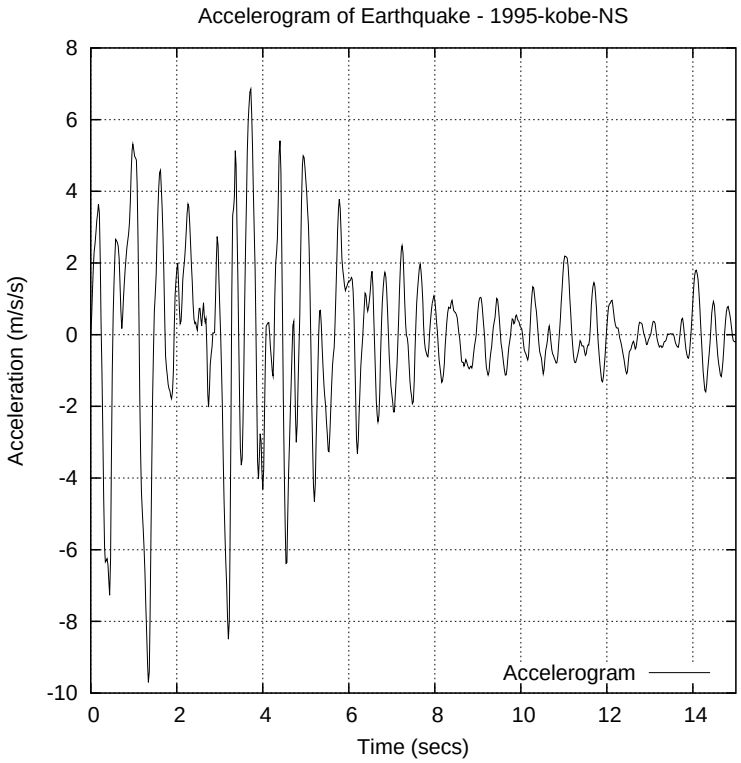

Figure 4.3: 1995 Kobe Accelerogram.

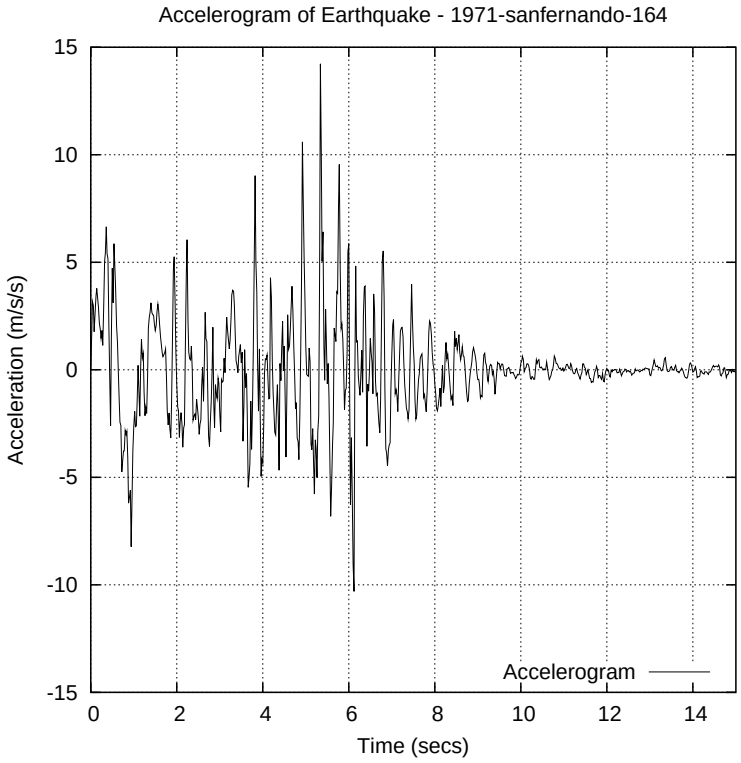

Figure 4.4: 1971 San Fernando Accelerogram.

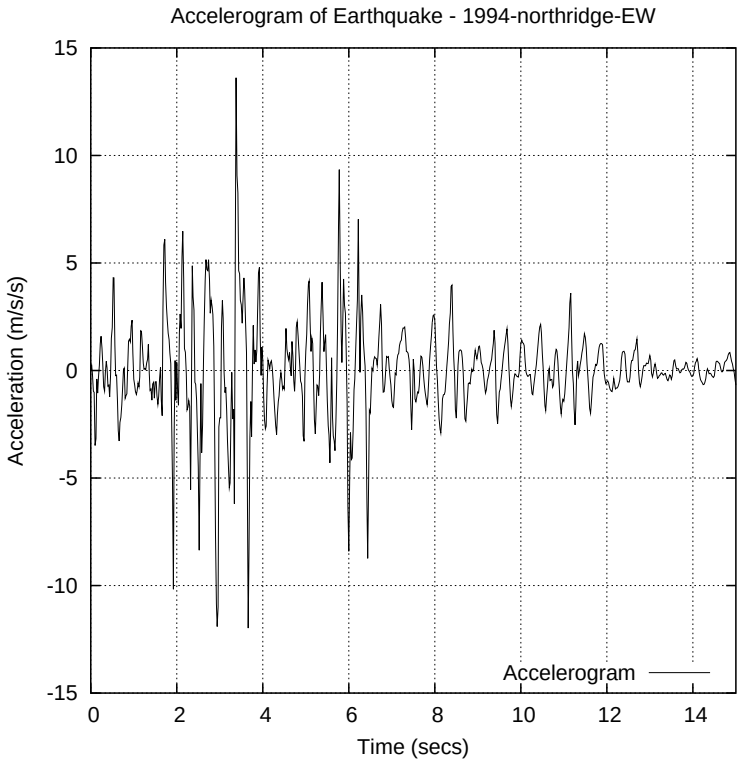

Figure 4.5: 1994 Northridge Accelerogram.

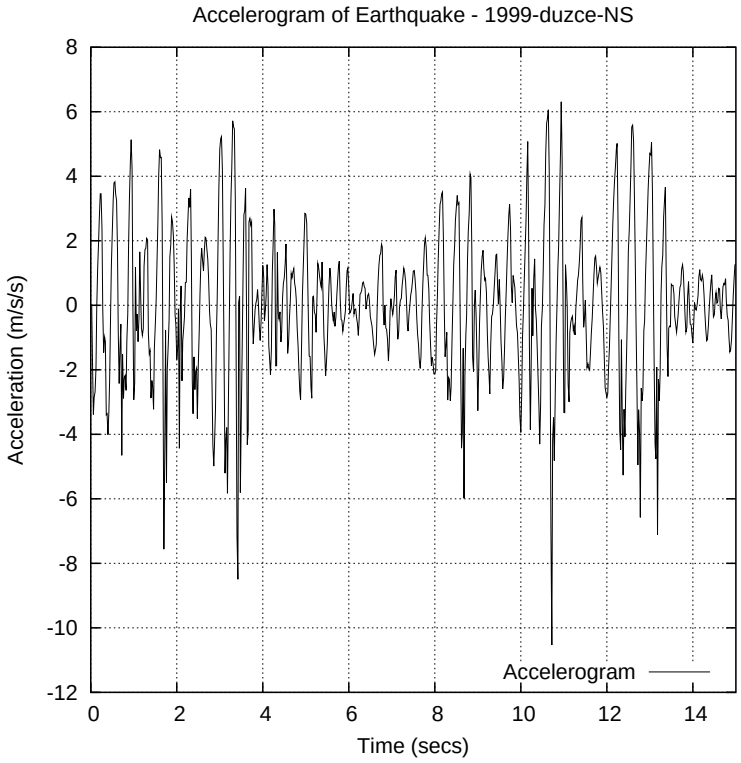

Figure 4.6: 1999 Duzce Accelerogram.

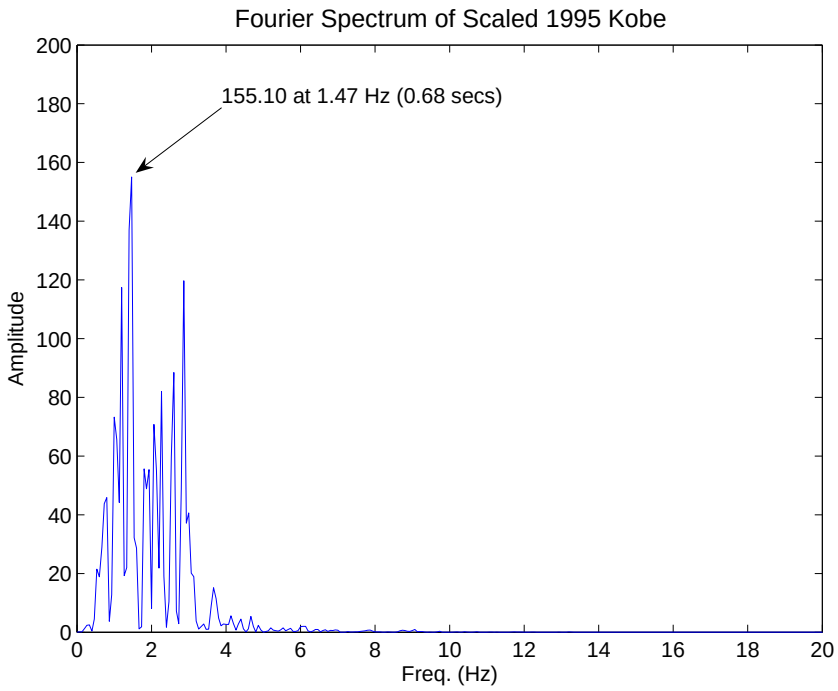

Figure 4.7: Fourier Spectrum for 1995 Kobe Accelerogram.

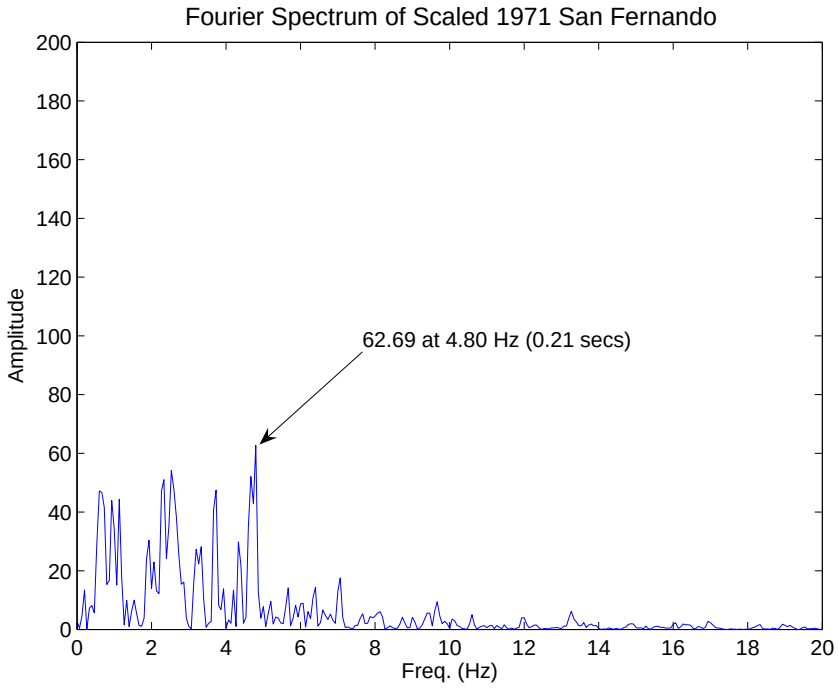

Figure 4.8: Fourier Spectrum for 1971 San Fernando Accelerogram.

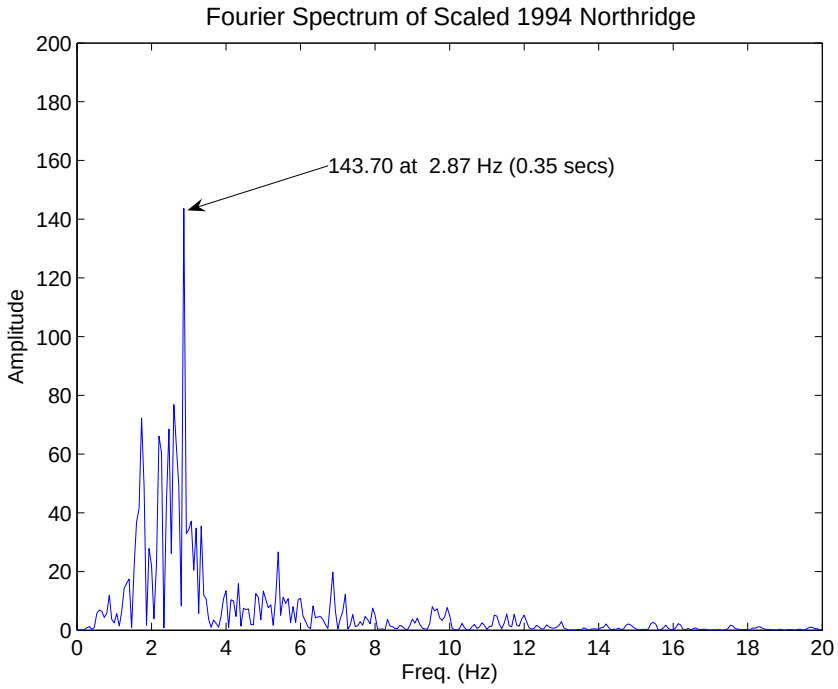

Figure 4.9: Fourier Spectrum for 1994 Northridge Accelerogram

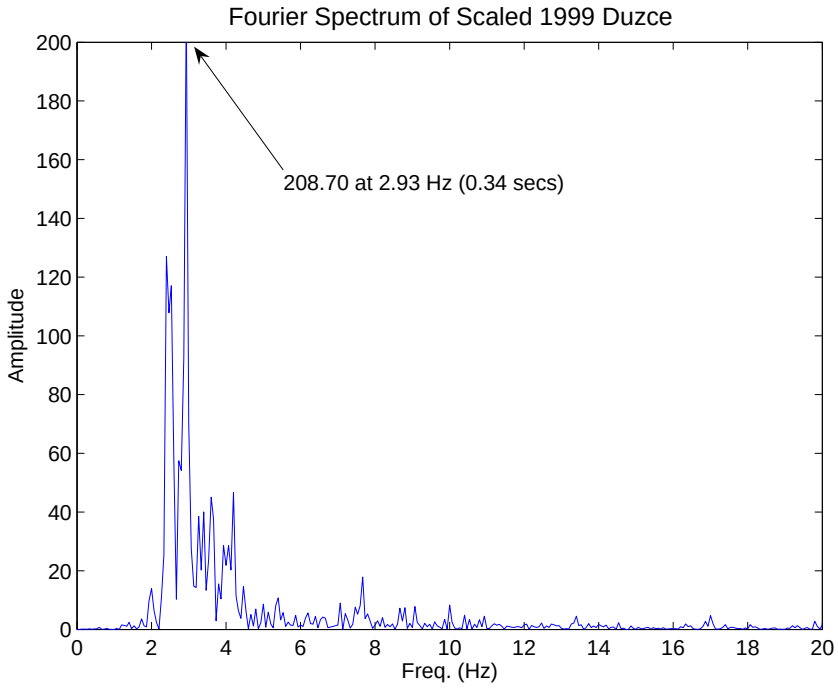

Figure 4.10: Fourier Spectrum for 1999 Duzce Accelerogram.

Earthquake	Motion Scale Factor	Arias Intensity (m/sec)	PGA (g)
1971 San Fernando	1.186	12.07	1.451
1994 Northridge	0.779	12.07	1.388
1995 Kobe	1.205	12.07	0.989
1999 Duzce	1.131	12.07	1.073

Table 4.2: Severe EQ Scaled Components: Scaling Factor, Arias Intensity, PGA

Earthquake	Velocity (cm/sec)		Fourier Peak (secs)
	Min.	Max.	
1971 San Fernando	-30.69	181.30	0.21
1994 Northridge	-104.30	44.08	0.35
1995 Kobe	-100.30	90.27	0.68
1999 Duzce	-44.34	32.76	0.34

Table 4.3: Severe EQ Scaled Components: Peak Velocity and Fourier Amplitude

2. Arias intensity incorporates the severity of motions over the full range of recorded frequency, whereas, PGA is often associated only with high-frequency motion.

The scaling procedure constrains each ground motion to have equal Arias Intensity and adjusts the scaling factors so that the average peak ground acceleration has a desired level. Mathematically, if $\ddot{x}_{ig}(t)$ is the i-th ground motion acceleration, then we seek scaling coefficients k_i so that:

$$\frac{\pi}{2g}\int_0^{10} k_1^2\ddot{x}_{1g}^2(\tau)d\tau = \frac{\pi}{2g}\int_0^{10} k_2^2\ddot{x}_{2g}^2(\tau)d\tau = \cdots = \frac{\pi}{2g}\int_0^{10} k_6^2\ddot{x}_{6g}^2(\tau)d\tau = \text{constant}. \tag{4.1}$$

The Arias Intensity and average PGA for the scaled ground motion accelerograms are 12.07 m/sec and 1.225g, respectively. Tables 4.2 and 4.3 show results of the scaling procedures, including the ground motion scaling factor, Arias Intensity, PGA, minimum and maximum ground velocities, and the period at which the peak Fourier

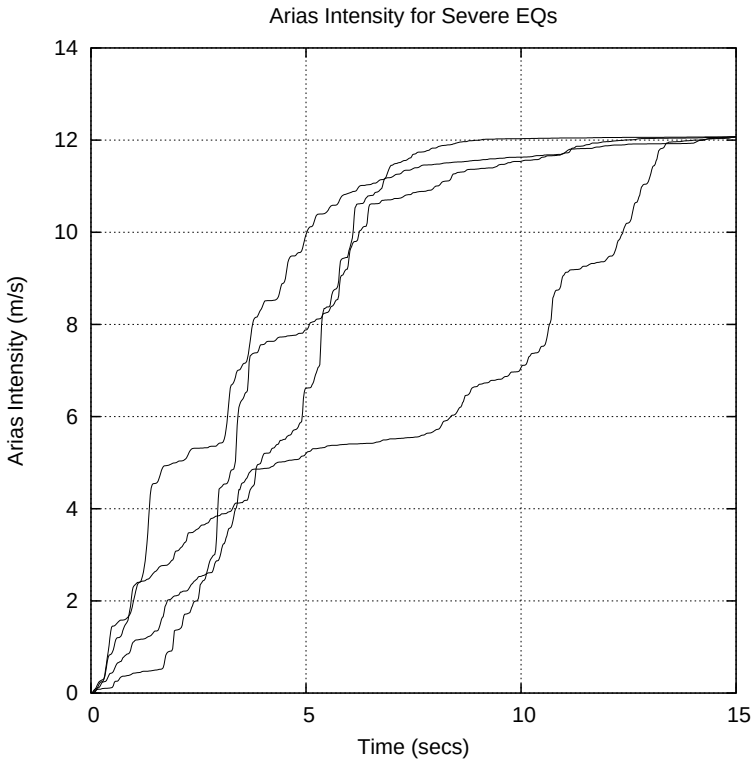

Figure 4.11: Arias Intensities versus Time for Scaled Ground Motion Accelerograms

transform occurs. The time variation in Arias Intensity for each of the four scaled ground motions is shown in Figure 4.11.

4.4 Bang-Bang Control Strategies

The purpose of this section is to assess the impact of the control algorithm strategy on nonlinear system-level behavior; for details on underlying behavior, see equation 1.1. Time history analyses are computed for two control methodologies:

Control Methodology 1. Consists of an actively controlled, nonlinear, base-isolated mass-spring-damper system with the same section, material, and actuator properties as previously described. This simplified approach to control assumes that the structural system properties will remain constant throughout the analyses – but, of course, they don't. Prior to the commencement of time

history computations, $\mathbf{B^T S}$ is calculated using values of α, β, $\mathbf{M}$, and $\mathbf{K}$ based on the elastic stiffness of the base isolator. Herein, this control methodology will be called constant stiffness (K) bang-bang (CKBB) control.

Control Methodology 2. Consists of an actively controlled, nonlinear, base-isolated mass-spring-damper system with the same section, material, and actuator properties as previously described. The goals of this methodology are to systematically refine the control algorithm based upon real-time values of the system parameters (including nonlinear force-displacement behavior of the isolation devices). A naive implementation would simply compute $\mathbf{B^T S}$ at each time-step. Instead, we note that at any point in time, the system can only be in one of two states: (1) pre-yield (initial) structural stiffness, or (2) post-yield (tangent) structural stiffness. $\mathbf{B^T S}$ was calculated prior to the time history using the base isolator stiffness based on both the preyield and postyield states. When the tangent stiffness of the base isolator is used to calculate $\mathbf{B^T S}$, equation 3.53 is not applicable. This is due to the fact that equation 3.53 was derived based on the relationship between the damping and stiffness (and mass) being $\mathbf{C} = \alpha\mathbf{M} + \beta\mathbf{K}$. However, since we are not varying the damping as a function of time, the Lyapunov equation (1.11) must be solved. During each time step of the analysis, an appropriate $\mathbf{B^T S}$ was selected. Herein, this control methodology will be called variable stiffness (K) bang-bang (VKBB) control.

To benchmark the improvements in system response due to the presence of active control, we compute a third time history response for base isolation alone. By comparing contours of time history response for control methodologies 1 and 2, we hope to determine if the simplifying assumptions in control methodology 1 are sufficient for design purposes. And by comparing control methodologies 1 and 2

to the ensemble of time history responses corresponding to base isolation alone, we hope to assess the impact that active control can have as a supplement to base isolation.

4.4.1 Constant Stiffness Bang-Bang Control (CKBB)

Before bang-bang control can be applied to equation of motion, 1.1, $\mathbf{B^T S}$ must first be calculated. For both the control methodologies, the potential energy in the structure will be minimized (i.e., a = b = 1). Therefore, equation 4.2 is applicable:

$$\mathbf{B^T S} = \left[\begin{array}{cc} \frac{\mathbf{H^T}}{2} & \frac{\mathbf{H^T M}(\alpha \cdot \mathbf{M} + \beta \cdot \mathbf{K})^{-1}}{2} \end{array} \right]. \tag{4.2}$$

Equation 4.2 evaluates to a (1×10) matrix.

Equations 4.3 through 4.5 show the values for α, β, and the matrices $\mathbf{H}$, $\mathbf{M}$, and $\mathbf{K}$ that are directly substituted into equation 4.2:

$$\alpha = 0.4170 \text{ Hz}; \quad \beta = 0.0039 \text{ secs}; \quad \mathbf{H} = \begin{bmatrix} 1 \\ 0 \\ 0 \\ 0 \\ 0 \end{bmatrix}, \tag{4.3}$$

$$\mathbf{M} = \begin{bmatrix} 160,000 & 0 & 0 & 0 & 0 \\ 0 & 160,000 & 0 & 0 & 0 \\ 0 & 0 & 160,000 & 0 & 0 \\ 0 & 0 & 0 & 160,000 & 0 \\ 0 & 0 & 0 & 0 & 160,000 \end{bmatrix} kg, \tag{4.4}$$

$$\mathbf{K} = \begin{bmatrix} 177,000 & -150,000 & 0 & 0 & 0 \\ -150,000 & 300,000 & -150,000 & 0 & 0 \\ 0 & -150,000 & 300,000 & -150,000 & 0 \\ 0 & 0 & -150,000 & 300,000 & -150,000 \\ 0 & 0 & 0 & -150,000 & 150,000 \end{bmatrix} kN/m, \quad (4.5)$$

and equation 4.6 shows the resultant matrix:

$$\mathbf{B^T S} = \begin{bmatrix} 0.500 & 0 & 0 & 0 & 0 & 0.250s & 0.186s & 0.144s & 0.119s & 0.106s \end{bmatrix}. \quad (4.6)$$

Matrix terms on the right-hand side of equation 4.6 are annotated with "s" indicating that the velocity terms have their own units.

4.4.2 Variable Stiffness Bang-Bang Control (VKBB)

For both control methodologies, the application of VKBB control is only slightly more difficult than CKBB control. Since the only nonlinearity present in our numerical examples comes in the form of a bilinear base isolator stiffness, $\mathbf{B^T S}$ must be calculated exactly twice. Equation 4.7 shows the stiffness matrix, $\mathbf{K}$ that is directly substituted into equation 4.2. $\mathbf{H}$ and $\mathbf{M}$ are as shown in equations 4.3 and 4.4:

$$\mathbf{K} = \begin{bmatrix} 154,500 & -150,000 & 0 & 0 & 0 \\ -150,000 & 300,000 & -150,000 & 0 & 0 \\ 0 & -150,000 & 300,000 & -150,000 & 0 \\ 0 & 0 & -150,000 & 300,000 & -150,000 \\ 0 & 0 & 0 & -150,000 & 150,000 \end{bmatrix} kN/m. \quad (4.7)$$

At each time step, the structural stiffness state must be determined and the corresponding $\mathbf{B^T S}$ substituted in the equation of motion. It is important to note, however, that when the post-yield tangent stiffness is employed in the $\mathbf{B^T S}$ compu-

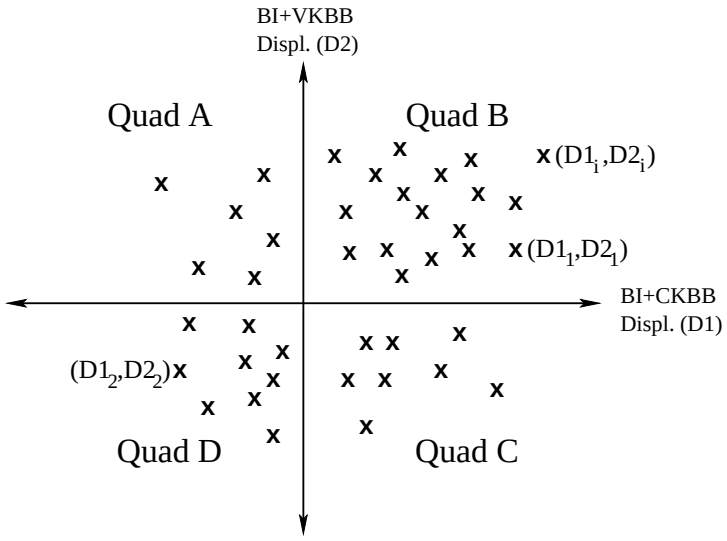

Figure 4.12: Symbolic Representation for Scatter Diagram of Displacement Data Points generated by Control Methodologies 1 and 2. The horizontal axis is base isolation plus constant stiffness bang-bang control (BI+CKBB). The vertical axis is base isolation plus variable stiffness bang-bang control (BI+VKBB).

tation, the relationship $\mathbf{C} = \alpha\mathbf{M} + \beta\mathbf{K}$ no longer holds, and hence, equation 3.53 is no longer valid. We circumvent this problem by computing a numerical solution to the Lyapunov equation. The result is:

$$\mathbf{B^T S} = \left[\begin{array}{ccccccccc} 0.619 & -0.06 & -0.035 & -0.016 & -0.008 & 0.293s & 0.21s & 0.157s & 0.127s & 0.113s \end{array} \right]. \tag{4.8}$$

The matrix elements in equations 4.6 and 4.8 have similar numerical values. The left-hand side of 4.8 evaluates to 0.619-0.06-0.035-0.016-0.008 = 0.5, which is identical to element(1,1) in equation 4.6. In equation 4.6 the sum of elements (1,6) through (1,10) is 0.805s. The same sum in 4.8 is 0.90s. The small increase in velocity coefficient values, as γ decreases from 0.18 to 0.03, is completely consistent with predictions made by the symbolic analysis.

4.4.3 Framework for Comparison of Control Strategies

In this section we present a simple framework for quantitatively evaluating the similarity between components of response in the time-history analyses.

Scatter Diagram. Figure 4.12 is a symbolic representation of the relationship of two random variables. This statistical evaluation considers the two time history base isolator displacements, D1 and D2, when base isolation (BI) + CKBB and BI+VKBB control is used, respectively. The probability mass density of (D1, D2) response coordinates can be represented in a scatter diagram. The number of data points in each quadrant of the scatter diagram is shown in Table 4.5.

Correlation Coefficients. The average values of the D1 and D2 are given by:

$$\overline{D1} = \frac{1}{N}\sum_{i=1}^{i=N} D1_i, \quad \overline{D2} = \frac{1}{N}\sum_{i=1}^{i=N} D2_i, \tag{4.9}$$

Measures of variance are given by [20]:

$$\sigma_{D1}^2 = \frac{1}{N}\sum_{i=1}^{i=N} \left(D1_i - \overline{D1}\right)^2. \tag{4.10}$$

$$\sigma_{D2}^2 = \frac{1}{N}\sum_{i=1}^{i=N} \left(D2_i - \overline{D2}\right)^2. \tag{4.11}$$

Measures of co-variance for displacements D1 and D2 are as follows:

$$\mu_{D1D2} = \frac{1}{N}\sum_{i=1}^{i=N} \left(D1_i - \overline{D1}\right) \cdot \left(D2_i - \overline{D2}\right) \tag{4.12}$$

With equations 4.9 through 4.12 in place, the correlation coefficient for "D1 and D2" is as follows:

$$\rho_{D1D2} = \frac{\mu_{D1D2}}{\sigma_{D1}\sigma_{D2}} \tag{4.13}$$

Because the mean square values are always positive, the correlation coefficient will always lie in the interval $[-1, 1]$ (i.e., $-1 < \rho_{D1D2} < 1$). One special case occurs when the variables D1 and D2 are statistically independent; $\mu_{D1D2} = 0$ and, hence, ρ_{D1D1} also equals 0. Based on our symbolic analysis of a simplified 2-DOF system, we expect the displacements, D1 and D2 to be strongly correlated – hence, ρ_{D1D2} should evaluate to a numerical value close to 1. The averages, standard deviations, co-variances, and correlation coefficients are given in table 4.6.

4.5 Summary of Results

Time history analyses are computed for 20 seconds at discrete intervals of 0.02 seconds. For the time interval $t \in [0, 15]$ seconds the structural system is subject to ground motion excitations plus external actuator forces applied by the control system. From $t \in [15, 20]$ seconds, the dynamic vibration is determined by the actuator forces alone.

Structural Drifts and Base Shear Forces. Figures 4.13 through 4.16 show time histories of structural drifts at the base isolator (node 1) corresponding to the scaled Kobe, San Fernando, Northridge, and Duzce ground motion inputs. Each plot contains contours of displacement for the constant stiffness (i.e., base isolation + CKBB) and variable stiffness (i.e., base isolation + VKBB) control strategies. To benchmark improvements in performance, a third contour for base isolation alone is also shown. A summary of peak values in base drift, structural drift, and base shear force for each of the three control cases is given in table 4.4. It is evident that, on average, peak displacements for constant stiffness bang-bang control (CKBB) are

21% smaller than those occurring for base isolation alone. With the sole exception of the 1971 San Fernando earthquake, CKBB increases structural drift by a modest amount. Thus, while active control works to decrease peak lateral displacements at the top of the isolator, these improvements in system performance must be "traded off" against a slight increase in internal forces and element-level displacements within the main structural system.

	Base Drift (mm)			**Structural Drift (mm)**			**Base Shear (kN)**		
Earthquake	BI	BI+ CKBB	BI+ VKBB	BI	BI+ CKBB	BI+ VKBB	BI	BI+ CKBB	BI+ VKBB
1971 San Fernando	447.60	368.90	368.90	12.38	12.29	12.29	2294.0	1940.0	1940.0
1994 Northridge	206.80	175.30	175.30	9.26	12.86	12.86	1210.0	1068.0	1068.0
1995 Kobe	260.70	203.00	203.00	8.31	10.15	10.15	1453.0	1193.0	1193.0
1999 Duzce	31.13	22.04	22.04	5.43	10.31	10.31	419.3	378.4	378.4

Table 4.4: Simulation Results: Peak Base/Structural Drifts and Base Shears

Earthquake	Quad A	Quad B	Quad C	Quad D	Total
1971 San Fernando	0	198	0	802	1000
1994 Northridge	0	645	0	355	1000
1995 Kobe	0	222	0	778	1000
1999 Duzce	0	270	0	730	1000

Table 4.5: Data Points in Each Quadrant of Scatter Diagram

Earthquake	Avg. D1 (mm)	Avg. D2 (mm)	Std. D1 (mm)	Std. D2 (mm)	Cov. D1,D2 (mm^2)	Corr. D1,D2
1971 San Fernando	-4.58	-4.58	80.61	80.61	6498.00	1
1994 Northridge	4.19	4.19	24.83	24.83	616.60	1
1995 Kobe	-6.13	-6.72	55.03	55.09	3031.00	0.9999
1999 Duzce	-2.29	-2.29	6.01	6.01	36.05	1

Table 4.6: Statistical Comparison of Time-Histories of Displacement. Measures include average values, standard deviations, covariances, and correlation coefficients

The summary of statistical metrics in table 4.6 shows an exact correlation in displacements (i.e., $\rho = 1$) generated by BI+CKBB and BI+VKBB for three of the ground motion inputs, and an extremely strong correlation in displacements generated by the 1995 Kobe earthquake.

The cause-and-effect and sensitivity analysis predictions enabled by symbolic analysis of the two-DOF system (for details, see section 3.3), correspond well to numerical results from time history analysis of the five-DOF model. Readers should note the dominance of first mode vibrations in both the elastic and inelastic states: ($\Gamma_1 = 1.11$ in the elastic state and $\Gamma_1 = 1.02$ in the inelastic state). For a 2-DOF model with γ varying between $0.03 \leq \gamma \leq 0.18$ and $\tau = 0.00265$ secs^2, Figures 3.7 through 3.9 validate these observations show that there will be very little change in the velocity coefficients of $\mathbf{B^T S}$.

Nonlinear Force-Displacement Response. Figures 4.17 through 4.20 show time histories of force-displacement in the base isolator (node 1) generated by the scaled Kobe, San Fernando, Northridge, and Duzce ground motion inputs. As expected, peak overall displacements are dominated by the contribution of plastic deformations of the base isolator. The tangent stiffness (i.e., slope of the force-displacement curve) in the pre- and post-yield domains is consistent with the material and section properties described in Section 4.1 and illustrated in Figure 4.2.

Internal Element and Actuator Forces. Figures 4.21 through 4.24 show time histories of internal element forces and actuator forces for system responses generated by the scaled Kobe, San Fernando, Northridge, and Duzce ground motion inputs. In our symbolic analysis for the bang-bang control of a one-degree of freedom system – see Figures 3.1 through 3.3 for the forced vibration case and Figures 3.4 through 3.6 for the free vibration case – we demonstrated that actuator force is "almost in phase" with velocities and and "almost completely out of phase" (i.e.,

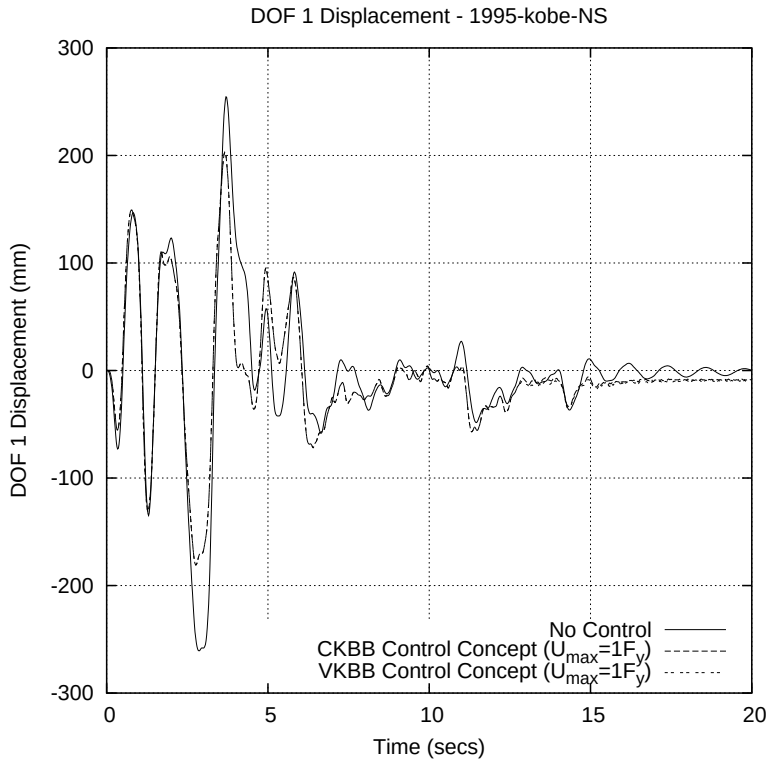

Figure 4.13: CKBB/VKBB Control Comparison: Base Isolator Drift for 1995 Kobe

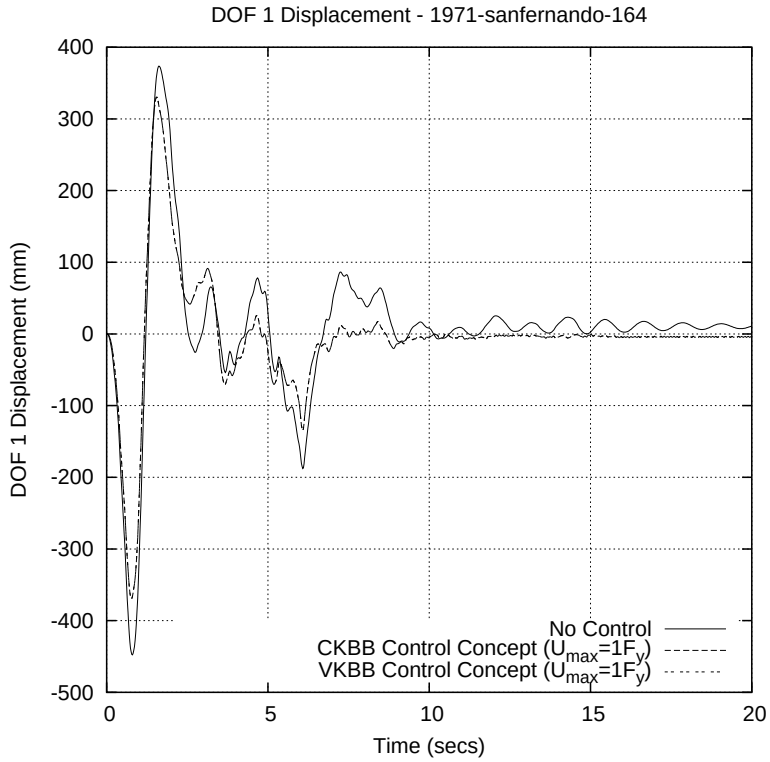

Figure 4.14: CKBB/VKBB Control Comparison: Base Isolator Drift for 1971 San Fernando

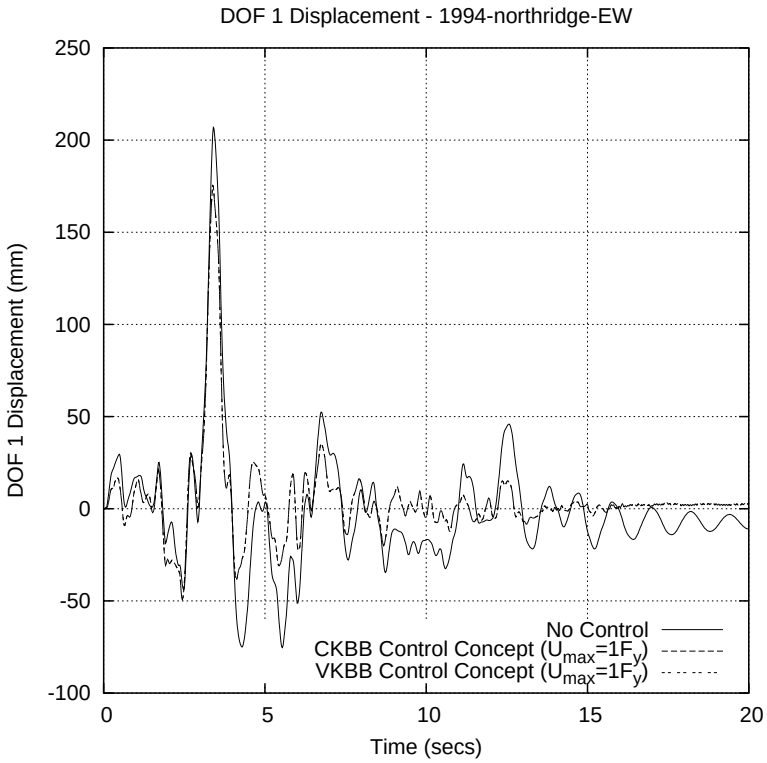

Figure 4.15: CKBB/VKBB Control Comparison: Base Isolator Drift for 1994 Northridge

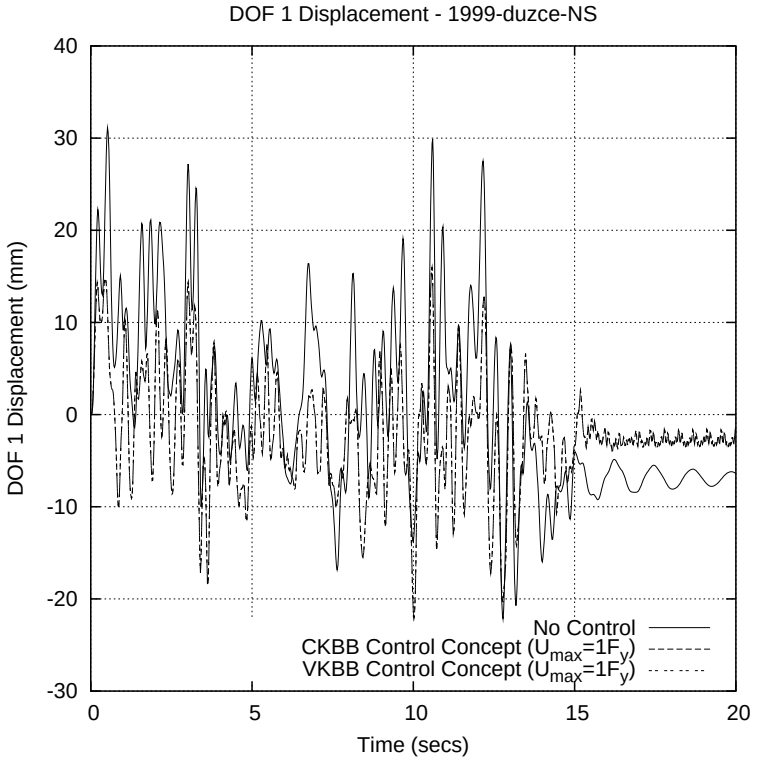

Figure 4.16: CKBB/VKBB Control Comparison: Base Isolator Drift for 1999 Duzce

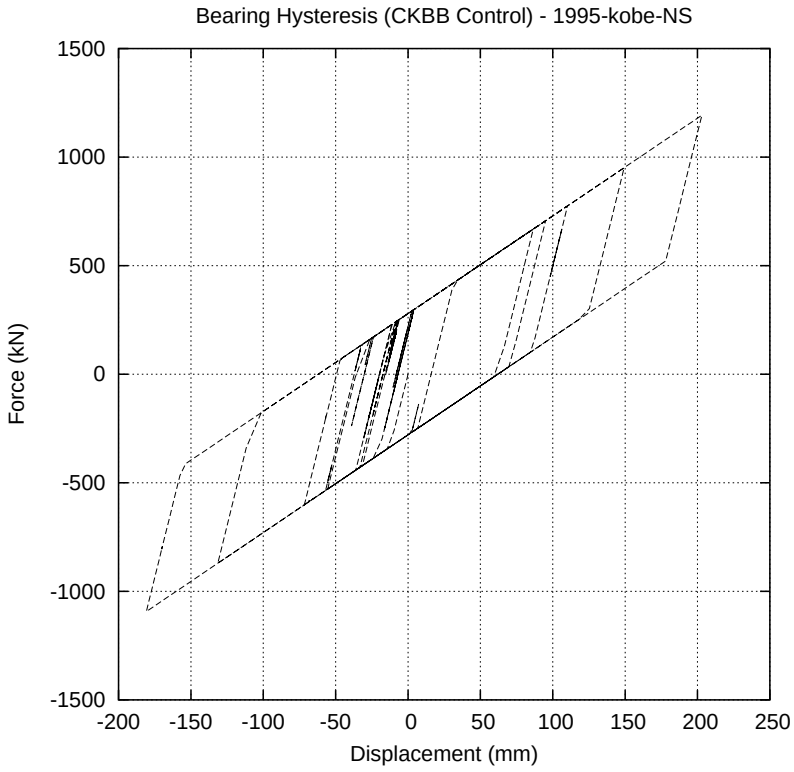

Figure 4.17: Base Isolator Hysteresis: 1995 Kobe.

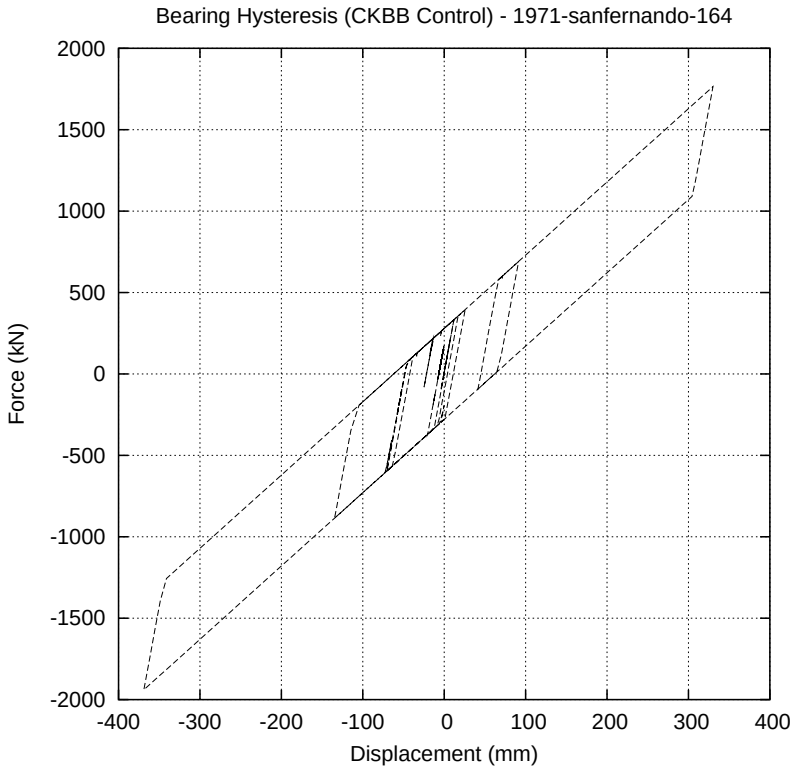

Figure 4.18: Base Isolator Hysteresis: 1971 San Fernando

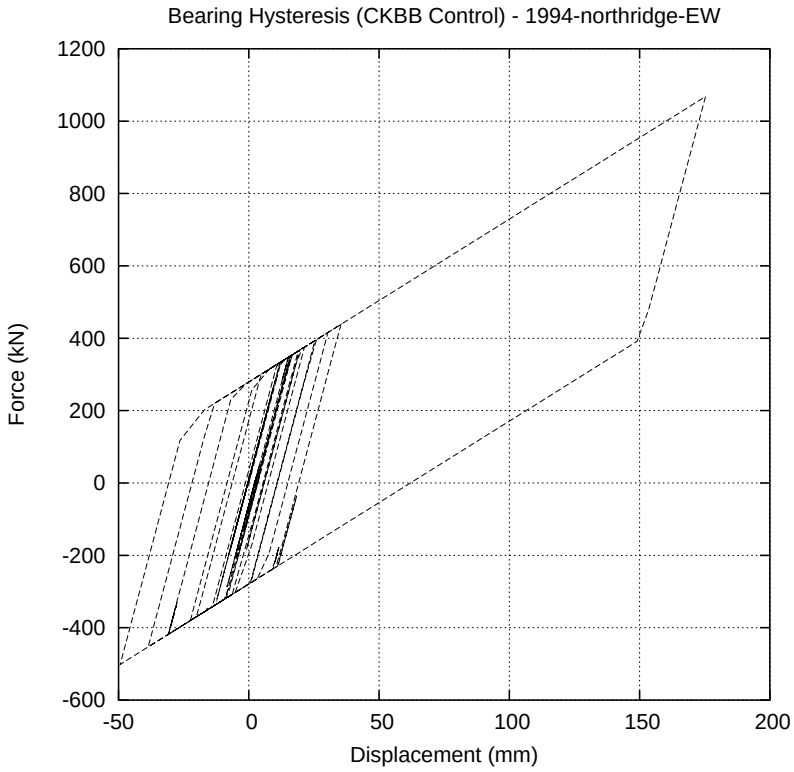

Figure 4.19: Base Isolator Hysteresis: 1994 Northridge

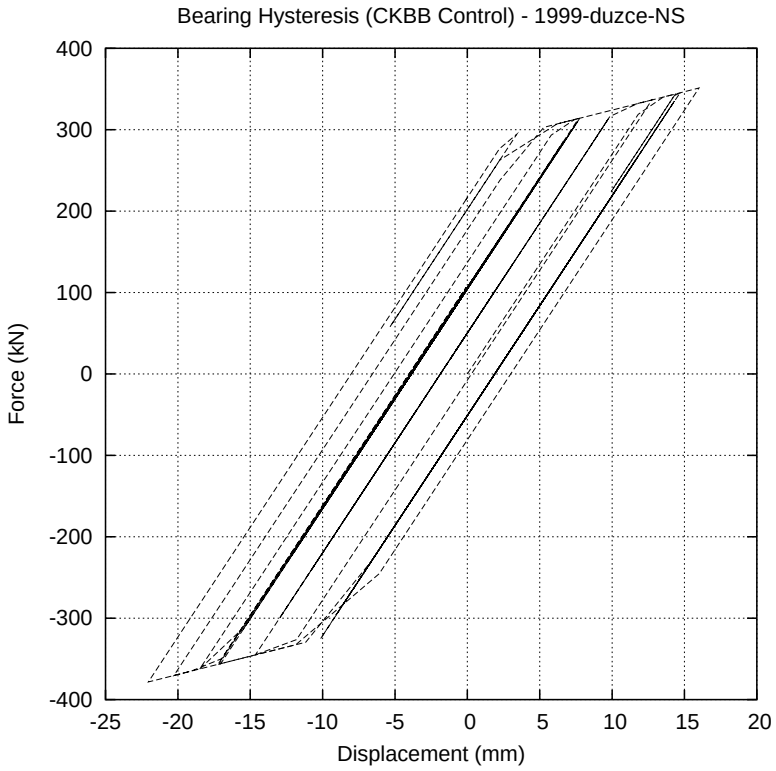

Figure 4.20: Base Isolator Hysteresis: 1999 Duzce

$\pi/2$ radians) with displacements. (This relationship between bang-bang control actuator forces and displacements and velocities is investigated further in a paper by Sebastianelli and Austin [64]). Figures 4.21 and 4.22, in particular, validate this prediction.

Notice, however, that at the end of the displacement-time histories for all the earthquakes, the top of the base isolator oscillates around a zero displacement and the actuator force switches between $\pm u_{max} = 350$ kN at a high frequency. During the "post ground shaking" phase of the time-history response, the actuator adds very little value in terms of reduced displacements and it should be turned off!

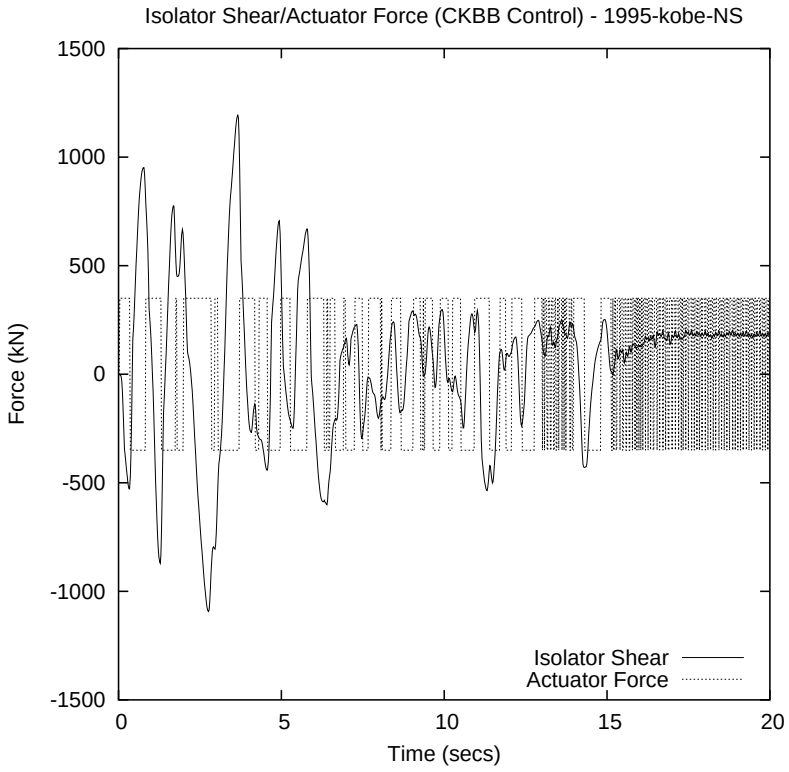

Figure 4.21: Isolator/Actuator Force: 1995 Kobe

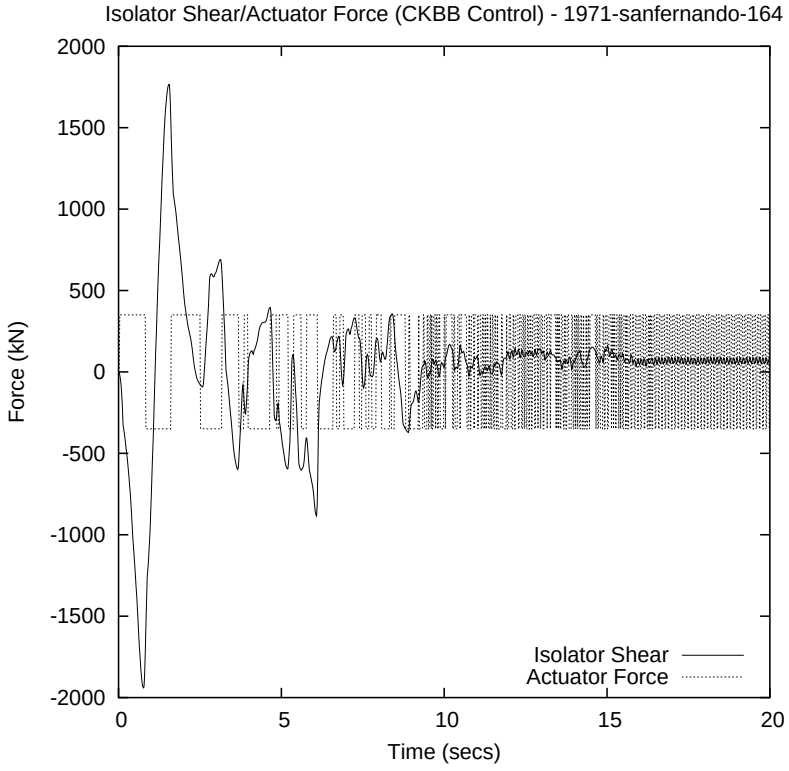

Figure 4.22: Isolator/Actuator Force: 1971 San Fernando

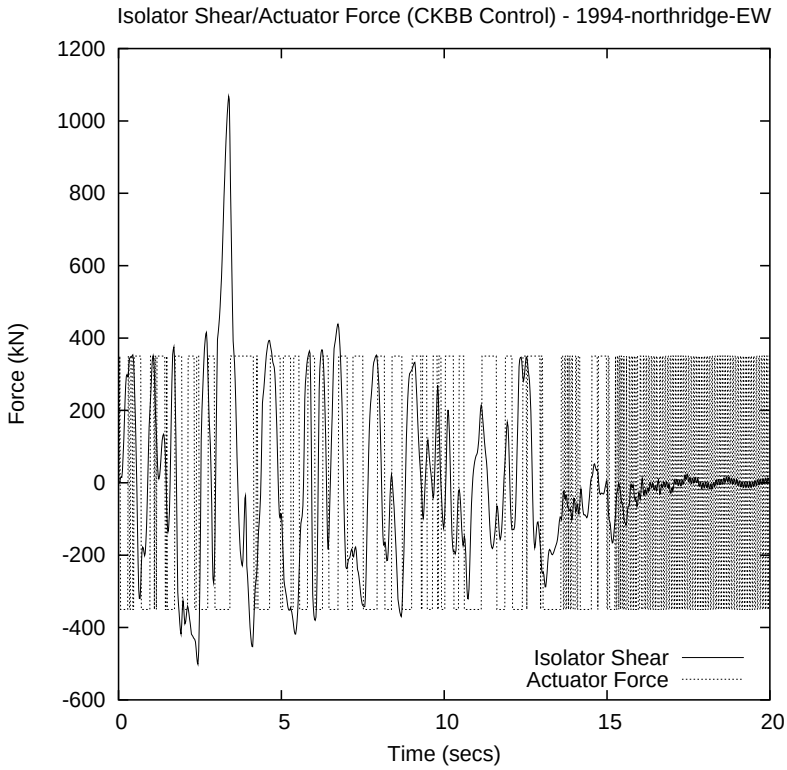

Figure 4.23: Isolator/Actuator Force: 1994 Northridge

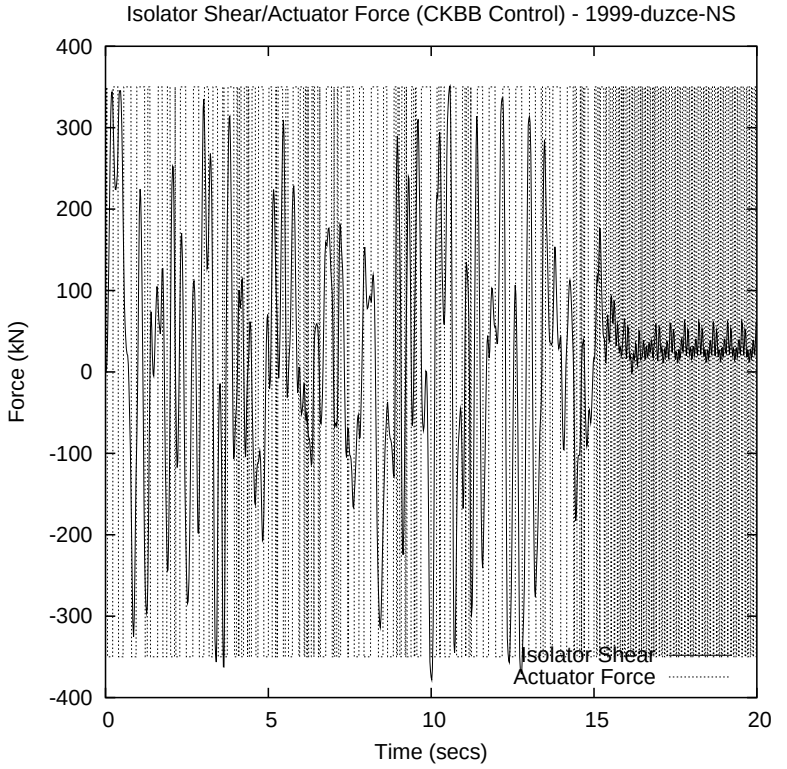

Figure 4.24: Isolator/Actuator Force: 1999 Duzce

Chapter 5

Energy- and Power-Balance Analysis

5.1 Background

Ideas in energy-based design date back to Housner [34, 35] in the 1950s, and have recently been revised by a number of researchers, including Powell and Allahabadi [56], Fajfar [28], and Bertero and co-workers [85, 89]. Generally speaking, these papers fall into three categories: (1) proposals for empirical design methods based upon energy ideas, (2) uses of energy in the performance assessment of energy dissipation devices and/or structural system configurations, and (3) analytical procedures for energy-balance calculations. As a result of this work, it is now understood that use of energy concepts provides:

1. A theoretical framework for connecting estimates of seismic input energy to spatial and temporal distributions of energy demand on structural subsystems and elements. The energy capacity of a structure is represented by the elastic capacity plus energy dissipation capacity associated with damping and key structural elements undergoing cyclic nonlinear deformations.

2. A rational means for accurately estimating the capacity of a structure. For example, it is now widely recognized that levels of damage caused by earthquakes do not depend on peak displacements alone. Instead, the cumulative damage from numerous inelastic cycles should be taken into account [28, 56].

The use of energy concepts in seismic design and analysis is appealing because very complex spatial and temporal distributions of linear/nonlinear deformations can

be represented by mathematical scalars (i.e., simple mathematical models). From a numerical analysis viewpoint, an energy balance check provides a means of validating the computations are stable and accurate.

5.2 Formulation of Energy-Balance Equations

Equation of Motion.

The left-hand side of Figure 5.1 shows the coordinate scheme for dynamics of a multi-degree of freedom structure subject to a horizontal time-varying base motion (actuators not shown). With respect to an absolute coordinate scheme, the equations of equilibrium, given in equation 1.1 may also be written as:

$$\mathbf{M}\ddot{x}_t(t) + \mathbf{F}(\dot{x}(t), x(t)) = \mathbf{H}u(t) \tag{5.1}$$

with initial conditions $x_t(0)$ and $\dot{x}_t(0)$. Here $x_t(t) = [x_{1t}(t), x_{2t}(t) \ ... \ x_{nt}(t)]^T$ is a $(n \times 1)$ vector of *absolute* system displacements, $\mathbf{M}$ is a $(n \times n)$ mass matrix, and $\mathbf{F}(\dot{x}(t), x(t))$ is a $(n \times 1)$ vector of straining and damping forces depending on displacements and velocities measured *relative* to the base motion. In other words, $\mathbf{F}(\dot{x}(t), x(t)) = \mathbf{F}_{\text{damping}}(\dot{x}(t), x(t)) + \mathbf{F}_{\text{straining}}(\dot{x}(t), x(t))$. As in section 1.3, $\mathbf{H}$ is an n x p matrix that designates the location of the controller(s), while $u(t)$ is a p-dimensional vector that represents the control force of p-number of controllers.

The relationship between absolute and relative displacements is simply given by:

$$x_t(t) = x(t) + rx_g(t) \tag{5.2}$$

where $x_g(t)$ is the horizontal ground displacement and $\mathbf{r}$ is a $(n \times 1)$ vector describing the movement in each of the structural degrees of freedom due to a unit ground displacement, Substituting equation 5.2 into 5.1 and rearranging terms gives:

$$\mathbf{M}\ddot{x}(t) + \mathbf{F}(\dot{x}(t), x(t)) = \mathbf{H}u(t) - \mathbf{M}r\ddot{x}_g(t) \tag{5.3}$$

The right-hand side of Equation 5.3 is a vector of equivalent external loads applied at the nodal degrees of freedom caused by the earthquake ground motions plus, actuator forces applied to the external degrees of freedom. As before, $\ddot{x}_g(t)$ is the ground acceleration at time t. Note that in equation 1.1, $\mathbf{F}(\dot{x}(t), x(t))$ is express as the damping ($\mathbf{C}\dot{x}(t)$) and stiffness ($\mathbf{K}x(t)$) of the structure.

In moving from equations 5.1 to 5.3 we are removing the effects of rigid-body displacements from the problem formulation. From a computational standpoint, this is desirable because matrix equations 5.3 may be written entirely in terms of relative displacements (and ground displacements).

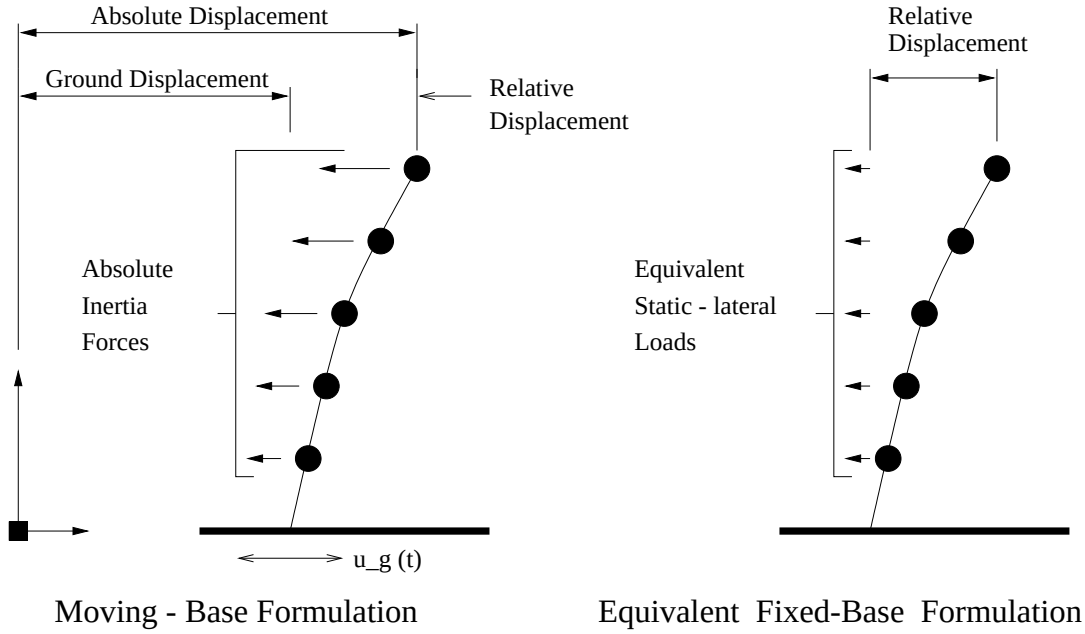

Figure 5.1: Moving- and Equivalent-base Models of System Response (forces due to active control not shown)

Energy-Balance Equations.

Let $\mathbf{R}(\dot{x}(\tau), x(\tau))$ be a force that depends on displacements $x(\tau)$ and velocities $\dot{x}(\tau)$. The work done by $\mathbf{R}(\cdots)$ over the time interval $\tau \in [0, t]$ is denoted $W(t)$, and is given by:

$$\mathrm{W(t)} = \int_0^t \dot{x}^T(\tau) \cdot \mathbf{R}(\dot{x}(\tau), x(\tau)) d\tau \tag{5.4}$$

At the highest level of abstraction the energy balance equations can be written:

$$\mathbf{W}_{\mathrm{int}}(t) + \mathbf{T}(t) = \mathbf{W}_{\mathrm{act}}(t) + \mathbf{W}_{\mathrm{eq}}(t) = \mathbf{W}_{\mathrm{ext}}(t), \tag{5.5}$$

where $\mathbf{W}$, without subscripts, represents work done and $\mathbf{T}$ represents kinetic energy. Equation 5.5 states that the work done by external loads/forces is converted to kinetic energy and/or internal energy. In this section we derive energy balance equations for (1) the moving base formulation, and (2) the equivalent fixed-base formulation. Energy balance equations have been formulated by Austin and Lin [5] in both the moving- and fixed-base coordinate frames. These energy balance equations are modified to account for the work done by the active control and used in energy-balance assessment.

Concept of Positive Versus Negative Work. The work done by a force acting on a body can by either positive or negative. Work done by a force is positive if the applied force has a component in the direction of the displacement; hence, work done by a force is negative if the applied force has a component in the direction opposite of the displacement. For example, when a body is falling, the force of gravity is acting in the downward direction. The displacement is also in the downward direction. Thus the work done by the gravitational force on the body is positive. Now consider the same body being lifted in a upward direction. In this case, the force of gravity is still acting in a downward direction, but the displacement of the body is in a upward direction. The work done by the force of gravity on the body

is negative [81].

5.3 Energy-Balance Equations for Equivalent Fixed-Based (or Relative) System

Substituting equation 5.1 into 5.4 and rearranging terms gives:

$$\int_0^t \dot{x}^T(\tau)\mathbf{M}\ddot{x}(\tau)d\tau+\int_0^t \dot{x}^T(\tau)\mathbf{F}(\dot{x}(\tau),x(\tau))d\tau = \int_0^t \dot{x}^T(\tau)\mathbf{H}u(\tau)d\tau-\int_0^t \dot{x}^T(\tau)\mathbf{M}r\ddot{x}_g(\tau)d\tau \tag{5.6}$$

The left-most term represents the work done by nodal inertia forces. The second term represents the work done by internal forces – due to condensation of boundary nodes, internal energy can be expressed in terms of relative displacements and velocities alone. The first term on the right-hand side represents the work done by the actuator forces $\mathbf{H}u(t)$ moving through relative displacements $x(t)$. The right-most term represents work done by equivalent static lateral nodal forces -$\mathbf{M}r\ddot{x}_g(t)$ moving through relative displacements $x(t)$. Integrating the left-most term by parts gives the kinetic energy, $\mathbf{T}(x(t))$, associated with relative displacements alone–it equals the integral of work done by equivalent static lateral node forces over the time interval [0, t].

5.4 Discrete Approximation for Energy-Balance Equations

Discrete approximation of the energy balance equations is necessary when they are being used in a iterative, time-step analysis. Discrete approximation of the energy balance equations for only the fixed-base (or relative) coordinate frame is considered here.

The internal work, $\mathbf{W}_{\text{int}}(t+\Delta t)$, represents the work done by the internal nodal forces moving through the degree of freedom displacements, and is given by

$$\mathbf{W}_{\text{int}}(t+\Delta t) = \mathbf{W}_{\text{int}}(t) + \int_t^{(t+\Delta t)} \dot{\mathbf{W}}_{\text{int}}(\tau) d\tau. \tag{5.7}$$

For damped systems, internal nodal forces, $\mathbf{F}_{\text{int}}$, are the sum of damping and straining force components. The rate of internal work is given by:

$$\dot{\mathbf{W}}_{\text{int}}(t) = \dot{x}(t)^T \mathbf{F}_{\text{int}}(t) = \dot{x}(t)^T \Big[\mathbf{F}_{\text{straining}}(t) + \mathbf{F}_{\text{damping}}(t)\Big]. \tag{5.8}$$

Substituting 5.8 into 5.7 and approximating the integral by the trapezoidal rule gives

$$\mathbf{W}_{\text{int}}(t+\Delta t) = \mathbf{W}_{\text{int}}(t) + \frac{\Delta t}{2}(\dot{x}(t)^T \mathbf{F}_{\text{int}}(t) + \dot{x}(t+\Delta t)^T \mathbf{F}_{\text{int}}(t+\Delta t)). \tag{5.9}$$

The work done by externally applied nodal loads is given by

$$\mathbf{W}_{\text{ext}}(t+\Delta t) = \mathbf{W}_{\text{ext}}(t) + \int_t^{(t+\Delta t)} \dot{\mathbf{W}}_{\text{ext}}(\tau) d\tau. \tag{5.10}$$

For the equivalent fixed-base formulation, the rate of work done by earthquake loads is $\dot{W}_{\text{eq}}(t) = -\dot{x}^T(t)\mathbf{M}r\ddot{u}_g(t)$. Approximating equation 5.10 by the trapezoidal rule gives

$$\mathbf{W}_{\text{eq}}(t+\Delta t) = \mathbf{W}_{\text{eq}}(t) + -\frac{\Delta t}{2}(\dot{x}(t)^T \mathbf{M}r\ddot{x}_g(t) + \dot{x}(t+\Delta t)^T \mathbf{M}r\ddot{x}_g(t+\Delta t)). \tag{5.11}$$

Similarly, the rate of work done by actuator forces is $\dot{W}_{\text{act}}(t) = \dot{x}^T(t)\mathbf{H}u(t)$. Approximating equation 5.10 by the trapezoidal rule gives

$$\mathbf{W}_{\text{act}}(t+\Delta t) = \mathbf{W}_{\text{act}}(t) + \frac{\Delta t}{2}(\dot{x}(t)^T \mathbf{H} u(t) + \dot{x}(t+\Delta t)^T \mathbf{H} u(t+\Delta t)). \quad (5.12)$$

The kinetic energy at time t is given by:

$$\int_0^t \dot{x}^T(\tau)\mathbf{M}\ddot{x}(\tau)d\tau = \frac{1}{2}\Big[\dot{x}^T(\tau)\mathbf{M}\dot{x}(\tau)\Big]_0^t = \mathbf{T}(\dot{x}(t)). \quad (5.13)$$

Chapter 6

Control Concept Performance Assessment

6.1 Objectives and Scope

For a wide range of moderate-to-large ground motion events, base isolated structures are expected to exhibit nonlinear displacement behavior at the isolator level, leaving the main structural system undamaged. While quantitative measurements such as peak values of velocity are a good indicator of non-structural damage [40], energy- and power-balance metrics of system performance provide a means for accurately estimating the capacity of a structure to resist forces elastically and dissipate energy associated with damping and key structural elements undergoing cyclic nonlinear deformations. Accordingly, in this chapter we exercise the theoretical framework for energy- and power-balance analysis by computing the time-history response of a six-DOF nonlinear mass-spring-damper system subject to an ensemble of moderate and severe ground excitations, plus constant stiffness bang-bang (CKBB) control. The purposes of the numerical experiment are three-fold:

1. To calculate the work done by the base isolators, superstructure, and actuators,

2. To assess the ability of present-day actuator technologies to deliver actuator power requirements estimated through simulation, and

3. To identify and quantitatively evaluate situations (e.g., moderate versus severe earthquake; expected versus unexpected ground motions) when CKBB control has the potential for adding significant value to overall performance, compared to base isolation alone.

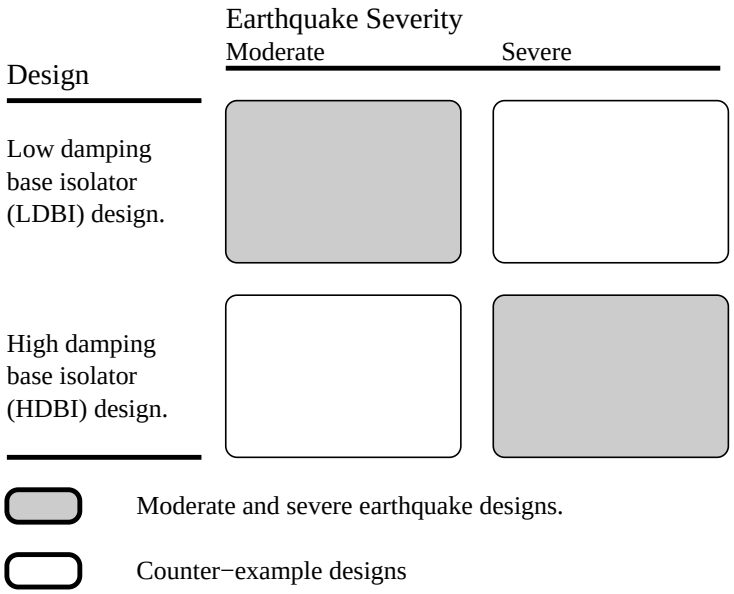

Figure 6.1: Scope of Case Study and Counter-Example Designs covered by the Numerical Experiments

Item 3 can be derived, in part, from the first two objectives and time histories of base drift. The scope of this chapter is restricted to constant stiffness bang-bang (CKBB) control; this decision is enabled by findings in section 3.3.

The numerical experiment covers the range of cases shown in figure 6.1. The shaded boxes show the two case-study designs: (1) a low damping base isolation (LDBI) system designed to withstand ground motions of moderate intensity, and (2) a high damping base isolation (HDBI) system designed to withstand ground motions of severe intensity. Details of the LDBI and HDBI design procedures will be explained in section 6.2.2. The unfilled boxes show the two design counter-examples: (1) the LDBI system is subject to a severe earthquake, and (2) the HDBI system is subject to a moderate earthquake. The purpose of the counter-examples is to see how well CKBB control works when seismic events of an unexpected size occur. To quantify improvements in performance due to control, the actively controlled time history responses are benchmarked against corresponding LDBI/HDBI systems responses for base isolation alone. All numerical computations are implemented with

the Aladdin scripting language [6, 7].

6.2 Actively Controlled Mass-Spring-Damper System

Figure 6.2 shows an elevation view of the six-DOF idealized mass-spring-damper model. This model has previously been employed by Ramallo et al. [57], which in turn can be traced to a five-story building model used by Kelly et al. [41]. Tables 6.1 and 6.2 summarize the structural parameters for the low damping base isolator (LDBI) design. For both the LDBI and HDBI designs the mass and damping properties are as shown in table 6.1. Table 6.3 summarizes the structural parameters for the high damping base isolator (HDBI) design. LDBI and HDBI designs are discussed in section 6.2.2. Boundary conditions for the model are full-fixity at the base and full-fixity against vertical displacements and rotations at nodes 2 through 6.

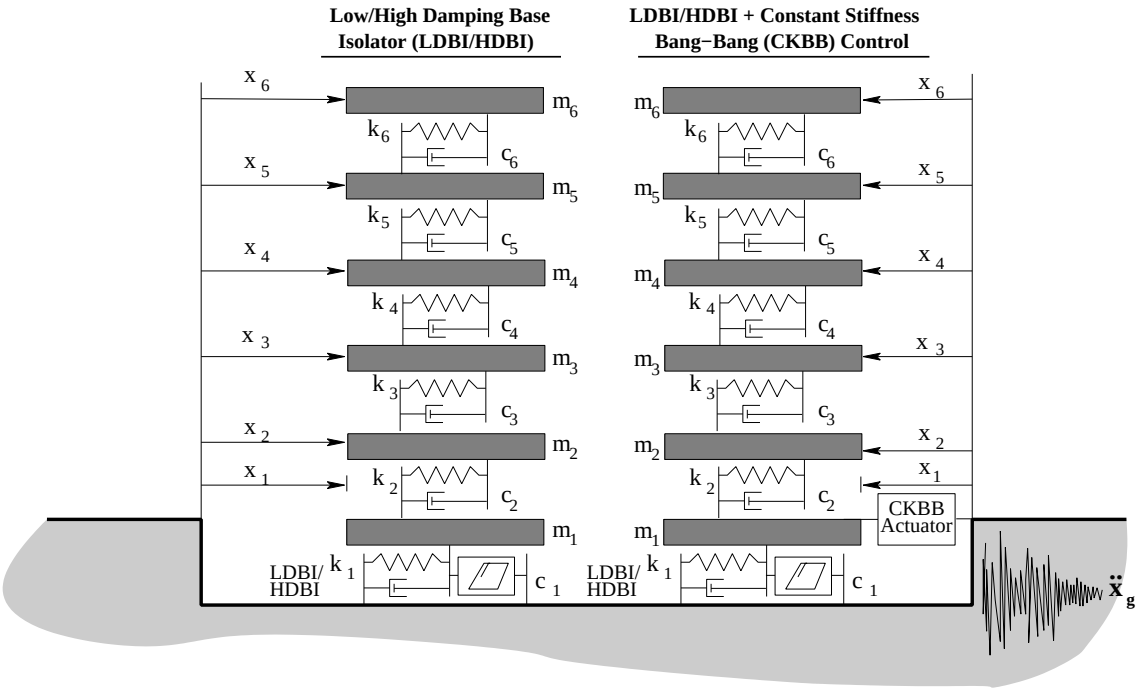

Figure 6.2: Elevation View of 6 DOF Linear/Nonlinear Mass-Spring-Damper System

	Floor	Damping	Stiffness (kN/m)	
DOF/Mode	Mass (kg)	(kN·s/m)	Pre-yield	Post-yield
1	6,800	3.74	1,392	232
2	5,897	67	33,732	33,732
3	5,897	58	29,093	29,093
4	5,897	57	28,621	28,621
5	5,897	50	24,954	24,954
6	5,897	38	19,059	19,059

Table 6.1: Mass, Damping and Stiffness Properties of Six-DOF Mass-Spring-Damper Model with Low Damping Base Isolator (LDBI)

	Period (secs)		Part. Factor (Γ)	
DOF/Mode	Pre-yield	Post-yield	Pre-yield	Post-yield
1	1.05	2.50	1.05	1.01
2	0.18	0.18	0.06	0.01
3	0.10	0.10	0.01	0.00
4	0.07	0.07	0.01	0.00
5	0.05	0.05	0.00	0.00
6	0.05	0.05	0.00	0.00

Table 6.2: Natural Periods of Vibration and Modal Participation Factors for Six-DOF Mass-Spring-Damper Model: with Low Damping Base Isolator (LDBI)

	Stiffness (kN/m)		Period (secs)		Part. Factor (Γ)	
DOF/Mode	Pre-yield	Post-yield	Pre-yield	Post-yield	Pre-yield	Post-yield
1	2,320	232	0.83	2.50	1.08	1.01
2	33,732	33,732	0.18	0.18	0.09	0.01
3	29,093	29,093	0.10	0.10	0.02	0.00
4	28,621	28,621	0.07	0.07	0.01	0.00
5	24,954	24,954	0.05	0.05	0.01	0.00
6	19,059	19,059	0.05	0.05	0.00	0.00

Table 6.3: Properties of Six DOF Mass-Spring-Damper Model with High Damping Base Isolator (HDBI)

6.2.1 Modeling Damping Mechanisms

In this dissertation, base isolation alone is considered the baseline damping mechanism against which the performance of base isolation + CKBB control will be evaluated. Modeling approaches for these two damping mechanisms are as follows:

1. **Base Isolation (BI) Alone.** The BI element is modeled as a bilinear solid with a force-displacement relationship that follows the kinematic hardening rule. This element was used by Lin [44] and is a model of a laminated rubber BI with a lead core. The initial and post-yield shear stiffnesses of the isolator are $K_{initial}$ and K_{yield}, respectively. The latter is generated by the stiffness of the rubber, and is fixed at ($K_{yield} = 232$ kN/m), as to give a 2.5 second fundamental post-yield period. Pre-yield to post-yield ratios, as well as the isolator yield force, F_y, are left as design parameters; the design details are discussed in section 6.2.2. The scope of this dissertation is restricted to two values that give good performance for both moderate and severe ground motions. Viscous damping from the rubber is assumed to be 2% critical damping.

2. **Base Isolation (BI)+Constant Stiffness Bang-Bang (CKBB) Control.** In the second model, the BI mechanism is supplemented by a controllable actuator that switches from one extreme to another (i.e., the control force is always exerting its maximum force in either the positive or negative direction). Solutions to the CKBB control problem are based on energy-inspired formulations of the Lyapunov equation, the details of which may be found in section 1.6.

It is important to emphasize that the BI in each of these two systems is identical (i.e., CKBB control *supplements* the BI damping mechanism). The only difference between these two systems is that one only has a BI passive damping mechanism, and the other has both a BI passive damping mechanism and a CKBB control active damping mechanism.

6.2.2 Base Isolator (BI) Design

Ramallo et al. [57] considers two parameters in the design of the BI, the total yield force, F_y, which is expressed as a fraction of the total structural weight, and the pre-yield to post-yield stiffness ratio of the BI, $K_{initial}/K_{yield}$. To obtain a post-yield fundamental period of 2.5 seconds, the post-yield stiffness is fixed at $K_{yield} = 232$ kN/m. The research supporting the low- and high-damping base isolator design procedures is as follows:

1. **Low Damping Base Isolator (LDBI).** Skinner et al. [65] suggest that for earthquakes having the "severity and character" of El Centro, typical values of the yield force (F_y) should be around 5% of the total structural weight. Park and Otsuka [53] recommend that F_y range from 4.3 to 5% of the total structural weight for moderate earthquakes (peak ground acceleration (PGA) of 0.35g). In a third study by Ramallo et al. [57], plots of base drift and structural acceleration as a function of F_y for several values of the stiffness ratio, $K_{initial}/K_{yield}$ were constructed for two- and six-DOF models. The latter study suggests that in order to obtain moderate base drift and acceleration reduction for a ground excitation with PGA=0.35g, use $F_y = 5\%$ of the total structural weight and $K_{initial}/K_{yield} = 6$. This low damping base isolation system falls into the "Class (ii): lightly damped" category of Skinner et al. [65].

2. **High Damping Base Isolator (HDBI).** For severe earthquake events, such as the Kobe and Northridge earthquakes, Ramallo et al. [57] found that in order to obtain significant reductions in base drift and moderate accelerations, BI yield strengths and stiffness ratios need to be increased (relative to optimal values for moderate ground motions). Similar observations are reported by Park and Otsuka [53]. They found that for severe ground motion attacks (i.e.,

PGA of 1.225g), system performance is best when F_y in the range 14 to 18% of total structural weight.

Hence, in this dissertation, the low damping base isolation (LDBI) design has F_y = 14.46 kN (which is 5% of the building weight) and $K_{initial}/K_{yield} = 6$. As noted by Ramallo et al. [57], the LDBI design is typical of low damping isolation systems used in engineering practice, is readily attainable using current technology, and follows standard AASHTO code procedures [1]. The high damping base isolator (HDBI) design has a yield force of F_y = 43.39 kN = 15% of the building weight and a stiffness ratio of $K_{initial}/K_{yield} = 10$. HDBI designs are not widely used in practice at this time. This may change, however, since there is now significant concern [31, 32, 68] that base isolated buildings may not be able to accommodate severe near-fault earthquakes.

The results of this dissertation will evaluate under which conditions CKBB control is most likely to be beneficial to base isolation. Based on four design-based scenarios (a full description of these scenarios is given in section 6.4), we will compare the performance of LDBI to LDBI+CKBB control damping mechanism. Likewise, we compare the performance of HDBI to HDBI+CKBB.

6.2.3 Actuator Placement and Characteristics

This section describes issues associated with actuator placement and performance (i.e., actuator force/reach and on/off characteristics).

Actuator Placement. Housner et al. [33] and Reinhorn et al. [58] state that one potential reason for supplementing passive base-isolated structures with active control is that the combination of active control with base isolation can potentially achieve both low interstory drift, and at the same time, limit the maximum base

displacement with a single set of control forces. Hence, in this dissertation, the effect of CKBB control will be illustrated with a single actuator located at the top of the BI (degree of freedom 1).

Duration of Performance. In section 4.5, it was shown that at the end of the displacement-time histories for all the earthquakes used in the simulations, the top of the base isolator oscillates around a zero displacement and the actuator force switches between $\pm u_{max} = 350$ kN at a high frequency; this adds very little value in terms of reduced displacements. Also, near the end of the ground excitation, the actuator dominates the response of the structure and is likely injecting mechanical energy into the structural system. This input of mechanical energy into the structural system has the potential to destabilize the system in a bounded input/bounded output sense. It will be discussed in section 6.3 that moderate ground excitations are constrained to the same Arias Intensity at the end of the time history; likewise, the Arias Intensity is constrained for each accelerogram in the severe classification.

Since Arias Intensity accounts for energy characteristics of the accelerogram throughout the entire duration of ground excitation, we will use this parametric to limit the duration in which the actuator is on. Arias Intensity is described in section 4.3. In this dissertation, when the Arias Intensity for a particular accelerogram reaches 90% of its constrained value (1.29 m/sec and 10.86 m/sec for moderate and severe earthquakes, respectively), the actuator will be turned off. Figure 6.3 shows the actuator being turned off when an Arias Intensity of 10.86 m/sec is reached for the 1971 San Fernando earthquake. The 1971 San Fernando earthquake reaches an Arias Intensity of 10.86 m/sec 6.62 seconds into the time history. This actuator force time history is for a scenario in which a high damping base isolator supplemented with CKBB control is subjected to the 1971 San Fernando earthquake. The scenarios which we evaluate in this dissertation are discussed in section 6.4.

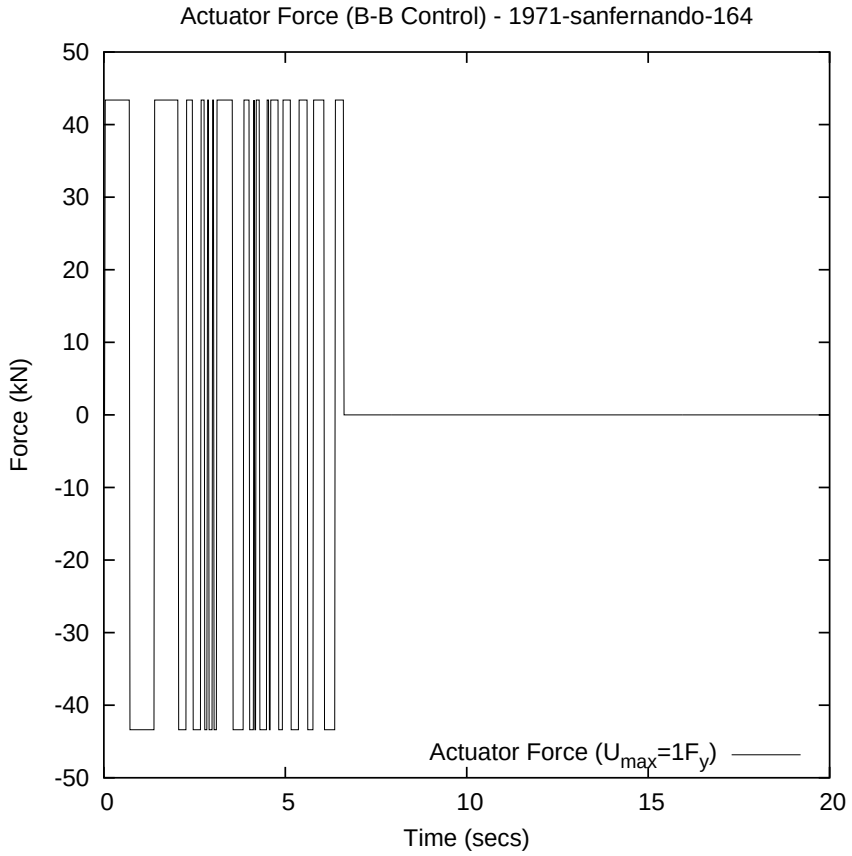

Figure 6.3: Actuator Time History Subjected to 1971 San Fernando

Magnitude of Actuator Force. In order to provide for a fair comparison between the performance of a passive BI damping mechanism and a hybrid LDBI/HDBI+CKBB damping mechanism, the maximum force, u_{max}, that the actuator can exert is limited. We proceed under the assumption that the LDBI/HDBI+CKBB will not add value to the overall system performance unless the passive and active damping components can work in concert. Skinner et al. [65], Wang and Liu [90], Park and Otsuka [53], and Ramallo et al. [57] have shown that LDBI and HDBI perform well for moderate and severe ground excitations with yield forces, F_y, equal to 5% and 15% of the total weight of the building, respectively. Thus, for a fair comparison, when CKBB control is used, the magnitude of the actuator force will be associated with the LDBI and HDBI as follows: for LDBI designs, $u_{max} = F_y = 14.46$ kN,

and for HDBI designs, u_{max} =F_y = 43.39 kN. Furthermore, in this dissertation, the actuator is assumed ideal, i.e., it can exert the required high-speed switching forces that are required for CKBB control and it can exert these dissipative forces without time delay or actuator dynamics.

6.3 Ground Excitation

All of the accelerograms used in this dissertation were scaled from accelerograms obtained from the Pacific Earthquake Engineering Research (PEER) Center Strong Motion Database [27]. Johnson et al. [36] and Spencer et al. [68] point out the recent concern regarding the effectiveness of base isolation to protect structures against near-source, high-velocity, severe earthquakes. Hence, the library of earthquake records used in this dissertation are broken into two classifications, namely, moderate and severe earthquakes. Figures 6.6 through 6.9 show the moderate classification of earthquakes used here – the 1940 El Centro, 1979 El Centro, and 1992 Landers earthquakes. The severe earthquakes used here are the same as those used section 4.3 and shown in figures 4.3 through 4.6 – the 1971 San Fernando, 1994 Northridge, 1995 Kobe, and 1999 Duzce earthquakes. The same preprocessing of earthquakes was followed here as in section 4.3. Specifically, the scaled design ground motions were obtained by first isolating the worst fifteen second sample of each record. Each record was then translated along the y-axis to remove residual velocity effects. Moderate and severe earthquake records were then scaled in the following manner:

Moderate Earthquake Events. The Arias Intensity [4] was constrained to the same value at the end of each earthquake record. These earthquake records were then scaled such that the average peak ground acceleration (PGA) is 0.35g. The resultant Arias Intensity for these scaled earthquakes was 1.438 m/sec. Figures 6.4 and 6.5

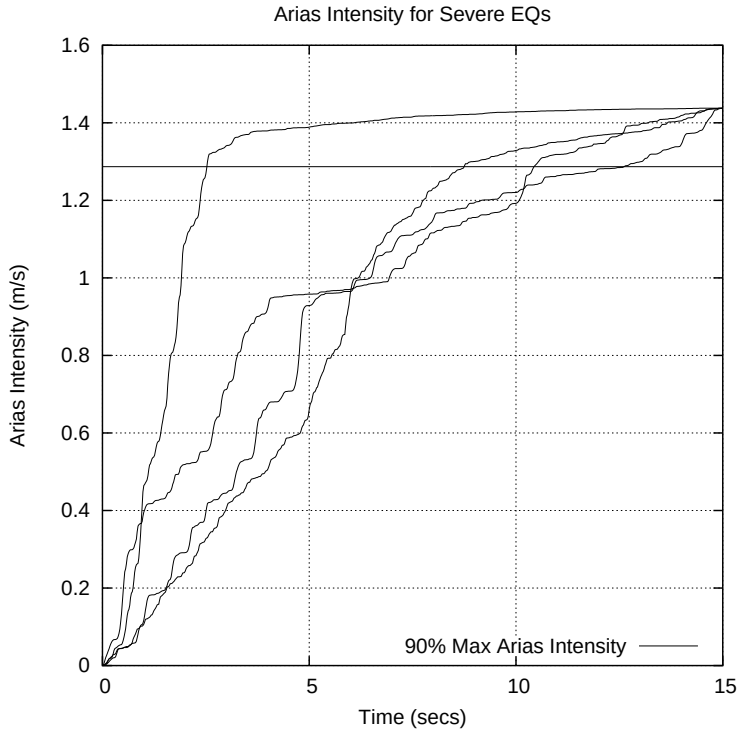

Figure 6.4: Arias Intensities for Moderate Ground Excitations

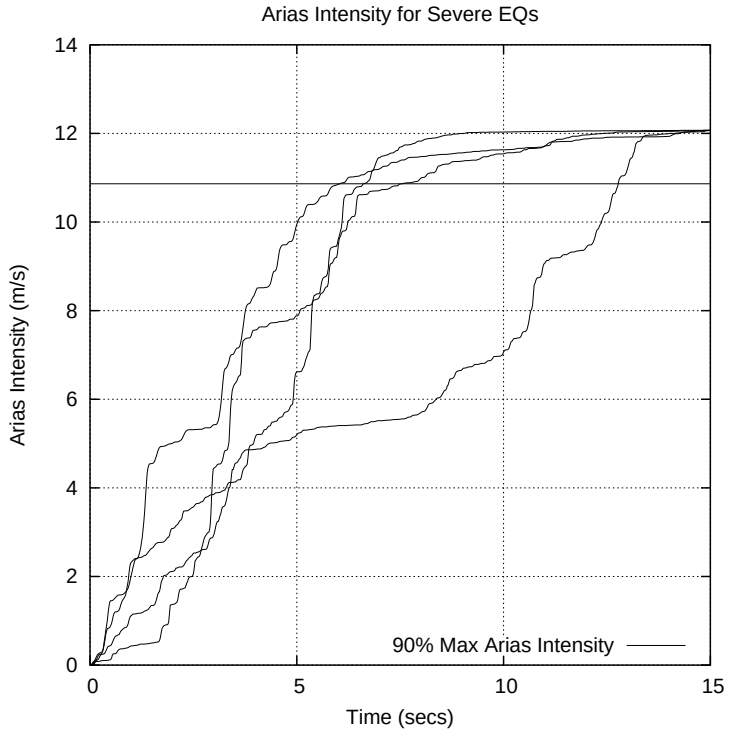

Figure 6.5: Arias Intensities for Severe Ground Excitations

show the constrained Arias Intensity for the moderate and severe classifications of earthquakes, respectively. Earthquakes used in this dissertation that fall into the moderate category are:

- 1940 El Centro – north-south component of the May 19, 1940, Imperial Valley, CA. USA. earthquake (unscaled magnitude 7.0). Recorded at the 117 El Centro Array #9 substation (United States Geological Survey (USGS) station 117). The closest distance of the substation to the fault rupture is 8.3 kilometers.

- 1979 El Centro – 3° north-north-west component of the October 15, 1979, Imperial Valley, CA. USA. earthquake (unscaled magnitude 6.5). Recorded at the 6618 Agrarias substation (Universidad Nacional Autonoma de Mexico (UNAM)/ University of California San Diego (UCSD) station 6618). The closest distance of the substation to the fault rupture is 12.9 kilometers.

- 1987 Whittier – 9° north-north-west component of the October 1, 1987, Whittier, CA. USA. earthquake (unscaled magnitude 6.0). Recorded at the Arcadia - Campus Drive substation (University of Southern California (USC) station 90093). The closest distance of the substation to the fault rupture is 12.2 kilometers.

- 1992 Landers – east-west component of the June 28, 1992, Landers, CA. USA. earthquake (unscaled magnitude 7.3). Recorded at the 22170 Joshua Tree substation (California Division of Mines and Geology (CDMG) station 22170). The closest distance of the substation to the fault rupture is 11.6 kilometers.

The average distance to fault rupture is 11.2 kilometers.

Earthquake	Motion Scaling Factor	Arias Intensity (AI) (m/sec)	Time at 90% AI (secs)	PGA (g)	Velocity (cm/sec) Min.	Velocity (cm/sec) Max.	Period of Fourier Peak (secs)
1940 El Centro	1.031	1.43	10.52	0.323	-17.94	35.64	0.68
1979 El Centro	0.983	1.43	8.78	0.364	-33.60	24.08	0.58
1987 Whittier	1.296	1.43	2.54	0.388	-16.70	28.85	0.29
1992 Landers	1.140	1.43	12.78	0.324	-39.34	26.44	0.75
1971 San Fernando	1.186	12.07	6.62	1.451	-30.69	181.30	0.21
1994 Northridge	0.779	12.07	7.56	1.388	-104.30	44.08	0.35
1995 Kobe	1.205	12.07	6.04	0.989	-100.30	90.27	0.68
1999 Duzce	1.131	12.07	12.78	1.073	-44.34	32.76	0.34

Table 6.4: Scaled Components of Moderate Ground Motion Excitations

Severe Earthquake Events. As done in section 4.3, the Arias Intensity [4] was constrained to the same value at the end of each earthquake record. These earthquake records were then scaled such that the average PGA is 1.225g. The resultant Arias Intensity for these scaled earthquakes was 12.07 m/sec. The average distance of the substation to fault rupture is 7.3 kilometers. Further detail regarding the severe earthquake events used here may be found in section 4.3.

Average PGA of 0.35g (for the moderate earthquakes) and 1.225g (for the severe earthquakes) corresponds well with the definitions of moderate and severe earthquake events used by Park and Otsuka [53] and Ramallo et al. [57], respectively. Table 6.4 summarizes the scaled ground motion scaling factor, Arias Intensity, PGA, minimum and maximum ground velocities, and the period at which the peak Fourier transform occurs for the moderate and severe classification of earthquakes used here. Figures 4.7 through 4.10 show the Fourier spectras for the earthquakes in the severe classification and figures 6.10 through 6.13 show the Fourier spectras for earthquakes in the moderate classification.

6.4 Results

This section compares the performance of our scaled 6-DOF model with a LDBI/HDBI to one with LDBI/HDBI+CKBB control. The results are categorized into scenario points of view. Due to the probability-based nature of a structure being subjected to its maximum capable earthquake, it is useful to consider in ascertaining the full range of benefits of supplemental damping forces, such as CKBB control, practical scenarios where a structure is subjected to magnitudes of earthquakes other than its maximum capable earthquake. In this section, we consider the results of our scaled 6-DOF model from the viewpoint of four practical scenarios:

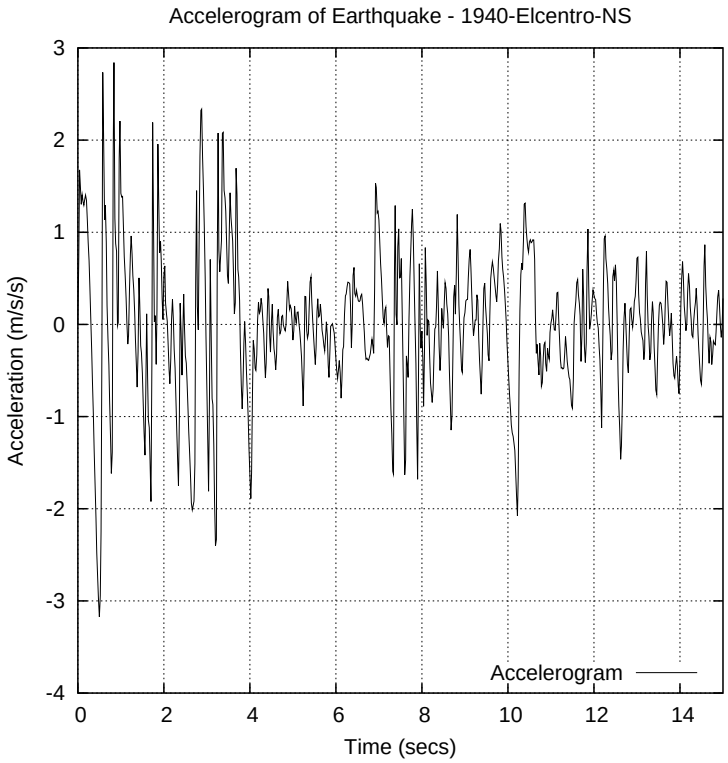

Figure 6.6: 1940 El Centro Accelerogram.

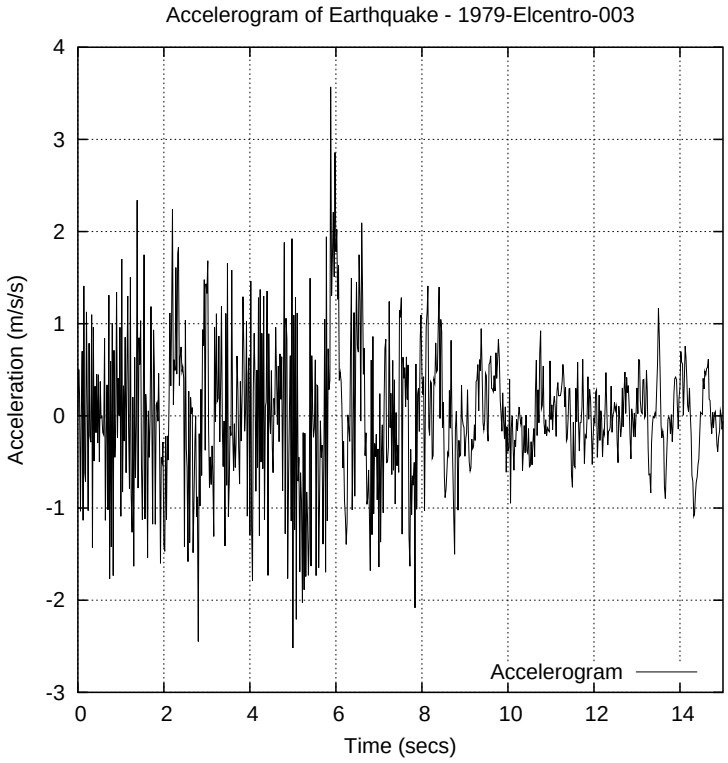

Figure 6.7: 1979 El Centro Accelerogram.

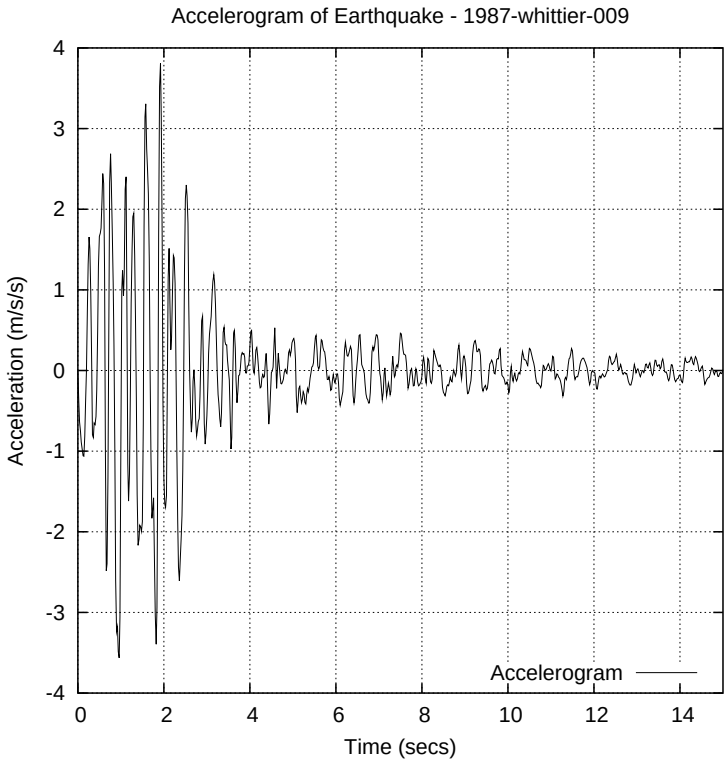

Figure 6.8: 1987 Whittier Accelerogram.

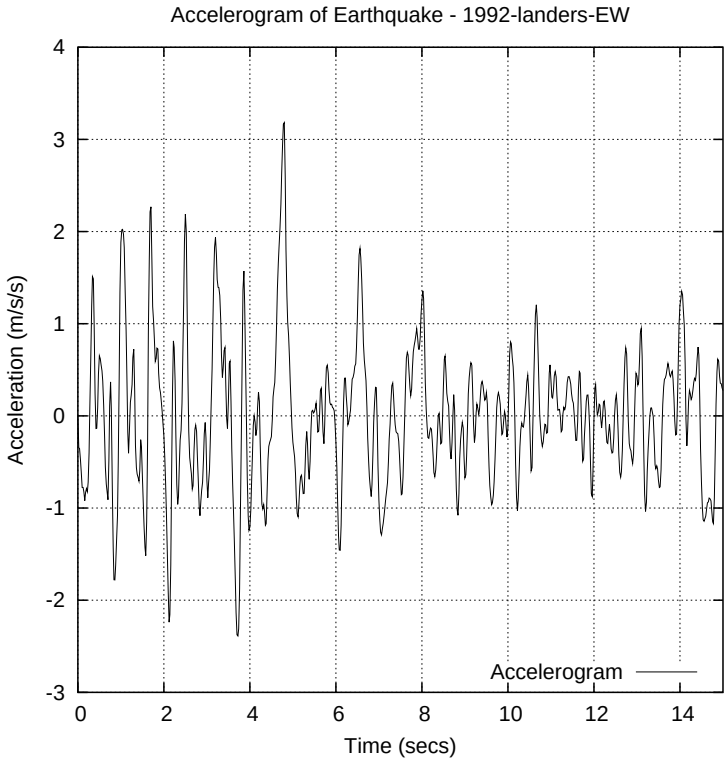

Figure 6.9: 1992 Landers Accelerogram.

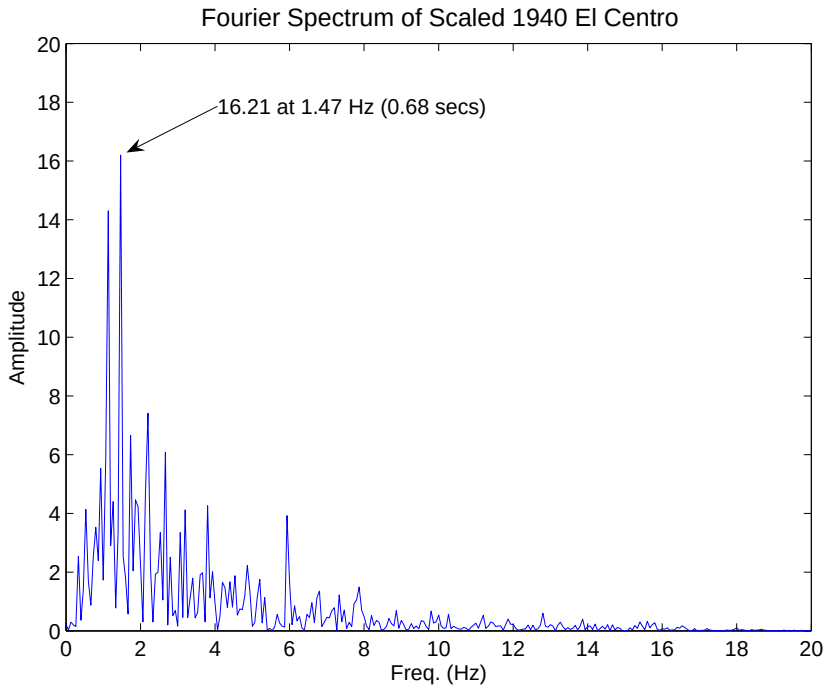

Figure 6.10: Fourier Spectrum for 1940 El Centro Accelerogram.

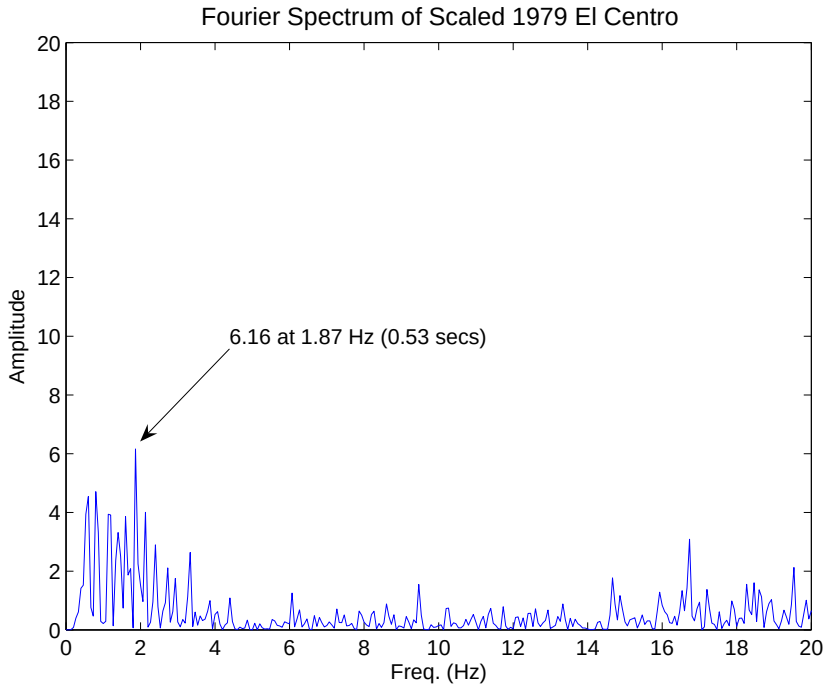

Figure 6.11: Fourier Spectrum for 1979 El Centro Accelerogram.

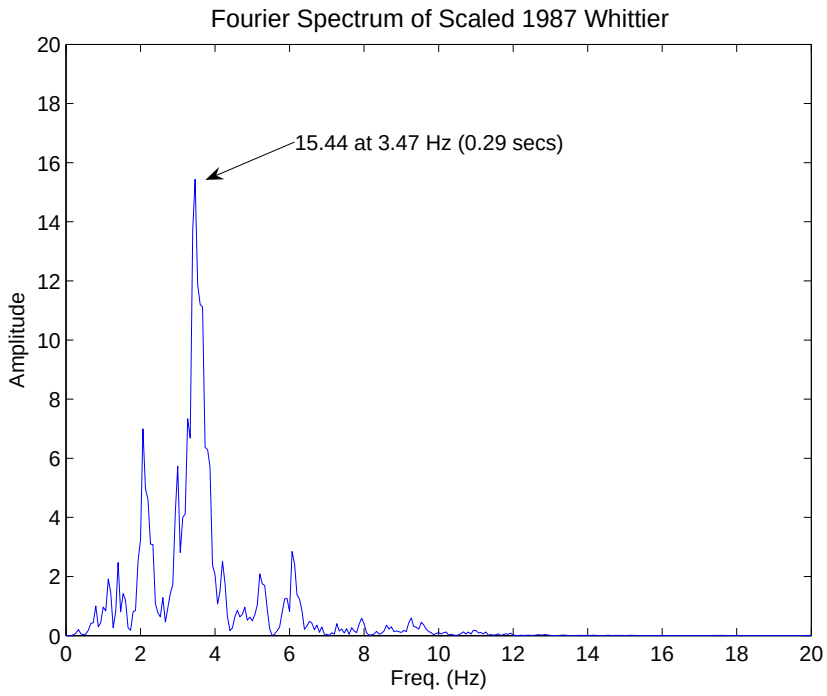

Figure 6.12: Fourier Spectrum for 1987 Whittier Accelerogram.

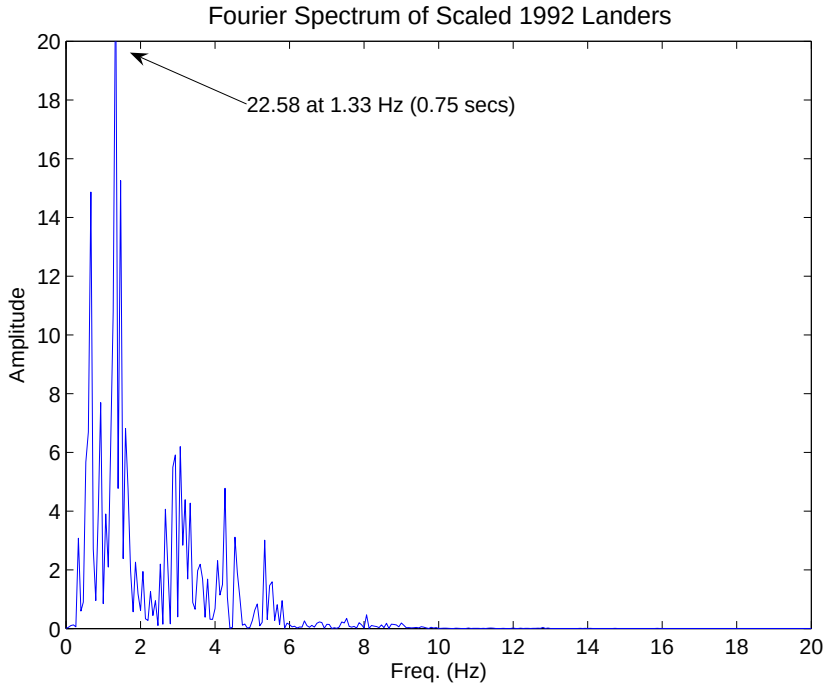

Figure 6.13: Fourier Spectrum for 1992 Landers Accelerogram.

1. A moderate severity BI/CKBB control design (LDBI and LDBI+CKBB) subjected to a moderate ground excitation (a El Centro characteristic earthquake),

2. A moderate severity BI/CKBB control design (LDBI and LDBI+CKBB) subjected to a severe ground excitation,

3. A high severity BI/CKBB control design (HDBI and HDBI+CKBB) subjected to a moderate ground excitation, and

4. A high severity BI/CKBB design (HDBI and HDBI+CKBB) subjected to a a severe ground excitation (a Northridge characteristic earthquake).

One and four cover the scenarios of expected ground motion attack. Two and three are the scenario counter-examples.

Tables 6.5 through 6.8 show the peak base drifts, isolator work done, structural drifts, structural work done, actuator work done, and actuator power requirements for each of these scenarios. The objective is two-fold: (1) to assess when CKBB control is most likely to be beneficial to base isolation, and (2) quantitatively determine the work done and power required by the actuator.

6.4.1 LDBI/LDBI+CKBB Control: Moderate Earthquakes

In this scenario, LDBI and LDBI+CKBB control damping mechanisms are subjected to moderate ground excitations. Ramallo et al. [57] found that LDBI was optimally designed to minimize base drift and structural acceleration for El Centro (moderate, i.e., PGA $\sim$0.35g) characteristic ground excitations. Table 6.5 summarizes the peak value results for this scenario. Section B.1 in the appendix contains figures showing the time histories of the base drifts, base isolator hysteresis, base isolator work done, superstructure work done, actuator work done, and actuator

power required for this scenario. For all earthquakes, the peak base drift was reduced when LDBI+CKBB control versus LDBI alone was used; the average percentage of this base drift reduction was 44%. This was associated with marginal increases in the peak structural drift. For all earthquakes used, the peak amount of work done by the base isolator decreased, and in 2 out of the 4 earthquakes, the work done by the superstructure increased; though both increases and decreases in the work done by the superstructure were minimal. The average work done and power required by the actuator are 7.08 kJ and 5.63 kW, respectively.

6.4.2 LDBI/LDBI+CKBB Control: Severe Earthquakes

In this scenario, LDBI and LDBI+CKBB control damping mechanisms are subjected to severe ground excitations (i.e., PGA $\sim$1.225g). This scenario represents a base-isolated structure that is subjected to an unexpectedly severe, yet conceivable, earthquake. Table 6.7 summarizes the peak value results for this scenario. Section B.2 in the appendix contains figures showing the time histories of the base drifts, base isolator hysteresis, base isolator work done, superstructure work done, actuator work done, and actuator power required for this scenario. For all earthquakes except the 1999 Duzce, the peak base drift was reduced when LDBI+CKBB control versus LDBI alone was used; the average percentage of this base drift reduction was 11%. The peak structural drift was virtually unchanged for all earthquakes except the 1999 Duzce which resulted in a tripling of its structural drift when LDBI+CKBB was used. For all earthquakes used, the peak amount of work done by the base isolator decreased, and in 3 out of 4 earthquakes, the work done by the superstructure decreased when LDBI+CKBB control was used. The average work done and power required by the actuator are 26.29 kJ and 15.55 kW, respectively.

	Base Drift (mm)		Structural Drift (mm)		Isolator Work (kJ)		Structural Work (kJ)		Actuator Work (kJ)	Actuator Power (kW)
Earthquake	LDBI	LDBI+ CKBB	LDBI	LDBI+ CKBB	LDBI	LDBI+ CKBB	LDBI	LDBI+ CKBB	LDBI+ CKBB	LDBI+ CKBB
1940 El Centro	79.82	45.89	0.77	1.88	10.44	6.91	2.33	2.42	8.46	5.68
1979 El Centro	155.80	68.03	1.22	1.74	14.28	4.34	4.43	2.37	4.19	5.45
1987 Whittier	72.58	33.50	0.74	1.64	2.35	1.48	1.32	2.12	2.90	4.70
1992 Landers	162.30	125.90	1.25	1.77	20.21	11.14	6.05	3.49	12.78	6.67

Table 6.5: 6-DOF Peak Values for LDBI & LDBI+CKBB: Moderate EQs

	Base Drift (mm)		Structural Drift (mm)		Isolator Work (kJ)		Structural Work (kJ)		Actuator Work (kJ)	Actuator Power (kW)
Earthquake	LDBI	LDBI+ CKBB	LDBI	LDBI+ CKBB	LDBI	LDBI+ CKBB	LDBI	LDBI+ CKBB	LDBI+ CKBB	LDBI+ CKBB
1971 San Fernando	529.80	454.50	3.26	3.26	59.27	45.77	52.08	41.48	37.96	24.27
1994 Northridge	238.80	211.00	1.79	1.92	21.17	17.81	12.27	12.13	18.88	12.87
1995 Kobe	354.60	251.50	2.36	2.19	49.69	42.33	38.93	26.93	33.86	18.65
1999 Duzce	39.16	43.02	0.80	2.41	5.16	4.44	3.01	4.97	14.47	6.40

Table 6.6: 6-DOF Peak Values for LDBI & LDBI+CKBB: Severe EQs

6.4.3 HDBI/HDBI+CKBB Control: Moderate Earthquakes

In this scenario, HDBI and HDBI+CKBB control damping mechanisms are subjected to moderate ground excitations. Since small and moderate earthquakes are more frequent than severe earthquakes, the likelihood is greater for a structure to be subjected to a moderate earthquake than a severe earthquake. In fact, the United States Geological Survey (USGS) tracks numerous earthquakes everyday from around the world of magnitude>5.0 at its website [87]. This scenario represents a base-isolated structure that is designed for a severe ground motion, but is subjected to a more likely moderate earthquake. Table 6.7 summarizes the peak value results for this scenario. Section B.3 in the appendix contains figures showing the time histories of the base drifts, base isolator hysteresis, base isolator work done, superstructure work done, actuator work done, and actuator power required for this scenario. For all earthquakes, the peak base drift was reduced when HDBI+CKBB control versus HDBI alone was used; the average percentage of this base drift reduction was 52%. However, this is associated with large increases in the peak structural drift. For all earthquakes used, the peak amount of work done by the base isolator decreased, and the amount of the work done by the superstructure increased when HDBI+CKBB control was used. The average percentage increase of peak superstructure work done when HDBI+CKBB control was used is 349%. The average work done and power required by the actuator are 5.85 kJ and 11.54 kW, respectively.

6.4.4 HDBI/HDBI+CKBB Control: Severe Earthquakes

In this scenario, HDBI and HDBI+CKBB control damping mechanisms are subjected to severe ground excitations. Park and Otsuka [57] found that HDBI was optimally designed to for Northridge characteristic ground excitations. This HDBI

	Base Drift (mm)		Structural Drift (mm)		Isolator Work (kJ)		Structural Work (kJ)		Actuator Work (kJ)	Actuator Power (kW)
Earthquake	HDBI	HDBI+ CKBB	HDBI	HDBI+ CKBB	HDBI	HDBI+ CKBB	HDBI	HDBI+ CKBB	HDBI+ CKBB	HDBI+ CKBB
1940 El Centro	71.09	30.83	1.74	5.16	22.06	1.46	4.07	14.03	5.43	9.37
1979 El Centro	74.57	23.17	1.57	4.40	11.35	0.86	1.70	12.69	8.36	7.43
1987 Whittier	56.28	28.16	1.74	4.86	6.96	3.49	4.02	4.02	4.51	18.77
1992 Landers	79.21	53.72	1.67	4.39	24.77	3.10	2.89	17.49	5.09	10.58

Table 6.7: 6-DOF Peak Values for HDBI & HDBI+CKBB: Moderate EQs

	Base Drift (mm)		Structural Drift (mm)		Isolator Work (kJ)		Structural Work (kJ)		Actuator Work (kJ)	Actuator Power (kW)
Earthquake	HDBI	HDBI+ CKBB	HDBI	HDBI+ CKBB	HDBI	HDBI+ CKBB	HDBI	HDBI+ CKBB	HDBI+ CKBB	HDBI+ CKBB
1971 San Fernando	424.50	276.00	3.59	4.68	97.23	45.62	38.23	17.77	62.10	47.54
1994 Northridge	173.00	105.90	2.21	4.26	34.27	23.03	13.78	12.15	42.90	38.68
1995 Kobe	188.20	220.70	2.80	4.36	104.40	72.28	23.77	20.90	73.99	52.82
1999 Duzce	68.62	42.53	1.97	5.00	7.10	4.20	5.83	14.20	36.31	20.63

Table 6.8: 6-DOF Peak Values for HDBI & HDBI+CKBB: Severe EQs

design is not common in practice, but due to the significant concern (for example, Hall et al. [31], Heaton et al. [32], and Spencer et al. [68]) of base-isolated buildings to accommodate severe near-fault earthquakes this alternative design is considered in this dissertation. Table 6.7 summarizes the peak value results for this scenario. Figures 6.14 through 6.18 show the time histories of the base drift, base isolator hysteresis, base isolator work done, superstructure work done, actuator work done, and actuator power required for 1971 San Fernando earthquake for this scenario. Section B.4 in the appendix contains figures showing the time histories of the base drifts, base isolator hysteresis, base isolator work done, superstructure work done, actuator work done, and actuator power required for 1994 Northridge, 1995 Kobe, and 1999 Duzce earthquakes. For all earthquakes except the 1995 Kobe, the peak base drift was reduced when HDBI+CKBB control versus HDBI alone was used; the average percentage of this base drift reduction was 24%. This reduction in peak base drift was associated with modest increases in the peak structural drift. For all earthquakes used, the peak amount of work done by the base isolator decreased, and in 3 out of 4 earthquakes, the work done by the superstructure decreased when HDBI+CKBB control was used. The average work done and power required by the actuator are 53.83 kJ and 39.92 kW, respectively.

6.5 Summary

The objectives of this numerical evaluation of our control concept were two-fold. First, to assess from a energy- and power-balance and base drift points of view when CKBB control is most likely to be beneficial to base isolation, and second to compare the demands on actuator power to actuator technology. We felt that energy based metrics were useful because they provide a means for accurately estimating the capacity of a structure to resist forces elastically and dissipate energy

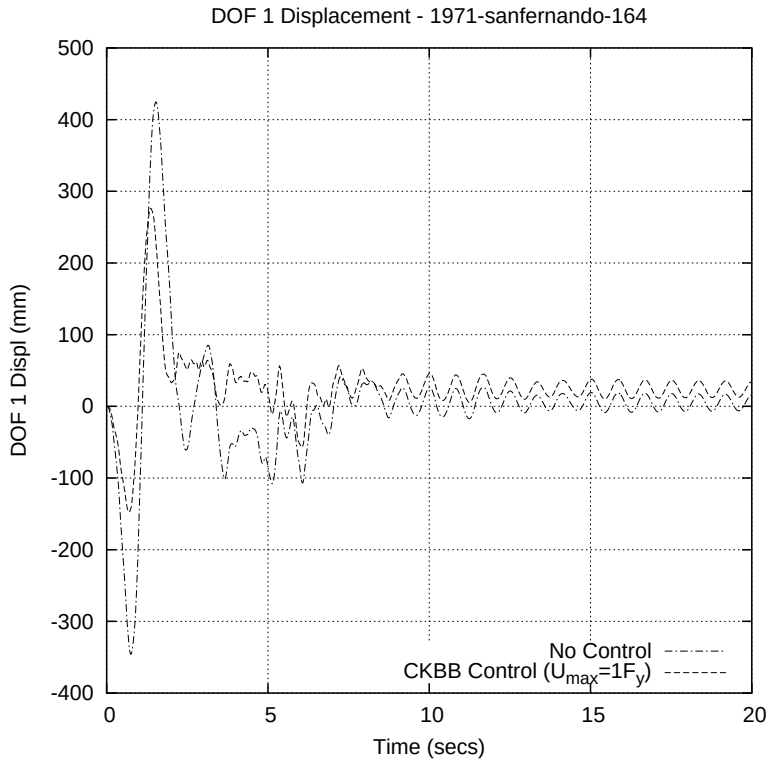

Figure 6.14: Comparison of HDBI/HDBI+CKBB Control: Base Drift for 1971 San Fernando

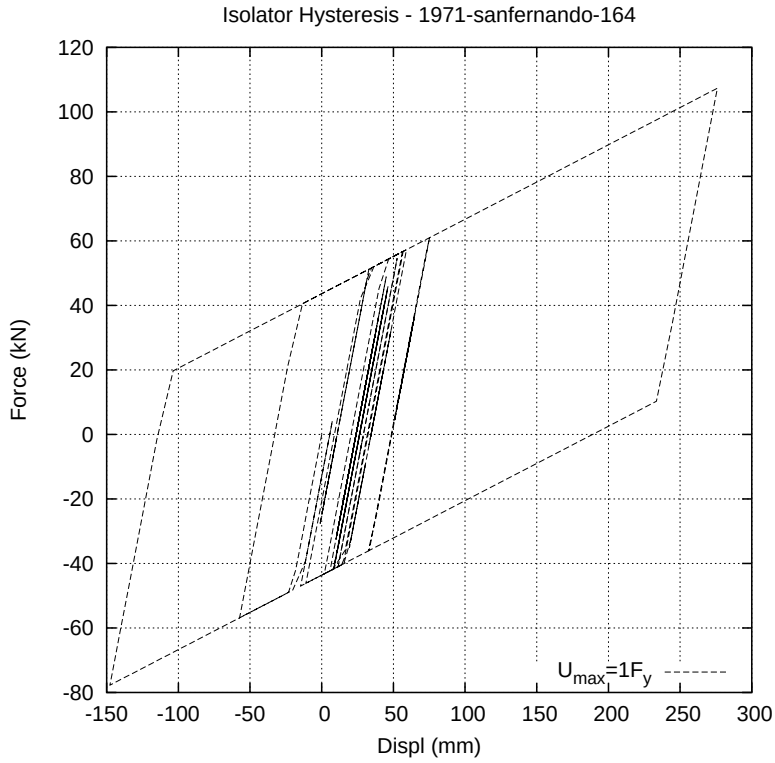

Figure 6.15: HDBI+CKBB Control: Base Isolator Hysteresis for 1971 San Fernando

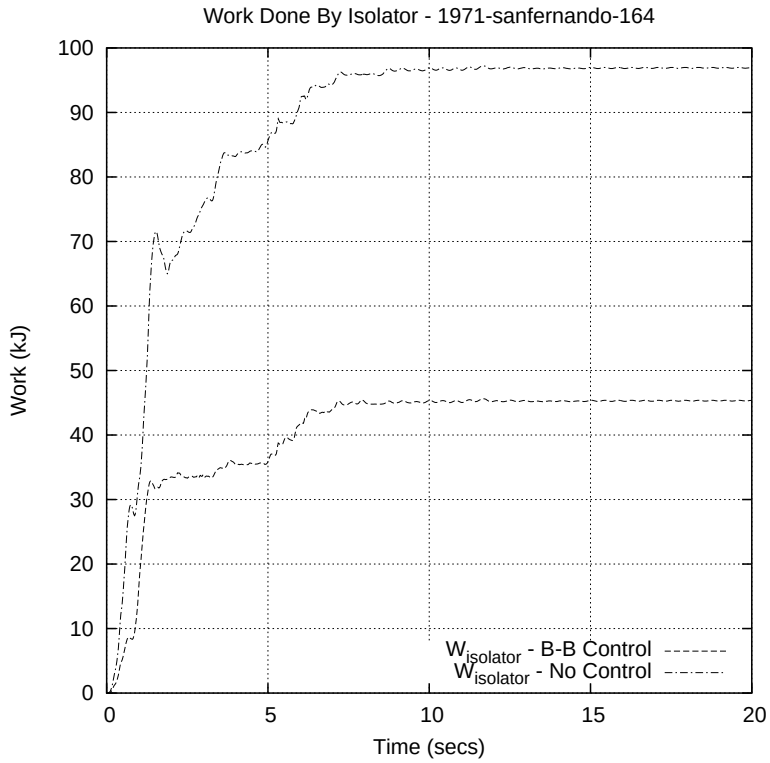

Figure 6.16: Comparison of HDBI/HDBI+CKBB Control: Base Isolator Work Done for 1971 San Fernando

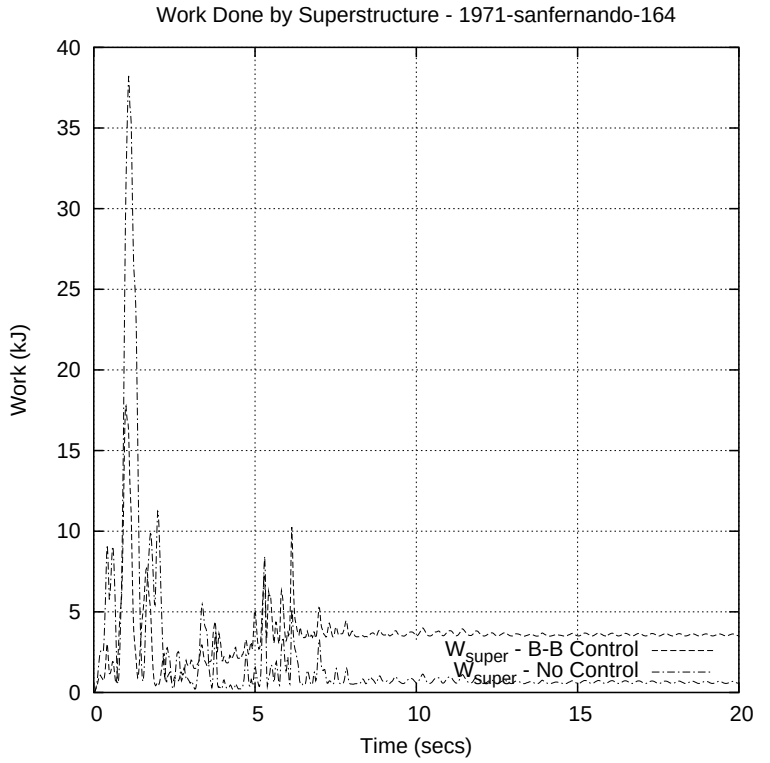

Figure 6.17: Comparison of HDBI/HDBI+CKBB Control: Superstructure Work Done for 1971 San Fernando

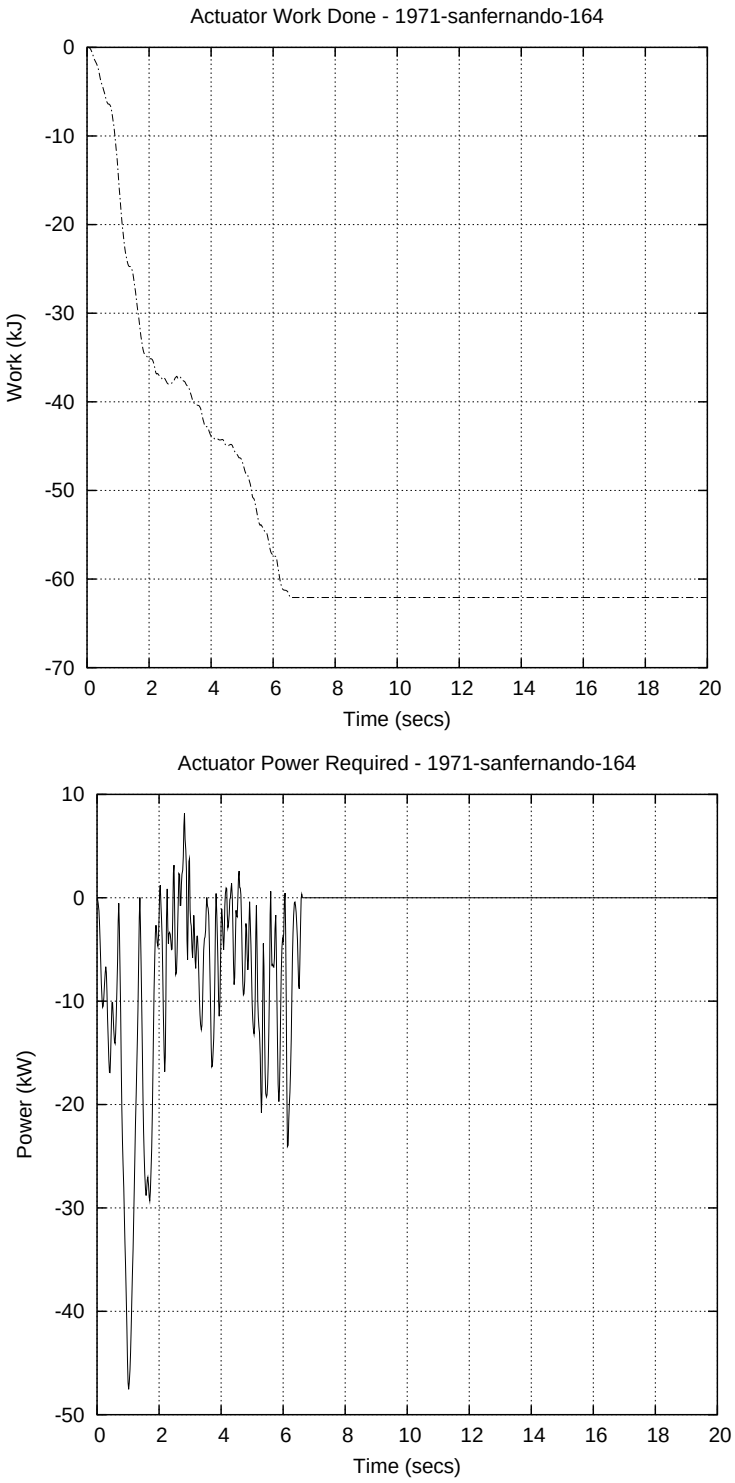

Figure 6.18: HDBI/CKBB Control: Actuator Work Done/Power Required for 1971 San Fernando

associated with damping and key structural elements undergoing cyclic nonlinear deformations. Also, since the control objective of CKBB control is energy-based, analyzing the system response from an energy point of view has helped us to validate the CKBB control theoretical formulation.

We began by formulating the energy- and power-balance equations for a base-isolated structure supplemented with constant stiffness bang-bang (CKBB) control. For the numerical experiments, the structural properties (mass, stiffness and damping matrices) of our 6-DOF scaled model are well referenced in the literature. We employ two different base isolators and associated CKBB control designs: a low damping base isolator (LDBI) with and without supplemental CKBB control, and a high damping base isolator (HDBI) with and without supplemental CKBB control. The maximum capable earthquake for the former is an earthquake of the size and "characteristic" of the 1940 El Centro earthquake (PGA$\sim$0.35g) while the maximum capable earthquake for the latter is the 1994 Northridge earthquake (PGA$\sim$1.225g).

The findings of our evaluation of our control concept are as follows:

1. There were trade-offs occurring between the amount of work being done by the base isolator, superstructure, and actuator. The scenario in which HDBI+CKBB control is subjected to moderate earthquakes results in the greatest average percent reduction in work done by the base isolator (81%); it also results in the greatest average percent increase in the work done by the superstructure (349%). It appears that for this scenario the actuator with peak force equal to 43.39 kN dominants the response of the structure and injects mechanical energy in the system that must be dissipated by the superstructure. The scenario in which HDBI+CKBB control is subjected to severe earthquakes results in a significant, but not overwhelming, average percent reduction in isolator work done (39%), but also in three of four time histories an average percent

decrease in structural work done (26%). It appears that for this scenario, the actuator with peak force again equal to 43.39 kN does work towards dissipating the earthquake and base isolator energy and does not dominant the response of the structure but rather absorbs some energy that would otherwise be injected into the superstructure if only base isolation were used. This conclusion leads to future work in the area of an adaptive bang-bang control strategy that would optimally make these trade-offs between work done by the base isolator, superstructure, and actuator based on earthquake energy input into the structure.

2. In most, but not all of our time histories, the addition of CKBB control to base isolation alone reduced the base drift. The percent change in base drift when base isolation alone is compared to base isolation supplemented with CKBB control ranged from a percent increase of 17% which occurred during the scenario of HDBI+CKBB control subjected to severe earthquake to a percent decrease of 69% which occurred during the scenario of HDBI+CKBB control subjected to a moderate earthquake.

3. In general, CKBB control is most beneficial to base isolation when severe ground motions are encountered. For the scenario when LDBI+CKBB control is subjected to severe earthquakes, the highest base drifts we calculated are reduced in all but one time history when CKBB control was added. The work done by the superstructure is likewise decreased in all but one time history when CKBB control was added. However, since the base drift is reduced by an average of only 11%, an adaptive bang-bang control algorithm that appropriately increases actuator force may improve performance. Base drifts, structural work, and actuator work for the scenario when HDBI+CKBB control is subjected to severe earthquakes follow a similar pattern.

4. For the scenarios where LDBI+CKBB control is subjected to moderate earthquakes and HDBI+CKBB control is subjected to severe earthquakes (design case scenarios), the addition of CKBB control generally reduces the base drift and reduces modestly the amount of work done by the structure. However, in the case of LDBI+CKBB control being subjected to moderate earthquakes, the value of these apparent pros seems questionable.

5. In all of our time histories, the addition of CKBB control to base isolation alone reduced the amount of work done by the base isolator. This validates the theoretical energy-based control objective formulation. Since our control objective was to minimize the amount of total potential energy in the system, we would expect the energy to be reduced in the element that is closest to the actuator (i.e., the base isolator).

6. For our scaled model, actuators were modeled as having a maximum peak force of 14.46 kN and 43.39 kN. For a similar full scale structure, depending on the scaling factor, table 2.1 shows that several semiactive actuators that are currently being produced that would be able to generate the required force within milliseconds with very little power (some even operating with batteries). In the event of a large scaling factor, the required actuator forces can be generated with parallel configurations of dampers based on the current technology shown in table 2.1.

Chapter 7

Conclusions

7.1 Intellectual Contributions

The intellectual contributions of this dissertation are:

1. A closed-form solution (equation 3.53) to the structural bang-bang control problem that may be directly substituted into the equation of motion for a multi-degree of freedom system (equation 1.14). This solution is based on the Lyapunov function (equation 1.10) and on a control objective of minimizing the potential energy in the structural system. It is exact for structures with a uniform mass (i.e., $m_1 = m_2 = \ldots = m_n$) and linear viscous damping of the form $\mathbf{C} = \alpha \cdot \mathbf{M} + \beta \cdot \mathbf{K}$.

2. Developed an exact, closed-form equation expressing the forced, steady-state and free vibration bang-bang control response for a 1-DOF system. For the forced, steady-state and free vibration cases, see equations 3.24 and 3.40, respectively. Showed for the case of a forced, steady-state and free vibration response, the relationship between the behavior of bang-bang control and velocity and displacement for a 1-DOF system (figures 3.1 through 3.5). Showed through numerical experiments of a 5-DOF system (section 4.5) that these equations are good representations of the relationship between the behavior of bang-bang control and the velocity and displacement of the DOF where the control force acts for higher DOF systems.

3. Developed closed-form equations expressing the relationship between the velocity and displacement bang-bang control coefficients and base isolator stiff-

ness for a 2-DOF system (equations 3.68 through 3.70); they are shown graphical in figures 3.7 through 3.9). These equations are exact for structures with a uniform mass (i.e., $m_1 = m_2 = \ldots = m_n$) and linear viscous damping of the form $\mathbf{C} = \alpha \cdot \mathbf{M} + \beta \cdot \mathbf{K}$ and are based on linear, elastic theory. Showed through numerical experiments of a 5-DOF system (section 4.5) that these equations are good representations of the relationship between velocity and displacement bang-bang control coefficients and base isolator stiffness for higher DOF systems.

4. Developed an understanding of when bang-bang control is likely to be beneficial to base isolation (section 6.5). The numerical response of base isolated structures supplemented with and without bang-bang control were compared. For specific earthquake severities, base isolator designs were identified which are likely to benefit from bang-bang control.

7.2 Conclusions

The objective of this dissertation has been to investigate the potential benefits and opportunities for using bang-bang control as a supplement to base isolation. We began by analyzing a control design matrix ($\mathbf{Q}$) that gives the bang-bang control objective (equation 1.10) well defined physical meaning. Wu et al. [94] give several suggestions for $\mathbf{Q}$ (equation 1.18). Using these suggestions for $\mathbf{Q}$, we employed linear matrix algebra and symbolic analysis software to derive symbolic expressions for bang-bang control, expressed in terms of solutions to the Lyapunov equation, the system parameters (m, k, ...) and state (i.e., displacements and velocities). The investigations included: (1) Symbolic analysis for 1 and 2 DOF systems, (2) Symbolic analysis for n-DOF systems, and (3) Effect of bang-bang control strategy on nonlinear deformations in base isolators. These investigations showed that

a simplified closed-form symbolic solution (equation 3.53) to the Lyapunov equation is possible based on the control objective of minimizing the potential energy in the structural system. This solution is exact for an n-DOF structure with uniform masses (i.e., $m_1 = m_2 = \ldots = m_n$) and linear viscous damping of the form $\mathbf{C} = \alpha \cdot \mathbf{M} + \beta \cdot \mathbf{K}$. The simplified symbolic solution to the Lyapunov equation derived in this dissertation allows for the identification of cause-and-effect relationships between the control algorithm parameters and properties of the dynamical system (e.g., damping matrices), which in turn affects the ensuing system response. This provided a pathway for us to further analysis the behavior of bang-bang control in relationship to displacement and velocity system response.

We showed that for the forced, steady-state and free vibration cases, a 1-DOF system is very nearly in-phase but opposite in direction to the system velocities (i.e., 90° out of phase and opposite in direction to the system displacements). This relationship is shown in figures 3.1 through 3.6. In regard to the effect of localized, nonlinear system displacements on the bang-bang velocity and control coefficients, we showed that for a 2-DOF system with a mass/stiffness ratio (τ) of $0.0001\ \text{sec}^2 \leq \tau \leq 0.010\ \text{sec}^2$, and base isolator to superstructure stiffness ratio (γ) varying between $0.03 \leq \gamma \leq 0.18$, the bang-bang velocity and displacement coefficients do not vary significantly. VKBB control is more difficult to incorporate into the equation of motion since the control algorithm is dependent on the linear or nonlinear state of the structure. This observation along with a insignificant loss of accuracy while using CKBB control provides justification for using the simpler CKBB control strategy. Numerical studies (chapter 4) of a 5-DOF system verify these conclusions and show their applicability to higher DOF systems.

In the second part of this dissertation, we assess from a energy- and power-balance and base drift viewpoint, when CKBB control is most likely to be beneficial

to base isolation. We felt that energy-based metrics were useful because they provide a means for accurately estimating the capacity of a structure to resist forces elastically and dissipate energy associated with damping and key structural elements undergoing cyclic nonlinear deformations. Also, since the control objective of CKBB control is energy-based, analyzing the system response from an energy point-of-view has helped us to validate the CKBB control theoretical formulation.

We began by formulating the energy- and power-balance equations for a base-isolated structure supplemented with CKBB control (section 5.2 through 5.4). Numerical studies used a scaled 6-DOF model that is well referenced in the literature and employed two different base isolator designs: a low damping base isolator (LDBI) and a high damping base isolator (HDBI). The design used for the LDBI is typical of that used for base isolators in practice. Our models were subjected to both low (PGA$\sim$0.35g) and high (PGA$\sim$1.225g) severity ground excitations.

Our numerical studies showed that there are trade-offs occurring between the work done by the base isolator, superstructure, and actuator. This is highlighted when a HDBI+CKBB control design is considered and the only variable is the severity of the ground motion. For a moderate ground motion, the actuator injects mechanical energy into the superstructure and for a severe ground motion it doesn't (i.e., the actuator protects the superstructure). This points to a need for an adaptive bang-bang control strategy that would optimally make trade-offs between the work done by the base isolator, superstructure, and actuator based on the earthquake energy input to the structure (for this scenario, reducing the actuator force may have been beneficial). In general, the addition of CKBB control to base isolation reduced the amount of base drift; however, sometimes at the expense of work done by the superstructure. Also, CKBB control seems to be particularly beneficial to base isolation when severe ground motions are encountered (section 6.4). However,

for the case when a LDBI+CKBB control design is subjected to a severe ground motion, an adaptive bang-bang control strategy that increased the actuator force may have been beneficial. In all the time histories, the amount of work done by the base isolator was reduced with the addition of CKBB control to base isolation. This validates the theoretical energy-based control objective formulation. Table 2.1 shows that several semiactive actuators are currently capable of producing, within milliseconds and with very little power, the actuator force required by a full-scale structure.

Interesting Aside Regarding CKBB Control Being "Nearly" in Phase With Velocity. We showed through symbolic analysis and numerical experiment that bang-bang control is nearly in phase, but opposite in direction to the velocity. We thought that it would be interesting to see the effect of implementing the following simple control algorithm (until the Arias Intensity = 90% maximum):

$$\mathbf{U} = \begin{cases} u_{max} & \text{if } \dot{x}_1(t) < 0 \\ -u_{max} & \text{otherwise} \end{cases} \tag{7.1}$$

Figure 7.1 shows the displacement time histories of DOF 1 when the 6-DOF model used in chapter 6 is subjected to the 1971 San Fernando earthquake. CKBB control is used in one time history and the simple control algorithm expressed by equation 7.1 is used in the other. There is little difference between the two. This shows that the complexity associated with bang-bang control (and even CKBB control) may be unwarranted. This should be an area of future work.

7.3 Anticipated Benefits

Anticipated benefits of this dissertation are the following:

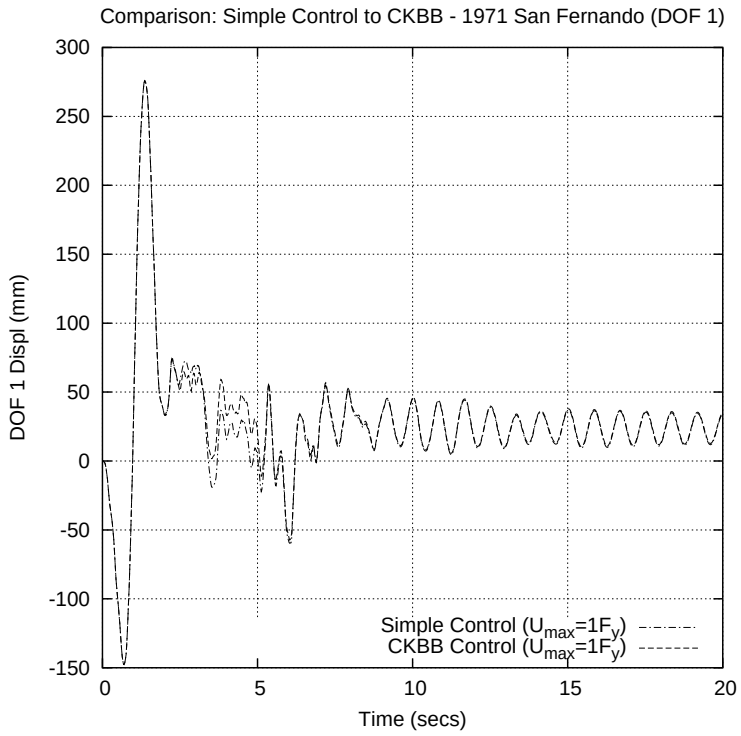

Figure 7.1: Comparison: Simple Velocity-Based to CKBB Control for 1971 San Fernando

1. Modern structural control algorithms obscure interpretation of the underlying physical mechanisms and "cause-and-effect" relationships governing performance. Our closed-form Lyapunov solution (see equation 3.53) to the structural bang-bang control problem allows one to analyze and understand the mechanisms affecting the behavior of bang-bang control. Indeed, we have already seen some of these benefits by being able to analysis our Lyapunov solution to express relationships for a 1-DOF system between bang-bang control and velocities and displacements of the DOF where the control force acts. It is anticipated that this understanding will lead to a better acceptance of this technology in the structural community.

2. Varying the bang-bang control algorithm dependent on the linear or nonlinear state of the structure is difficult to incorporate into the equation of motion.

This complexity is furthered if the base isolator is represented by a complicated hysteresis model (i.e., the Bouc-Wen model; for further information on the Bouc-Wen model, see Wen [91]). This dissertation shows that this complexity is unwarranted in base-isolated structures in which the first mode dominates, has a mass/stiffness ratio (τ) of 0.0001 sec^2 $\leq \tau \leq$ 0.010 sec^2, and base isolator to superstructure stiffness ratio (γ) varies between $0.03 \leq \gamma \leq 0.18$ (see section 4.5). In other words, the bang-bang control algorithm may use linear properties of the structure throughout the entire time history without significant loss of accuracy for base-isolated structures with the aforementioned parameters.

3. Trade-offs occur between the amount of work being done by the base isolator, superstructure, and actuator. For the scenario in which a high damping base isolator with bang-bang control is subjected to a moderate earthquake (see section 6.4.3), the actuator injects mechanical energy into the system (possibly destabilizing it). When the same base isolator with bang-bang control is subjected to a severe earthquake, the actuator does not inject mechanical energy into the system, but dissipates the earthquake and base isolator energy that would otherwise be injected into the superstructure. This research highlights the need for an adaptive bang-bang control strategy. It is anticipated that future research would use the understanding of the mechanisms affecting the behavior of bang-bang control and the metrics (i.e., base and structural drift and base, structural, and actuator work done) highlighted in this dissertation to develop and assess this new adaptive control strategy.

7.4 Directions for Future Work

The work described in this dissertation is simply one step in a long-term research objective aimed at development of analytical procedures and general guidelines to help engineers design structures protected by hybrid passive/active control.

Throughout this dissertation we have employed simplifying assumptions to facilitate insight into cause-and-effect relationships and numerical studies. One simplifying assumption is that the magnitude of the control force is not allowed to vary throughout the time history. We showed in section 6.4.3 that this potentially may lead to the actuator injecting mechanical energy into the system (e.g., when a HDBI supplemented with CKBB control is subjected to a moderate earthquake). This may lead to the actuator destabilizing the structure. With this in mind, there is a need for future work in the area of adaptive bang-bang control that would optimally make trade-offs between the work done by the base isolator, superstructure, and actuator based on the earthquake energy input to the structure.

In regard to moving from symbolic analysis and prototype-level numerical studies to a full-scale experimental dissertation, several assumptions would need to be re-examined. They include:

1. **Singular Control-Force Delivery Requirement.** Since bang-bang control laws lead to a singular control-force delivery requirement, servo-hydraulic actuators are not suitable for this kind of control law due to high-speed switching of control forces that are needed to meet this requirement. Therefore, modification is necessary for practical application of bang-bang control laws to civil engineering structures. Wu and Soong [93] propose a method of approximating this singular control requirement using series of polynomial functions. Therefore a discontinuous function, such as the control-force delivery require-

ment for bang-bang control may be approximated as a series of polynomials as proposed by Wu and Soong [93].

2. **Availability of State Variables.** In this dissertation, it is assumed that the state variables i.e., the displacements and velocities at each degree of freedom are readily measurable. The bang-bang control algorithm is dependent on the availability of the state variables, (see equation 1.14). Dyke et. al. [24] points out that accurate measurement of displacements and velocities is difficult to achieve since during a seismic event the foundation of the structure is moving with the ground. It is suggested that since accelerometers are readily available and an inexpensive measurement of accelerations at strategic points on the structure is an ideal solution to this problem. Also, Chung et. al. [18] point out that the error in the observability of these state variables along with structural controllability issues and on-line computational errors tend to accumulate rapidly and may degrade the structural performance seriously or produce instability.

3. **Time Delay.** In the analyses presented in this dissertation, time delay is not taken into account; however, time delay between the measured variables and the application of the control forces can not be eliminated. Chung et. al. [18] points out that time lag diminished control effects for a real system as compared to an ideal one. Since phase lag is proportional to time delay and modal frequency, the effect of time delay may be very serious for higher modes even with small amounts of time delay. Chung et. al. [18, 19] developed a phase shift method for SDOF systems which compensates for time delay in the modal domain.

4. **Actuator Location.** In the derivations and numerical experiment in this dissertation, a single actuator is located at the top of the base isolator (DOF 1).

The reasoning for the location of this actuator is that for base-isolated structures the main potential benefit is believed to lie in the ability of active control to limit the maximum base displacement while the base isolation limits inter-story drift and absolute acceleration [33]. Brown, Ankireddi, and Yang [12], studied the problem of actuator and sensor placement for multi-objective control. A linear quadratic Gaussian control algorithm that synthesizes Pareto optimal trade-off curves was used to determine the optimal location of actuators and sensors in this parametric study. Cheng and Jiang [16] used a statistical method for determining the optimal placement of control devices and showed that optimal placement of control devices resulted in better performance because less control force was required to reduce structural seismic response to a given level.

Appendix A

Scalability of Solutions to the Lyapunov Matrix Equation

The following matrix equations prove that when the total potential energy and/or kinetic energy of a structure is minimized, under certain restrictions on the form of the mass, damping, and stiffness matrices, the solution to the Lyapunov matrix equation for a 1-DOF system is scalable to an n-DOF system. These restrictions on the form of the mass, damping, and stiffness matrices are as follows:

1. The mass matrix, $\mathbf{M}$, must be diagonal and uniform (i.e., $m_1 = m_2 = ... = m_n$).

2. Linear viscous damping (in the form $\alpha \cdot \mathbf{M} + \beta \cdot \mathbf{K}$) must be present in the system.

3. The structural stiffness matrix, $\mathbf{K}$, must be well-conditioned.

Consider a 1-DOF system with stiffness, k, mass, m, and linear viscous damping, c= $\alpha \cdot m + \beta \cdot k$. For the following general choice of $\mathbf{Q}$,

$$\mathbf{Q} = \begin{bmatrix} k^\star & 0 \\ 0 & 0 \end{bmatrix}, \tag{A.1}$$

where $k^\star$ is a real, positive number, the solution to the Lyapunov matrix equation for $\mathbf{S}$ is as follows:

$$\mathbf{S} = \begin{bmatrix} \frac{mk^\star}{2(\alpha \cdot m + \beta \cdot k)} + \frac{(\alpha \cdot m + \beta \cdot k)k^\star}{2k} & \frac{mk^\star}{2k} \\ \frac{mk^\star}{2k} & \frac{m^2 k^\star}{2k(\alpha \cdot m + \beta \cdot k)} \end{bmatrix}. \tag{A.2}$$

Substituting equation 1.4 (the defination for $\mathbf{A}$) into the matrix equation $\mathbf{A^T S} + \mathbf{SA} = -\mathbf{Q}$, and noting that $\mathbf{K^T} = \mathbf{K}$ and $\mathbf{M^T} = \mathbf{M}$, we have:

$$\mathbf{A^T S + SA} = \begin{bmatrix} \mathbf{0} & -([\mathbf{K}][\mathbf{M^{-1}}]) \\ [\mathbf{I}] & -([\mathbf{C}][\mathbf{M^{-1}}]) \end{bmatrix} \mathbf{S} + \mathbf{S} \begin{bmatrix} \mathbf{0} & [\mathbf{I}] \\ -([\mathbf{M^{-1}}][\mathbf{K}]) & -([\mathbf{M^{-1}}][\mathbf{C}]) \end{bmatrix} = -\mathbf{Q}. \tag{A.3}$$

Now notice that the matrix elements of equation A.2 are symbolic expressions expressed as fractions. For the matrix counterpart of equation A.2, one can either pre- or post-multiply the matrix expression appearing as the denuminator of each matrix element. We investigate both scenarios to ascertain if, and under what conditions, the symbolic form for the SDOF system will scale to a MDOF system.

A.1 Pre-Multiplication Matrix Strategy for S

Using pre-multiplication to calculate the matrix **S** (see equation A.2) and substituting the analogous matrix equation of equation A.2 into equation A.3, gives the following results:

A.1.1 Matrix Product $\mathbf{A^T S}$:

$$\text{Element 1-1} = -\frac{1}{2}[\mathbf{K^{-1}}][\mathbf{K}][\mathbf{K^\star}] = -\frac{1}{2}[\mathbf{K^\star}] \tag{A.4}$$

$$\text{Element 1-2} = -\frac{1}{2}[\mathbf{K}][\mathbf{M^{-1}}][\mathbf{K^{-1}}][\mathbf{C^{-1}}][\mathbf{M}][\mathbf{M}][\mathbf{K^\star}] \tag{A.5}$$

$$\text{Element 2-1} = \frac{1}{2}[\mathbf{C^{-1}}][\mathbf{M}][\mathbf{K^\star}] + \frac{1}{2}[\mathbf{K^{-1}}][\mathbf{C}][\mathbf{K^\star}] - \frac{1}{2}[\mathbf{C}][\mathbf{M^{-1}}][\mathbf{K^{-1}}][\mathbf{M}][\mathbf{K^\star}] \tag{A.6}$$

$$\text{Element 2-2} = \frac{1}{2}[\mathbf{K^{-1}}][\mathbf{M}][\mathbf{K^\star}] - \frac{1}{2}[\mathbf{C}][\mathbf{M^{-1}}][\mathbf{K^{-1}}][\mathbf{C^{-1}}][\mathbf{M}][\mathbf{M}][\mathbf{K^\star}] \tag{A.7}$$

A.1.2 Matrix Product **SA** :

$$\text{Element 1-1} = -\frac{1}{2}[\mathbf{K^{-1}}][\mathbf{M}][\mathbf{K^{\star}}][\mathbf{M^{-1}}][\mathbf{K}] \tag{A.8}$$

$$\text{Element 1-2} = \frac{1}{2}[\mathbf{C^{-1}}][\mathbf{M}][\mathbf{K^{\star}}] + \frac{1}{2}[\mathbf{K^{-1}}][\mathbf{C}][\mathbf{K^{\star}}] - \frac{1}{2}[\mathbf{K^{-1}}][\mathbf{M}][\mathbf{K^{\star}}][\mathbf{C}][\mathbf{M^{-1}}] \tag{A.9}$$

$$\text{Element 2-1} = -\frac{1}{2}[\mathbf{K^{-1}}][\mathbf{C^{-1}}][\mathbf{M}][\mathbf{M}][\mathbf{K^{\star}}][\mathbf{K}][\mathbf{M^{-1}}] \tag{A.10}$$

$$\text{Element 2-2} = \frac{1}{2}[\mathbf{K^{-1}}][\mathbf{M}][\mathbf{K^{\star}}] - \frac{1}{2}[\mathbf{K^{-1}}][\mathbf{C^{-1}}][\mathbf{M}][\mathbf{M}][\mathbf{K^{\star}}][\mathbf{C}][\mathbf{M^{-1}}] \tag{A.11}$$

It is easy to see that when $[\mathbf{K^{\star}}] = [\mathbf{K}]$ and $[\mathbf{M}]$ is diagonal and uniform (i.e., $m_1 = m_2 = \ldots = m_n$) equations A.4 through A.11 simplify. Substituting $[\mathbf{K^{\star}}] = [\mathbf{K}]$ into equations A.4 through A.11, assuming a diagonal and uniform mass matrix, $[\mathbf{M}]$, and substituting this resultant into equation A.3 results in the following:

$$\mathbf{A^T S + SA} = \begin{bmatrix} -[\mathbf{K}] & \mathbf{0} \\ \begin{pmatrix} \frac{1}{2}[\mathbf{C^{-1}}][\mathbf{M}][\mathbf{K}] + \frac{1}{2}[\mathbf{K^{-1}}][\mathbf{C}][\mathbf{K}] \\ -\frac{1}{2}[\mathbf{C}] - \frac{1}{2}[\mathbf{K^{-1}}][\mathbf{C^{-1}}][\mathbf{M}][\mathbf{K}][\mathbf{K}] \end{pmatrix} & \begin{pmatrix} [\mathbf{K^{-1}}][\mathbf{M}][\mathbf{K}] - \frac{1}{2}[\mathbf{C}][\mathbf{K^{-1}}][\mathbf{C^{-1}}][\mathbf{M}][\mathbf{K}] \\ -\frac{1}{2}[\mathbf{K^{-1}}][\mathbf{C^{-1}}][\mathbf{M}][\mathbf{K}][\mathbf{C}] \end{pmatrix} \end{bmatrix}, \tag{A.12}$$

Note the following equalities:

1. $[\mathbf{K^{-1}}][\mathbf{C}][\mathbf{K}] = [\mathbf{C}]$
2. $[\mathbf{K^{-1}}][\mathbf{C^{-1}}][\mathbf{M}][\mathbf{K}] = [\mathbf{C^{-1}}][\mathbf{M}]$
3. $[\mathbf{C}][\mathbf{K^{-1}}][\mathbf{C^{-1}}] = [\mathbf{K^{-1}}]$
4. $[\mathbf{C^{-1}}][\mathbf{M}][\mathbf{K}][\mathbf{C}] = [\mathbf{M}][\mathbf{K}]$

Substituting these equalities into equation A.12 and simplifying terms gives:

$$\mathbf{A^T S + SA} = \begin{bmatrix} -[\mathbf{K}] & \mathbf{0} \\ \mathbf{0} & \mathbf{0} \end{bmatrix} = -\mathbf{Q}. \tag{A.13}$$

A.2 Post-Multiplication Matrix Strategy for S

Using post-multiplication to calculate the matrix **S** (see equation A.2) and substituting the analogous matrix equation of equation A.2 into equation A.3, gives the following results:

A.2.1 Matrix Product $\mathbf{A^T S}$:

$$\text{Element 1-1} = -\frac{1}{2}[\mathbf{K}][\mathbf{K^\star}][\mathbf{K^{-1}}] \tag{A.14}$$

$$\text{Element 1-2} = -\frac{1}{2}[\mathbf{K}][\mathbf{M}][\mathbf{K^\star}][\mathbf{K^{-1}}][\mathbf{C^{-1}}] \tag{A.15}$$

$$\text{Element 2-1} = \frac{1}{2}[\mathbf{M}][\mathbf{K^\star}][\mathbf{C^{-1}}] \tag{A.16}$$

$$\text{Element 2-2} = \frac{1}{2}[\mathbf{M}][\mathbf{K^\star}][\mathbf{K^{-1}}] - \mathbf{\frac{1}{2}}[\mathbf{C}][\mathbf{M}][\mathbf{K^\star}][\mathbf{K^{-1}}][\mathbf{C^{-1}}] \tag{A.17}$$

A.2.2 Matrix Product $\mathbf{SA}$:

$$\text{Element 1-1} = -\frac{1}{2}[\mathbf{M}][\mathbf{K^\star}][\mathbf{K^{-1}}][\mathbf{M}][\mathbf{K}] \tag{A.18}$$

$$\text{Element 1-2} = \frac{1}{2}[\mathbf{M}][\mathbf{K^\star}][\mathbf{C^{-1}}] + \frac{1}{2}[\mathbf{C}][\mathbf{K^\star}][\mathbf{K^{-1}}] - \frac{1}{2}[\mathbf{M}][\mathbf{K^\star}][\mathbf{K^{-1}}][\mathbf{M^{-1}}][\mathbf{C}] \tag{A.19}$$

$$\text{Element 2-1} = -\frac{1}{2}[\mathbf{M}][\mathbf{M}][\mathbf{K}^\star][\mathbf{K}^{-1}][\mathbf{C}^{-1}][\mathbf{M}^{-1}][\mathbf{K}] \tag{A.20}$$

$$\text{Element 2-2} = \frac{1}{2}[\mathbf{M}][\mathbf{K}^\star][\mathbf{K}^{-1}] - \frac{1}{2}[\mathbf{M}][\mathbf{M}][\mathbf{K}^\star][\mathbf{K}^{-1}][\mathbf{C}^{-1}][\mathbf{M}^{-1}][\mathbf{C}] \tag{A.21}$$

As with the pre-multiplication strategy for calculating $\mathbf{S}$, when $[\mathbf{K}^\star] = [\mathbf{K}]$ and $[\mathbf{M}]$ is diagonal and uniform (i.e., $m_1 = m_2 = \ldots = m_n$) equations A.14 through A.21 simplify. Substituting $[\mathbf{K}^\star] = [\mathbf{K}]$ into equations A.14 through A.21, assuming a diagonal and uniform mass matrix, $[\mathbf{M}]$, and substituting this resultant into equation A.3 results in the following:

$$\mathbf{A^T S + SA} = \begin{bmatrix} -[\mathbf{K}] & -\frac{1}{2}[\mathbf{K}][\mathbf{M}][\mathbf{C^{-1}}] + \frac{1}{2}[\mathbf{M}][\mathbf{K}][\mathbf{C^{-1}}] \\ \frac{1}{2}[\mathbf{M}][\mathbf{K}][\mathbf{C^{-1}}] - \frac{1}{2}[\mathbf{M}][\mathbf{C^{-1}}][\mathbf{K}] & \frac{1}{2}[\mathbf{M}] - \frac{1}{2}[\mathbf{C}][\mathbf{M}][\mathbf{C^{-1}}] \end{bmatrix}. \tag{A.22}$$

Note the following equalities:

1. $[\mathbf{K}][\mathbf{C^{-1}}] = ([\mathbf{K}][\mathbf{C^{-1}}])^\mathbf{T} = [\mathbf{C}]^\mathbf{T}[\mathbf{K}]^\mathbf{T} = [\mathbf{C^{-1}}][\mathbf{K}]$
2. $[\mathbf{C}][\mathbf{M}][\mathbf{C^{-1}}] = [\mathbf{M}]$
3. $[\mathbf{K}][\mathbf{M}] = ([\mathbf{K}][\mathbf{M}])^\mathbf{T} = [\mathbf{M}]^\mathbf{T}[\mathbf{K}]^\mathbf{T} = [\mathbf{M}][\mathbf{K}]$

Substituting these equalities into equation A.22 and simplifying terms gives:

$$\mathbf{A^T S + SA} = \begin{bmatrix} -[\mathbf{K}] & \mathbf{0} \\ \mathbf{0} & \mathbf{0} \end{bmatrix} = -\mathbf{Q}. \tag{A.23}$$

Appendix B

Figures: Chapter 6

B.1 LDBI and LDBI+CKBB Control: Moderate Earthquakes

Base Isolator Drift: LDBI/LDBI+CKBB Designs

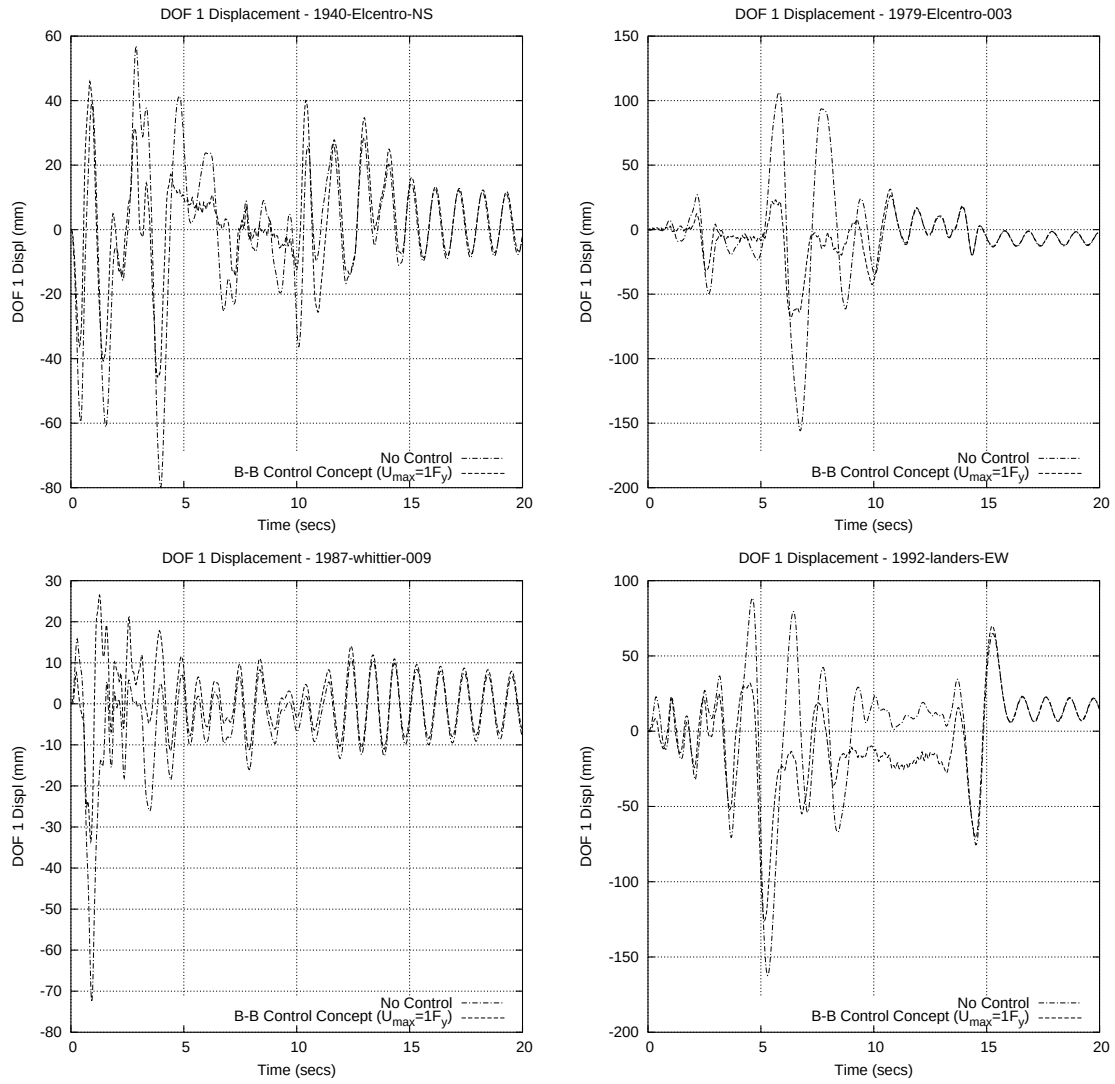

Figure B.1: Moderate EQs: 1940 El Centro, 1979 El Centro, 1987 Whittier, 1992 Landers.

Hystersis Curves: LDBI+CKBB Design

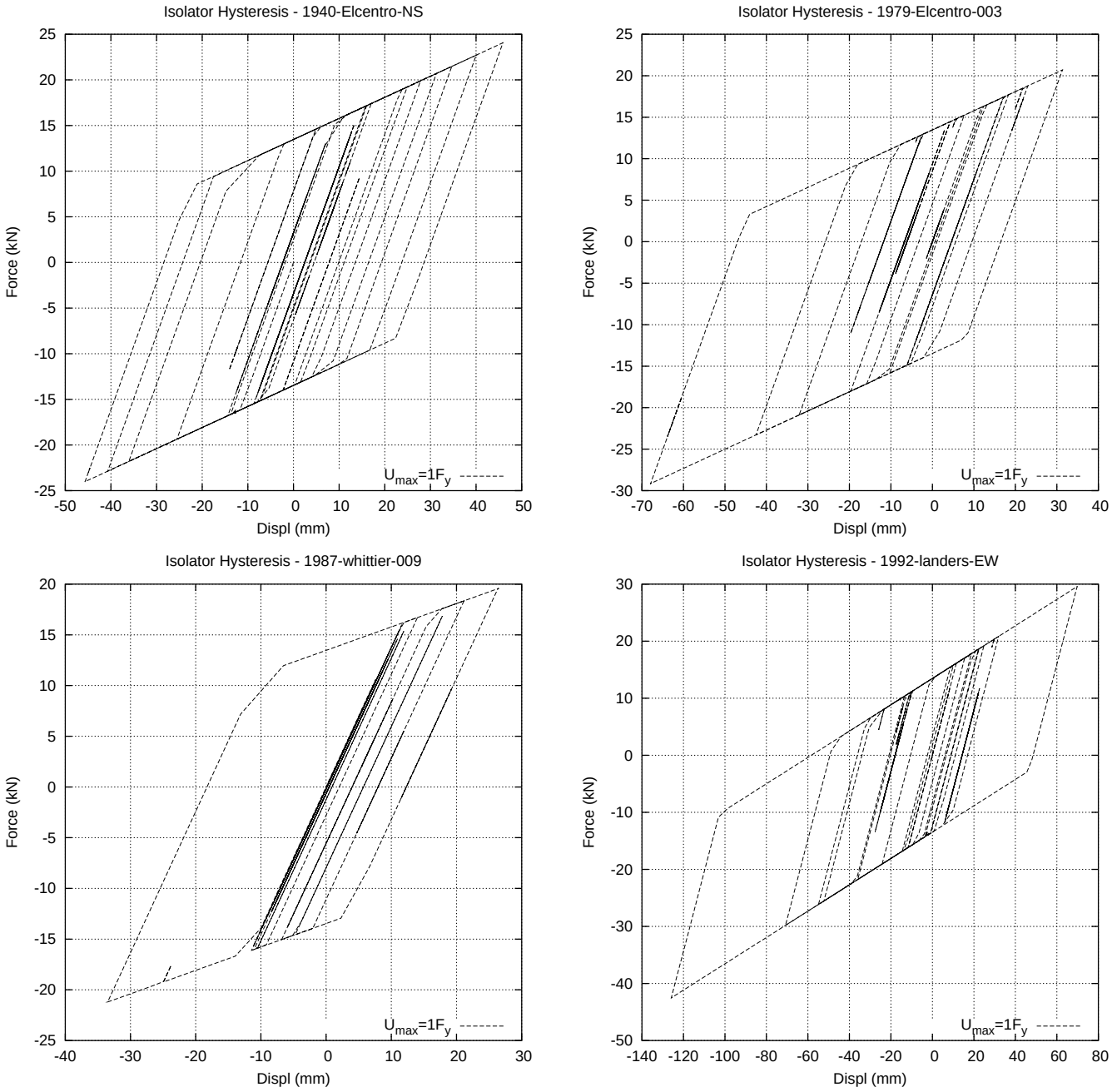

Figure B.2: Moderate EQs: 1940 El Centro, 1979 El Centro, 1987 Whittier, 1992 Landers.

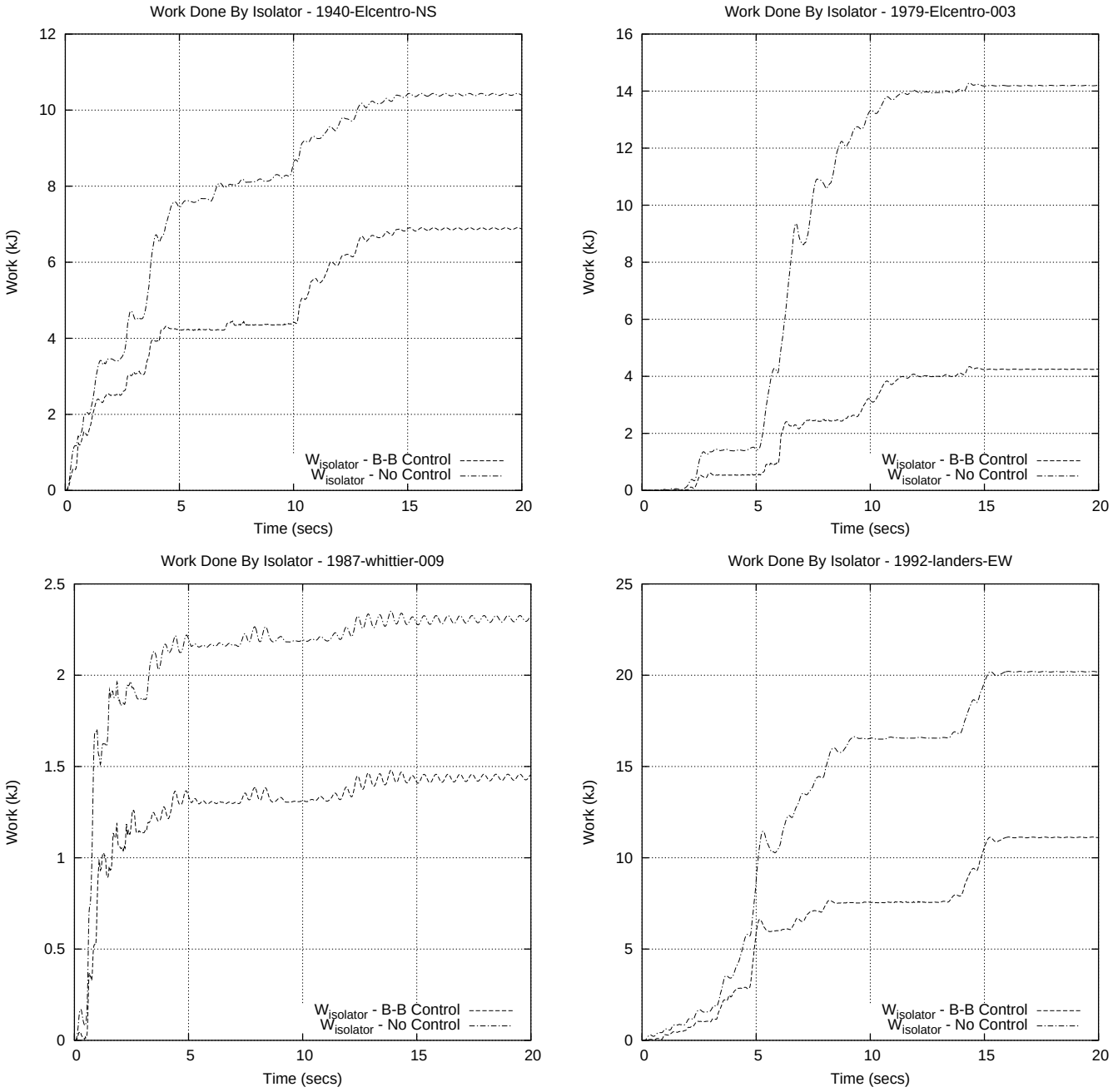

Figure B.3: Moderate EQs: 1940 El Centro, 1979 El Centro, 1987 Whittier, 1992 Landers.

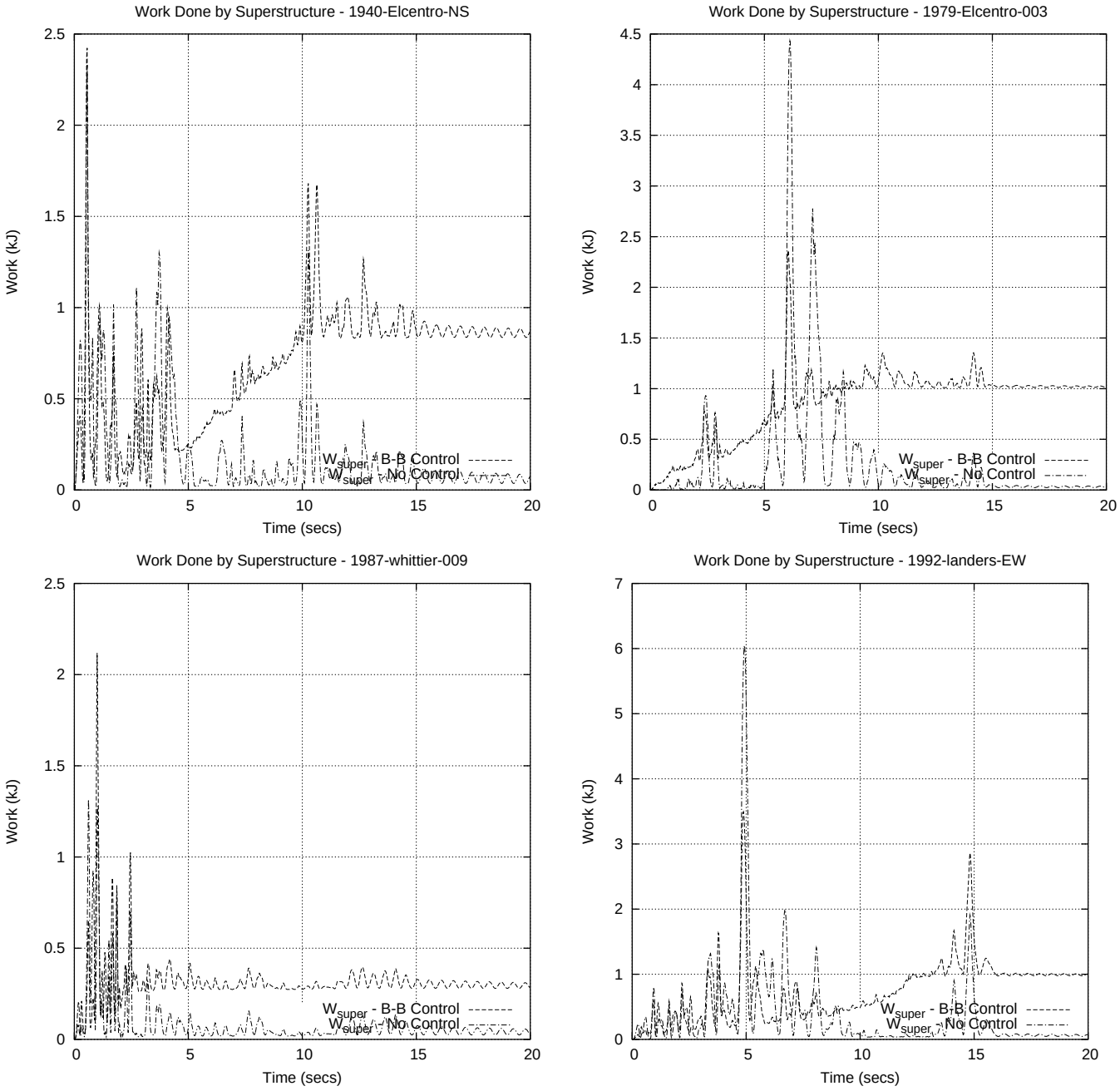

Figure B.4: Moderate EQs: 1940 El Centro, 1979 El Centro, 1987 Whittier, 1992 Landers.

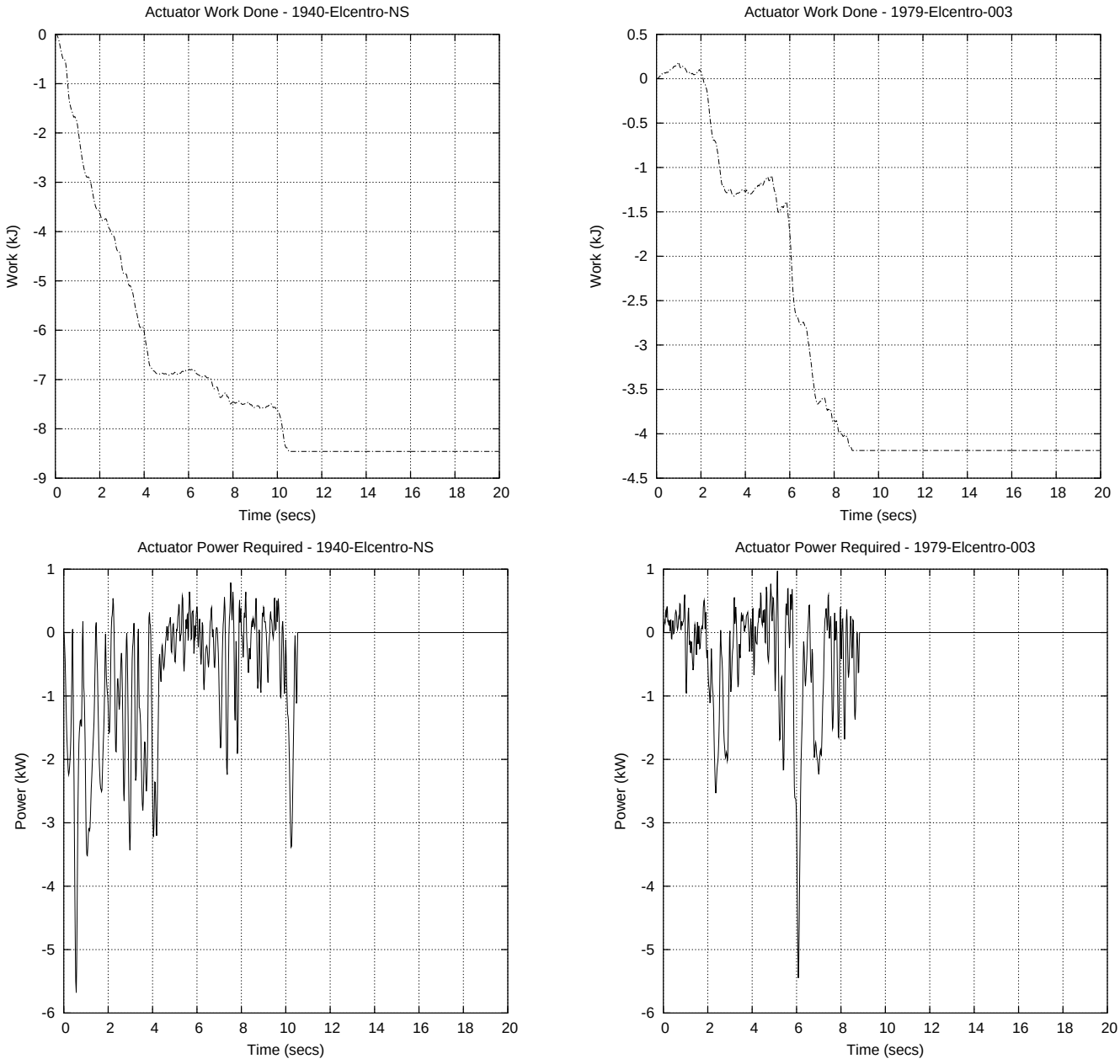

Figure B.5: Moderate EQs: 1940 El Centro and 1979 El Centro.

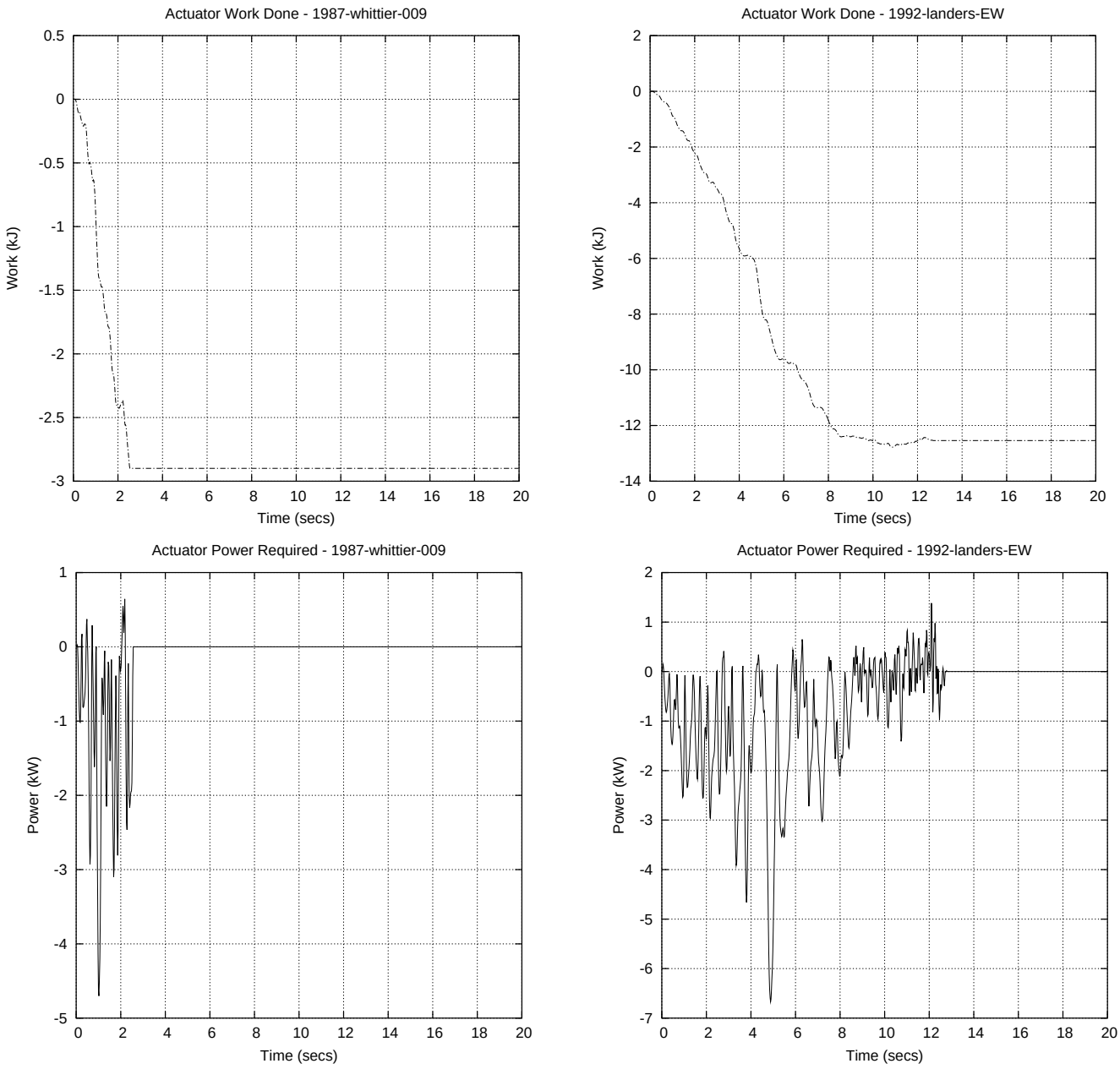

Figure B.6: Moderate EQs: 1987 Whittier and 1992 Landers.

B.2 LDBI and LDBI+CKBB Control: Severe Earthquakes

Base Isolator Drift: LDBI/LDBI+CKBB Designs

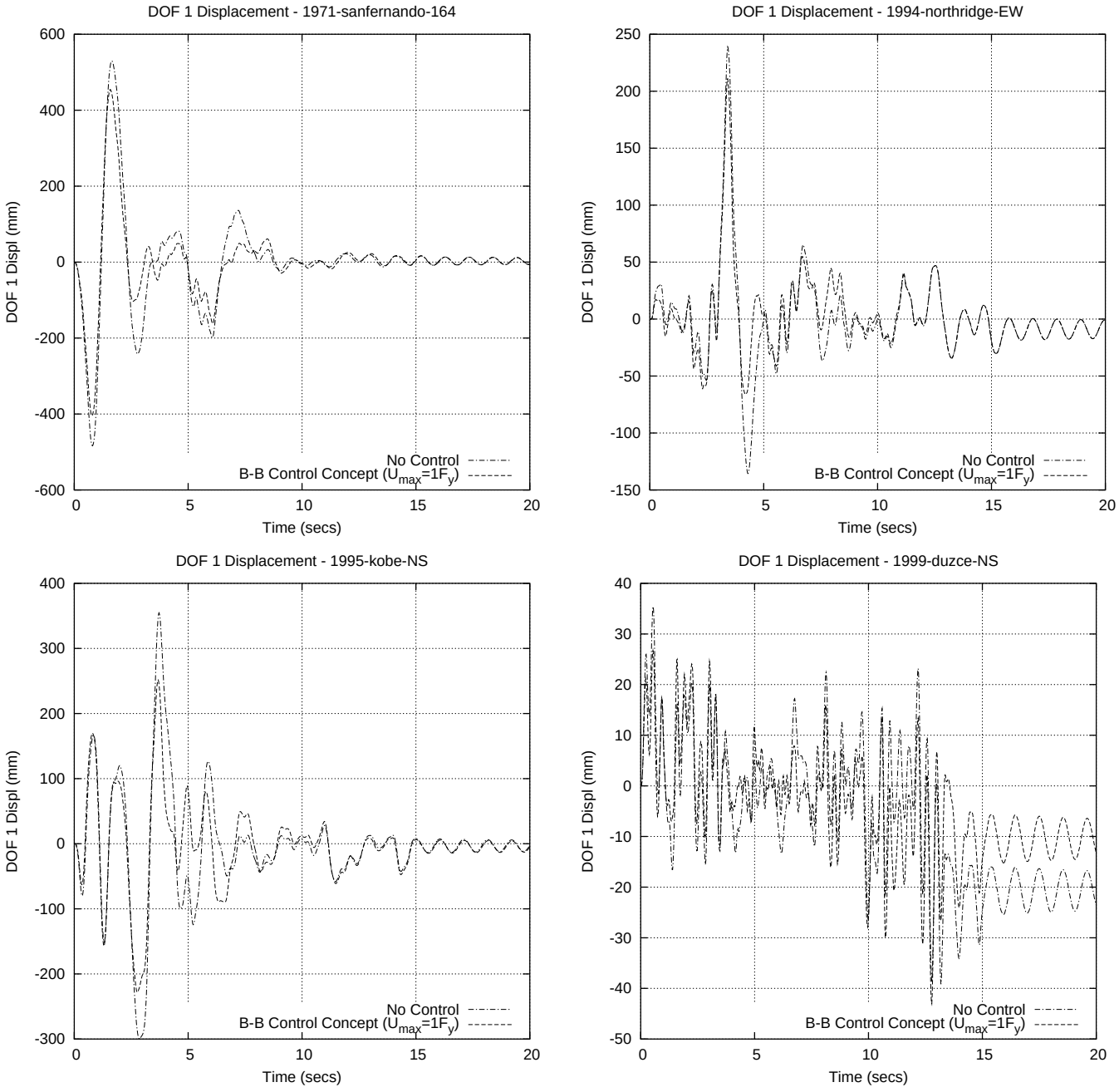

Figure B.7: Severe EQs: 1971 San Fernando, 1994 Northridge, 1995 Kobe, 1999 Duzce.

Hystersis Curves: LDBI+CKBB Design

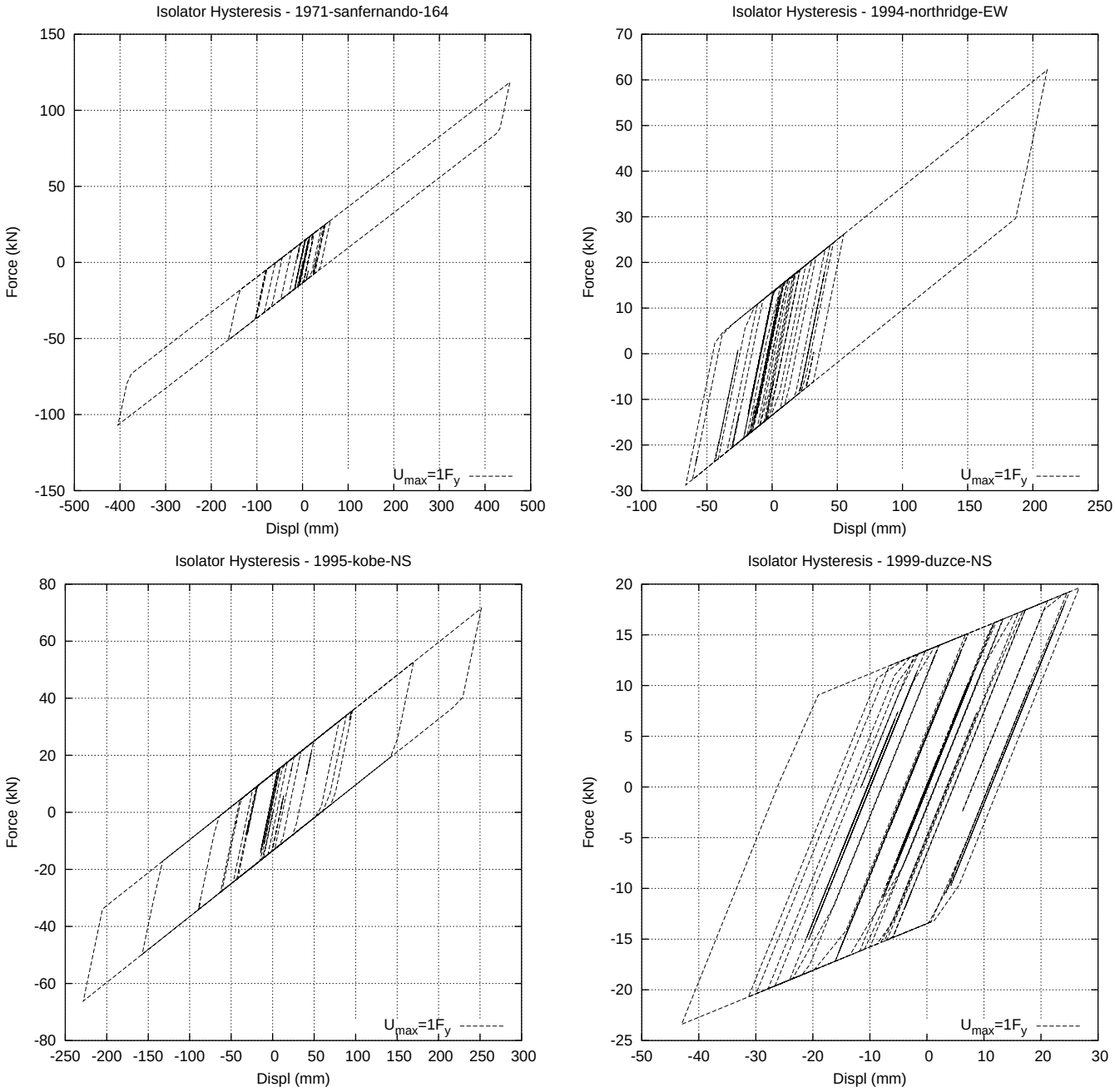

Figure B.8: Severe EQs: 1971 San Fernando, 1994 Northridge, 1995 Kobe, 1999 Duzce.

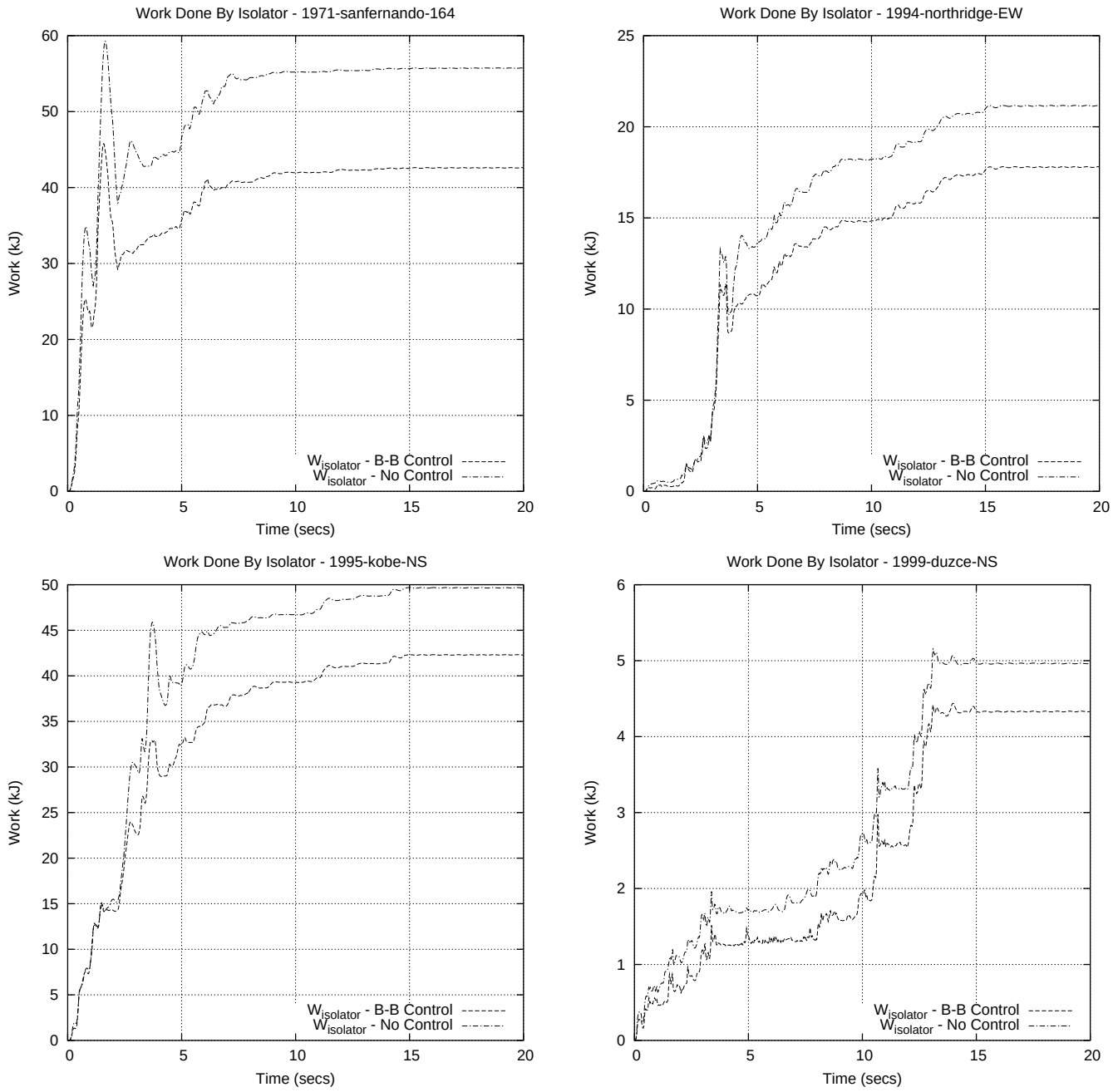

Figure B.9: Severe EQs: 1971 San Fernando, 1994 Northridge, 1995 Kobe, 1999 Duzce.

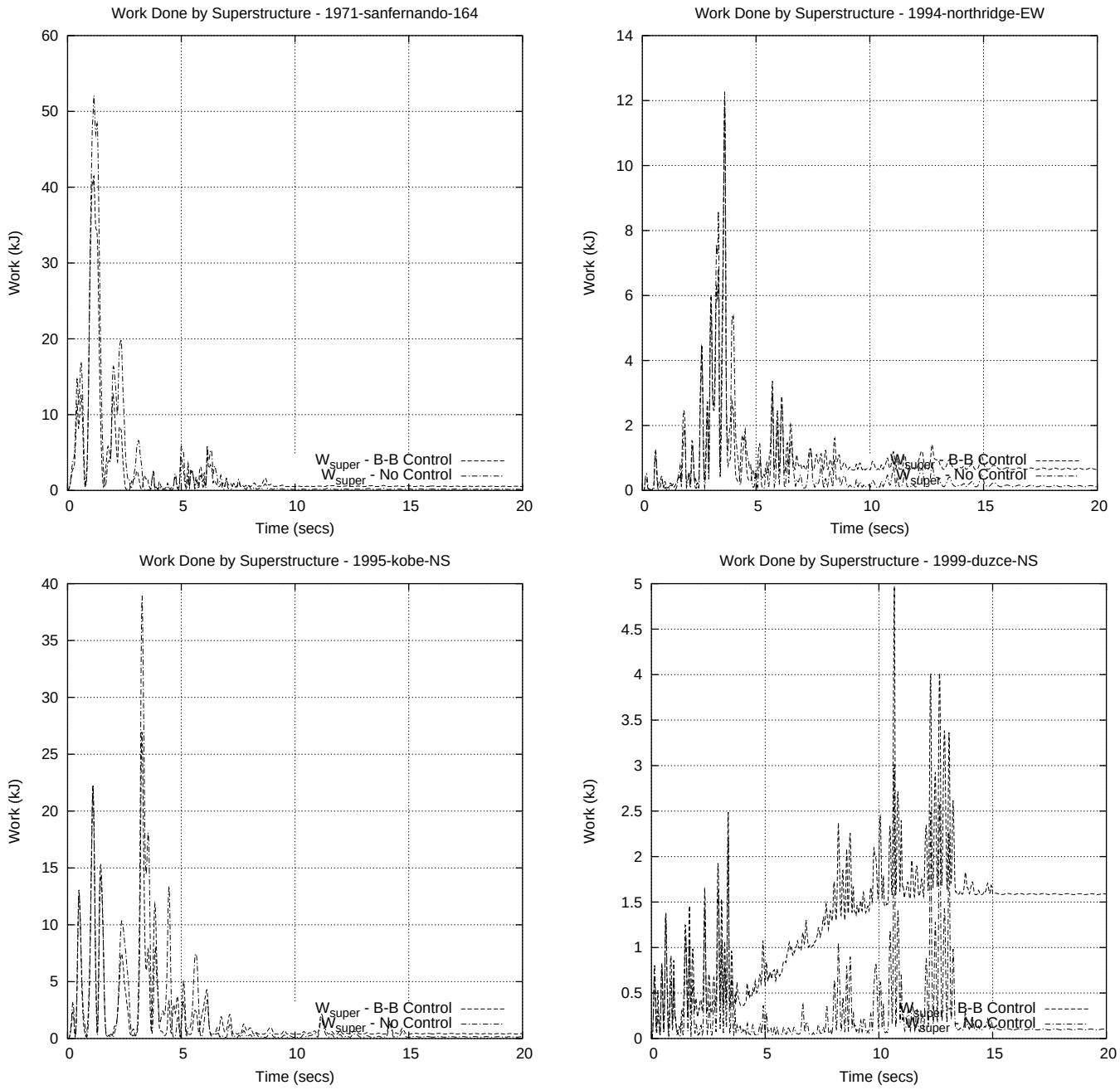

Figure B.10: Severe EQs: 1971 San Fernando, 1994 Northridge, 1995 Kobe, 1999 Duzce.

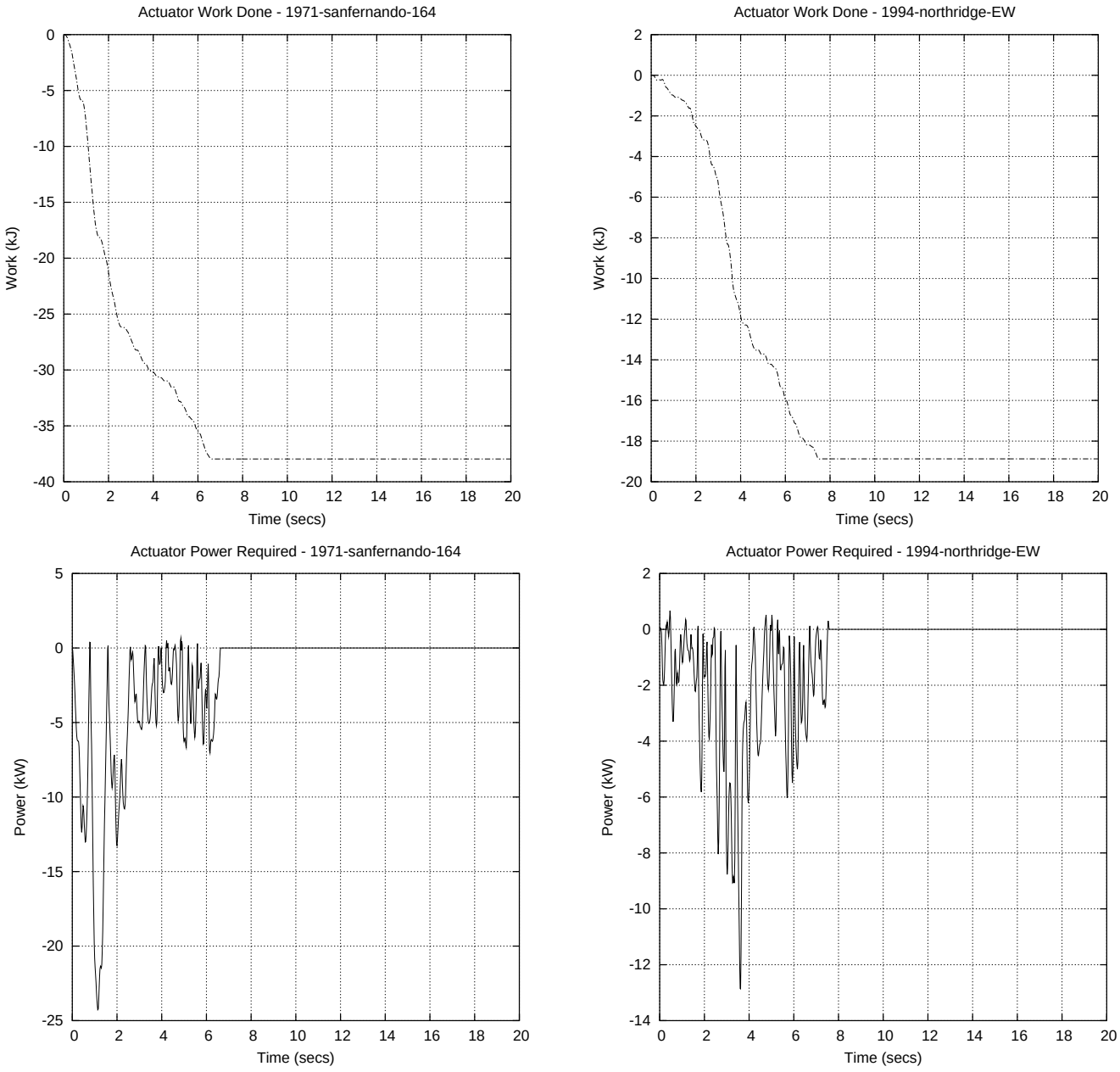

Figure B.11: Severe EQs: 1971 San Fernando and 1994 Northridge.

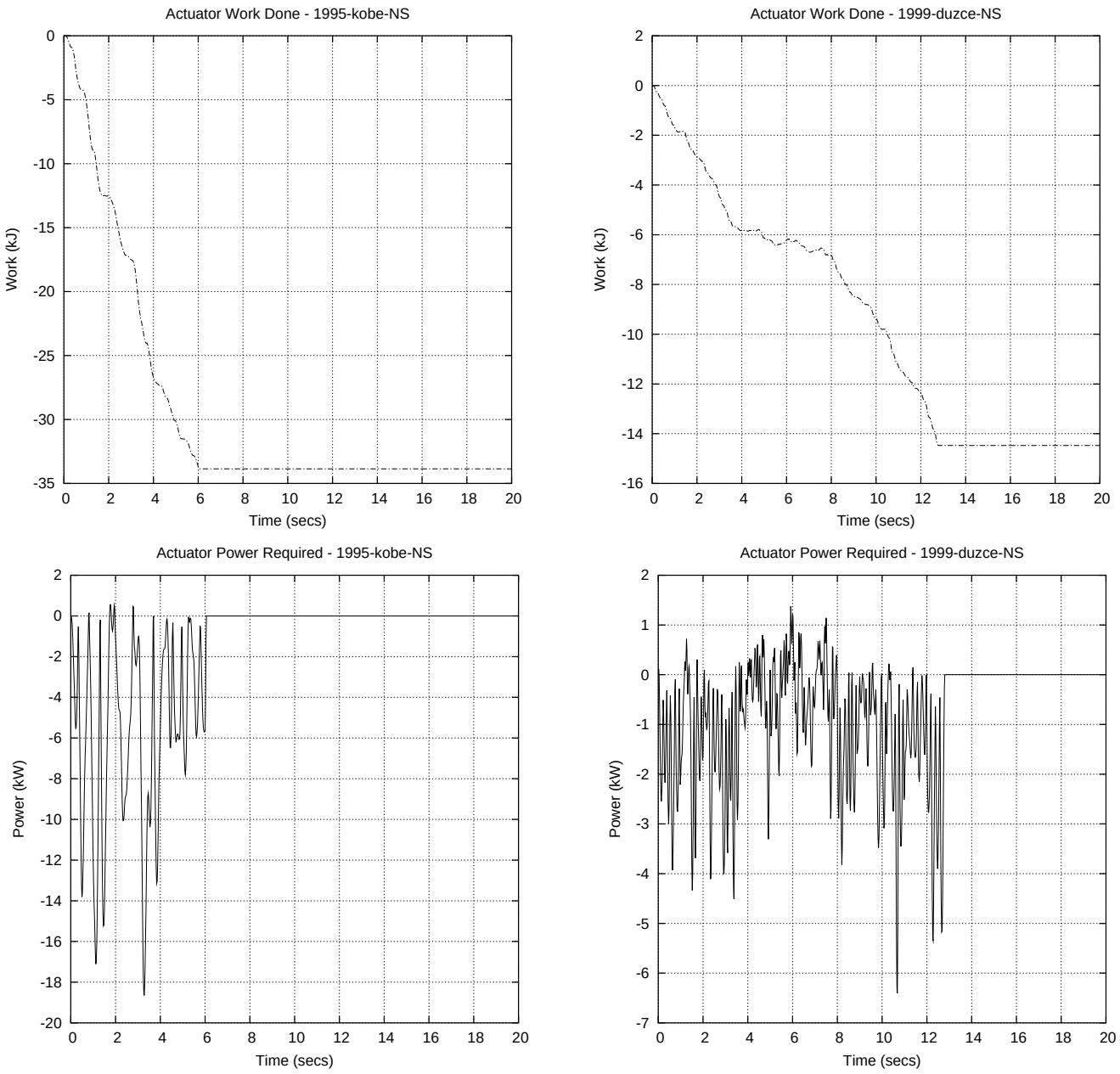

Figure B.12: Severe EQs: 1995 Kobe and 1999 Duzce.

B.3 HDBI and HDBI+CKBB Control: Moderate Earthquakes

Base Isolator Drift: HDBI/HDBI+CKBB Designs

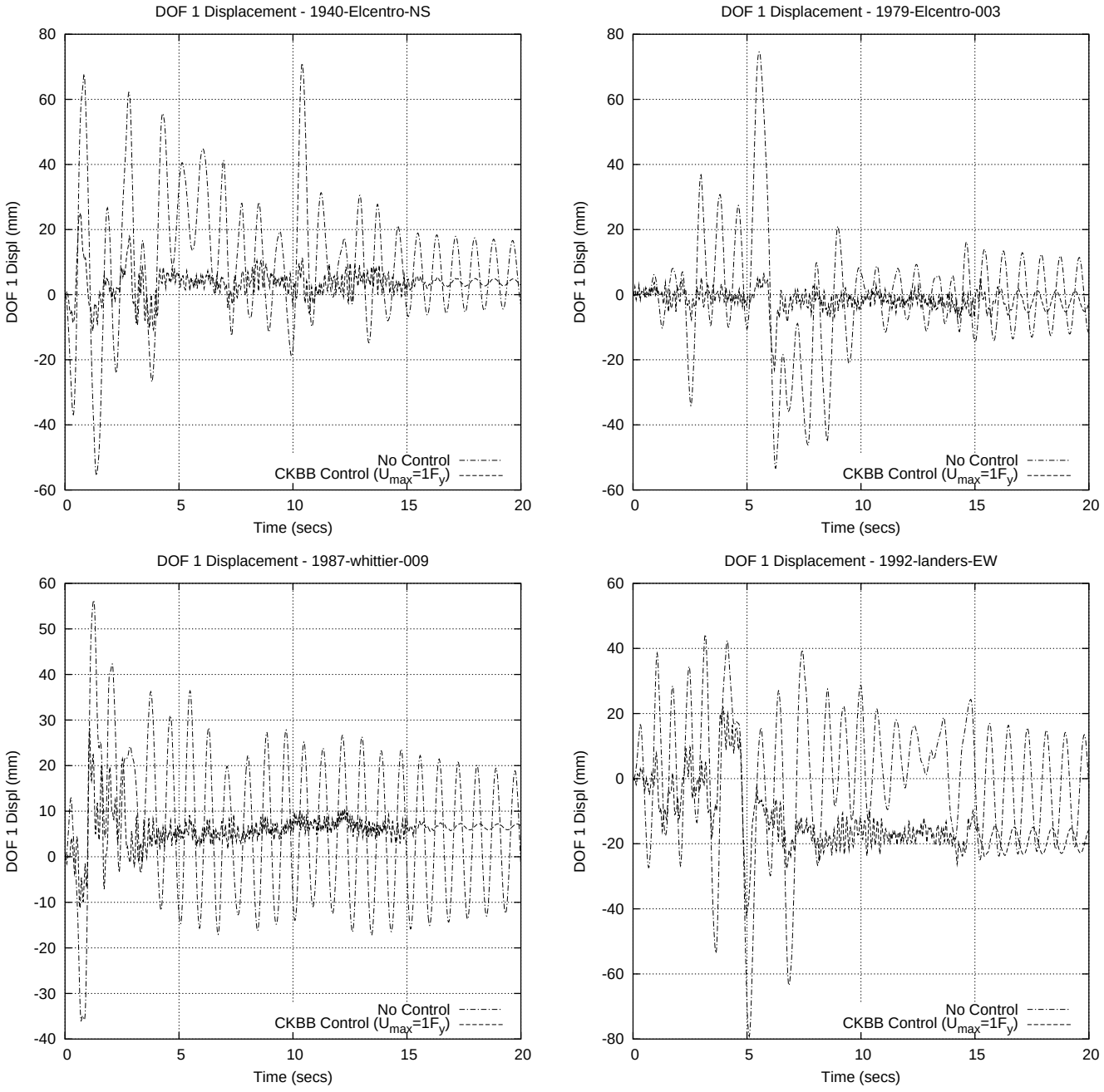

Figure B.13: Moderate EQs: 1940 El Centro, 1979 El Centro, 1987 Whittier, 1992 Landers.

Hystersis Curves: HDBI+CKBB Design

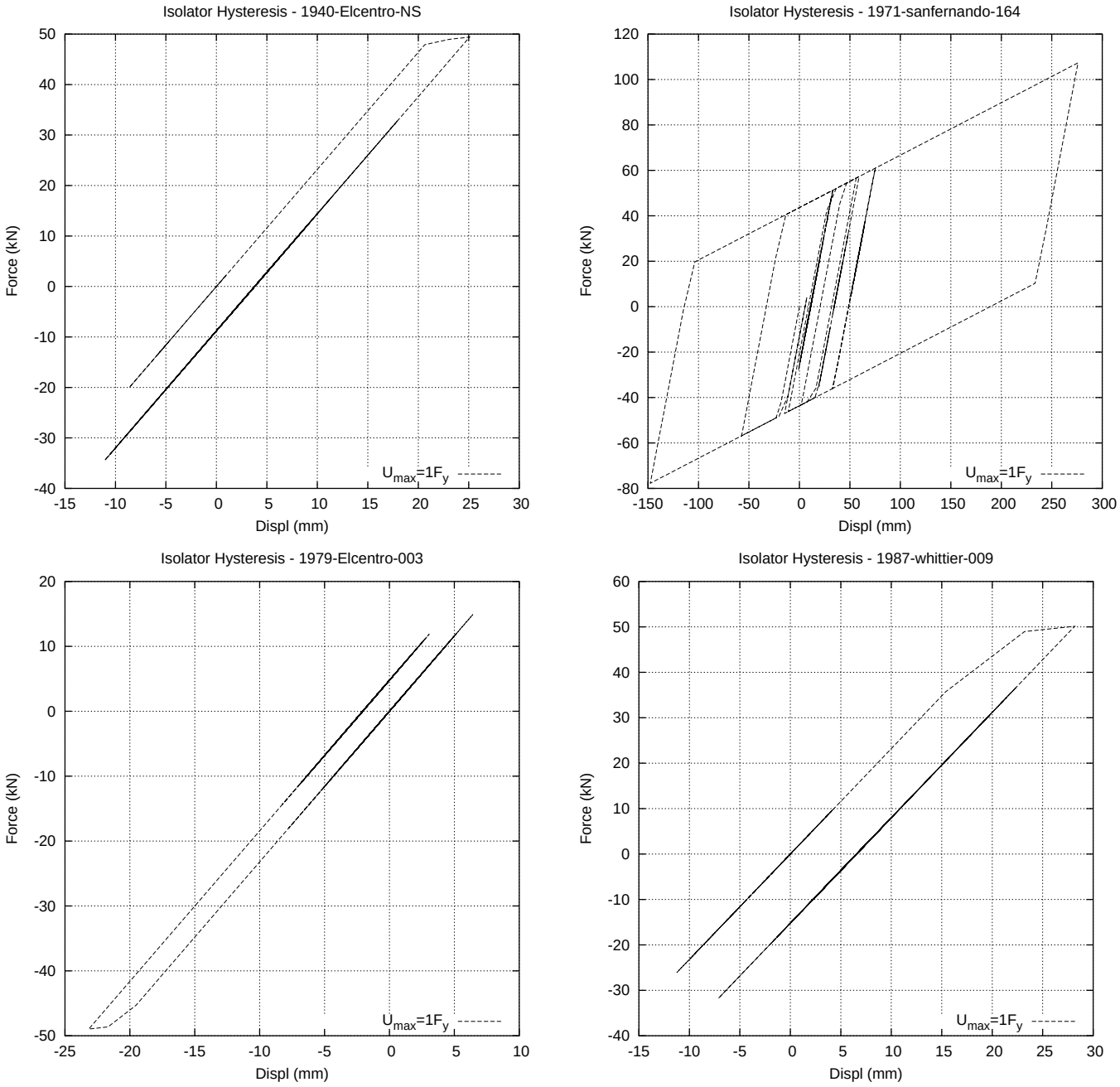

Figure B.14: Moderate EQs: 1940 El Centro, 1979 El Centro, 1987 Whittier, 1992 Landers.

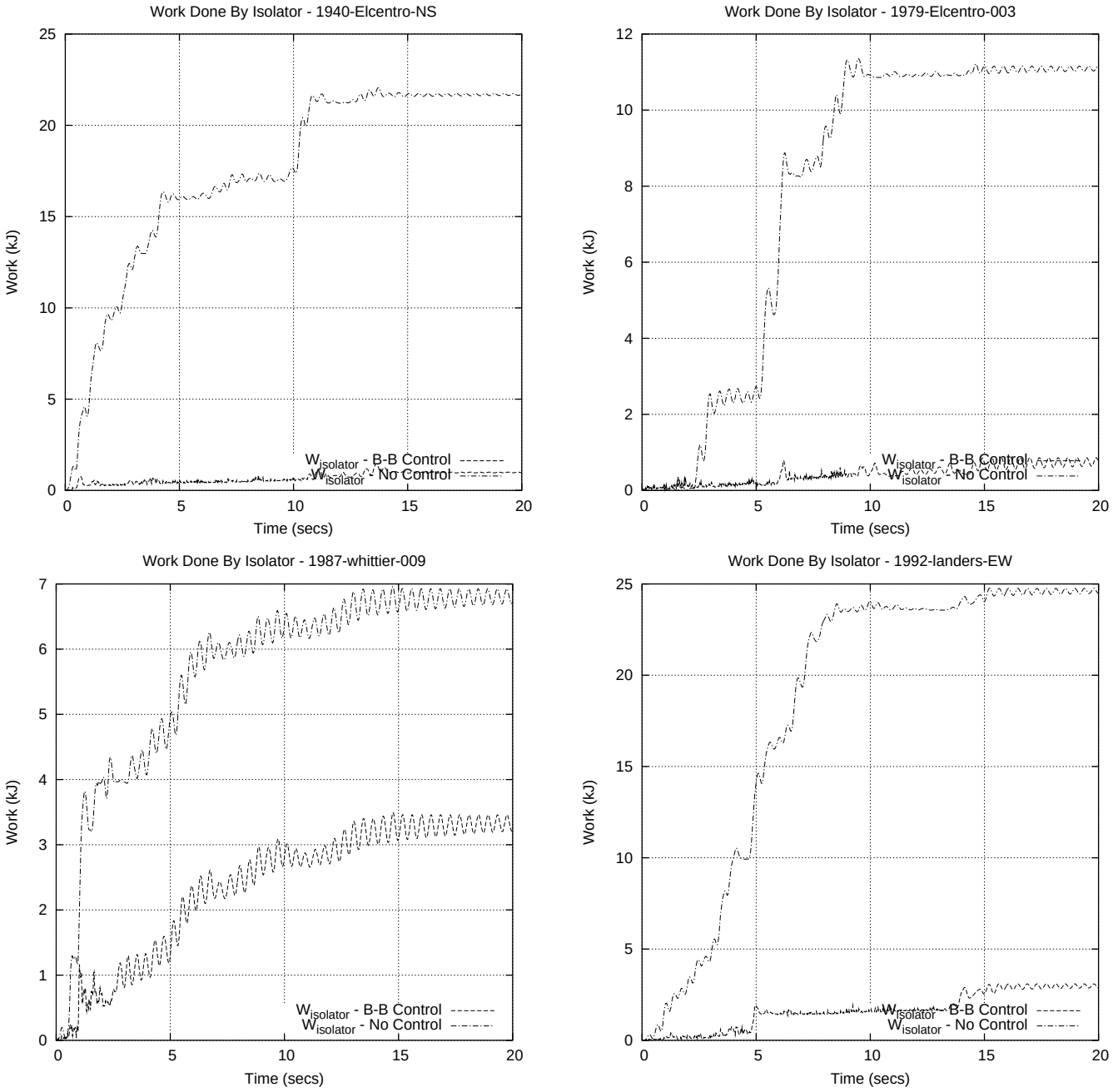

Figure B.15: Moderate EQs: 1940 El Centro, 1979 El Centro, 1987 Whittier, 1992 Landers.

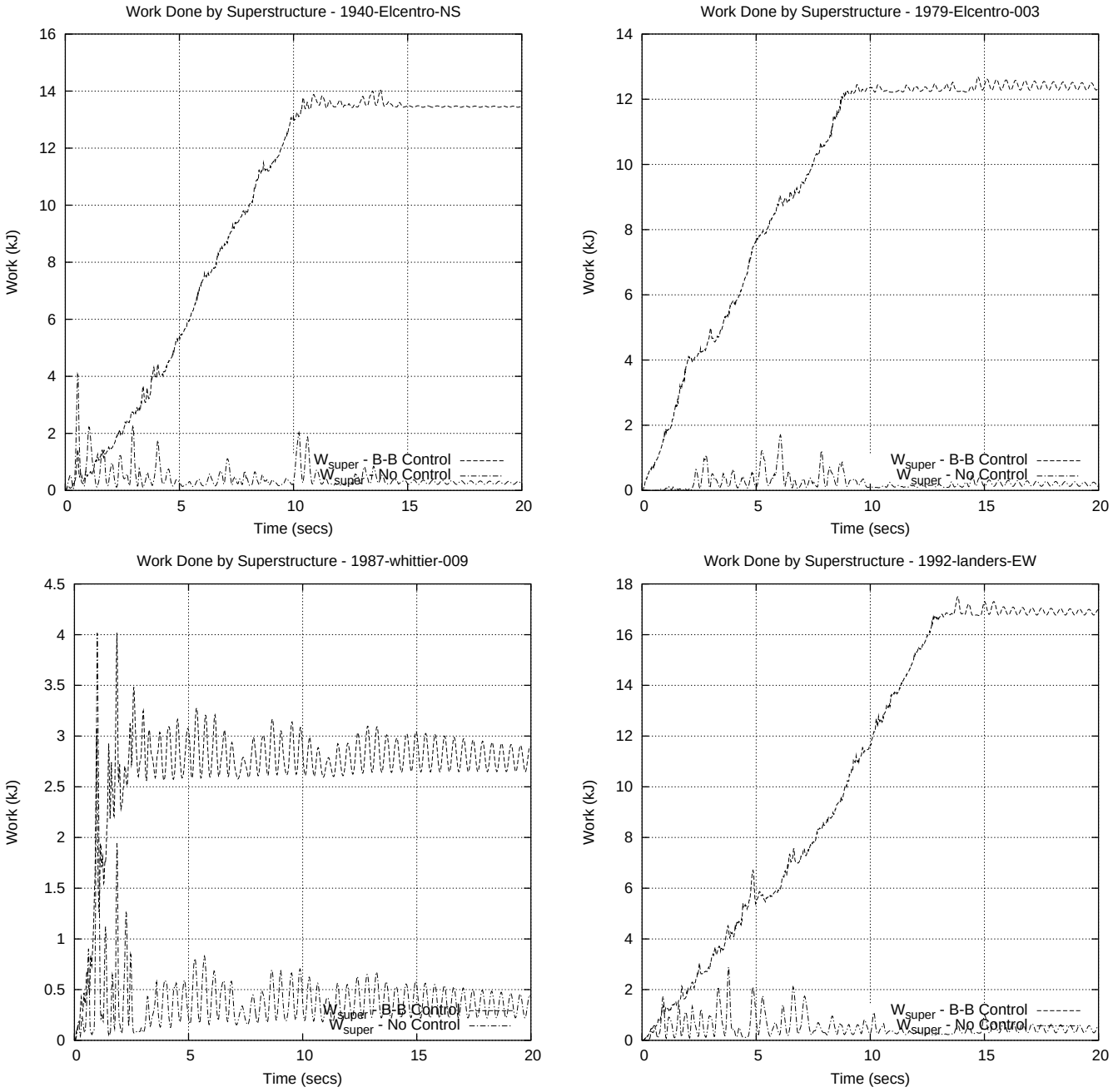

Figure B.16: Moderate EQs: 1940 El Centro, 1979 El Centro, 1987 Whittier, 1992 Landers.

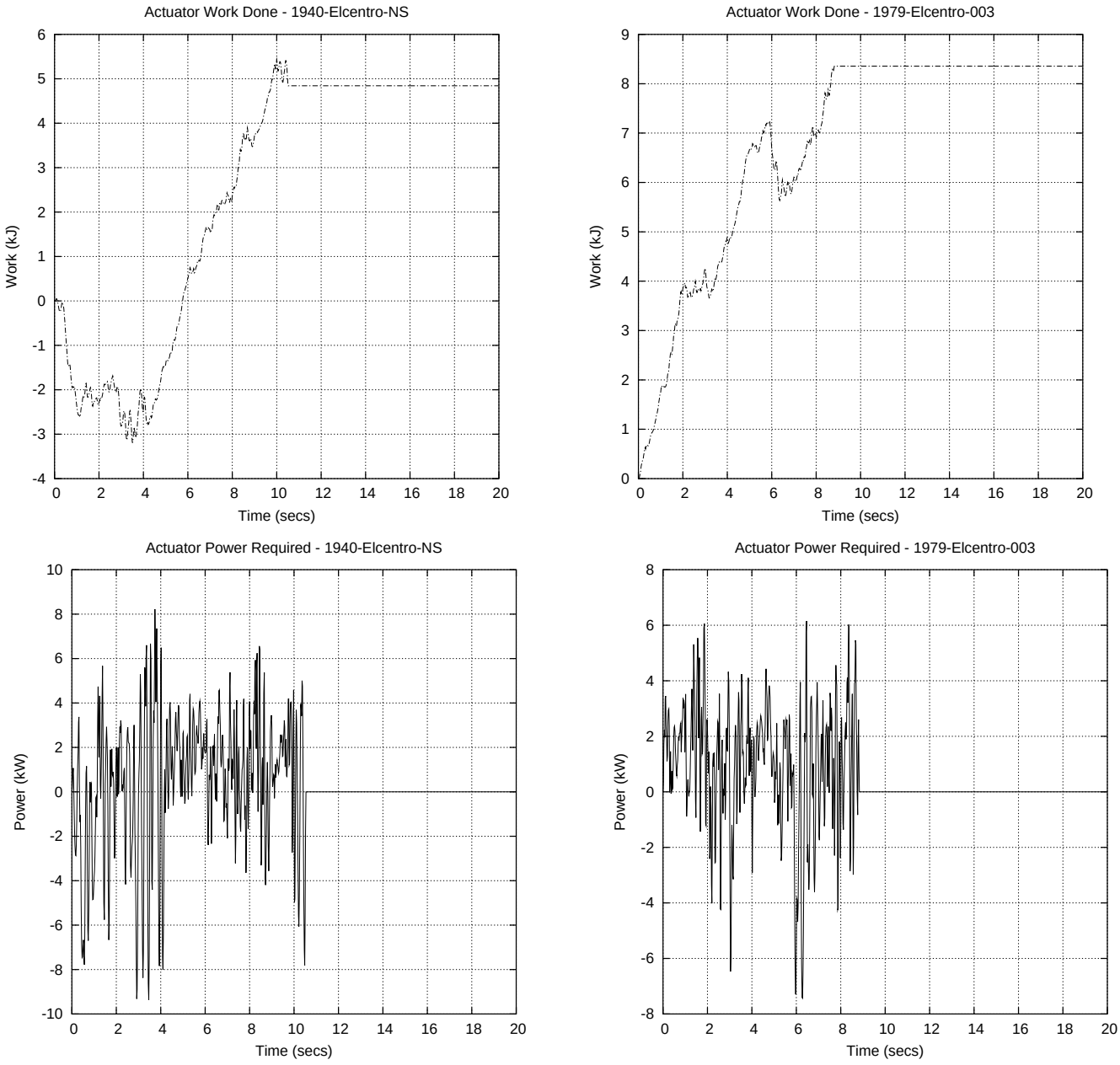

Figure B.17: Moderate EQs: 1940 El Centro and 1979 El Centro.

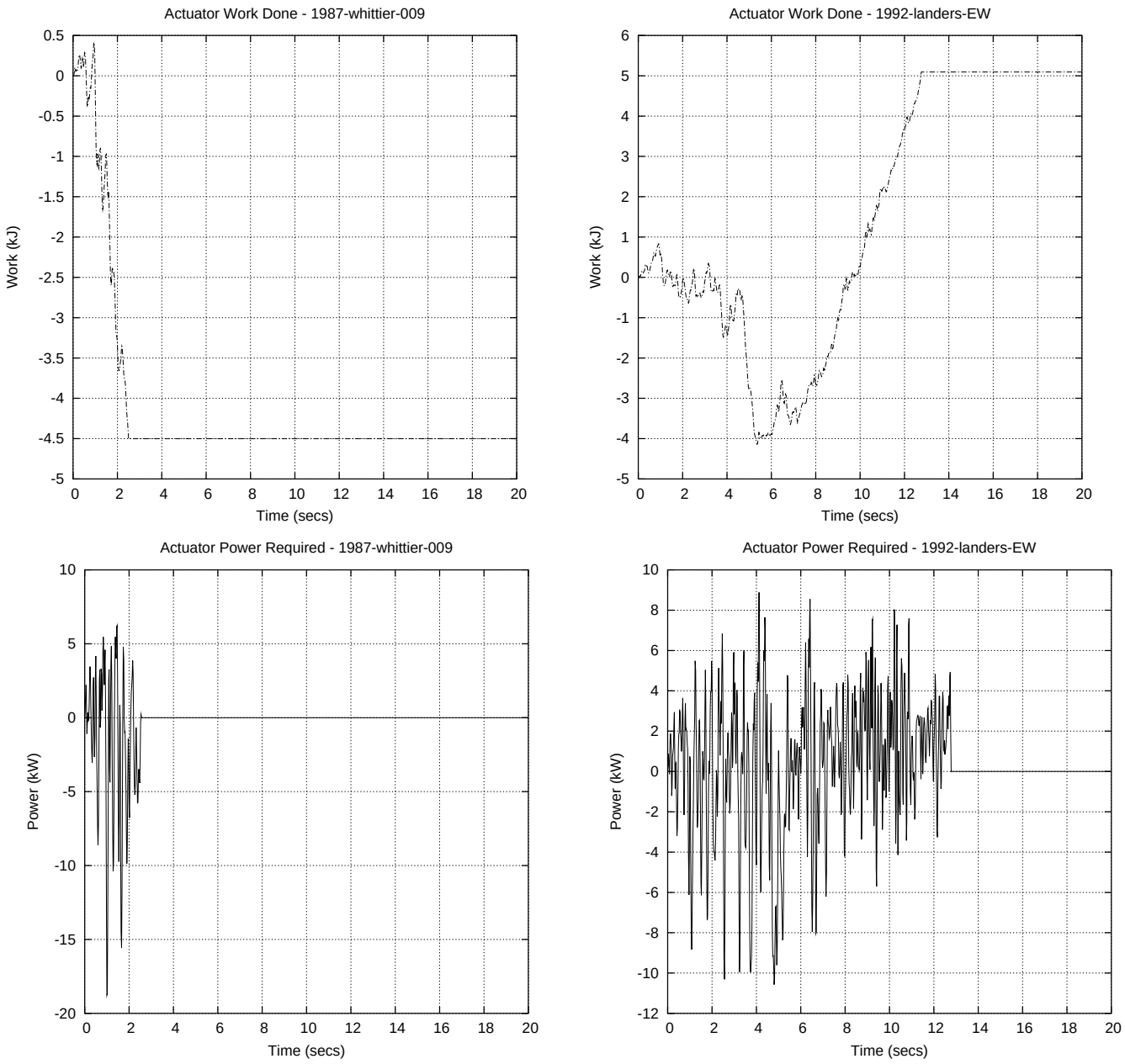

Figure B.18: Moderate EQs: 1987 Whittier and 1992 Landers.

B.4 HDBI and HDBI+CKBB Control: Severe Earthquakes

Base Isolator Drift: HDBI/HDBI+CKBB Designs

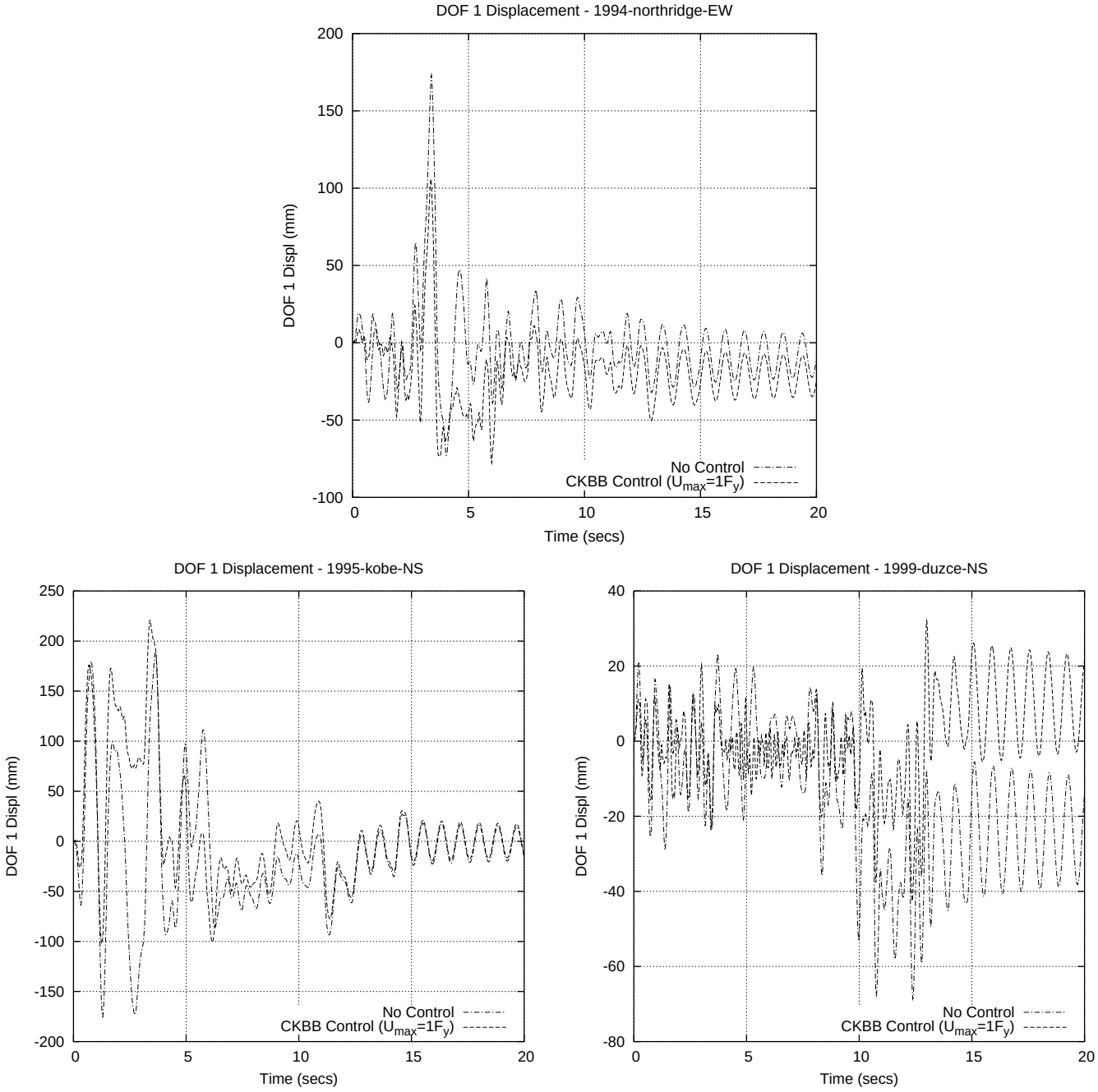

Figure B.19: Severe EQs: 1994 Northridge, 1995 Kobe, 1999 Duzce.

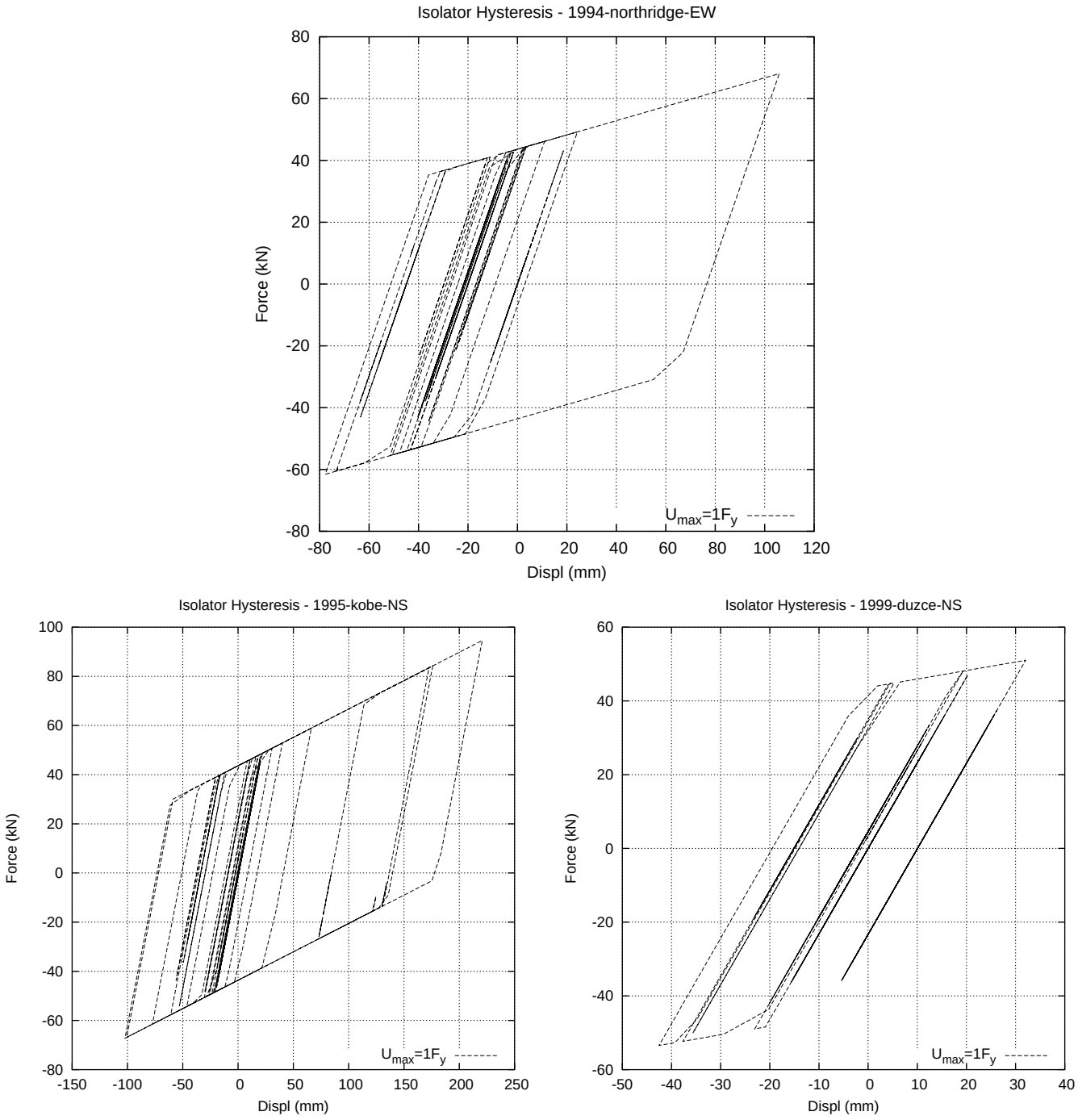

Figure B.20: Severe EQs: 1994 Northridge, 1995 Kobe, 1999 Duzce.

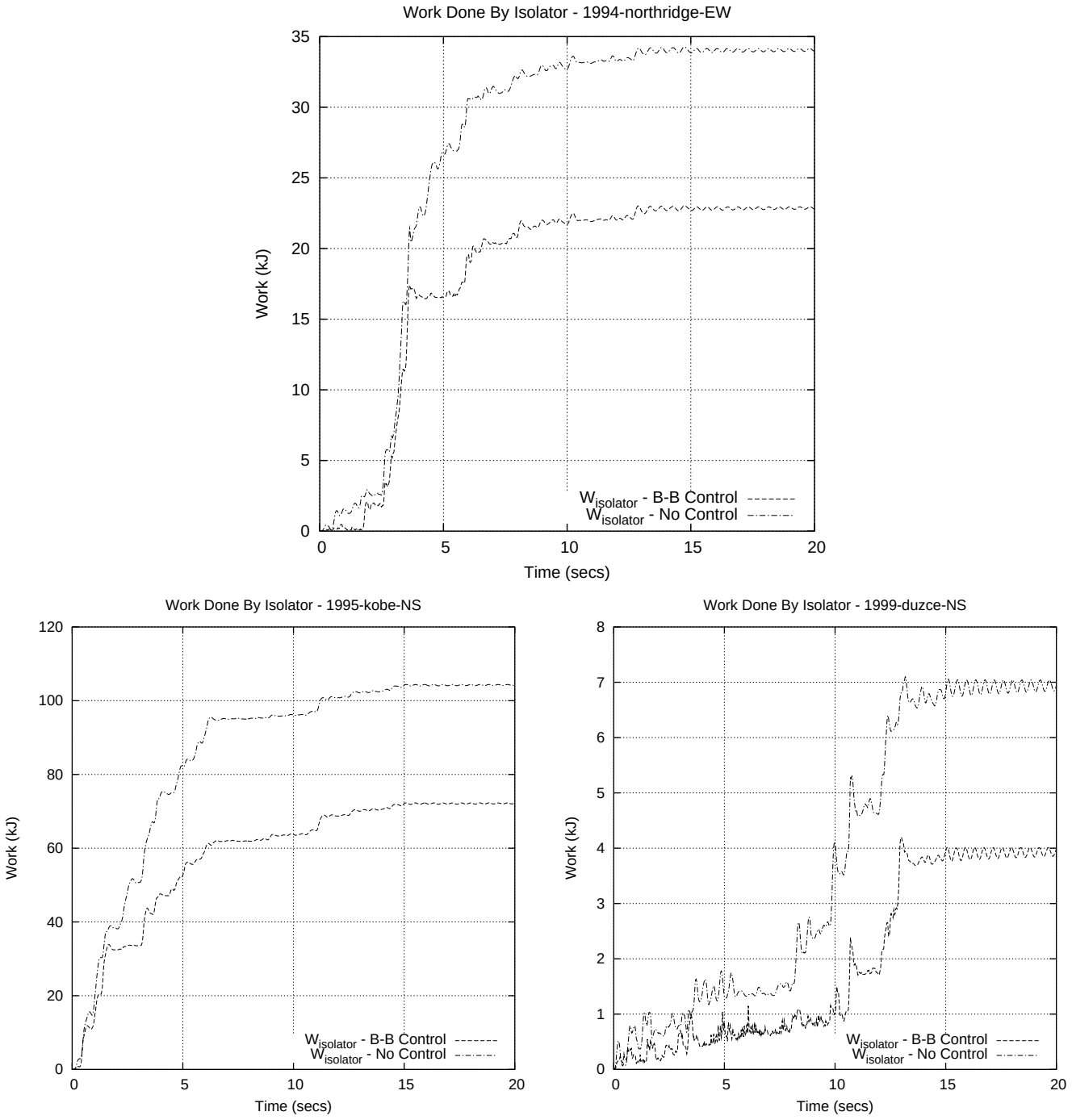

Figure B.21: Severe EQs: 1994 Northridge, 1995 Kobe, 1999 Duzce.

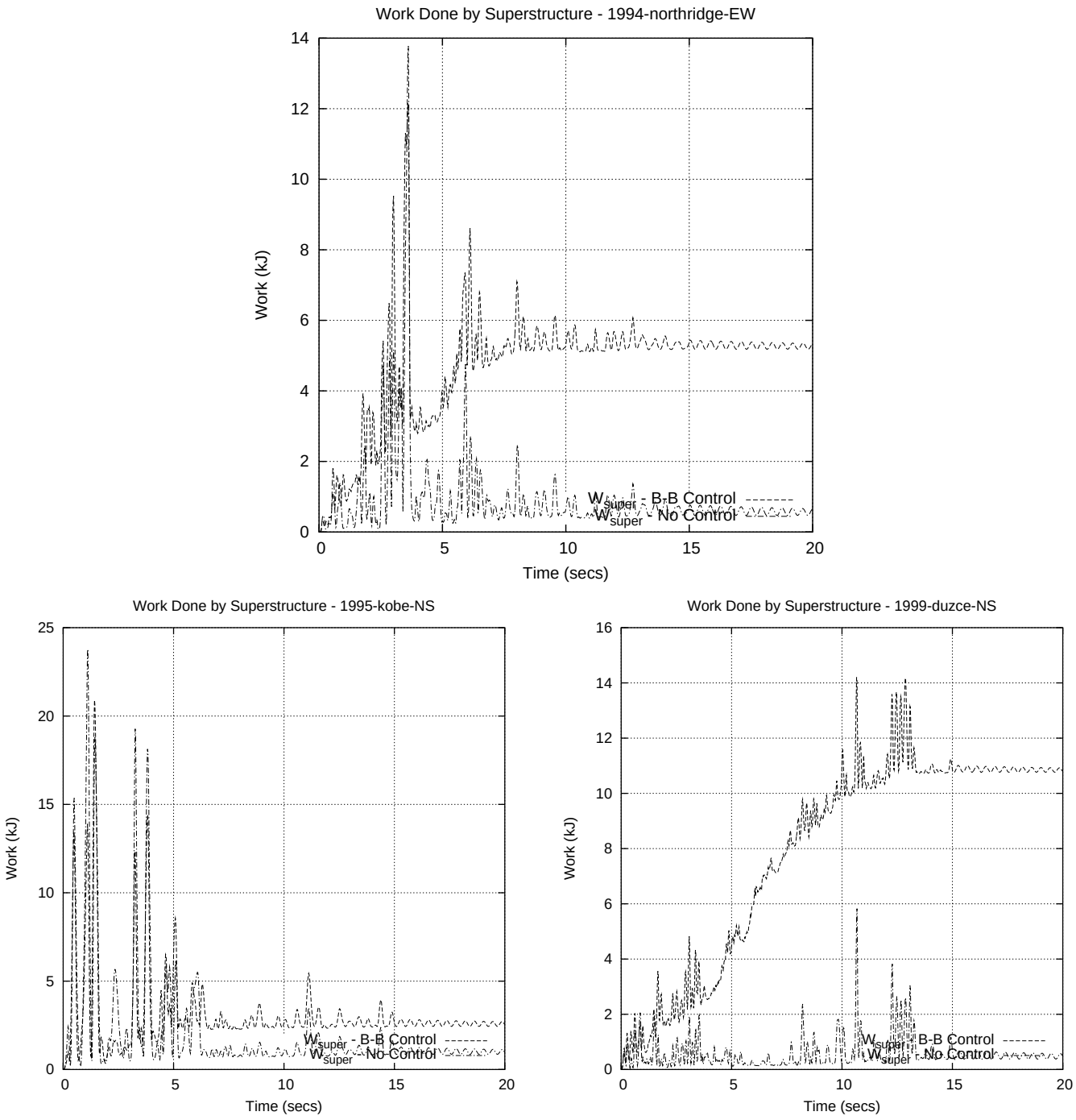

Figure B.22: Severe EQs: 1994 Northridge, 1995 Kobe, 1999 Duzce.

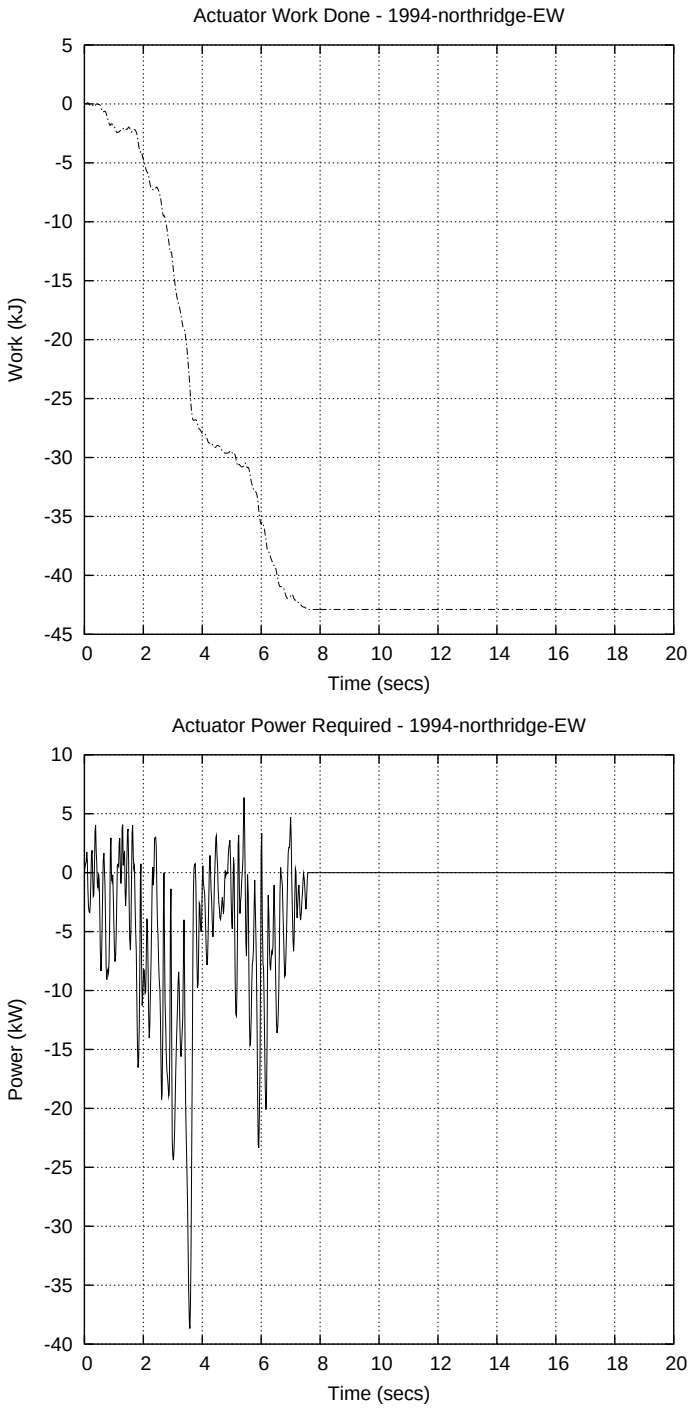

Figure B.23: Severe EQs: 1994 Northridge.

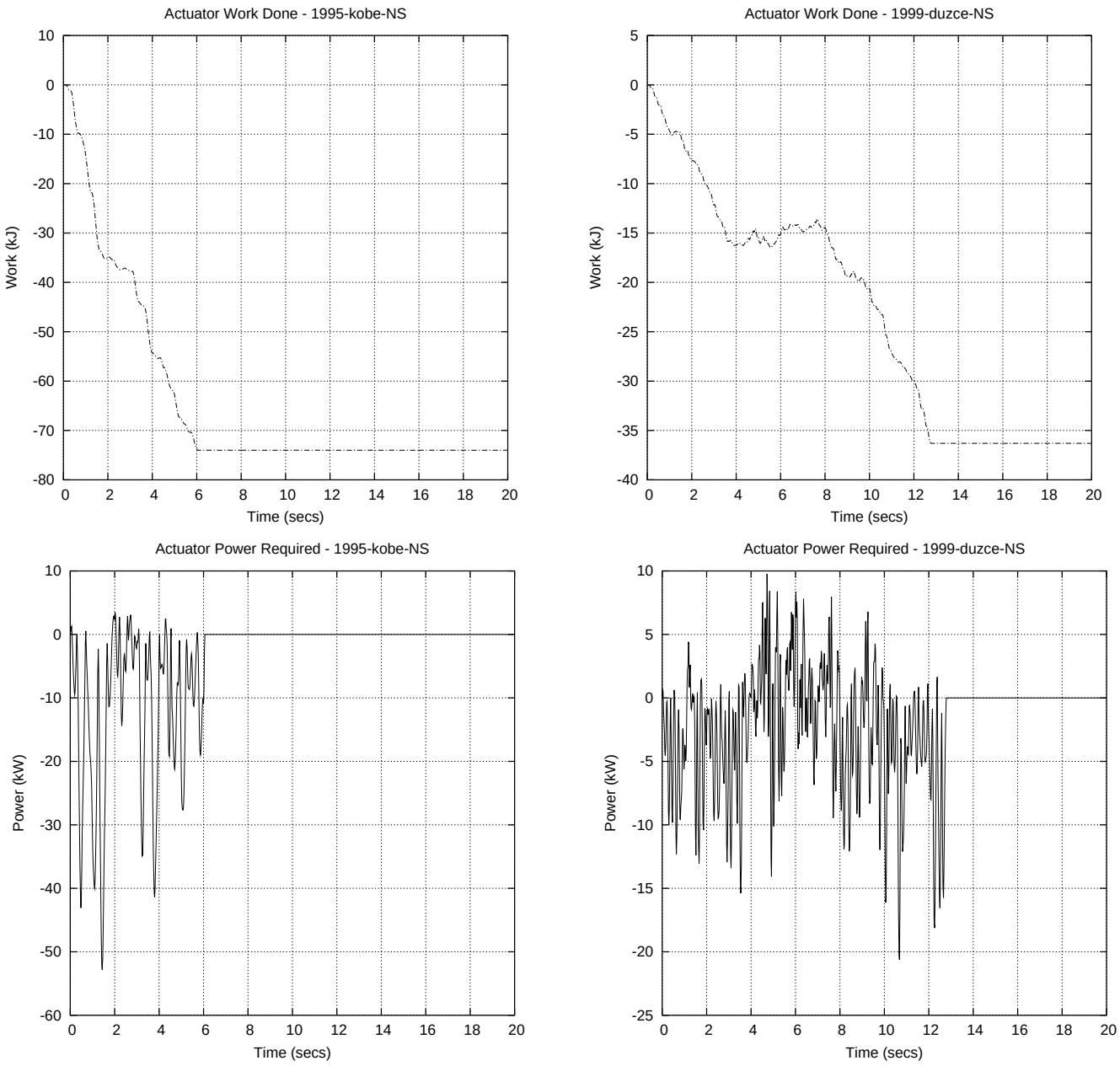

Figure B.24: Severe EQs: 1995 Kobe and 1999 Duzce.

Appendix C

Notation

The following symbols are used in this dissertation:

A = forcing function amplitude;

C = viscous damping matrix;

DOF = degree of freedom;

E = Young's Modulus of Elasticity;

F(.) = (n $\times$ 1) vector of straining and damping forces;

F_y = yield force;

g = acceleration due to gravity;

I = moment of inertia;

J = energy (Joules);

K = global stiffness matrix;

k = element-level stiffness matrix;

M = mass matrix;

n = number of degrees of freedom in global structural model;

N = work (Newtons);

R(.) = (n $\times$ 1) vector of general forces, and, (n $\times$ 1) vector of residual forces in (nonlinear) Newmark integration;

$\mathbf{r}$ = (n $\times$ 1) vector describing the movement of each structural degree of freedom due to a unit ground displacement;

$\mathbf{Q}$ = control design matrix variable;

$\mathbf{S}$ = solution matrix to Lyapunov equation;

T = kinetic energy, and, natural period of vibration;

z = vector of system displacements concatenated with system velocities;

t = time (sec);

$x(t)$ = (n $\times$ 1) vector of displacements at structural degrees of freedom;

$\dot{x}(t)$ = (n $\times$ 1) vector of velocities at structural degrees of freedom;

$\ddot{x}(t)$ = (n $\times$ 1) vector of accelerations at structural degrees of freedom;

$\mathbf{W}$ = work done by internal/external loads;

α = mass coefficient for damping;

β = stiffness coefficient for damping; ratio of forcing function frequency to system natural, free-vibration frequency;

γ = base isolator stiffness scaling parameter;

λ = bang-bang control costate vector;

ξ = ratio of system damping to critical damping value;

ρ = ratio of initial system displacement $\times$ free-vibration frequency of undamped system ($x(0)\omega_o$) to initial system velocity ($\dot{x}(0)$); statistical correlation coefficient;

τ = ratio of superstructure mass to superstructure stiffness for a 2-DOF system;

ω_d = free-vibration frequency of a damped system;

ω_o = free-vibration frequency of a undamped system;

$\triangle t$ = time increment in Newmark integration.

Subscripts:

damping = damping forces;

e = elastic stiffness matrix;

eff = effective stiffness and effective mass;

ext = external loads;

g = ground motion;

int = internal loads;

straining = straining forces;

t = tangent stiffness matrix, and, total displacement, velocity, or acceleration;

1,2 = damping matrix coefficients.

BIBLIOGRAPHY

[1] AASHTO. *Guide Specifications for Seismic Isolation Design.* 1991.

[2] Andriono T., Carr A.J. A Simplified Earthquake Resistant Design Method for Base Isolated MultiStorey Buildings. *Bulletin of the New Zealand National Society for Earthquake Engineering*, 24(3):238–250, September 1991.

[3] Andriono T., Carr A.J. Reduction and Distribution of Lateral Seismic Forces on Base Isolated Mutli-Storey Structures. *Bulletin of the New Zealand National Society for Earthquake Engineering*, 24(3):225–237, September 1991.

[4] Arias, A. *A Measure of Earthquake Intensity in Seismic Design for Nuclear Power Plants.* MIT Press, 1970. Hansen R., ed.

[5] Austin, M. A., and Lin, W. J. Energy-Balance Assessment of Isolated Structures. *Journal of Engineering Mechanics*, 130(3):347–358, 2003.

[6] Austin, M. A., Lin, W. J., and Chen, X. G. Structural Matrix Computations with Units. *Journal of Computing in Civil Engineering*, 14(3):174–182, 2000.

[7] Austin M. A., Chen X. G., Lin W-J. ALADDIN: A Computational Toolkit for Interactive Engineering Matrix and Finite Element Analysis. Technical Report TR95-74, Institute for Systems Research, University of Maryland, College Park, December 1995.

[8] Austin, M. A., Pister, K. S., Mahin, S. A. A Methodology for the Probabilistic Limit States Design of Earthquake Resistant Structures. *Journal of the Structural Division, ASCE*, 113(8):1642–1659, August 1987.

[9] Austin, M. A., Pister, K. S., Mahin, S. A. Probabilistic Limit States Design of Moment Resistant Frames Under Seismic Loading. *Journal of the Structural Division, ASCE*, 113(8):1660–1677, August 1987.

[10] Belanger, P. R. *Control Engineering : A Modern Approach*. Saunders College Publishing, Fort Worth, TX, 1995.

[11] Bellman, R., Glicksberg, I., and Gross, O. On the Bang-Bang Control Problem. *Quarterly of Applied Mathematics*, 14(1):11–18, 1956.

[12] Brown, A. S., Ankireddi, S., and Yang, H. T. Actuator and Sensor Placement For Multiobjective Control of Structures. *Journal of Structural Engineering*, 125(7):757–765, 1999.

[13] Cai, G., Huang, J., Sun, F., and Wang, C. Modified Sliding-Mode Bang-Bang Control for Seismically Excited Linear Structures. *Earthquake Engineering and Structural Dynamics*, 29.

[14] Carlson, J. D., and Spencer, B. F., Jr. MR Fluid Dampers for Semi-Active Seismic Control. In *Proceeding of 3rd Int. Conference on Vibration Control*, volume III, pages 35–40, 1996.

[15] Casciati, F. and Yao, T. Comparison of Strategies for the Active Control of Civil Structures. In *Proceeding of First World Conference on Structural Control*, volume WA1.

[16] Cheng, F. Y. and Jiang, H.

[17] Chopra, A. K. *Dynamics of Structures: Theory and Applications to Earthquake Engineering*. Prentice Hall, 1995.

[18] Chung, L. L., Lin, R. C., Soong, T. T., and Reinhorn, A. M. Experimental Study of Active Control for MDOF Seismic Structures. *Journal of Engineering Mechanics*, 115(8):1609–1627, 1989.

[19] Chung, L. L., Reinhorn, A. M., and Soong, T. T. Experiments on Active Control of Seismic Structures. *Journal of Engineering Mechanics*, 114:241–256, 1988.

[20] Clough, R. W., Penzien, J. *Dynamics of Structures*. McGraw-Hill, New York, New York, 1993.

[21] Connor, J.J. *Introduction to Structural Motion Control*. Pearson Education, Inc., 2003.

[22] Dorey, A. P. and Moore, J. H. *Advances in Actuators*. Institute of Physics Publishing, Bristol, England, 1996.

[23] Dyke, S. J., Spencer B. F., Jr., Quast, P., and Sain, M. K. Experimental Study of a Active Mass Damper Using Acceleration Feedback Control Strategies. In *Proceeding ASCE Engineering Mechanics Spec. Conference*, pages 1227–1230. ASCE, New York, 1995.

[24] Dyke, S. J., Spencer, B. F., Jr., Quast, P., Sain, M. K., Kaspari, D. C., and Soong, T. T. Acceleration Feedback Control of MDOF Structures. *Journal of Engineering Mechanics*, 122(9):907–918, 1996.

[25] Dyke, S. J., Spencer, B. F., Jr., Sain, M. K., and Carlson, J. D. Modeling and Control of MR Dampers for Seismic Response Reduction. *Smart Mater. Struct.*, 5:565–575, 1996.

[26] Dyke, S. J., Spencer, B. F., Jr., Sain, M. K., and Carlson, J. D. An Experimental Study of MR Dampers for Seismic Protection. *Smart Mater. Struct.*, 7:693–703, 1998.

[27] Earthquake Engineering Research Center, UC Berkeley. Pacific Earthquake Engineering Research (PEER) Strong Motion Database. *http://peer.berkeley.edu/smcat/index.html*.

[28] Fajfar P. Equivalent Ductility Factors, Taking Into Account Low-Cycle Fatigue. *Earthquake Engineering and Structural Dynamics*, 21:837–848, 1992.

[29] Field, R. V., Jr., Voulgaris, P. G., and Bergman, L. A. Probabilistic Stability Robustness of Structural Systems. *Journal of Engineering Mechanics*, 122(10):1012–1021, 1996.

[30] Ghobarah A., Ali H.M. Seismic Design of Base-Isolated Highway Bridges utilizing Lead-Rubber Bearings. *Canadian Journal of Civil Engineering*, 17:413–422, 1990.

[31] Hall, J. F., Heaton, T. H., Halling, M. W., and Wald, D. J. Near-Source Ground Motion and its Effects on Flexible Buildings. *Earthquake Spectra*, 11(4):569–605, 1995.

[32] Heaton, T. H., Hall, J. F., Wald, D. J., and Halling, M. W. Response of High-Rise and Base-Isolated Buildings in a Hypothetical Mw 7.0 Blind Thrust Earthquake. *Science*, 267.

[33] Housner, G. W., Bergman, L. A., et al. Structural Control: Past, Present, and Future. *Journal of Engineering Mechanics*, 123(9):897–971, 1997.

[34] Housner G.W. Limit Design of Structures to Resist Earthquakes. In *Proceedings of the World Conference on Earthquake Engineering*, Berkeley,California, 1956. Earthquake Engineering Reseach Center.

[35] Housner G.W. Behavior of Structures During Earthquakes. *Journal of the Structural Division, ASCE*, 85(4):109–124, April 1959.

[36] Johnson, E. A., Ramallo, J. C., Spencer, B. F., Jr., and Sain, M. K. Intelligent Base Isolation Systems. In *Proceedings of the Second World Conference on Structural Control*, 1998.

[37] Kailath, T. *Linear Systems*. Prentice-Hall, London, England, 1980.

[38] Kaufman, H., Bar-Kana, I., and Sobel, K. *Direct Adaptive Control Algorithms*. Springer-Verlag New York, Inc., N.Y., 1994.

[39] Kayen, R. E. and Mitchell, J. K. Variation of the Intensity of Earthquake Motion Beneath the Ground Surface. In *Proceeding of the Sixth National Conference on Earthquake Engineering*, 1998. Seattle, May 31 - June 4.

[40] Kelly, J. M. and Tsai, H. Seismic Response of Light Internal Equipment in Base Isolated Structures. Report No. UCB/SESM-84/17, Department of Structural Engineering and Structural Mechanics, Berkeley, CA, September 1984.

[41] Kelly, J. M., Leitmann, G., and Soldatos, A. G. Robust Control of Base-Isolated Structures Under Earthquake Excitation. *Journal of Optimization Theory and Applications*, 53(2):159–180, 1987.

[42] Korbori, T., Takahashi, M., Nasu, T., Niwa, N., and Ogasawara, K. Seismic Response Controlled Structure with Active Variable Stiffness System. *Earthquake Engineering and Structural Dynamics*, 22:925–941, 1993.

[43] Kurata, N., Kobori, T., Takahashi, M., Niwa, N., and Kusino, H. Shaking Table Experiment of Active Variable Damping System. In *Proceeding of the First World Conference on Structural Control*, volume 2.

[44] Lin, W. J. Modern Computational Environments for Seismic Analysis of Highway Bridge Structures, 1997. Doctoral Dissertation.

[45] Lou, J. Y. K., Lutes, L. D., and Li, J. J. Active Tuned Liquid Damper for Structural Control. In *Proceeding of First World Conference on Structural Control*, volume TP1.

[46] Madden, G. J., Wongprasert, N., and Symans, M. D. Experimental Verification of Seismic Response of Building Frame with Adaptive Sliding Base-Isolation System. *Journal of Structural Engineering*, 128(8):1037–1045, 2002.

[47] Makris, N. Rigidity-Plasticity-Viscosity : Can Electrorheological Dampers Protect Base-Isolated Structures from Near-Source Earthquakes. *Journal of Engineering and Structural Dynamics*, 26:571–591, 1997.

[48] Mayes R.L., Buckle I.G., Kelly T.R., Jones L. AASHTO Seismic Isolation Design Requirements for Highway Bridges. *Journal of the Structural Division, ASCE*, 118(1):284–304, January 1992.

[49] Naeim, F. and Kelly, J. *Design of Seismic Isolated Structures*. John Wiley and Sons, 1998.

[50] Nagarajaiah, S. and Mate, D. Semi-Active Control of Continuously Variable Stiffness System. In *Proceeding of Second World Conference on Structural Control*, volume 1.

[51] Nagarajaiah, S. and Varadarajan, N. Novel Semiactive Variable Stiffness Tuned Masss Damper With Real Time Tuning Capability. In *Proceeding of 13th Engineering Mechanics Conference*, 2000. (on CD ROM), Reston, VA.

[52] Newmark N.M., Hall W.J. *Earthquake Spectra and Design. A Primer*. Earthquake Research Institute, Berkeley, CA, 1982.

[53] Park, J. and Otsuka, H. Optimal Yield Level of Bilinear Seismic Isolation Devices. *Earthquake Engineering and Structural Dynamics*, 28.

[54] Patten, W., Sack, R., and He, Q. Controlled Semiactive Hydraulic Vibration Absorber for Bridges. *Journal of Structural Engineering*, 122(2):187–192, 1996.

[55] Patten, W., Sun, J., Li, G. Kuehn, J., and Song, G. Field Test of an Intelligent Stiffener for Bridges at the I-35 Walnut Creek Bridge. *Earthquake Engineering and Structural Dynamics*, 28(2):109–126, 1999.

[56] Powell G. H., Allahabadi R. Seismic Damage Prediction by Deterministic Methods: Concepts and Procedures. *Earthquake Engineering and Structural Dynamics*, 16:719–734, 1988.

[57] Ramallo, J. C., Johnson, E. A., and Spencer, B. F., Jr. "Smart" Base Isolation Systems. *Journal of Engineering Mechanics*, 128(10):1088–1099, 2002.

[58] Reinhorn, A. M., Soong, T. T., and Wen, C. Y. Base-isolated Structures with Active Control. In *Proceedings of Pressure Vessels and Piping (PVP) Conference*, volume PVP-127, pages 413–420, 1987.

[59] Robinson, W. H. Lead-Rubber Hysteretic Bearings Suitable for Protecting Structures During an Earthquake. *Earthquake Engineering and Structural Dynamics*, 10:593–602, 1982.

[60] Sack, R. L. and Patten, W. Semi-Active Hydraulic Structural Control. In *Proceeding of International Workshop on Structural Control*, volume NISTIR 5923. edited by G.W. Housner and S.F. Masri.

[61] Schemmann, A. G. and Smith, H. A. Vibration Control of Cable-Stayed Bridges -Part 1: Modeling Issues. *Earthquake Engineering and Structural Dynamics*, 1998.

[62] Schemmann, A. G. and Smith, H. A. Vibration Control of Cable-Stayed Bridges -Part 2: Control Analyses. *Earthquake Engineering and Structural Dynamics*, 1998.

[63] Schemmann, A. G., Smith, H. A., Bergman, L. A., Dyke, S. J. Feasibility Study: Control of a Cable-Stayed Bridge Model Part I: Problem Definition. In *Proceedings of the Second World Conference on Structural Control*, 1998.

[64] Sebastianelli, R. R., Jr., and Austin, M. A. Phase Analysis of Actuator Response of Semi-Active Bang-Bang Control of Base Isolated Structures. *Earthquake Engineering and Structural Dynamics in press.*

[65] Skinner, R. I., Robinson, W. H., and McVerry, G. H. *An Introduction to Seismic Isolation.* Wiley Publishing, Chichester, England, 1993.

[66] Skinner, R. I., Robinson, W. H., McVerry, G. H. *An Introduction to Seismic Isolation.* John Wiley & Sons, Inc., 1993.

[67] Spencer, B. F., Jr. Civil Engineering Applications of Smart Damping Technology. In *Proceeding of 5th Int. Conference on Vibration Control*, pages 771–782, 2002. Nanjing, China.

[68] Spencer, B. F., Jr. and Nagarajaiah, S. State of the Art of Structural Control. *Journal of Structural Engineering*, pages 845–856, July 2003.

[69] Spencer, B. F., Jr. and Sain, M. K. Controlling Buildings: A New Frontier in Feedback. *IEEE Control System Magazine*, 17(6):19–35, 1997.

[70] Spencer, B. F., Jr., Christenson, R. E., Dyke, S. J. Next Generation Benchmark Control Problem for Seismically Excited Buildings. In *Proceedings of the Second World Conference on Structural Control*, 1998.

[71] Spencer, B. F., Jr., Dyke, S. J., Deoskar, H. S. Benchmark Problems in Structural Control -Part 1: Active Mass Driver System. In *Proceedings of the ASCE Struc. Congress XV*, volume 2, pages 1265–1269.

[72] Spencer, B. F., Jr., Dyke, S. J., Sain, M. K., and Carlson, J. D. Phenomenological Model of a Magnetorheological Damper. 123(3):230–238, 1997.

[73] Spencer, B. F., Jr., Sain, M. K. Controlling Buildings: A New Frontier in Feedback. *IEEE Control Systems*, 17(6), 1997.

[74] Spencer, B. F., Jr., Sain, M. K., Won, C. H., Kaspari, D., Jr., and Sain, P. M. Reliability-Based Measures of Structural Control Robustness. *Structural Safety*, 15:111–129, 1994.

[75] Spencer, B. F., Jr., Suhardjo, J., and Sain, M. K. Frequency Domain Optimal Control Strategies for Aseismic Protection. 118(12):2463–2481, 1992.

[76] Spencer, B. F., Jr., Timlin T. L., Sain, M. K., and Dyke, S. J. Series Solution of a Class of Nonlinear Optimal Regulators. *Journal of Optimization Theory and Applications*, 91(5):321–345, 1996.

[77] Spencer, B. F., Jr., Yang, G., Carlson, J. D., Sain, M. K. "Smart" Dampers for Seismic Protection of Structures: A Full-Scale Study. In *Proceeding of*

Second World Conference on Structural Control, volume 1, pages 417–426. Wiley, New York, 1999.

[78] Stengel, R. F. *Stochastic Optimal Control: Theory and Application*. Wiley Publishing, New York, NY, 1986.

[79] Suhardjo, J. Frequency Domain Techniques for Control of Civil Engineering Structures with Some Robustness Considerations, 1990. Doctoral Dissertation.

[80] *Dynamic Structural Design : An Inverse Approach*. WIT Press, 2000.

[81] The Physics Classroom and Mathsoft Engineering and Education, Inc. The Work-Energy Theorem. *http://www.physicsclassroom.com/*.

[82] Turkington D.H., Carr A.J., Cooke N., and Moss P.J. Design Method for Bridges on Lead-Rubber Bearings. *Journal of the Structural Division, ASCE*, 115(12):3017–3030, December 1989.

[83] Turkington D.H., Carr A.J., Cooke N., and Moss P.J. Seismic Design of Bridges on Lead-Rubber Bearings. *Journal of the Structural Division, ASCE*, 115(12):3000–3016, December 1989.

[84] Tyler R.G. Rubber Bearings in Base Isolated Structures : A Summary Paper. *Bulletin of the New Zealand National Society of Earthquake Engineering*, 24(3), September 1991.

[85] Uang C.M., Bertero V.V. Evaluation of Seismic Energy in Structures. *Earthquake Engineering and Structural Dynamics*, 19:77–90, 1990.

[86] Earthquake Regulations for Seismic-Isolated Structures : Appendix Chapter 16. *International Conference of Building Officials*, 1997.

[87] United States Geological Survey (USGS) Earthquake Hazards Program. Recent World Earthquakes. *http://earthquake.usgs.gov/recenteqsww/*.

[88] Varadarajan, N. and Nagarajaiah, S. Wind Response Control of Building with Variable Stiffness TMD Using Empirical Mode Decomposition. 130(4):451–458, 2003.

[89] Vision 2000 Committee. Performance Based Seismic Engineering of Buildings. Volume 1 : Interim Recommendations and Conceptual Framework, Structural Engineers Association of California, College Park, MD 20742, April 1995.

[90] Wang, Y. P., and Liu, C. J. Active Control of Base-Isolated Structures Under Strong Earthquakes. In *Proceeding of the Fifth USA National Conference on Earthquake Engineering*, volume 1. Chicago, July 10-14.

[91] Wen, Y. K. Method for Random Vibration of Hysteretic Systems. *Journal of Engineering Mechanics*, 102(2):249–263, 1976.

[92] Wonham, W. M. and Johnson, C. D. Optimal Bang-Bang Control with Quadratic Performance Index. *Journal of Basic Engineering*, 86:107–115, 1964.

[93] Wu, Z., and Soong, T. T. Modified Bang-Bang Control Law for Structural Control Implementation. *Journal of Engineering Mechanics*, 122(8):771–777, 1996.

[94] Wu, Z., Soong, T. T., Gattulli, V., and Lin, R. C. Nonlinear Control Algorithms for Peak Response Reduction. Technical Report NCEER-95-0004, National Center for Earthquake Engineering Research, State University of New York at Buffalo, Buffalo, NY. 14261, February 1995.

[95] Xu, Y. L., Qu, W. L., and Ko, J. M. Seismic Response Control of Frame Structures Using MR/ER Dampers. 29:557–575, 2000.

[96] Yang, J. N., Wu, J. C., Reinhorn, A. M., Riley, M. Schmitendorf, W. E., and Jabbari, F. Experimental Verifications of H_∞ and Sliding Mode Control for Seismic-Excited Buildings. In *Proceeding of First World Conference on Structural Control*, volume TP4.

[97] Yang, J. N., Wu, J. C., Samali, B., and Agrawal, A. K. A Benchmark Problem For Response Control of Wind-Excited Tall Buildings, 1997. Benchmark Problem Package.

[98] Yao, J. T. P. Concept of Structural Control. *J. Struct. Div.*, 98:1567–1574, 1972.

[99] Yoshioka, H., Ramallo, J. C., and Spencer, B. F., Jr. Smart Base Isolation Strategies Employing Magnetorheological Dampers. *Journal of Engineering Mechanics*, 128(5):540–551, 2002.

[100] Zhou, K., Doyle, J. C., and Glover, K. *Robust and Optimal Control*. Prentice-Hall, Inc, Englewood Cliffs, N.J., 1996.

[101] Zhu, G., Rotea, M. and Skelton, R. E. A Convergent Algorithm for the Output Covariance Constraint Control Problem. *Journal of Control and Optimization*, 35(1):341, 1997.